Universitat Autònoma de Barcelona

FAIM-L participation in Alzheimer's Disease and other tauopathies: Deciphering the role of FAIM-L in tau ubiquitination, synaptic maintenance, and memory function during the development of tau pathology

Raquel Badillos Rodríguez

PhD thesis

FAIM-L participation in Alzheimer's Disease and other tauopathies:

Deciphering the role of FAIM-L in tau ubiquitination, synaptic maintenance, and memory function during the development of tau pathology

Raquel Badillos Rodríguez

Doctorat en Neurociències

Institut de Neurociències

Universitat Autònoma de Barcelona

Desembre del 2022

FAIM-L participation in Alzheimer's Disease and other tauopathies:

Deciphering the role of FAIM-L in tau ubiquitination, synaptic maintenance, and memory function during the development of tau pathology

Memòria de tesi doctoral presentada per Raquel Badillos Rodríguez per optar al grau de Doctora en Neurociències per la Universitat Autònoma de Barcelona.

Aquest treball ha estat realitzat al grup de Senyalització Cel·lular i Apoptosi de l'Institut de Recerca de Vall d'Hebron (VHIR), i al Departament de Bioquímica i Biologia Molecular i Institut de Neurociències de la Universitat Autònoma de Barcelona (UAB), sota la direcció dels doctors Joan X. Comella i Montse Solé.

Tanmateix, aquest ha estat parcialment finançat per les següents entitats: Ministerio Economía, Industria y Competitividad (BES-2017-080846), Ministerio de Ciencia e Innovación (SAF2016-80236-R i PID2019-107286RB- I00), CIBERNED (CB06/05/1104) i la Generalitat de Catalunya (2017SGR996).

Doctoranda Director Directora

Raquel Badillos Rodríguez Joan X. Comella Montse Solé

Desembre del 2022

Para mi familia,

para mis dos estrellas.

ABSTRACT

ABSTRACT

Alzheimer's disease (AD) is the most prevalent type of dementia worldwide and one of the most relevant disorders among a group of neurodegenerative diseases named tauopathies. These diseases are characterized by the aberrant modification and progressive accumulation of the protein tau. Tau protein, initially described to stabilize microtubules, participates in other multiple cellular processes, including DNA repair, synaptic plasticity, and mitochondrial maintenance. Consequently, it is an essential protein for cellular homeostasis but also can become the trigger of the neuronal failure and loss associated to this type of diseases, especially to AD. Our group has been centred in the study of the neuro-specific long isoform of the Fas Apoptotic Inhibitory Molecule, FAIM-L. Furthermore, we have been pioneers in describing unique roles of this protein through its capacity to inhibit certain non-apoptotic functions of caspase-3. Importantly, our group was the first in linking FAIM-L to neurodegeneration by finding it decreased in both AD patients and in a mouse model of the disease. Since FAIM-L is implicated in the correct control of apoptosis and synaptic processes, we propose that its loss may be promoting the progression of AD. To explore this hypothesis, we aimed to elucidate the molecular mechanisms involved in FAIM-L reduction and the consequences of its decrease. Additionally, we have analysed the functional implications of FAIM-L levels restoration using *in vivo* adeno-associated viral injections. Therefore, we would like to propose FAIM-L as a potential therapeutical target for AD.

Importantly, we found that the reduction of FAIM-L was directly linked to tau pathology and was not directly dependent on amyloid-β pathology. Also, by using the Frontotemporal Dementia linked to Parkinsonism (FTDP-17) mouse model, the PS19 mice, we proved that this decrease occurs before other

pathological alterations such as synaptic impairment and reactive gliosis and that it is associated to a decrease in XIAP levels and an anomalous increase in global ubiquitination. This early reduction of FAIM-L in the course of the pathology offers a new therapeutic window that is clearly supported by the results obtained after FAIM-L modulation *in vivo*. Our novel findings show that FAIM-L expression restoration in the hippocampus of the PS19 mice completely avoided dendritic spine loss and helped maintaining synaptic integrity by preventing PSD95 and mGluR2 losing the postsynaptic compartment. Consequently, FAIM-L overexpression prevented brain atrophy as well as learning and memory impairment in our model. The relationship between FAIM-L and tau pathology is reinforced by our *in vitro* experiments in which we were able to describe, for the first time, that FAIM-L reduction depends on the increase in phosphorylation levels of tau and, indeed, to report a functional connection between these two proteins. In this work, we also demonstrate that FAIM-L interacts with both wild-type and mutant tau isoforms and avoids its ubiquitination.

In summary, our results confirm FAIM-L implication in AD but also settle it an essential element for neuronal survival, synaptic maintenance and cognition. Also, these findings allow to suggest that FAIM-L confers early protection from tau-associated alterations and place it as a potential target for therapeutic approaches, not only for AD but possibly for FTDP-17 and the rest of tauopathies.

RESUMEN

La enfermedad de Alzheimer (EA) es el tipo de demencia más prevalente a nivel mundial y uno de los trastornos más relevantes dentro de un grupo de enfermedades neurodegenerativas denominadas tauopatías. Estas enfermedades se caracterizan por la modificación aberrante y acumulación progresiva de la proteína tau. Esta proteína, descrita inicialmente como estabilizadora de microtúbulos, participa también en múltiples procesos celulares, incluidos la reparación del ADN, la plasticidad sináptica y el mantenimiento de la función mitocondrial. Por ello, además de ser un elemento esencial para la homeostasis celular, tau también puede desencadenar el mal funcionamiento y la pérdida neuronal asociados a este tipo de enfermedades, especialmente a la EA. Nuestro grupo se ha centrado en el estudio de la isoforma larga neuroespecífica de la Molécula Inhibidora de la Apoptosis Fas, FAIM-L. Además, hemos sido pioneros en describir funciones únicas de esta proteína basadas en su capacidad de inhibir ciertas funciones no apoptóticas de la caspasa-3. Junto a esto, nuestro grupo fue también el primero en vincular FAIM-L con la neurodegeneración, al encontrar que se encuentra disminuido tanto en pacientes con EA como en un modelo de ratón de dicha enfermedad.

Dado que FAIM-L está implicado en el correcto control de la apoptosis y los procesos sinápticos, proponemos que su pérdida puede estar favoreciendo la progresión de la EA. Para explorar esta hipótesis, nuestro objetivo fue dilucidar los mecanismos moleculares involucrados en la reducción de FAIM-L y las consecuencias de su disminución. Además, hemos querido analizar las implicaciones funcionales de la restauración de los niveles de FAIM-L *in vivo* mediante el uso de inyecciones virales con vectores adeno-asociados. Con

todo ello, nos gustaría proponer FAIM-L como un potencial diana terapéutica para la EA.

En este trabajo, observamos que la reducción de FAIM-L estaba directamente relacionada con la patología tau mientras que no dependía directamente de la patología β-amiloide. Además, utilizando el modelo murino de Demencia Frontotemporal ligada a Parkinsonismo (FTDP-17), el ratón PS19, comprobamos que esta disminución se producía previamente al desarrollo de otras alteraciones patológicas como el deterioro sináptico y la gliosis. Además, pudimos ver que estaba asociada a una disminución de los niveles de XIAP y a un aumento anómalo de la ubiquitinación global. Esta reducción temprana de FAIM-L en el curso de la patología ofrece una nueva ventana terapéutica que está claramente avalada por los resultados obtenidos tras la modulación de FAIM-L *in vivo*. Nuestros nuevos hallazgos mostraron que la restauración de la expresión de FAIM-L en el hipocampo de los ratones PS19, evitó por completo la pérdida de espinas dendríticas y ayudó a mantener la integridad sináptica mediante la prevención de la pérdida de las proteínas PSD95 y mGluR2 en el compartimento postsináptico. En consecuencia, la sobreexpresión de FAIM-L previno la atrofia cerebral y el deterioro del aprendizaje y la memoria en nuestro modelo. Adicionalmente, gracias a nuestros experimentos *in vitro*, pudimos reforzar a relación entre FAIM-L y la patología de tau. Con ellos, pudimos describir que la reducción de FAIM-L depende del aumento en los niveles de fosforilación de tau. Además, hemos podido reportar una conexión funcional entre estas dos proteínas. En este trabajo, demostramos, por primera vez, que FAIM-L interactúa con las isoformas *wild-type* y mutante de tau y evita su ubiquitinación.

En resumen, nuestros resultados confirman la implicación de FAIM-L en la EA pero también lo establecen como un elemento esencial para la

supervivencia neuronal, el mantenimiento sináptico y la memoria. Además, estos hallazgos permiten sugerir que FAIM-L confiere una protección temprana frente a las alteraciones asociadas a tau. Por tanto, lo sitúan como una diana potencial para abordajes terapéuticos, no solo para la EA sino posiblemente para FTDP-17 y el resto de tauopatías.

RESUM

La Malaltia d'Alzheimer (MA) és el tipus de demència més prevalent a nivell mundial i un dels trastorns més rellevants dins un grup de malalties neurodegeneratives anomenades tauopaties. Aquestes malalties es caracteritzen per la modificació aberrant i acumulació progressiva de la proteïna tau. Tau va ser descrita inicialment com a estabilitzadora de microtúbuls, tot i que també participa en múltiples processos cel·lulars, inclosos la reparació de l'ADN, la plasticitat sinàptica i el manteniment de la funció mitocondrial. Per això, a més de ser un element essencial per a l'homeòstasi cel·lular, tau també pot desencadenar el mal funcionament i la pèrdua neuronal associats a aquest tipus de malalties, especialment a la MA. El nostre grup s'ha centrat en l'estudi de la isoforma llarga neuroespecífica de la Molècula Inhibidora de l'Apoptosi Fas, FAIM-L. A més, hem estat pioners a descriure funcions úniques d'aquesta proteïna basades en la seva capacitat d'inhibir certes funcions no apoptòtiques de la caspasa-3. Amb això, el nostre grup va ser també el primer a vincular FAIM-L amb la neurodegeneració, en descobrir que es trobava disminuïda tant en pacients amb la MA com en un model de ratolí d'aquesta malaltia.

Atès que FAIM-L està implicat en el correcte control de l'apoptosi i dels processos sinàptics, vam proposar que la seva pèrdua podia estar afavorint la progressió de la MA. Per explorar aquesta hipòtesi, el nostre objectiu va ser dilucidar els mecanismes moleculars involucrats en la reducció de FAIM-L, les conseqüències de la seva disminució i les implicacions funcionals de la restauració dels nivells de FAIM-L *in vivo* mitjançant l'ús d'injeccions virals amb vectors adeno-associats. Amb tot això, volem proposar FAIM-L com un element terapèutic potencial per a la MA.

En aquest treball, vam observar que la reducció de FAIM-L estava directament relacionada amb la patologia tau, mentre que no depenia de la patologia β-amiloide. A més, utilitzant el model murí de Demència Fronto-temporal lligada a Parkinsonisme (FTDP-17), el ratolí PS19, vam comprovar que aquesta disminució es produïa prèviament al desenvolupament d'altres alteracions patològiques com el deteriorament sinàptic i la gliosi. A més, vam poder veure que estava associada a una disminució dels nivells de XIAP i a un augment anòmal de la ubiquitinació global. Aquesta reducció primerenca de FAIM-L al curs de la patologia ofereix una nova finestra terapèutica que està clarament avalada pels resultats obtinguts després de la modulació de FAIM-L *in vivo*. Els nostres nous descobriments van mostrar que la restauració de l'expressió de FAIM-L a l'hipocamp dels ratolins PS19, va evitar per complet la pèrdua d'espines dendrítiques i va ajudar a mantenir la integritat sinàptica mitjançant la prevenció de la pèrdua de les proteïnes PSD95 i mGluR2 al compartiment post-sinàptic. En conseqüència, la sobre-expressió de FAIM-L va prevenir l'atròfia cerebral i el deteriorament de l'aprenentatge i la memòria al nostre model. Addicionalment, gràcies als nostres experiments *in vitro*, vam poder reforçar la relació entre FAIM-L i la patologia de tau. Amb ells, vam poder descriure que la reducció de FAIM-L depèn de l'augment dels nivells de fosforilació de tau. A més, vam reportar una connexió funcional entre aquestes dues proteïnes. En aquest treball, demostrem, per primer cop, que FAIM-L interactua amb les isoformes *wild-type* i mutant de tau i evita la seva ubiquitinació.

En resum, els nostres resultats confirmen la implicació de FAIM-L a l'EA però també l'estableixen com un element essencial per a la supervivència neuronal, el manteniment sinàptic i la memòria. A més, aquestes troballes permeten suggerir que FAIM-L confereix una protecció primerenca davant de les alteracions associades a tau. Per tant, el situen com a diana potencial per a

abordatges terapèutics, no només per a l'EA sinó possiblement per a FTDP-17 i la resta de tauopaties.

CONTENTS

ABBREVIATIONS

I. ABBREVIATIONS

5LO	5-lipoxygenase
AAV	Adeno-associate Virus
ACh	Acetylcholine
AD	Alzheimer's Disease
ADAM	A Disintegrin And Metalloprotease
ADDLs	Aβ Derived Diffusible Ligands
AGD	Argyrophilic Grain Disease
AGs	Argyrophilic Grains
AMPA	(Apha-amino-3-hydroxy-5-methyl-4-isoxazolepropionic acid)-ionotropic
AMPK	5′ Adenosine Monophosphate-Activated Protein Kinase
AP	Anteroposterior
APOE	Apolipoprotein E
APP	Amyloid Precursor Protein
Aβ	Amyloid-β
CB	Ceberellum
CBD	Corticobasal Degeneration
CDK5	Cyclin-Dependent Kinase 5
CFU	Colony-Formation Unit
CHIP	E3 ligase carboxy-terminus of Hsc70 Interacting Protein
CK1	Casein Kinase 1
CNS	Central Nervous System
CTE	Chronic Traumatic Encephalopathy
CX	Cortex
DCTN1	Dynactin Subunit 1
DG	Dentate Gyrus
DMEM	Dulbecco's Modified Eagle Medium

DMSO	Dimethylsulfoxide
DR	Death receptor
DUB	Deubiquitinase
DV	Dorsoventral
E1	Ubiquitin-activating enzyme-1
E2	Ubiquitin-conjugating enzyme-2
E3	Ubiquitin-protein ligase-3
ER	Endoplasmic reticulum
FAD	Familiar Alzheimer's Disease
FAIM	Fas Apoptotic Inhibitory Molecule
FAIM-L	Long isoform of Fas Apoptotic Inhibitory Molecule
FAIM-S	Short isoform of Fas Apoptotic Inhibitory Molecule
FasL	Fas Ligand
GGT	Globular Glial Tauopathy
GO	Gene Ontology
GSK-3β	Serine/threonine Glycogen Synthase Kinase-3β
HD	Huntington's Disease
HEPES	4-(2-hydeoxyethil)-1-Piperazineethanesulonic Acid
HIP	Hippocampus
HSP	Heat Shock Protein
Htt	Huntingtin
IAPs	Inhibitors of Apoptotic Proteins
iFBS	Heat-inactivated Fetal Bovine Serum
iHS	Heat-inactivated Horse Serum
IP	Inmunoprecipitation
ISR-1	Insulin Receptor Substrate 1
ISRβ	Insulin Receptor β
IκB	Inhibitor of NF-κB

KO	Knock-Out
LRRK2	Leucine-Rich Repeat Kinase 2
LTD	Long-Term Depression
LTP	Long-Term Potentiation
Lys	Lysine
MAPs	Microtubule-Associated Proteins
MARK	Microtubule Affinity-Regulating Kinase
MCI	Mild Cognitive Impairment
mGluR2	metabotropic Glutamate Receptor 2
ML	Mediolateral
MOMP	Mitochondrial Outer Membrane Permeabilization
MT	Microtubule
MTB	Microtubule-binding
nAChR	Nicotinic acetylcholine receptor
NF-κB	Nuclear Factor kappa-light-chain-enhancer of activated B cells
NFTs	Neurofibrillar Tangles
NGF	Nerve Growth Factor
NMDA	N-methyl-D-aspartate
NOLT	Novel Object Location Test
NORT	Novel Object Recognition Test
OF	Open Field
Park2	Ub ligase Parkin 2
PART	Primary Age-Related Tauopathy
PBS	Phosphate-Buffered Saline
PCD	Programmed Cell Death
PD	Parkinson’s Disease
PEG	Polyethylene Glycol

PEI	Polyethylenimine
Pen	Penicillin
PFC	Prefrontal Cortex
PHFs	Paired Helical Filaments
PiD	Pick's Disease
PKA	AMP-dependent Protein Kinase A
PP1	Protein Phosphatase-1
PP2A	Protein Phosphatase-2A
PP5	Protein Phosphatase-5
PrP	Prion Protein
PSD	Post Synaptic Density
PSD95	Postsynaptic Density Protein 95
PSEN1	Presenilin 1
PSEN2	Presenilin 2
PSMs	Peptide Spectrum Matches
PSP	Progressive Supranuclear Palsy
PTM	Post-translational Modification
RBP	RNA Binding Proteins
RIP	Receptor-Interacting protein
ROS	Reactive Oxygen Species
RS	Richardson's Syndrome
RT	Room Temperature
sAPPα	Released soluble APP alpha
SF	Straight Filament
shRNA	Short-hairpin RNA
SMA	Spinal Muscular Atrophy
SOD1	Superoxide Dismutase 1
SP	Senile plaque

STR	Striatum
Strep	Streptomicin
TIA1	T-cell Intracellular Antigen 1
TNFα	Tumor Necrosis Factor alpha
TRAF6	TNF Receptor Associated Factor 6
Ub	Ubiquitin
UPS	Ubiquitin Proteasome System
UTR	Untranslated Region
WB	Western Blot
WT	Wild-Type
XIAP	X-linked Inhibitor of Apoptosis Protein

INTRODUCTION

IV. INTRODUCTION

Neurodegenerative diseases are characterized by the progressive loss of selective vulnerable populations of neurons and its functionality, which leads to a wide spectrum of clinical symptoms. Among them, those characterized by an aberrant accumulation of certain proteins, as a consequence of alterations in its structure, conformation, and/or functionality are known as proteinopathies. Inside this group, the aberrant accumulation of the protein tau gives name to tauopathies. Alzheimer's Disease (AD) is one of the most relevant in this last group, and despite not being a classical tauopathy is highly dependent of abnormal tau modifications. Along these pages, we will describe the basis of tauopathies, with special attention to AD, and we will review the two main cellular and molecular alterations underlying these diseases: the impaired proteostasis that cause protein aggregation and the main cell death process responsible of neurodegeneration, apoptosis. Importantly, we will settle the participation of the protein FAIM-L in all this context.

1. TAUOPATHIES

Tauopathies are the group of proteinopathies characterized by the deposition of abnormal microtubule-associated protein tau (*) in neurons and/or glia[1–4]. As other neurodegenerative diseases, tauopathies are clinically, morphologically, and biochemically heterogeneous. They can be categorized depending on the brain area affected, type of cellular vulnerability, and pathological alterations of tau. Usually, they are divided in primary and secondary tauopathies, depending on the principal pathological driving event (*see table 4 for more information*). Briefly, the term primary tauopathy refers to disorders in which tau deposition is the predominant feature and include

(*) All the information regarding tau structure, functionality and its implication in pathology are deeply described in the following section 1.3

diseases such as Pick's Disease (PiD) or the Corticobasal Degeneration (CBD). In contrast, secondary tauopathies correspond to those disorders mainly characterized by another pathological event that generally occurs before in the course of the pathology, but also course with tau abnormalities. This last group of diseases includes the Gerstman–Sträussler–Scheinker syndrome, the familial British and Danish dementias, the one of the most relevant diseases nowadays, Alzheimer's Disease (AD).

1.1 Alzheimer's Disease: a secondary tauopathy highly dependent on tau

AD is the most common type of neurodegenerative disease worldwide, affecting mostly to elder people. Nowadays, it is responsible of the 50-70% of all cases of dementia, a data that exponentially increases every year (an increase from 6.5 million to more than 15 million is expected by 2050)[5]. Its high socio-economic impact has placed AD as one of the most studied diseases among the scientific community.

AD is associated with a progressive loss of brain functions caused by an increasing neuronal degeneration and neuroinflammation[5]. This progressive neuronal degeneration derives from the toxic effect and accumulation of the two main proteins characterizing this disease: amyloid-β (Aβ) and tau protein.

Aβ pathology occurs early in the course of the disease, and it is reported altered even 15 years before cognitive decline[6]. For this reason, AD is classified as a secondary tauopathy, and several efforts have been placed on it to find effective therapies. In the past few years, several clinical trials have put to test monoclonal antibodies against Aβ (*see section 1.1.4.3*), but tbeir effectivity still remains unclear, and no successful treatment is available to date[7]. Then, after these aforementioned difficulties, special focus has placed on the next modification, tau. The contribution of tau in the progression of this

disease (*see section 1.1.4.4*), has settled AD as an important member of tauopathies. Therefore, the understanding of the primary tauopathies is an undoubtable tool to contribute to the understanding of this disease. During this first section of this Thesis, we will deeper analyze the history, etiology and neuro-pathophysiology underlying AD, to then, progressively introduce its dependence on tau pathology. Finally, focusing on AD, we also will include a review of the most used experimental strategy for studying neurodegenerative diseases: mouse models.

1.1.1 A little bit of history of AD

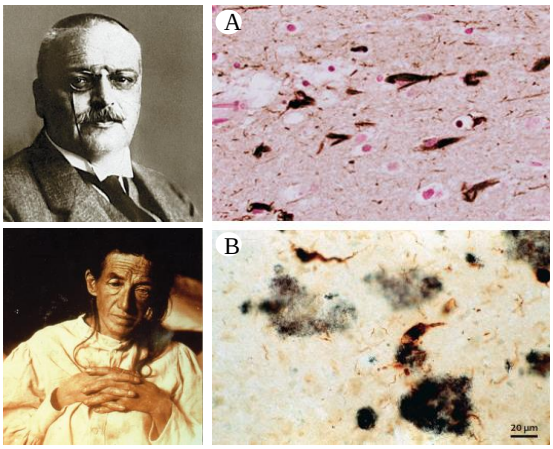

Figure 1. Discovery of the main hallmarks of AD. AD was discovered by Alois Alzheimer (*above*) in a female patient (*bellow*) coursing with memory disturbances and paranoid behaviours. Brain autopsy revealed the two main hallmarks of the disease: (A) tau neurofibrillary tangles (brown) and (B) senile plaques made of Aβ (dark blue) (here shown after immunohistochemistry with anti-tau and anti-Aβ antibodies). Adapted from (3).

Alois Alzheimer (**Figure 1**, *above*) reported the first case of AD in 1906. The patient, August D. (**Figure 1**, *below*) came to the Frankfurt Psychiatric Hospital in 1901 with paranoid symptomatology, sleep disorders, confusion, and disturbances in memory.

In 1906, at the 37th Meeting of South-West German Psychiatrist, Alois Alzheimer reported a ‘‘peculiar severe disease process of the cerebral cortex’’. He described the presence of two characteristic histological alterations in the brain. They would be later known as senile plaques (SP) and neurofibrillary tangles (NFTs)[8]. In

1910, and for the first time, Emil Kraepelin referred to this pathology with the term 'Alzheimer's disease''. It was not until 1984 when a uniform set of criteria was developed to maintain consistency in AD diagnosis.

1.1.2 Etiology: causes and risk factors

Sporadic AD is considered a multifactorial disease, associated with several risk factors. The principal one is age, but environmental factors (air pollution, diet, or infections) or diseases such as diabetes, obesity or hypertension can potentiate AD development. Genetic factors also have been considered as susceptibility factors[9]. In this regard, the most important risk factor for AD, after age, is *APOE* genotype[9,10]. Apolipoprotein E (ApoE) is a glycoprotein essential for lipid transport and injury repair in the brain[11]. Lately, it has been related to contribute to correct myelin production [12]. *APOE* gene codifies for 3 isoforms and the carriage of the ε4 alelle can increase the risk of AD up to 12-15 times compared to those who carry the ε3 allele[13].

Besides the sporadic form, dominantly inherited AD cases have also been described (known as familiar AD, FAD). This genetic variant of the disease presents clinical and pathological similarities with the sporadic AD but has an earlier age of onset (around 45 years). Mutations in the *APP*, presenilin 1 (*PSEN1)* and presenilin 2 (*PSEN2*) genes are the main responsible of familiar AD[14]. Interestingly, no mutations in the *MAPT* gene, the gene that codifies for tau protein, have been associated so far with AD.

1.1.3 Clinical symptoms

Cognitive impairment is the main clinical symptom in AD. The principal cognitive functions affected in AD are those responsible of memory, language, and executive and visuospatial tasks. A progressive loss of spatial cognition, executive function and working memory, which interferes with daily

functioning, finally leads to depression, anxiety, emotional loss of control, hallucinations and aggressive behaviours[15]. Non-amnesic symptoms such as visual difficulties or progressive aphasia are also present in patients suffering from AD[16]. Interestingly, clinical presentations observed during AD progression emerge following the specific distribution of the tau pathology in the brain[17].

1.1.4 Principal hallmarks and the neuropathology associated

AD is characterized by the aggregation and deposition of Aβ extracellular SPs and tau-containing intracellular NFTs (**Figure 2**)[18]. These aggregates, together with neuroinflammation and oxidative stress, lead to a progressive synaptic and neuronal loss[19,20]. At last instance, all these pathological events converge in brain atrophy and the classic cognitive impairment and behavioural changes.

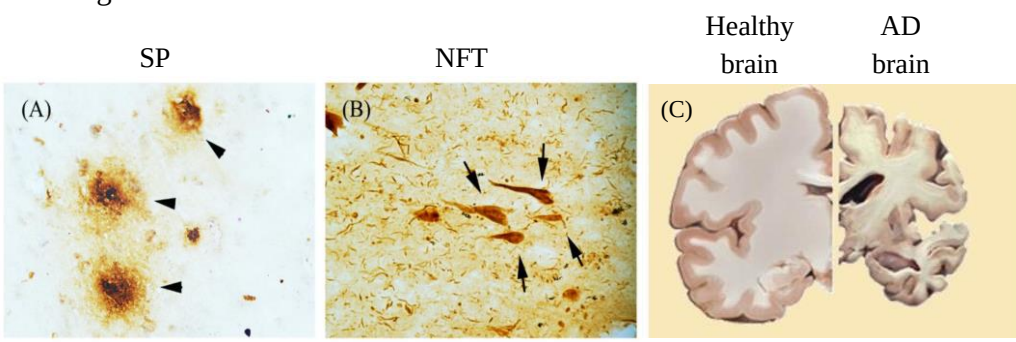

Figure 2. Major pathological hallmarks of AD. Immunohistochemistry microscopic images showing the accumulation of senile (or amyloid) plaques (A; arrowhead) and NFTs (B; arrows) in the hippocampus of AD patients. Consequently, a complex sequence of pathological events occurs and leads to a massive neuronal loss and brain atrophy at later stages of the disease (C). Modified from (21,22).

1.1.4.1 Senile plaques

SPs are extracellular deposits of Aβ protein, which is obtained after a sequential cleavage of the amyloid precursor protein (APP)[23]. The APP

protein is a type I transmembrane protein that can be cleaved by the non-amyloidogenic and the amyloidogenic pathways. In the first one, APP is cleaved by the A disintegrin and metalloprotease (ADAM) family of proteases, generating the released soluble APP alpha (sAPPα) peptide (**Figure 3A**, *left*).

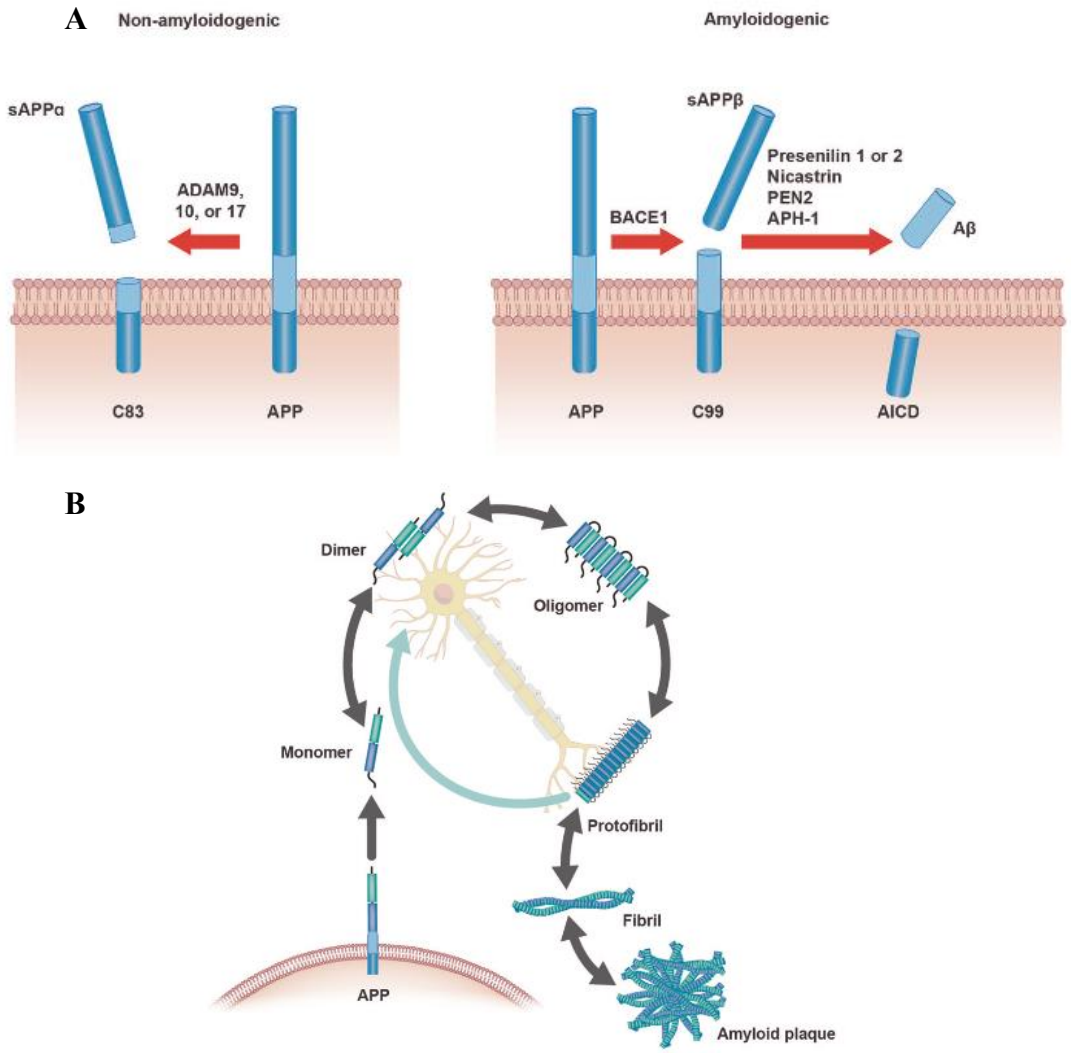

(legend in next page)

Figure 3. An imbalance between amyloidogenic and non-amyloidogenic pathways leads to the aberrant production of Aβ and its further aggregation. (A) In the non-amyloidogenic pathway (left), APP is cleaved by ADAM proteases generating the sAPPα peptide. In the amyloidogenic pathway (right), APP is first cleaved by β-secretases (β-APP-cleaving enzyme-1 or BACE1) generating the CTF-β fragment, which is subsequently cleaved by γ-secretases (PSEN1, PSEN2 proteins, Nicastrin, PEN2 or APH-1), producing the pro-aggregative peptide, Aβ. (B) This proteolytic processing releases amyloid-β into the extracellular space, where it progressively accumulates forming dimers, oligomers, protofibrils, fibrils and, finally amyloid plaques. Adapted from (26).

This peptide is involved in neuroprotection, synaptic plasticity, neurogenesis, and memory formation[24,25]. In the amyloidogenic pathway, APP is cleaved by different proteases with β-secretases and γ-secretases activity (resumed in **Figure 3A**, *right*). Then, they generate the Aβ peptide.

Aβ is also produced under physiological conditions, and seems to have relevant synaptic function[27]. However, an increased amyloidogenic cleavage, together with an impaired degradation of the resultant peptides, leads to Aβ accumulation. Thus, it progressively oligomerizes and aggregates into fibrillar forms. The accumulation of SPs contributes to synaptic impairment, neuroinflammation and at last instance, to neuronal death[20,28]. Dense accumulations of SPs are especially observed in the hippocampus, amygdala, and cerebral cortex in AD patients[29,30].

1.1.4.2 Neurofibrillary tangles

Hyperphosphorylation of tau protein, among other post-translational modifications (PTMs), leads to the progressive aggregation of the protein, first forming pre-tangles, then paired helical filaments (PHFs), and finally accumulating as NFTs [31]. NFTs are primarily intracellular, but at later stages, after the neuron dies, they can also be found extracellularly (**Figure 4**). These deposits are called ‘‘ghost tangles’’ and are also common in other tauopathies[32,33].

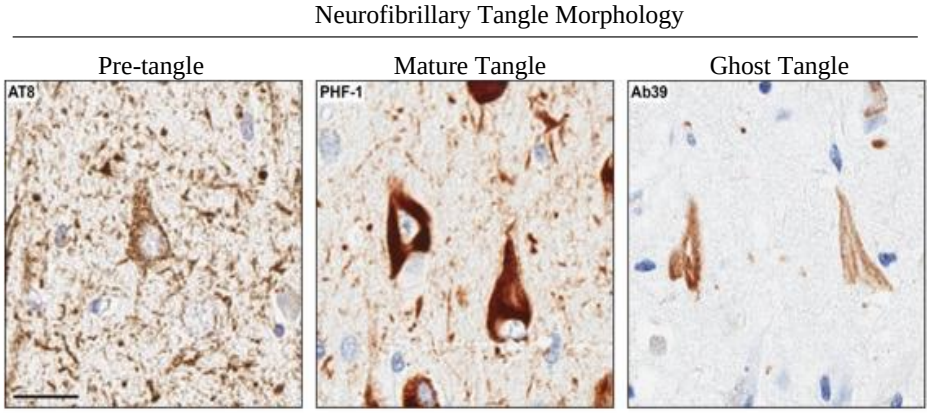

Figure 4. Neurofibrillary tangle maturation process in AD hippocampus. Pre-tangles have perinuclear accumulation of tau and progressively become mature tangles (NFTs) occupying all the neuron cytoplasm. Finally, remnants of mature tangles accumulate. AT8, PHF-1 and Ab39 antibodies were used to stain tau. Scale bar = 25 μm. Adapted from (31).

NFTs are mostly found in the soma of neurons, but can also be detected among axons and dendrites, contributing to the impairment of synaptic function. Interestingly, the presence of aggregated tau in the synaptic compartment allows its release to the extracellular space by synaptic activity. Then, it can be incorporated by postsynaptic neurons and glia[34,35]. Through this mechanism, tau can spread between neurons, promoting the progression of the disease[36].

1.1.4.3 Role of Aβ in AD: redefining the amyloid hypothesis

Aβ was firstly described to be accumulated during pathology in 1984. Then, it was identified in the meningovascular polymorphic deposits of patients with Down's Syndrome. Several years later, it would be also reported as the constituent of the SPs of AD[23,37]. Since then, it has been deeply related to the progression of the disease, especially when accumulated in oligomeric, poorly aggregated forms.

Accumulation of Aβ has been specially related to synaptic dysfunction by mediating acetylcholine (ACh) deficiency and glutamate excitotoxicity[38–40]. In fact, Aβ species have reported to promote the dysregulation of N-methyl-D-aspartate (NMDA) and, to a lesser extent (α-amino-3-hydroxy-5-methyl-4-isoxazolepropionic acid)-ionotropic (AMPA) glutamate receptors[41,42] (**Figure 5**). By these mechanisms it seems to be responsible of hippocampal synaptic failure in certain mouse models of the disease[43].

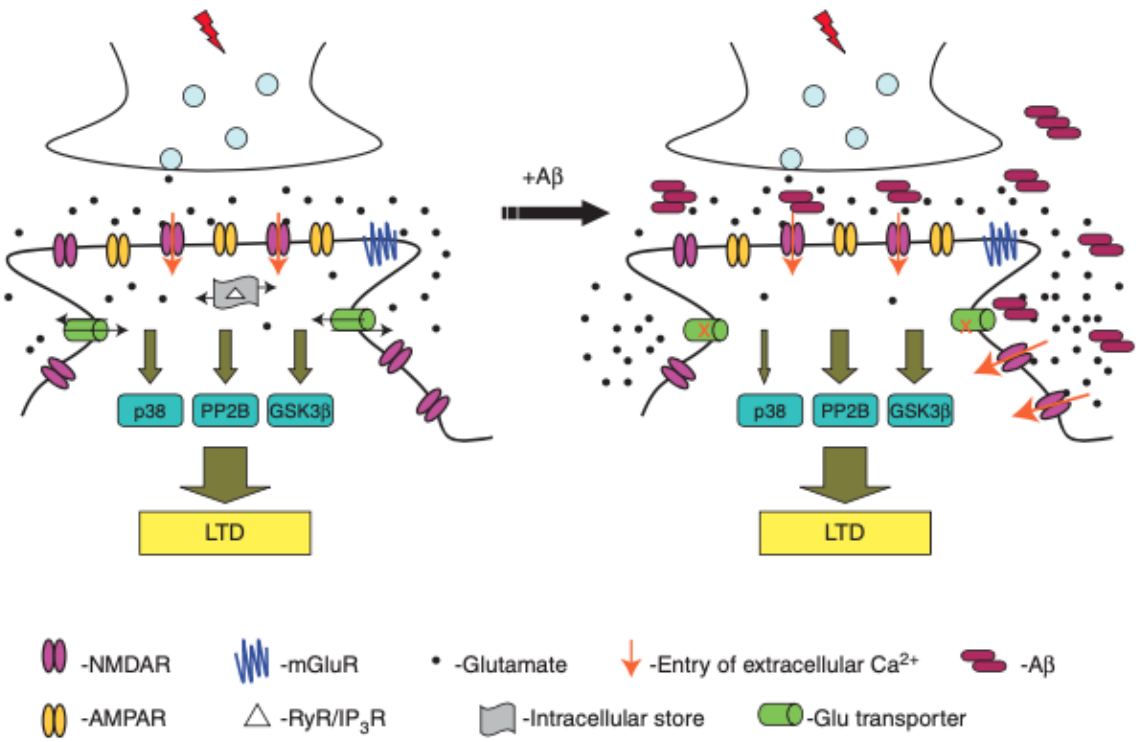

Figure 5. Aβ contributes to synaptic impairment. (*left*) Correct LTD requires accurate control of extracellular and intracellular flux of calcium. Its NMDA-mediated release leads to the activation of PP2B, GSK-3β, or p38 MAPK signaling pathways. (*right*) LTD is impaired in presence of oligomeric Aβ, which contributes to NMDA excitotoxicity and aberrant hyperactivation of the downstream pathways (*see legend*). From (44).

The discovery of APP and PSEN mutations causing FAD has permitted the development of mouse models coursing with Aβ pathology and reflecting AD alterations. Then, this has led for more than 25 years to believe that Aβ is the trigger of AD. During this time, several promising results have been made regarding Aβ and its utility as an early marker of the disease. Cortical Aβ deposition is reported around 15 years before dementia onset[45], offering a big gap for detention of the pathology during the prodromal stage. In this line, both Aβ-PET scans and blood-based assays have reported to closely approximate to neuropathology[46], and to provide an early detection of the pathology. However, when Aβ is targeted for therapy, clinical trials have reported undesired results. Various attempts have been made to develop agents that interferes with Aβ production. Among them, we can remark inhibitors for β- or γ secretases, developed to reduce the generation of Aβ peptides[47,48]. Other strategies have followed immunotherapeutic approaches attempting to remove the burden of Aβ from the brain. Several Aβ-specific antibodies have been designed to this end, but they have failed in phase II or III clinical trials. Some examples are Crenezumab[49], Solanezumab[50], Bapineuzumab[51], or Gantenerumab[52] or the newest one Aducanumab [53], whose efficiency is still under debate.

These unpromising results, together with the presence of Aβ deposits in aged people[54] without developing AD, or the absence of neuronal loss in animal models[55] have put in doubt that Aβ may be directly causing AD pathology and neuronal death. Conversely, progression of tau pathology better correlates with clinical dysfunction in AD patients[56]. Also, increasing evidence has pointed tau (and especially intermediate aggregated forms of tau) to be highly toxic for neurons and to be the main responsible of neurodegeneration. In this line, inverse correlations have been found between NFTs and the number of surviving neurons[57], while aberrant phosphorylation and fibrillation of tau

have been related to defects in mitochondrial integrity, DNA damage, alterations in proteostasis and synaptic failure[58]. Therefore, a more accurate vision of the amyloid hypothesis has been getting into consideration. According to this new vision, the deposition of Aβ within the brain has been proposed as a mechanism for directing tau spread and enhancing its pathology (**Figure 6**).

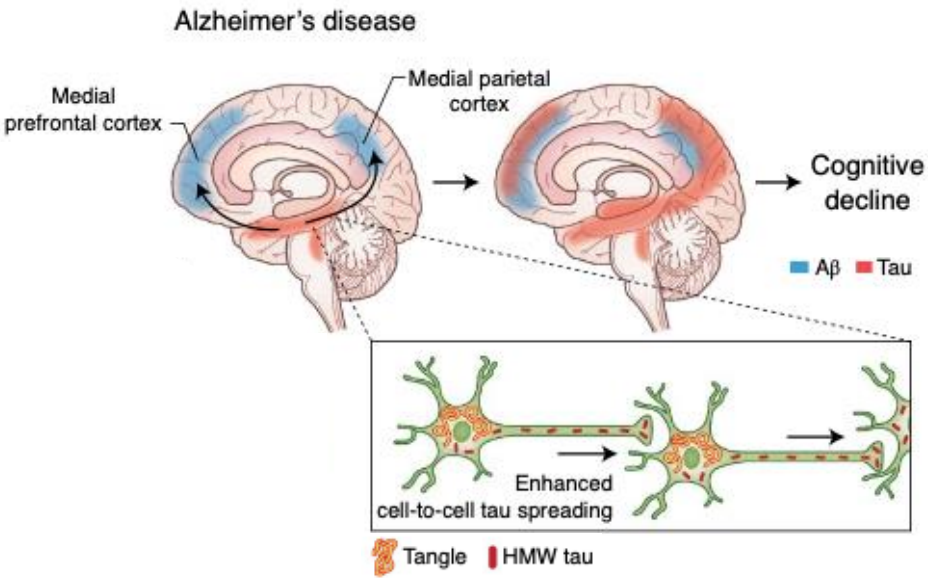

Figure 6. Prion-like propagation of AD pathology. The presence of senile plaques (blue) correlates with neuronal tau propagation from the parahippocampal gyrus into neocortical, coinciding with cognitive alterations. In neurons, Aβ aggregates have been considered to accelerate tau spreading within synapses in a prion-like manner. Adapted from (59).

Indeed, it has been considered that AD presents prion-like mechanisms used to spread tau aggregates across the brain[60,61]. This way, Aβ stimulates tau spread, and tau itself converts normal tau into pathological one in those non-affected areas. This way, both proteins contribute to propagate the pathology between cells and brain areas[62].

Altogether, despite Aβ has been classically considered a central element in AD progression, new insights have proposed tau as the main responsible of

the neuropathological changes. Consequently, the Amyloid hypothesis has been redefined proposing a synergy between the two proteins. Then, both proteins would be acting together to promote, for example, synaptic impairment[63] (**Figure 7**). Under these conditions, Aβ would be leading tau aberrant modifications and this last one, executing them.

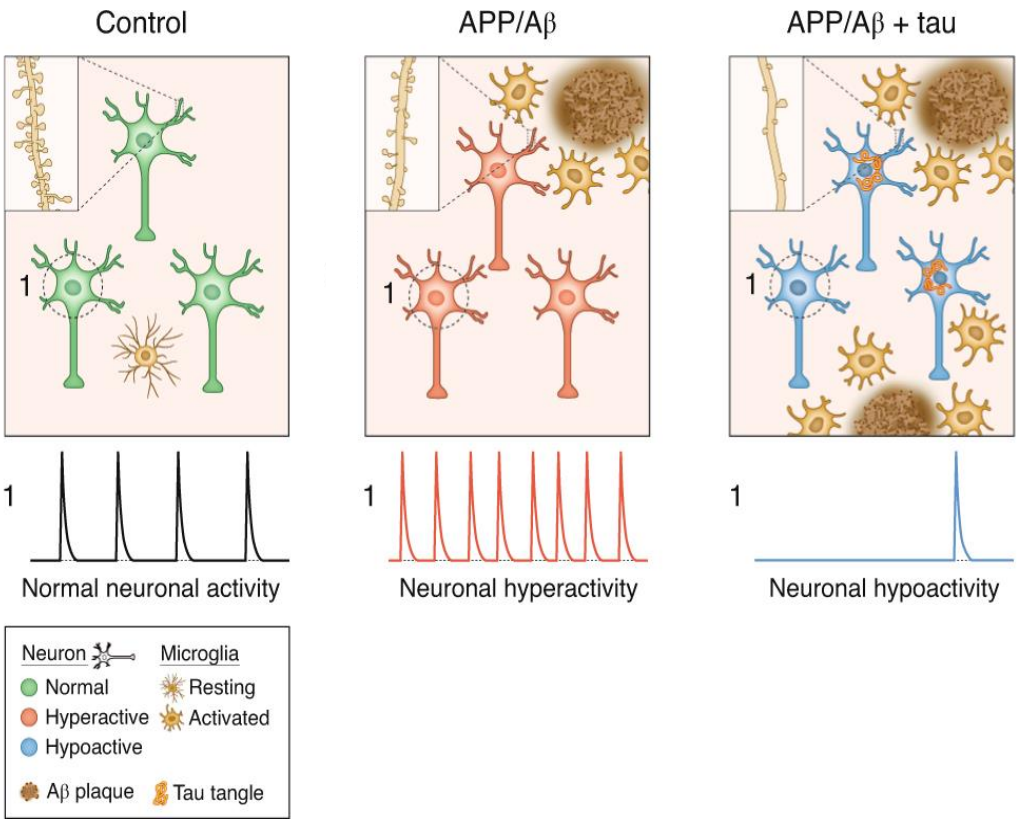

Figure 7. Synergic effect of Aβ and tau in synaptic malfunction. Aβ accumulation (middle panel) courses with hyperactive neurons, microglial activation and spine loss while combined presence of Aβ and tau pathology (right panel) is associated with suppressed neuronal activity, as well as with enhanced microglial activation and spine loss. Adapted from (59).

1.1.4.4 AD associated neuropathology: emerging role of tau

Thus, given these considerations, in the following paragraphs, we will describe the cellular alterations present in AD focusing on the paper of the more direct trigger, tau.

1.1.4.4.1 The loop between tau and dysfunctional proteostasis

The main feature of AD is the accumulation and aggregation of proteins due to defects in folding and clearance of damaged proteins. The principal strategy for protein degradation in cells is the ubiquitin proteasome system (UPS), and its dysfunction results in the accumulation of ubiquitin-immunopositive NFTs in case of AD[64,65]. Dysfunction of the UPS and its subunits can be associated to the accumulation pathological tau. More specifically, it impairs the 26S proteasome subunit and provokes cognitive dysfunction[66]. Because of that, impaired proteostasis has been considered as an early event in AD progression and to be highly related to synaptic failure[67].

1.1.4.4.2 Tau role in synaptic impairment

Synaptic and dendritic spine loss are strongly correlated with cognition impairment in patients of AD and constitute one of the early events reported in the disease[68,69]. There, the important physiological role of tau in synaptic maintenance (*see section 1.3.5.3)* and its excessive accumulation in dendrites under pathological conditions place tau as a main orchestrator of synaptic impairment (**Figure 8)**.

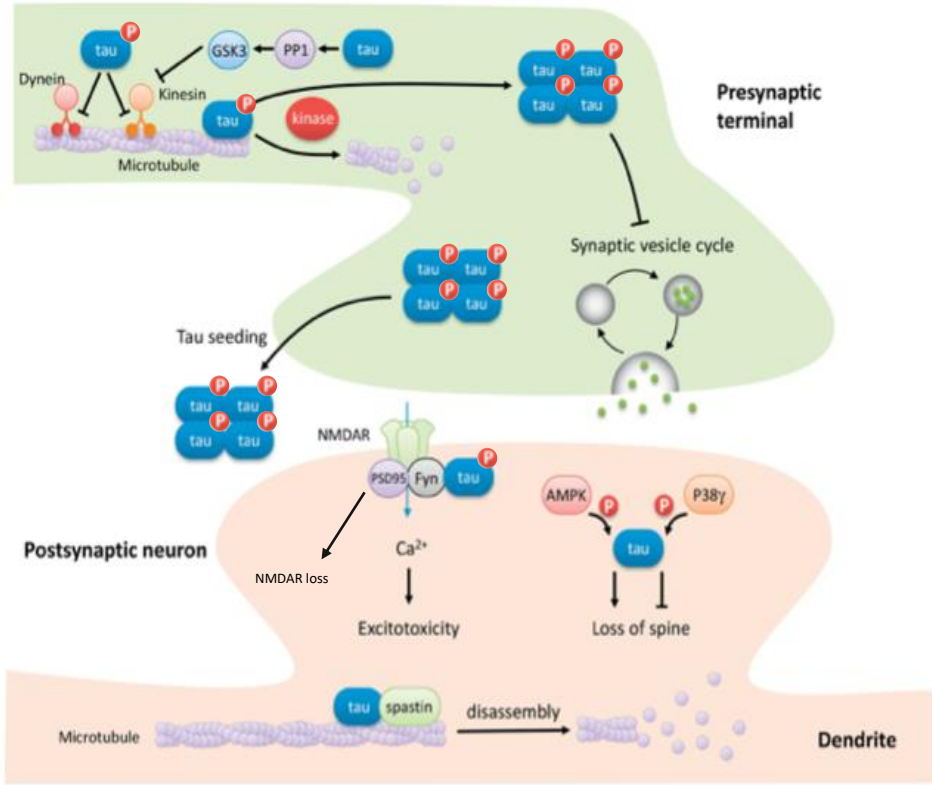

Figure 8. Synaptic dysfunction in presence of pathological tau. Impaired exocytosis and endocytosis and vesicular transport have been described to be altered in the pre-synaptic terminal in presence of pathological tau. Also, in the post-synaptic terminal, aberrant tau causes NMDAR dysfunction and loss, spine loss and excitotoxicity. Adapted from (70).

More specifically, tau loss-of-function results in a reduced release of presynaptic vesicles in the pre-synaptic compartment and an impaired maturation of dendritic spines at the postsynaptic terminals. For correct dendritic spine formation and maturation, controlled cytoskeletal destabilization is required. Tau controls microtubules (MTs) disassembly, so it becomes essential for this process. Particularly, this dynamism is ensured by a controlled caspase-mediated cleavage and degradation of tau protein[71]. Then, excessive activity of caspase-6 or caspase-3 results in an aberrant fragmentation of tau that finally is translated to synaptic structures degeneration[72]. Also, as tau and the kinase that phosphorylates it (the serine/threonine protein kinase GSK-3β) are required for AMPA and NMDA

receptors endocytosis[73], their impaired function leads to alterations in long-term potentiation (LTP) and long-term depression (LTD).

In this line, the generation of a tau *knock-out* (KO) or the *knock-down* of tau by short-hairpins (shRNAs) *in vitro*, which simulate tau misfunction, provokes the abolition of LTD[74]. Similarly, an excessive phosphorylation of tau, mediated by the serine/threonine protein kinase GSK-3β, causes tau translocation to the synapsis and its misfunction and induces aberrant LTD[75]

For controlling all these processes, neurons present high concentration of components involved in apoptotic cell death process in their synaptic terminals. As we will discuss later (*see section 3.2.4*), under physiological conditions, the apoptotic machinery can be accurately activated, without inducing cell death[76]. By this mechanism, apoptotic modulators can mediate clearance of harmed synapses or control LTD and neuritic processes[77,78]. Aberrant increase in oxidative stress or reduced energy availability can pathologically stimulate this cascade within synapses. Then, it results in an excessive elimination of synapses, dendrites or even axons[79,80].

1.1.4.4.3 Tau participation in neuroinflammatory response

AD pathogenesis is not restricted to the neuronal compartment and strongly interacts with immunological mechanisms in the brain. In fact, activated astrocytes and reactive microglia are commonly found around SP and present signs of functional impairment (**Figure 9**)[81]

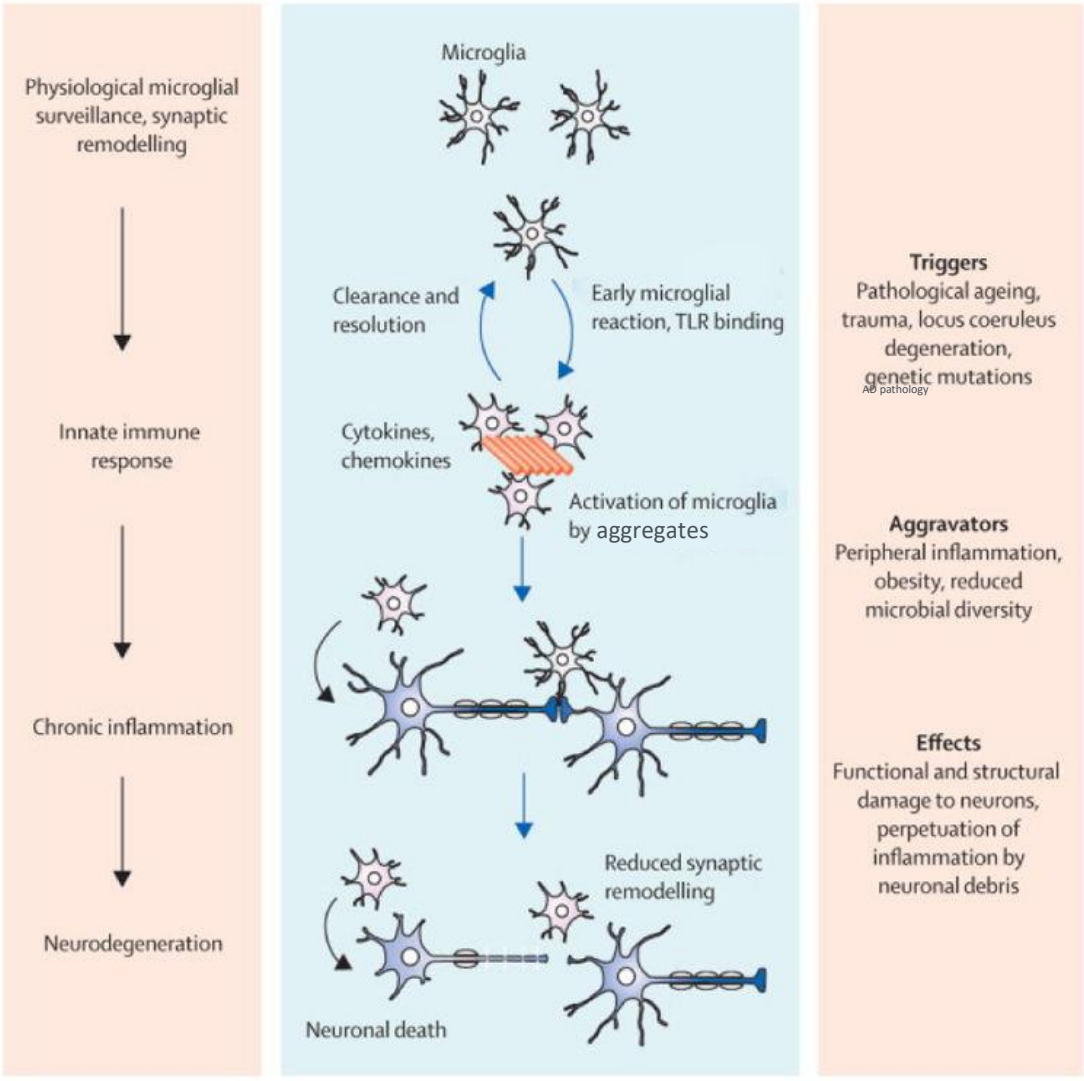

(legend in next page)

Figure 9. Sequence of pathological micro and astroglia activation in AD. (*upper panel*) Physiologically, glial cells contribute to synaptic clearance and remodelling. However, presence of Aβ aggregates impairs their functions and results in an acute inflammatory response. This response is thought to aid the clearance of the aggregates and to restore tissue homeostasis. However, during the neurotoxic context of AD, it turns into a chronic neuroinflammation, which finally ends in neuronal degeneration. (*lower panel*) CD11b-positive microglia (A, blue) and GFAP-positive astrocytes (C, blue) within an Aβ deposit (brown) in the parietal cortex of a human AD brain. Activated, Iba1-positive microglia (B, green) and GFAP-positive astrocytes (D, green) at Aβ plaque site (red) in APP/PS1 mouse. *Scale bar=25 or 50 μm*, as indicated. Adapted from (81).

Despite glial activation is usually more related to Aβ, tau has also been reported to activate microglia and astrocytes[82,83] in AD and other tauopathies[84–86]. Specifically, as pathological tau species can be secreted extracellularly, they can promote this aberrant activation and stimulate the release of cytokines such as IL-1β or TNF-α in AD[86]. These pro-inflammatory molecules can modulate tau kinases, enhancing tau pathology and self-perpetuating the disease (**Figure 10**).

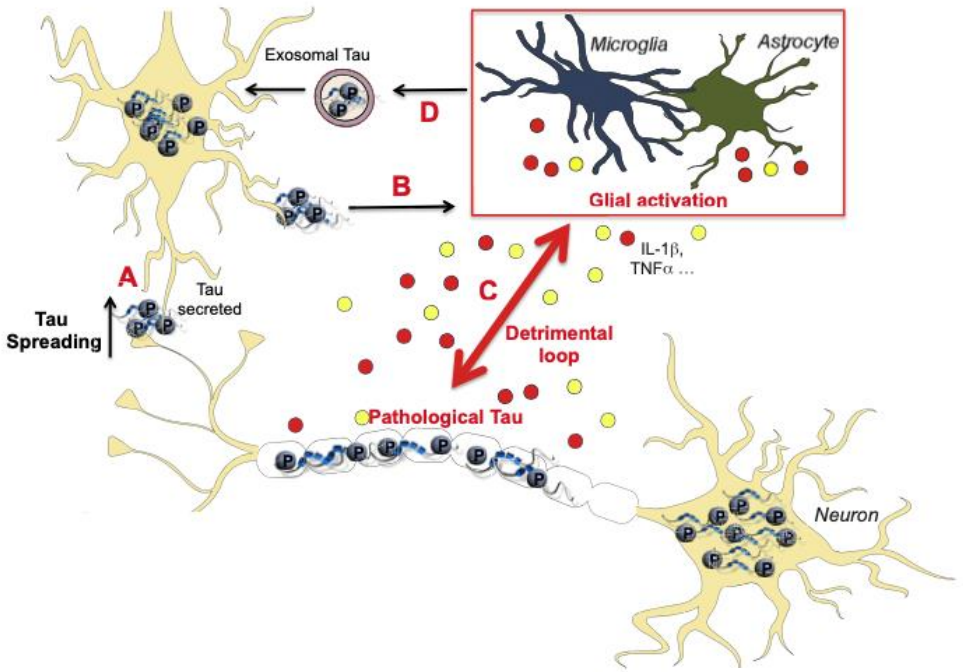

(legend in next page)

Figure 10. Immune response to tau pathology. Hyperphosphorylated pathological tau species are secreted extracellularly (A) and promote microglia and astrocyte activation (B). Then, they release IL-1β and TNF-α and contribute to the enhancement of the disease by promoting the activation of kinases, which aberrantly phosphorylate tau (C). Finally, microglia can phagocyte extracellular tau and release it through exosomes (D), contributing to the propagation of the disease. Adapted from (86).

1.1.5 Alzheimer's Disease mouse models

Mouse models constitute one of the most important tools to study the pathophysiology of neurodegenerative diseases and the development of new therapeutic strategies. The discovery of a genetic cause for both primary and secondary tauopathies has helped developing animal models that reproduce at least some of the events observed in these diseases. During this part, we will review the different models available for the AD study.

Importantly, in AD, only mutations related to Aβ pathology have been described. However, as AD pathology usually overlaps with primary tauopathies with a genetic inheritance[87], transgenic animals developing tau pathology, the *MAPT* mouse models, have been used for AD research together with the *APP* mouse models. They are based on missense mutations in the *MAPT* gene associated to a group of primary tauopathies named as Frontotemporal dementia and parkinsonism linked to chromosome 17 (FTDP-17). Also, in order to better board AD complexity, double transgenic animals have been also generated by combining APP and MAPT mouse models. Finally, with the intention to explore the sporadic origin of this disease, transgenic mouse models of risk factors for AD, such as ApoE, have been developed. Two examples are the APOE4 model[88], which replaces the mouse APOE4 allele for the human one, or the E4FAD model[89], generated after combination of the APOE4 model with the 5xFAD model.

1.1.5.1 *APP* mouse models

Mutations responsible of FAD are described in the *APP*, *PSEN1* and *PSEN2* genes. These mutations generally increase the production of Aβ, and displace $A\beta_{42}/A\beta_{40}$ ratio, with a higher production of $A\beta_{42}$. Consequently, they reproduce the affection in cell functions such as protein trafficking, cell adhesion or calcium homeostasis, and finally, aberrant apoptotic death[90]. The first generation of transgenic mice developed included human *APP* overexpression with or without FAD mutations. This expression is usually controlled by promoters such as Thy1 or prion protein PrP. The most used mutations are the Swedish (K670N/M671L), Dutch (E693Q) and London (V717I), which served to generate mouse models such as the APP23 or APPsl. Specifically, these models overexpress the human *APP* gene with the Swedish mutation and the Swedish and London mutations, respectively. Later, a second generation of mouse models such as the APPxPS1 or 5xFAD were generated by combining the overexpression of muted *APP* gene with the overexpression and mutation of the *PSEN1* genes. This way, an increased severity of Aβ pathology was achieved. Finally, a third generation of mouse models was developed by using *knock-in* of the *APP* gene. In these mice, murine *App* gene was modified in order to carry a humanized Aβ sequence, which ensured a proportion of the peptide equivalent to humans. As before, this strategy was also combined with the overexpression of muted *PSEN1* genes. A brief review of these models can be found in the following **Table 1** and further reviewed in ([55]).

Table 1. **Classical APP mouse models of AD**.

Model	Promoter	Mutation(s)	General features
APP23	Thy1	$APP^{KM670/671NL}$	Aβ (~6mo) Synaptic deficits (~3mo) Gliosis (~6mo) Neuronal loss (~12-15mo) Cognitive impairment (~3mo)
APPsl	Thy1	$APP^{KM670/671NL;V717I}$	Aβ (~14mo)
J20	PDGF-β	$APP^{KM670/671NL;V717F}$	Aβ (~8mo) Synaptic deficits (~3-6mo) Gliosis (~6mo) Neuronal loss (~3mo) Cognitive impairment (~4mo)
5xFAD	Thy1	$APP^{KM670/671NL;I716V;V717I}$ $PSEN1^{M146L;L286V}$	Aβ (~2mo) Synaptic deficits (~3-6mo) Gliosis (~3mo) Neuronal loss (~6mo) Cognitive impairment (~4mo)
APP/PS1	PrP	$APP^{KM670/671NL}$ $PSEN^{M146L}$	Aβ (~2mo) pTau (~2mo) Synaptic deficits (~3-6mo) Gliosis (~3mo) Neuronal loss (~6mo) Cognitive impairment (~7mo)

1.1.5.2 *MAPT* mouse models

As we have mentioned above, the discovery of FTD-linked mutations has facilitated the development of mouse models representing the tau pathology observed in primary tauopathies, but also in AD as secondary tauopathy. Methodologically speaking, these mice are FTDP-17 models. However, the crescent input overlapping this group of diseases with other tauopathies has extended their use to the rest of tauopathies (*see section 1.2)*. *MAPT* mouse models differ depending on the genetic enginery method used and the

isoforms, brain area or level of tau overexpression. Again, promoters such as PrP or Thy1 are frequently used to regulate tau expression. The first *MAPT* model established was the JNPL3 model[91], which overexpresses the human Tau containing the P301L mutation. Other models are the Tau^{P301S}, which was generated following the same strategy (*see the following section for more information*), or the model Tau^{VLM}, which incorporates three mutations (G272V, P301L and R406W). Generally, in these models, disease courses with enhanced tau pathology (aberrant modifications of tau and increased aggregation) and the associated neurotoxic effects, but also frequently presents motor deficits (mainly consequence of striatal affection, as happens in human diseases). A summary of these transgenic mouse models is represented in **Table 2**.

Table 2. MAPT mouse models

Model	Promoter	Mutation(s)	General features
PS19	PrP	Tau^{P301S}	NFTs (~6mo) Synaptic deficits (~3mo) Gliosis (~3-6mo) Neuronal loss (~8mo) Cognitive impairment (~6mo)
VLW	Thy1	$Tau^{G272V;P301L;R406W}$	No NFTs pTau (~8mo) Synaptic deficits (~8mo) Gliosis (~3-6mo) Neuronal loss (~8mo) Cognitive impairment (~8mo)
JNPL3	PrP	Tau^{P301L}	NFTs (~5mo) Synaptic deficits (~6mo) Gliosis (~10mo) Neuronal loss (~10mo) Cognitive impairment (~10mo)

1.1.5.2.1 Tau^{P301S} mouse model (PS19 line)

In this Thesis, we also have appealed to mouse models, and used a mouse model presenting the P301S mutation for our research trying to elucidate a small part of the pathological mechanisms underlying AD and other tauopathies. Two *MAPT* mouse models incorporate this mutation, the hTau^{P301S}, controlled by the Thy1.2 and the PS19 mice (from now also referred as Tau^{P301S}).

In our work, we have used this last one, which was generated by Yoshiyama et al.,[92] in 2007. It expresses the human 1N4R isoform of Tau with the mentioned P301S mutation (*see section 1.3.8*) under the PrP promoter. Tau^{P301S} affections are preferentially located in the hippocampus but become widespread to the neocortex, brainstem, spinal cord, and amygdala at later ages. Originally, it was first characterized by presenting an early synaptic loss and microglia reactivity (by 3 months-of-age). These alterations were found prior to NTFs formation, which was reported by 6 months. By this age, animals also presented astrogliosis as well. Neuronal loss was firstly reported in the hippocampus by 8 months-of-age, coinciding with cognitive deficits. This mouse model reported impaired spatial learning and memory ability in the Morris water maze[93] as well as compromised contextual fear conditioning memory[94]. Additionally, they were reported to course with motor deficits (clasping and limb retraction), which rapidly progressed to limb weakness and paralysis. About an 80% of PS19 mice died by 12 months (**Figure 10**).

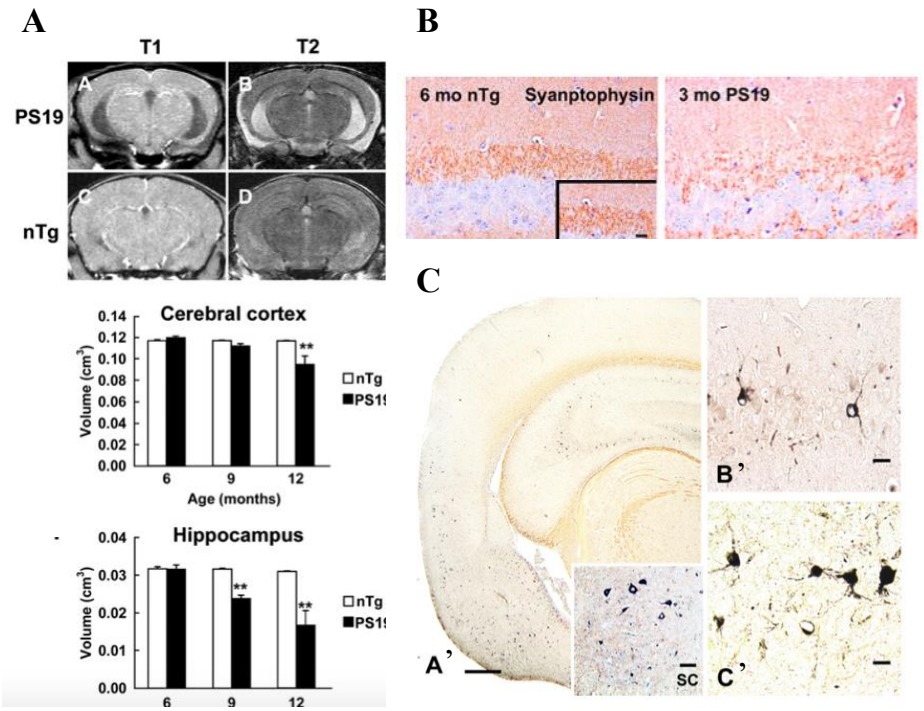

Figure 10. Pathological hallmarks reported in the original PS19 mice by Yoshiyama and colleagues. (A) PS19 mice showed an increased brain atrophy, starting at 9-months-old (mo) in the hippocampus and progressing to the cerebral cortex by 12mo. (B) Synaptic loss (measured by synaptophysin immunohistochemical staining) is observed in the CA3 region of the hippocampus in PS19 mice by 3mo compared to the 6mo non-transgenic (nTg) mice. (C) Gallyas silver impregnation of brain slices (A') from PS19 mice showed widespread formation of NFTs in the hippocampus (B') and amygdala (C') by 6mo. Adapted from (92).

Recent publications using this model have reported an attenuated development of tau pathology, where hyperphosphorylated tau inclusions, gliosis and cognitive impairment are initially observed in 9 months-old animals[95–97] and a significant neuronal death is only present after 12 months-of-age[98] (**Figure 11**).

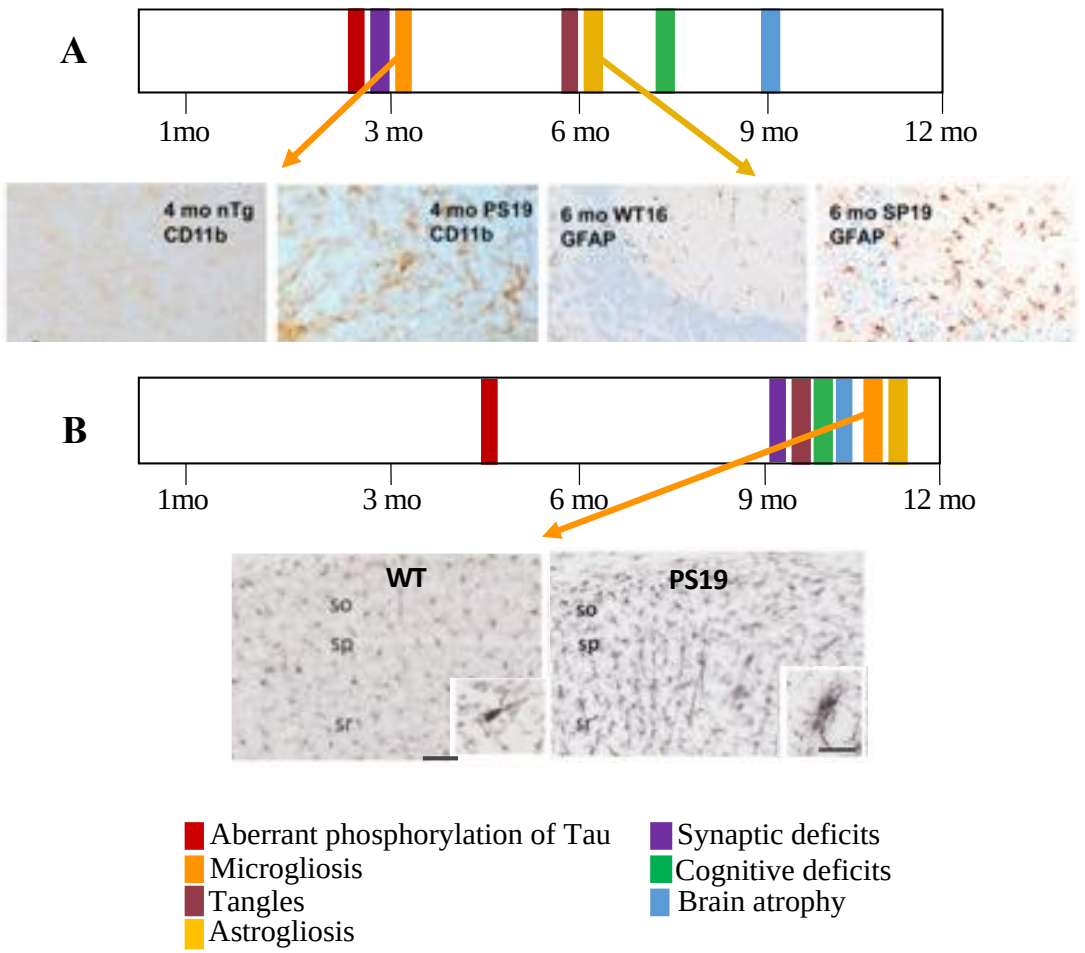

Figure 11. The onset of pathological modifications in the PS19 mice has been reported delayed during the last decade. (A) Time course of PS19 mice pathology as described by Yoshiyama et al. They observed microglia (*right*) and astrocyte (*left*) reactivity by 4 and 6-months-old (mo), respectively. (B) Recent studies have observed a delayed onset of the disease, often appearing within 9 and 12mo. Representative images of microglia activation are provided at the bottom of the panel. Adapted from (92,95).

1.1.5.3 Double-transgenic mice models

Lately, to compile both Aβ and tau pathology, double transgenic mice were developed (**Table 3**). Those mice generally develop both pathologies with a more severe tau pathology, further suggesting the idea that Aβ promotes tau alterations (*as reviewed in section 1.1.4.3*). The first double transgenic mouse

model was called TAPP mice[190]. Other example is the 3xTg mice, which overexpresses *APP*, *PSEN* and *MAPT* genes (with the Swedish, M146V and P301L mutations, respectively).

Table 3. List of double-transgenic mouse models for AD research

Model	Promoter	Mutation(s)	General features
Double transgenic mouse models			
TAPP	PrP	$APP^{KM670/671NL}$ Tau^{P301L}	Aβ (~9mo) NFTs (~6mo) Synaptic deficits (~6mo) Gliosis (~3mo) Neuronal loss (~8mo) Cognitive impairment (~3-6mo)
3xtg	Thy1.2	$APP^{KM670/671NL}$ $PSEN1^{M146V}$ Tau^{P301L}	Aβ (~6mo) NFTs (~12mo) Synaptic deficits (~6mo) Gliosis (~7mo) Neuronal loss (~8mo) Cognitive impairment (~3-6mo)

1.2 Primary tauopathies

Primary tauopathies account for an approximately 3% of all cases of dementia and have become the second or third most prevalent type of dementia in early-onset patients (below 65 years of age)[99]. Caused by the deposition of the tau protein, a better understanding of them has become essential to board tau contribution to AD. As mentioned, the finding of a genetic cause as responsible of some of them, has helped untangling the bases of tau pathology not only for AD but also for the other sporadic primary tauopathies. We have already commented how this discovery has helped to develop experimental tools such as animal models. Now, we will perform an analysis of this primary tauopathies, to understand this comparative analysis and their relationship. For that, we will start with a with a brief resume of the primary tauopathies with a

sporadic cause, named 3R, 4R and 3R/4R tauopathies and continue relating them and AD with those with a genetic cause.

1.2.1 Sporadic primary tauopathies

Classification of primary sporadic tauopathies has been complex because its pathophysiology and clinical features usually overlap between them. Thus, they are usually classified depending on the nature of tau protein present in aggregates (3R and/or 4R tau isoforms, *see section 1.3.2 for details*). Then, they are separated in 3R, 4R and 3R/4R tauopathies (equal ratio of both isoforms). A classification of the main primary tauopathies and their principal neuropathological features (**Figure 12**) are further explained next and recompiled at the end of this section in **Table 4**.

Figure 12. Characteristic neuropathological features of sporadic primary tauopathies. Different primary tauopathies are organized in columns and their corresponding molecular classification (3R, 4R and 3R/4R tau) is specified at the bottom. Micrographs show hippocampal sections immunostained with different antibodies, Bielschowsky or Gallyas Silver (as indicated) to mark the different aggregates appearing in each pathology: (a-d) Pick bodies, (e-g) astrocytic plaques, (h) balloon neuron, (i,j) tufted astrocyte, (k) coiled bodies (**l)** globose tangle formation, (m) lobular astrocytic inclusions (n), oligodendrocyte forming coiled bodies, (o-r) and globular oligodendroglial inclusions, (s, t) Granular fuzzy astrocytes, (u-x) AD like NFTs. PiD, Pick's disease; CBD, cCorticobasal degeneration, PSP, Progressive supranuclear palsy; GGT, Globular glial tauopathy; AGS, Argyrophilic grain disease; PART, Primary age-related tauopathy. Adapted from (100).

(figure in next page)

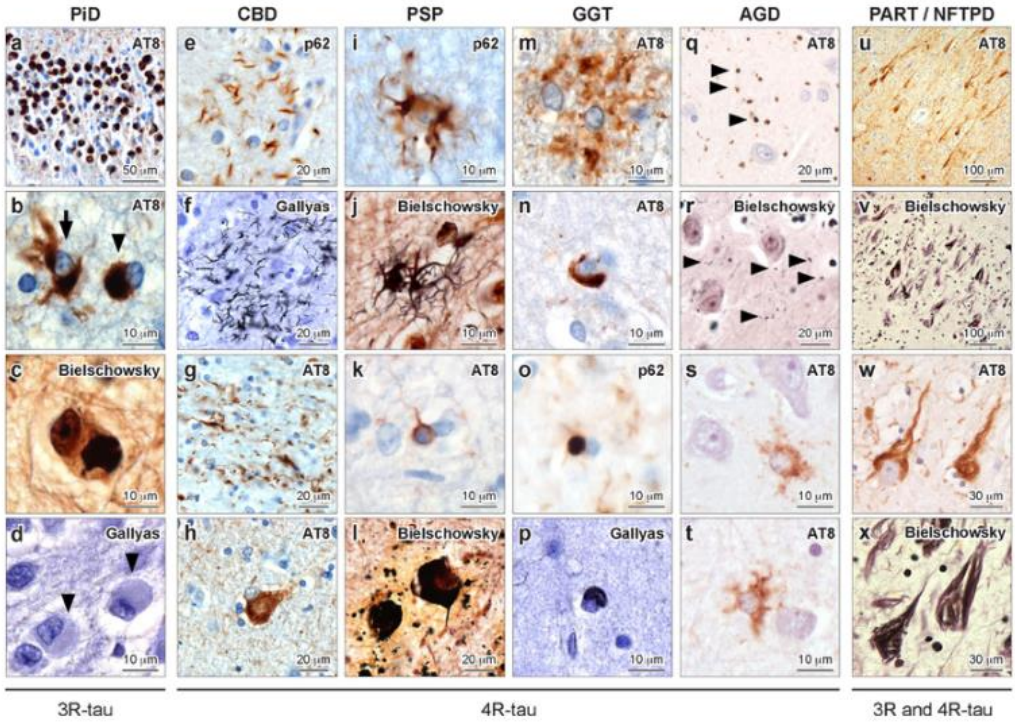

1.2.1.1 3R Tauopathies: Pick's disease

PiD is considered the unique tauopathy presenting a higher ratio of 3R tau isoform in its aggregates. They are spherical, non-argyrophilic and are called Pick bodies. They predominantly accumulate in granular cells of the dentate gyrus (DG), which progressively degenerate, acquiring a ballooned shape (Pick cells)[101].

1.2.1.2 4R Tauopathies

4R tauopathies are characterized by abnormal accumulation of 4R tau, and include Progressive supranuclear palsy (PSP), CBD, Argyrophilic grain disease (AGS) or the Globular glial tauopathy (GGT).

PSP presents these aggregates within neurons, oligodendrocytes and astrocytes[102,103]. These tau accumulatios are globose and predominantly

accumulate in subcortical structures, with special affection of the substantia nigra[104]. CBD courses with poorly aggregated tau deposits named ‘‘pre-tangles’’[3] in both neurons and glia, which also acquire ballooned shapes. *AGS* usually accompanies other 4R tauopathies and modifies their outcome and phenotype[105,106]. Lesions, known as argyrophilic grains (AGs) are mostly pre-tangled, and are present in neurons, oligodendrocytes, and astrocytes (named as granular/fuzzy astrocytes)[104,107]. GGT is characterized by the presence of non-argyrophilic and globular astrocytic inclusions, usually deposited in proximal processes (tufted astrocytes). Also, it presents argyrophilic globular inclusions in oligodendroglia (coiled bodies) [108].

1.2.1.3 3R/4R Tauopathies: chronic traumatic encephalopathy and primary age-related tauopathy

As mentioned, this group of primary tauopathies presents aggregates positive for both tau isoforms and include Chronic traumatic encephalopathy (CTE*)* or Primary age-related tauopathy (PART). *CTE* was firstly reported in boxers[109] and it is, to date, the only primary tauopathy, presenting an etiological environmental component (repetitive contusive head injuries). CTE and PART au inclusions are similar to the NFTs in AD and can be present both in neurons and glia in CTE, and only in neurons in PART. As for AD, they also can accumulate extracellularly (ghost tangles) at late stages of the disease[110,111].

Table 4: List of main primary tauopathies. Primary tauopathies can be divided into 3R and 4R disorders and course with heterogeneous neuropathology and symptomatology. Main information regarding primary tauopathies is reviewed in Dugger et al., 2017 and Kovacs et al., 2015[4,112].

Tauopathy	Tau isoform	Pathological hallmark	Cellular and anatomical vulnerability	Clinical features
Pick's disease *(PiD)*	3R	Pick bodies Pick cells	Neurons Frontal and temporal lobes	Frontotemporal dementia Progressive aphasia
Progressive supranuclear palsy *(PSP)*	4R	Globose NFTs Tufted astrocytes Oligodendroglia coiled bodies Neuropil threads	Neurons Oligodendrocytes Astrocytes Dentate nucleus Substantia nigra Subthalamic nucleus Superior colliculus	Parkinsonism Corticobasal syndrome Progressive gait freezing
Corticobasal degeneration *(CBD)*	4R	Pre-tangles Astrocytic plaques Neuropil threads Ballooned neurons	Neurons Oligodendrocytes Astrocytes Frontoparietal association cortices Substantia nigra	Progressive aphasia Corticobasal síndrome Atypical parkinsonism
Argyrophilic grain disease *(AGS)*	4R	Argyrophilic grains Ballooned neurons Coiled bodies Granular/Fuzzy astrocytes	Neurons Oligodendrocytes Astrocytes Anterior temporal lobe Amygdala Ambient gyrus Hippocampus	Mild cognitive impairment
Globular glial tauopathy (*GGT*)	4R	Non- and argyrophilic inclusions Coiled bodies Tufted astrocytes	Astrocytes Oligodendrocytes Frontal and motor cortices Temporal lobes	Frontotemporal dementia Richardson's syndrome Corticobasal syndrome

(continues in the next page)

Tauopathy	Tau isoform	Pathological hallmark	Cellular and anatomical vulnerability	Clinical features
Chronic traumatic encephalopathy *(CTE)*	3R/4R	Astrocytic tau tangles NFTs	Neurons Oligodendrocytes Astrocytes Frontal, temporal, and parietal lobes Sulci and vasculature	Behavioural and cognitive deficits
Primary age-related tauopathy *(PART)*	3R/4R	NFTs	Neurons Basal forebrain Brainstem Medial temporal lobe Olfactory bulb	Mild cognitive impairment

1.2.2 Genetic tauophaties: FTDP-17, a basis for understanding other taupathies

Primary tauopathies that have reported to present a familiar autosomal inheritance are included inside the group of FTDP-17. This genetic origin is mostly caused by the presence of mutations in the *MAPT* gene, which codifies for the protein tau (*see section 1.3.1*) and constitutes between a 5 and a 10% of all cases of primary tauopathies[113].

1.2.2.1 Epidemiology and etiology of FTDP-17

FTDP-17 is an extremely rare condition with a prevalence and incidence still unknown. Over 100 families with 38 different mutations in the MAPT gene have been identified worldwide. About 50–600 patients have been described until now, with fewer than 70 individuals still living[114].

The most common mutations in FTDP-17 are the missense mutations P301L and N279K, and the silent splice site mutation located 16 nucleotides after the splicing site (+16). The P301L mutation, together with the ΔK280, P301L or P301S mutations, become the most aggressive ones[115]. This last concept is based in the idea that they produce the largest effects regarding tau aggregation (*see Figure 23 in section 1.3.8)*.

1.2.2.2 FTDP-17 neuropathology and its relation to AD and other tauopathies

Several similarities have been reported in the past few years between FTLD-17 and the rest of primary and secondary tauopathies. Thus, these genetic tauopathies have served to study the various cellular mechanisms involved in distinctive forms of sporadic tauopathies[87,116,117]. Indeed, they have served to develop the previous reviewed rodent models and permitted to unveil the basis of tau pathology.

1.2.2.2.1 Common clinical symptoms and brain areas affected

FTDP-17 curses with heterogeneous behavioural, movement, language, and memory deficits[118,119] that progress complexly reflecting molecular alterations happening in the brain. Then, phenotypes vary not only between families carrying different mutations but also within families carrying the same mutation, and is not far away from that observed in other primary tauopathies or even in AD. This includes motor disabilities (extrapyramidal movements, ataxia, bradykinesia, or parkinsonism)[2,120], language disorders (progressive aphasia or apraxia of speech) and cognitive decline (progressive amnesia, aggression, disinhibition, or paranoid ideas)[121,122]. Also, as FTDP-17 also affects temporal lobes, it frequently courses with loss of episodic and semantic memories. These clinical features resemble those observed in PSP, CBD or

AD, respectively. More specifically, from the mutations already mentioned, the +16 intronic mutations presented similar clinical symptoms as AD, while the ΔK280 resembles the primary tauopathy *progressive supranuclear palsy* (PSP)[100,123]

Concrete clinical features usually reflect specific patterns of atrophy. Thus, FTDP-17 mostly affect frontotemporal cortex and temporal lobes, basal ganglia, substantia nigra and striatum[124]. The first ones justify the cognitive deficits aforementioned and match with the pattern observed in CBD and GGT. Then, the striatum atrophy explains the motor deficits usually reported in FTDP-17 patients, especially common among PSP patients, whose major common clinical features include parkinsonism or progressive gait freezing[124]. Progressive affection of these areas is also observed in AD, including even motor cortices and striatum[125,126].

1.2.2.2.2 Development of equivalent neuropathological traits

Affection of these areas results from the progressive accumulation of NTFs and argentophilic intraneuronal inclusions[127]. Importantly, these accumulations usually resemble aggregates observed in other tauopathies (they can be reviewed in [100] and ([87] and summarized in **Figure 13**). More specifically, the classical FTLD-17 with a P301L mutation has similar neuropathological features to the sporadic GGT. PSP and the CBD inclusions clear resemble those of cases of FTDP-17 caused by splicing mutations or the missense P301S mutation. They share same cell vulnerability affection or similar type of filamentous deposits[100]. Finally, pathology associated to several *MAPT* mutations is similar to that observed in *PSEN* mutations from early-onset familial AD. FTDP-17 V337M mutation, for example, shares same mechanisms that lead to the filamentous tau pathology in AD, with structurally similar pre-tangled forms[128].

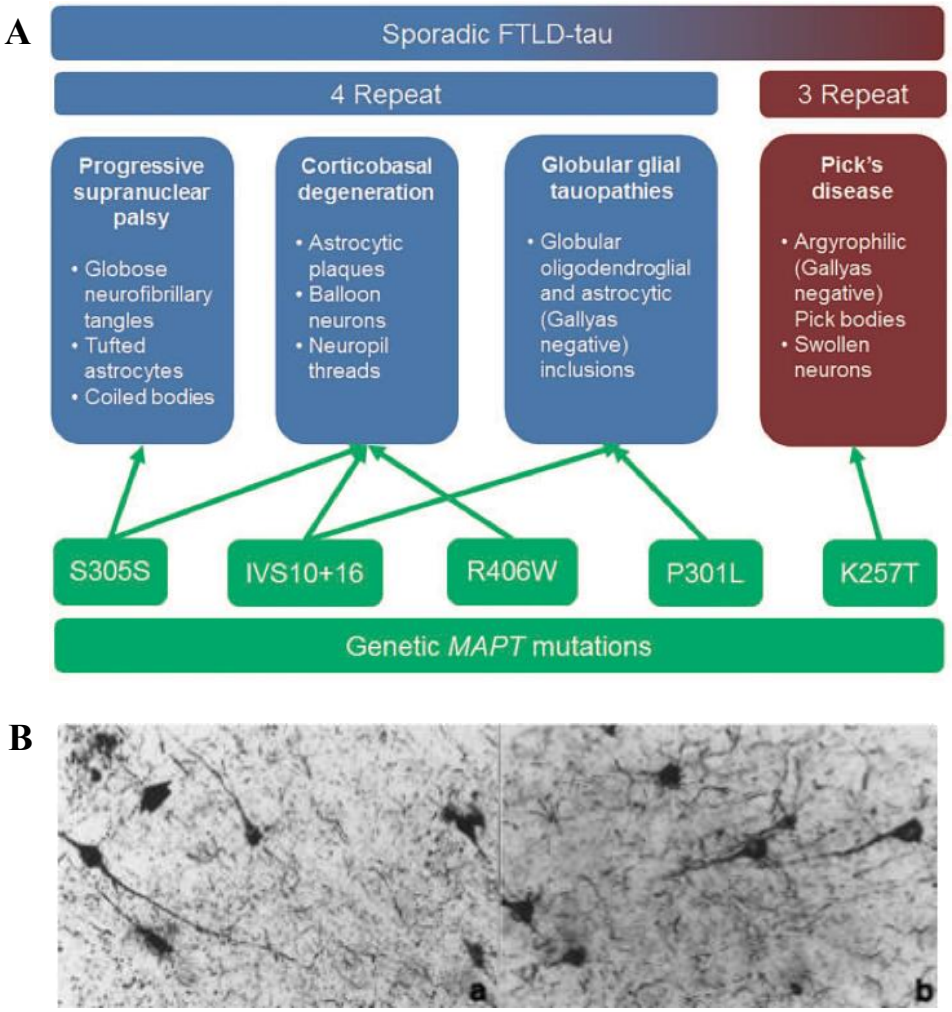

Figure 13. Neuropathological similarities between sporadic and genetic tauopathies. (A) Different FTDP-17 mutations in *MAPT* gene result in the accumulation of the same traits observed in other primary tauopathies, as indicated by arrows [100]. (B) This tau pathology resemblance is extended to AD (a), where phosphorylated tau pattern is highly similar to that observed in FTDP-17 caused by the V337M mutation (b). Adapted from (87,128).

1.3 Tau protein

As mentioned before, the common element and main hallmark underlying tauopathies is the accumulation of tau protein. For that, now, we will focus on dismantling the basis of this protein.

Neurons are differentiated, polarized cells whose functionality is extremely dependent on a well-equipped network. This system is required for the trafficking of vesicles and organelles along the cell and axons and for that, a strong and dynamic cytoskeleton is required. MTs constitute one of the main components of this cellular framework, together with microfilaments and intermediate filaments. They are dynamic structures whose sequential assembly and depolymerization ensures cell morphology. MTs stabilization is regulated by a group of proteins known as microtubule-associated proteins (MAPs) (**Figure 14**). This is formed by MAP1 (A and B), MAP2 and tau protein.

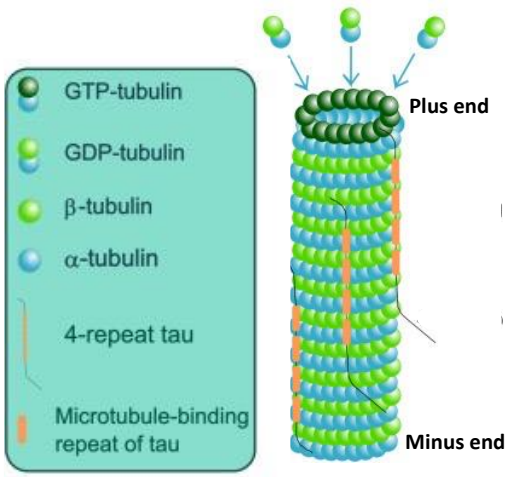

Figure 14. Microtubule (MT) structure is conserved by tau stabilization. α- and β-tubulins are added to the plus end of the MT to form a cylindric structure. This structure is stabilized by the longitudinal (or lateral) binding of tau protein and the addition of GTP-tubulin in the growing end, which prevents from its disassembly. Adapted from (129).

Tau protein was discovered in 1975 by Weingarten et al.,[130], as a protein which copurified with MTs and participated in tubulin polymerization. During the following sections we will explore tau production, structure, localization, and functional relevance in both physiological and pathological conditions. As a

brief fist read-out, tau was firstly proposed as a degradation product of other MAPs, but then proved to be an independent protein[131,132]. It is, in fact, a highly regulated protein codified by the *MAPT* gene and predominantly expressed in neurons. It is mostly cytosolic with predominant location in axons. Despite being classically defined to promote MTs assembly and stabilization, its participation is extended to other functions going from nuclear maintenance to synaptic functionality (*see section 1.3.5*).

1.3.1 *MAPT* gene

The human *MAPT* gene is located on human chromosome 17q21[133,134]. It is highly conserved between species, being expressed from *C. Elegans* and Drosophila to rodents, monkeys and humans. Its expression is mostly neuronal, with lower detection in peripheral tissues such as heart, kidney or lung[135]. Within the brain, tau is more abundant in the frontal and occipital cortices, with significantly reduced expression in putamen and cerebellum[136]. Expression of tau is controlled by specific neuronal transcription factors such as AP2 and SP1[137]. A deep analysis of the regulation of MAPT gene can be found in [138]

MAPT gene contains 16 exons (**Figure 15A**) and codifies for 6 different tau isoforms (**Figure 15B**)[133,134]. Exons 0 and 14 are part of the promoter region and part of the 3' untranslated region (UTR), respectively, and are not translated. Among the translated ones, exons 4A, 6, and 8 are expressed only in peripheral tissues, while exons 9, 11, and 12 encode the microtubule-binding (MTB) domains (R1, R3, and R4 domains, respectively) [116,139]. The exons 2, 3 and 10 are the responsible of the formation of these 6 isoforms mentioned.

1.3.2 Tau isoforms

In human brain, alternative splicing of the exons 2, 3 and 10 results in these 6 different isoforms of tau[140]. While exons 2 and 3 encode for two amino-terminal inserts, exon 10 encodes for an additional MTB domain repeat (R2). Exon 3 is only present together with exon 2, thus, generating 3 tau isoforms that can contain none, one or two amino-terminal inserts. The inclusion of the exon 10 supposes the addition of an extra MTB and the generation of isoforms with four MTB domains repeats. Altogether, alternative splicing of the *MAPT* gene results in the generation of 0N3R, 1N3R, 2N3R and 0N4R, 1N4R and 2N4R isoforms (**Figure 15B**).

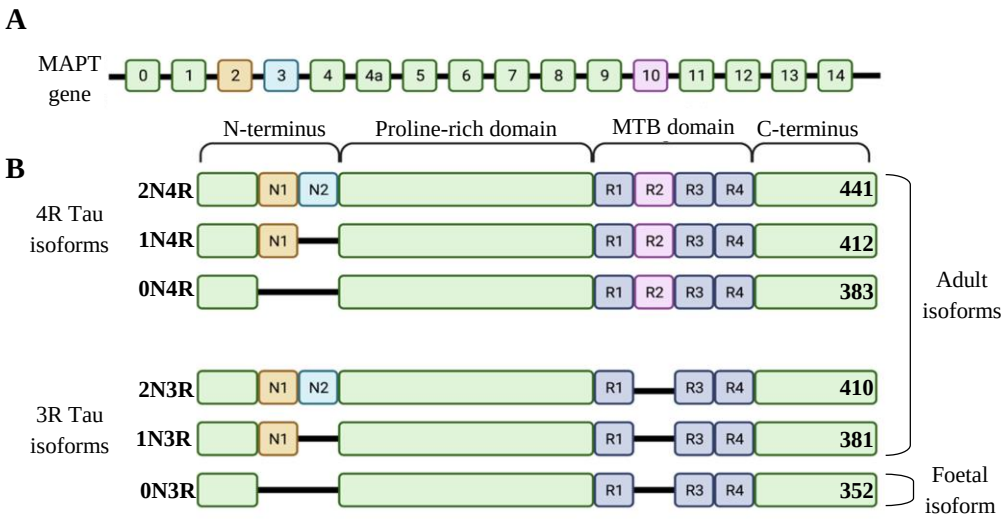

Figure 15. Structure of *MAPT* gene and Tau isoforms after alternative splicing. (A) Diagram of the exons of the human *MAPT* gene. (B) Presence of exons 2 (orange) and 3 (blue) determines the presence of none, one or two amino-terminal inserts (referred as ON, 1N or 2N). Inclusion of exon 10 implicates the presence of an additional MTB domain repeat (R2, shown in purple) and the generation of 4R isoforms. 0N3R isoform is exclusively expressed during development. Functional regions of the protein and isoform lengths are also indicated. Modified from (141).

The proportion of the different isoforms of tau changes during development and follows a different pattern among different species. In rodents, tau isoform expression shifts from 0N3R during brain maturation to only 4R isoform in adults. In humans, only 0N3R tau is also expressed in foetal brain and during first days of postnatal development. By contrast, during adulthood, all other isoforms are expressed in different ratios. Similar levels of 3R and 4R Tau isoforms are expressed, while the proportion of N isoforms varies. 1N tau isoform constitutes approximately a 50% of the total tau, being a 40% for 0N isoform and a 10% for 2N tau[136]. In addition, they present concrete cellular and subcellular localization. On one side, different neuron types seem to express different isoforms of tau[140]. As an example, hippocampal granular cells from DG only contain 3R isoforms. On the other hand, 2N isoforms present a preferential somatodendritic localization, while 1N isoforms are mostly expressed in axons. Despite the functional relevance of this distribution is still unknown, recent studies suggest that this differential pattern depends on the different capacity of the isoforms to bind to MTs [142].

1.3.3 Tau protein structure

Tau protein isoforms have a number of amino acids ranging between 352 and 441, with a molecular weight between 45 and 65 kDa. The structure of the protein consists in a highly acidic N-terminal domain followed by a proline-rich region. Next, and attached to the C-terminus, we found the MTB domains, the central component for tau interaction with MTs. MTB domains consist of 3 or 4 MTB repeats depending on the isoform (**Figure 16**).

Tau presents specific motifs in the proline-rich region (PPXXP or PXXP), which confer tau the ability to interact with proteins containing SH3 domains. Importantly, proteins containing this domain include tyrosine kinases such as Fyn, which link tau to cytoskeletal structure maintenance or synaptic

functions. Also, another two conserved sequences have been identified in the MTB domains, which are relevant for self-assembly of tau [143,144] (**Figure 16A**). They are named as PHF6 (VQIVYK) and PHF6* (VQIINK) peptides and are located at the beginning of the third and second repeat of the MTB domain, respectively. Thus, PHF6* is exclusive of 4R isoforms.

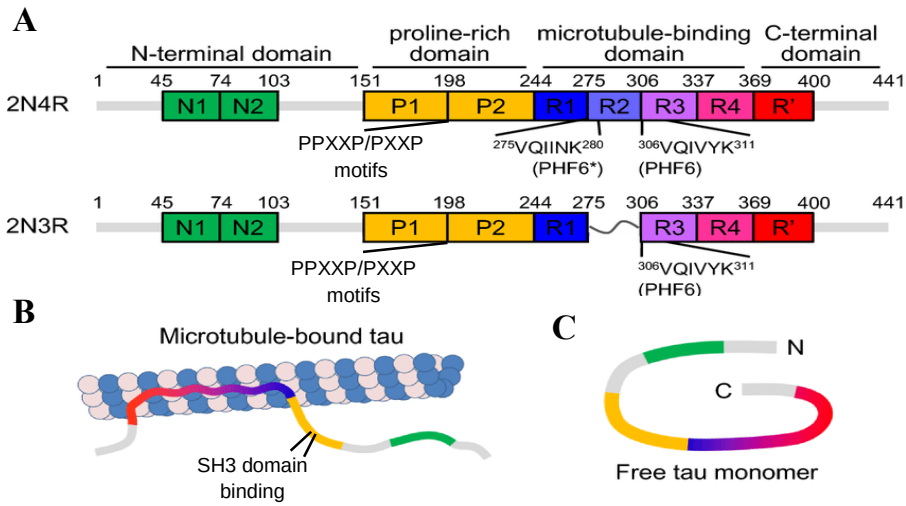

Figure 16. Structure and domains of human tau protein. (A) Tau protein is divided in 4 main domains: the N- and C-terminal domains, the proline-rich domain and the MTB domain. PPXXP and PXXP motifs are located in the proline-rich domain and allow tau to interact with proteins containing SH3 domains. MTB domains (3 or 4 repeats in 2N3R and 2N4R isoforms, respectively) permit the interaction with MTs and contain motifs involved in tau self-assembly (PHF6 and PHF6*), which are exposed after a conformational change from bended (C) to a lineal form (B). Adapted from (145).

1.3.4 Tau cellular and subcellular localization

In the brain, tau is mostly a neuronal protein with a heterogeneous pattern of expression between different neuronal types. However, transcriptomic studies revealed that oligodendrocytes and astrocytes can also express low levels of tau[146]. Regarding cellular distribution, tau becomes primarily axonal during neuronal maturation and polarization. It is mainly localized in the growth cone of the axon and shows a decreasing gradient of expression towards the soma.

Despite this, tau can also be detected in dendrites and in the synaptic compartment. Finally, tau is mostly a cytosolic protein, but it has been also identified attached to the cell membranes, which ensures cell polarization and organelles attachment to the cytoskeleton (the Golgi network, endoplasmic reticulum, and the plasma membrane[147,148], and in the nucleus. This widespread localization of tau explains its implication in several non-canonical functions, which will be further described in the next section.

1.3.5 Tau physiological functions

The principal and firstly described function of tau was the maintenance of stability and dynamism of MTs in the axon of mature neurons, but several non-standard functions have been described as well[149] (**Figure 17**).

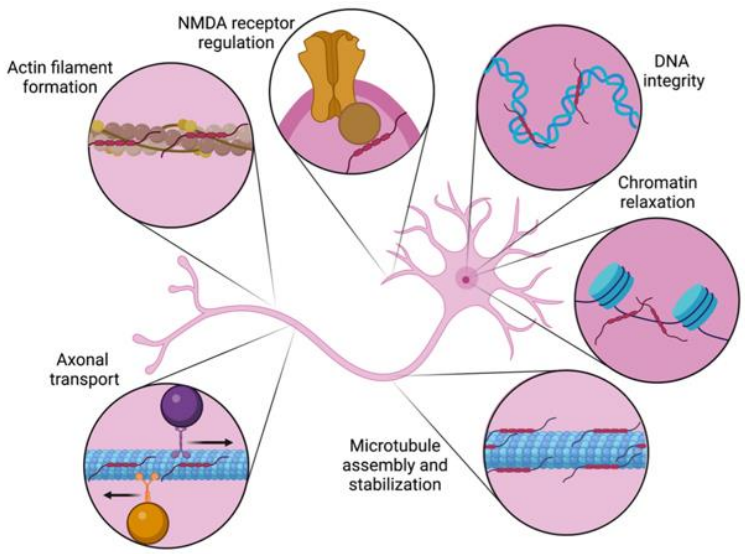

Figure 17. Tau main physiological functions in neurons. Tau was firstly described as a MTs stabilizer protein in axons. However, its presence in dendrites or nucleus confers to Tau additional roles in the maintenance of synaptic function and DNA integrity. Also, Tau participates in actin filament formation, among others. Adapted from (141).

These functions are due to the differential localization of tau above commented and are principally regulated by post-translational modifications of tau, which are further explained in the next section.

1.3.5.1 Regulation of axonal transport

Tau is able to regulate both anterograde and retrograde transport, ensuring neuronal transport of organelles, proteins and lipids from the soma to the axon and dendrites. This is directed by competing against dynein and kinesins for the MTs, but also by directly interacting with kinesins via its N-terminus[150,151].

1.3.5.2 Maintenance of cytoskeletal structure and actin filaments formation

Tau can directly interact with spectrin and actin filaments[152,153] through the MTB domain, helping the stabilization of MTs and the interaction with neurofilaments, and finally, guaranteeing cytoskeletal structure. In addition, tau can bind to phosphatidylinositol bisphosphate (PIP2), controlling other actin-binding proteins and participating in actin assembly[154].

1.3.5.3 Regulation of synaptic plasticity

Tau can be found in both pre- and post-synaptic compartments regulating several synaptic plasticity processes (*see Box 3, section 3.2.4 for a detailed information about synaptic plasticity*). It has been involved in spine remodelling[75,155] due to its capacity to interact with actin or the Src kinases family[156]. Also, it has been involved in LTD and LTP. Tau can interact with the SH3 domain of the kinase Fyn and regulate NMDA receptor recruitment and signalling[157]. In addition, it has been shown to associate with the post-synaptic density (PSD) complex helping to pair NMDA receptors to PSD95 protein[157–159].

1.3.5.4 Tau and mitochondria

By regulating axonal transport, tau is able to regulate mitochondria transport to presynaptic sites, an essential event for correct synaptic function. Also, as mitochondria are involved in the regulation of intracellular calcium and ATP levels, and these are critical for vesicle release, tau also participates in neurotransmission[160].

1.3.5.5 Tau in the nucleus

In the nucleus, tau is able to induce chromatic relaxation and its stabilization, further being able to regulate global transcription[149,161]. It also participates in the maintenance of genomic DNA integrity[162].

1.3.5.6 Tau and insulin

Finally, tau can also regulate the insulin-signalling pathway. Unless the mechanism is misunderstood, deletion of tau has been reported to cause higher phosphorylation of insulin receptor substrate 1 (IRS-1)[163] and an impaired hippocampal response to insulin, leading to insulin resistance[164].

1.3.5.7 Tau in glial cells

Even in low quantity, tau can be expressed in glial cells. To date, physiological functions of tau in astrocytes and microglia remain unknown, but in oligodendrocytes, tau has been described to participate in the myelination process by interacting with Fyn and stabilizing microtubule networks[165].

1.3.6 Post-translational modifications of tau and their implication in pysiology and neurodegeneration

As we previously introduced, tau localization, function and degradation are highly regulated by the addition of post-translationa modifications (PTMs) to the protein. Many PTMs have been described for tau, being phosphorylation the most studied one. Other modifications include ubiquitination, glycosylation, glycation, acetylation, oxidation SUMOylation, nitration, methylation and truncation [166]. Wesseling et al.,[167] provided a qualitative and quantitative profiling of the PTMs of tau by identifying 55 phosphorylation, 17 ubiquitination, 19 acetylation, and 4 methylation sites for tau. Most abundant PTMs and their patterns on tau are summarized in **Figure 18**.

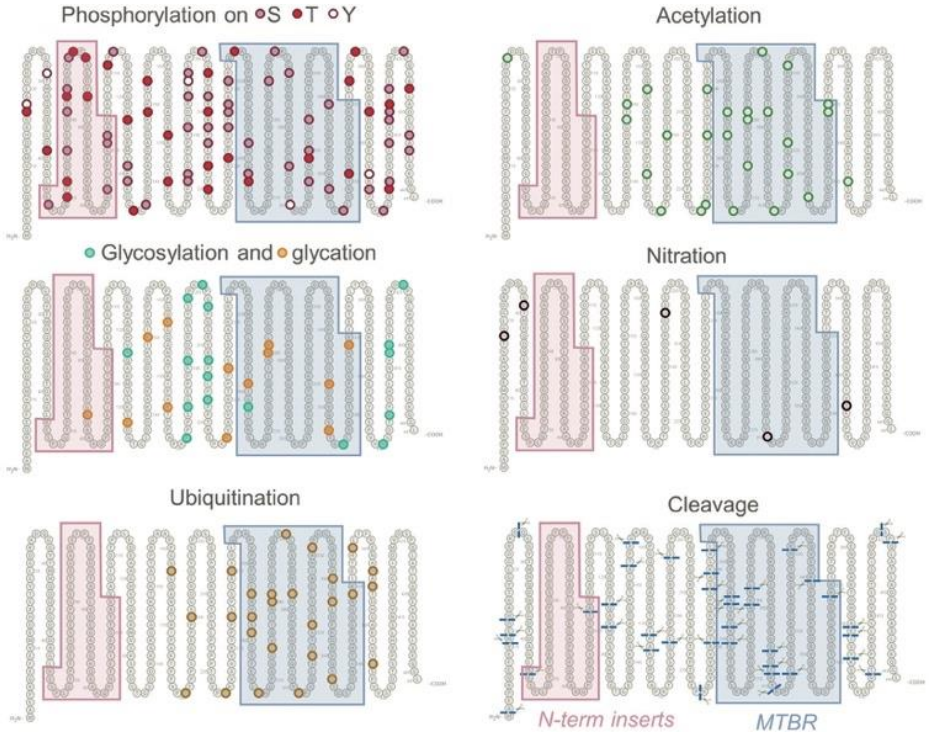

Figure 18. PTM patterns on Tau. While phosphorylation of Tau is distributed along the protein, other PTMs such as ubiquitination and acetylation are found clustered next to the MTB domains. Potential sites target of different proteases are shown in blue. Obtained from (166).

Importantly, these PTMs, and specially phosphorylation, have been recognized to contribute to neurodegeneration. Their implication in both physiological and/or pathological conditions is resumed in the following paragraphs.

1.3.6.1 Tau phosphorylation

The 2N4R isoform of tau has 85 phosphorylation residues (**Figure 19**) and has been described in many studies as a phosphoprotein. Tau phosphorylation is considered the principal PTM due to its capacity to regulate distribution, function, and degradation of tau in physiological conditions. As these requirements change during development, phosphorylation also changes progressively from especially high levels during foetal development to decreased ones in adulthood.

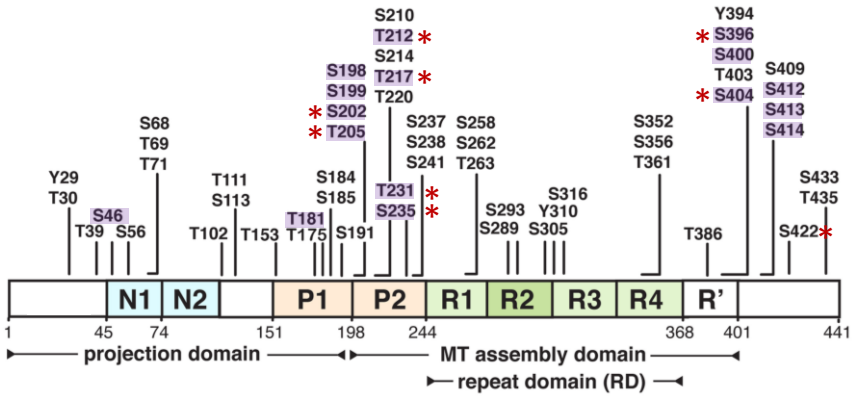

Figure 19. Phosphorylation residues of Tau. Phosphorylation sites are mostly clustered in the proline-rich domain of tau (P1 and P2) but distributed heterogeneously through all sequence. Residues phosphorylated under physiological conditions are marked in purple. In certain diseases, these residues become over-phosphorylated, together with additional phosphorylations in the rest of residues indicated. The red asterisk indicates those residues phosphorylated by GSK3-β. Interestingly, phosphorylation of S396 or S404 seem not to affect to its MTs binding. Adapted from (168).

As mentioned, phosphorylation serves as a signal for its localization and its affinity to MTs, then, being able to regulate both canonical and non-canonical functions of tau. In the axon, there is a proximo-distal gradient of tau phosphorylation: it is primarily dephosphorylated in the growth cone of the axon, while is more phosphorylated in the proximal axon and cell body[169]. Phosphorylated tau generally implies less affinity to bind MTs, so, this fact ensures MTs dynamism and efficient transport within the axon and helps regulating neurite outgrowth. In the nucleus, tau is mostly dephosphorylated, and its phosphorylation mediates its translocation outside it, and its attachment to cell membranes[170–172] This way, phosphorylation serves to control nuclear functions.

Finally, phosphorylation also promotes tau degradation through the proteasome or the autophagy-lysosomal pathway. This is achieved by the phosphorylation of serine or tyrosine residues from specific amino acid sequences known to serve as a degradation-signal motifs[173,174].

Given the implications of phosphorylation in tau functionality, a coordinated activity of kinases and phosphatases is necessary to maintain the phosphorylation status of tau under physiological conditions. Kinases reported to phosphorylate tau can be divided in three groups and include:

- *Proline-directed kinases*: glycogen synthase kinase-3 (GSK-3), cyclin-dependent kinase 5 (cdk5), and 5′ adenosine monophosphate-activated protein kinase (AMPK).
- *Non-proline directed kinases*: casein kinase 1 (CDK1), AMP-dependent protein kinase a (PKA), or microtubule affinity-regulating kinases (MARKs).
- *Tyrosine kinases* such as Fyn, Abl or Syk.

Several phosphatases have been described to counteract this kinase activity as well. They include protein phosphatase-1, -2A, and -5 (PP1, PP2A, and PP5A[166].

1.3.6.1.1 Pathological implications of tau phosphorylation

Due to its influence in tau localization and functions, phosphorylation status of tau is finely controlled by a kinase/phosphatase equilibrium. Then, an imbalance can provoke a mislocalization and a dysregulation of its functions. This is traduced into a gain of toxicity within the neuron, which is indeed the basis of a wide number of neurodegenerative diseases.

First insights regarding the pathogenicity of dysregulated phosphorylation of tau were described by Grundke-Iqbal et al., in 1986[175]. They demonstrated the presence of phosphorylated tau in the intracellular tau aggregates present in AD, the NFTs[157]. In fact, hyperphosphorylation of tau has been reported to impair its correct degradation and, usually in combination with other PTMs, increase its propensity to self-associate (*see section 1.3.7*), oligomerize and eventually form filamentous aggregates that will lead to the deposition of tau aggregates. Tau loss-of-function is observed at several levels, as described in the **Figure 20**.

Its inability to properly interact with MTs is traduced to cytoskeleton instability, axonal degeneration, and impaired axonal transport[176,177]. Deficient cell transport provokes a poor release of neurotransmitter vesicles at the synapsis, reducing neuronal excitability. There, an increment of phosphorylated tau also results in a reduction in the AMPA receptors, a promotion of LTD, a loss of synaptic integrity and, at last instance, memory impairment[157]. Also, its massive translocation to the soma alters its nuclear functions, altering chromatin relaxation or DNA repair processes.

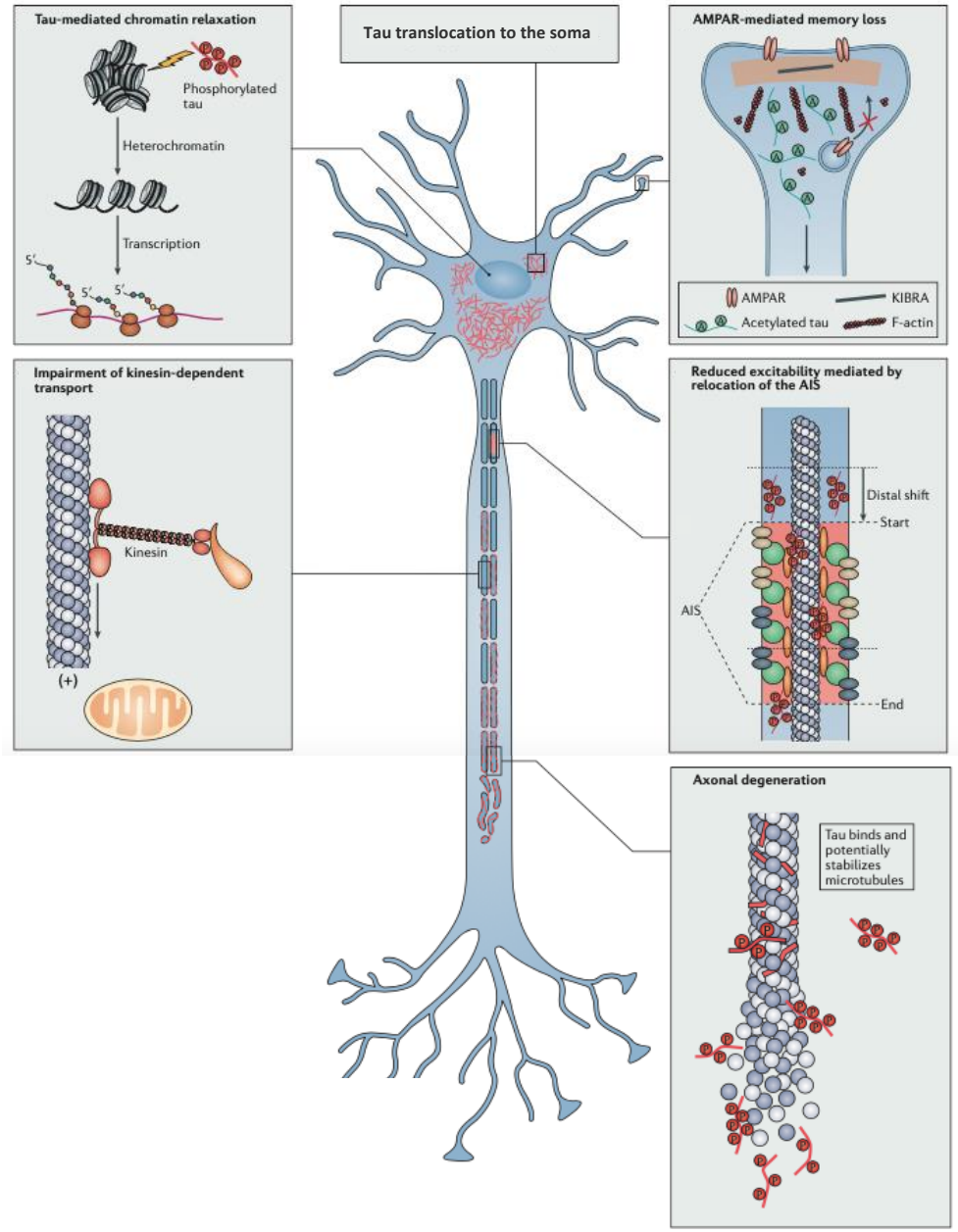

Figure 20. Pathological events resultant from the phosphorylation, aggregation and other PMTs of Tau. Nuclear and synaptic functions, axonal transport, and stability of MTs are impaired because of the progressive increment in phosphorylation of tau and the formation of aggregates. Adapted from (178).

1.3.6.2 Tau ubiquitination

Ubiquitination process will be deeply reviewed in **section 2** due to its implication in the protein aggregation characteristic of proteinopathies. However, among these paragraphs, we will review how this process, based on the covalent attachment of different patterns of ubiquitin (Ub) chains, impacts in tau physiological and pathological relevance.

Several of them are ubiquitinated by the E3 ligase carboxy-terminus of Hsc70 interacting protein (CHIP), which can ubiquitinate tau with Lys48- and Lys63-linked poly-Ub chains[179]. Also, it can be Lys63-linked poly-ubiquitinated by the TNF Receptor Associated Factor 6 (TRAF6) due to its E3 ligase activity and its interaction with tau through the SH3 domain. Lys48-linked poly-ubiquitination is the most common and most explored form of tau ubiquitination under physiological conditions. It serves as a signal for its proteasomal degradation.

On the other hand, Lys63-linked poly-ubiquitination has been seen to mediate its degradation trough the lysosomal pathway[180]. Also, as TRAF6-mediated poly-ubiquitination at Lys63 has been linked to processes such as endocytosis, its action is considered to promote its endocytosis from cell membrane[181]. Finally, it possibly also enables nuclear tau functions, because Lys63 ubiquitin chain is known to permit recruitment of proteins in charge of DNA repair[182]. The physiological relevance of other ubiquitination patterns of tau is still unknown. Considering this, potential functions have been mostly described upon general functions of ubiquitin signalling (**Box 1**) and after the implications of aberrant ubiquitination in disease.

BOX 1
CELLULAR FUNCTIONS OF UB-CHAINS

- **Proteasomal degradation**: Lys48-linked poly-Ub
- **DNA repair and transcriptional regulation**:
  - Mono-Ub
  - Lys63- linked poly-Ub
  - Lys11-linked poly-Ub
- **Autophagy and endocytosis**: Lys63- linked poly-Ub
- **Signalling transduction**:
  - NF-κB: Lys63- and Lys11-linked poly-Ub
  - TNFα: Met1-linked ub
- **Mitochondrial homeostasis**: branched lys6-linked chains

1.3.6.2.1 Ubiquitination in pathological conditions

Ubiquitination of tau gains relevance upon pathological conditions. Protein aggregates are frequently positive for Ub (*see box 2, section 2.4*). More importantly, less aggregated forms of tau (such as the PHFs) have been also reported to be ubiquitinated. This PHFs are mostly mono-ubiquitinated, but they are also positive for Lys48-, Lys63-, Lys6, Lys11-, and Met1-linked poly-ubiquitin chains[179,183,184].

Majorly, pathological ubiquitination has been related with an increased tendency to aggregation. According to this, from those reported, mono-ubiquitination of tau has specifically been observed to impair its MTs binding[185]. Also, these mentioned CHIP and TRAF6-mediated hyper-ubiquitinations (Lys63-linked) have been reported to promote aggregates formation under pathological conditions[186], and in case of Lys63-linked chains

they have also been associated with enhanced seeding activity and propagation[187].

1.3.6.3 Tau truncation

In physiological conditions, tau can be cleaved by proteases such as calpain[188], Cathepsin D[189] or caspases -3 and -6 as a mechanism of turnover. In fact, tau presents PEST domains in both N- and C-terminal regions[190], which serve as a rapid proteolytic signal for its degradation.

1.3.6.3.1 Aberrant cleavage of Tau

Excessive truncation of tau (e.g. due to an increased caspase activity) together with the inability to correctly degrade it, generates toxic and pro-aggregative fragments of the protein. Then, it is a common feature of the different tauopathies, and it is frequently observed among aggregates[135,191,192]. Despite aberrant truncation can be mediated by several caspases[193], the action of caspase-3 in an aspartate residue (Aps421) seems to appear early in the progression of certain pathologies, generating a highly toxic 43 kDa peptide known as Tau-C3 with high tendency to assembly[194,195].

1.3.6.4 Other post-translational modifications

Functional implications of other PTMs are barely studied. However, several have been described, habitually, accompanying tau phosphorylation. Also, most of them are potentially implicated to the progression of tauopathies.

Tau can be *acetylated* in several lysine residues of the proline-rich and MTB domains. Indeed, tau acetylation of the Lys280 has been detected in brains from AD, CBD, and PSP patients, and considered as an early marker of AD[167]. *N- and O-glycosylation* plays a role in the nuclear mislocalization of tau[196]. *Glycation* of tau (condensation of a sugar aldehyde or ketone group in a lysine

residue) has been reported to promote oxidative stress and has been detected in PHFs[197,198].

1.3.7 Tau aggregation: the pathological hallmark of tauopathies

Tau monomer is an intrinsically disordered protein without defined secondary or tertiary structures. Under physiological conditions, tau is soluble, and this solubility can be attributed to the high positive charge surrounding the MTB domain. Intramolecular interactions between N- and C-terminal regions of tau lead to the formation of a ‘‘paper-clip’’ structure, which maintains its monomeric structure. The induction of negative charges (anionic or hydrophobic), for example, by phosphorylation[199] undergoes conformational changes in tau protein, promoting the opening of this “paper-clip” structure[200], and facilitating tau self-aggregation. This open structure promotes the exposition and interaction of the PHF6 and PH6* motifs located in the R2 and R3 domains, and the multiple assembly of the monomers forming β-sheets.

At the same time, tau can also acquire an α-helix secondary structure upon association with lipid membranes[201] which conforms the nucleus of oligomers and permits further polymerization[197]. This way, additional monomer incorporations lead to the formation of higher polymerized structures: the PHFs and straight filaments (SFs) (**Figure 21A**). Finally, sequential fragmentation and secondary nucleation events of this fibrillar forms, results in the formation of the largest aggregates (**Figure 21B**). They have different structural conformations and are distinctive from the different tauopathies. These include the NFTs observed in AD, or the spherical aggregates observed in PiD.

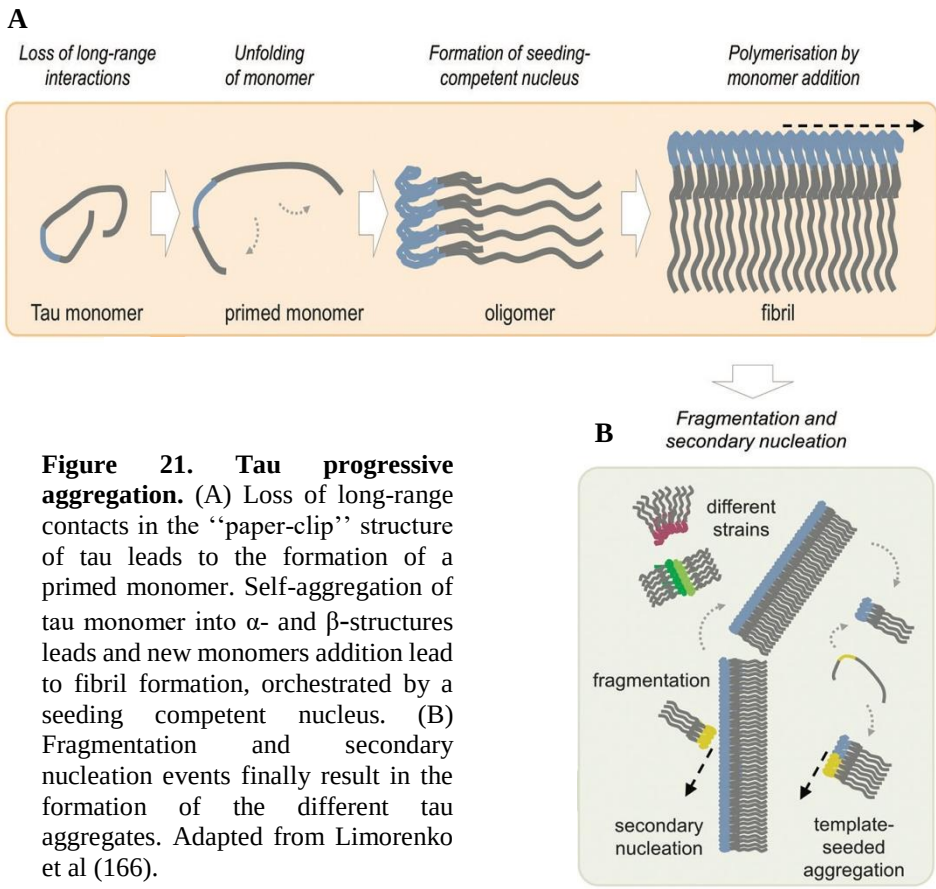

Figure 21. Tau progressive aggregation. (A) Loss of long-range contacts in the ‘‘paper-clip’’ structure of tau leads to the formation of a primed monomer. Self-aggregation of tau monomer into α- and β-structures leads and new monomers addition lead to fibril formation, orchestrated by a seeding competent nucleus. (B) Fragmentation and secondary nucleation events finally result in the formation of the different tau aggregates. Adapted from Limorenko et al (166).

For many years, it was assumed that tau aggregates were the cause of neuronal toxicity in AD. However, recent studies have shown that prefibrillar tau oligomers are more responsible of tau’s toxicity. Although the exact mechanisms in which pre-tangled tau leads to neurodegeneration remain unclear, oligomeric tau has been demonstrated to interfere in genomic regulation, protein degradation, energy metabolism, intraneuronal transport and synaptic signalling, in the way we have already commented[94,202].

1.3.8 Mutations in the *MAPT* gene

So far, to understand the nature of AD and other tauopathies we had to introduce the group of FTDP-17 tauopathies, which raised after the discovery of mutations in the *MAPT* gene. We have mentioned the most prevalent and aggressive mutations and shared that some of them present similarities with other tauopathies. We have also commented how they have served to the development several rodent models. After that, we already know that the P301L mutation is a missense mutation that provokes the rapid formation of tau aggregates, highly similar to those observed in the CBD. Also, we have mentioned that this mutation was used to generate the first MAPT mouse model, the JNPL3. Now, once we had explored tau gene and the properties of this protein, we will focus on describing more accurately the basis and implications of these mutations.

To date, at least 37 mutations in *MAPT* gene have been identified (**Figure 22**) and include missense mutations that have consequences at the protein level, and mutations affecting the alternative splicing of tau. Initially, these mutations directly affect neurons but, on some occasions, they can also affect glial cells.

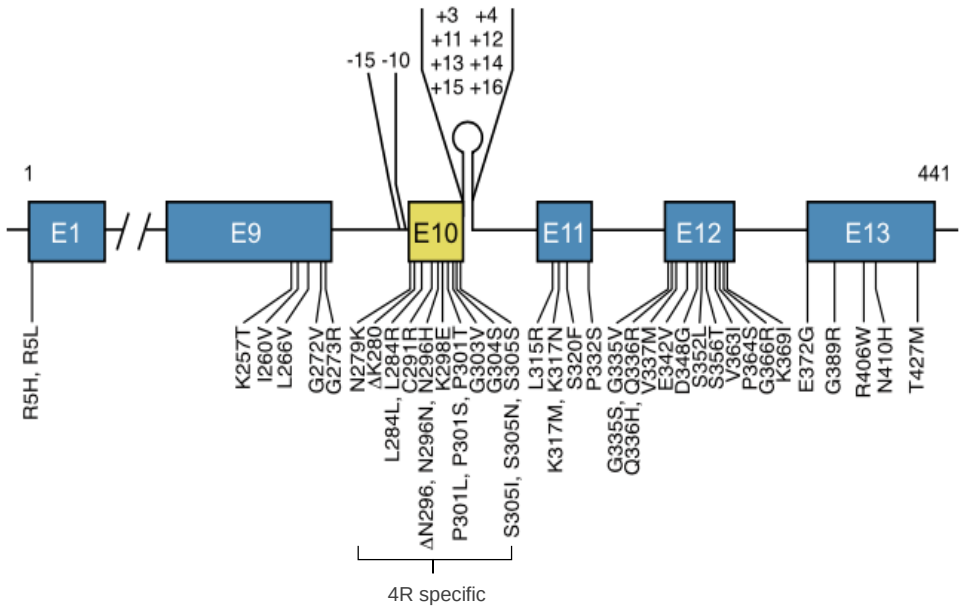

Figure 22. Mutations in the MAPT gene. *MAPT* mutations are mostly located in the MTB domain and can affect 4R/3R ratio, tau affinity for MTs and its capacity of self-aggregate. Some mutations are located inside the exon 10 (yellow) and only affect 4R isoforms (4R specific). Intronic mutations flanking the E10 are also shown. Adpated from (203).

Most of the *missense mutations* are clustered in the MTB domain and interfere with the capacity of tau to interact with MTs[204]. Therefore, they may directly confer tau the ability to form filaments (**Figure 23**). Also, some evidences report that those missense mutations can directly enhance tau phosphorylation, but this remains unclear[205,206]. This type of mutations includes P301L or P301S mutations. Both of them are located inside the exon 10, only affecting 4R isoforms and are reported to promote the exposition of the PHF6 and PHF6* domains, conformationally changing tau and enhancing its self-assembly[207,208].

Mutations that affect splicing are associated with the incorporation of exon 10, consequently, altering the 3R/4R ratio. This type of mutations and normally silent and intronic mutations found near the 5' splicing site of the exon 10 or

in its coding region. They are named depending on the number of residues numbered from the 5' splice site of the exon (e.g. -15 or +16; **Figure 22**, *upper panel*).

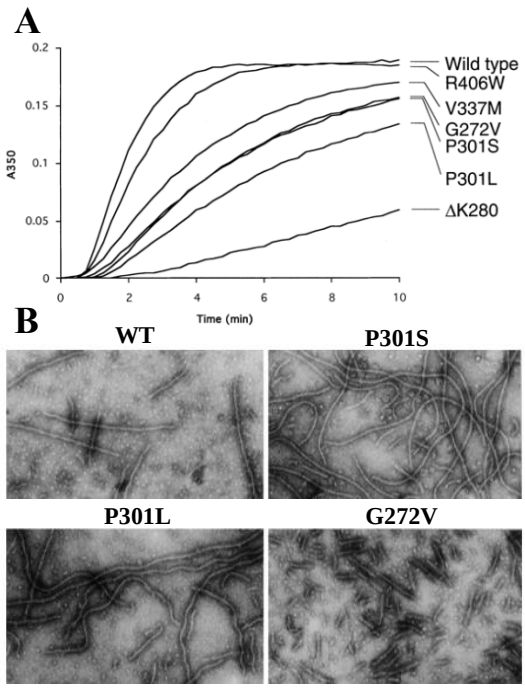

Figure 23: Effects of coding region mutations in tau on its ability of to promote microtubule assembly. (A) Polymerization of tubulin induced by WT tau and six mutant proteins (G272V, ΔK280, P301L, P301S, V337M, R406W), as measured over time by turbidimetry (A350). (B) Representative images of filaments assembled from WT and the mutant tau proteins P301S, P301L and G272V. Adapted from (116).

However, this group also includes missense mutations that can imbalance the ratio in both directions; for example, while N279K, L284L mutations promote the inclusion of the exon 10, the ΔK280 mutation decreases its splicing. Overproduction of tau isoforms with four MTBs has been related to a possible gain of toxic function due to an excess of tau over available binding sites on MTs[116].

2. MOLECULAR MECHANISMS OF PROTEOSTASIS: THE IMPORTANCE OF UBIQUITIN

Neuronal death gave name to neurogenerative diseases, being of the last events in the course of these pathologies, consequence of dysbalanced cellular processes and pronounced neuroinflammation. Among these alterations, impaired protein homeostasis and deficient quality control result in accumulation of specific protein aggregates which set the basis of a that group of neurodegenerative diseases called proteoinopathies. Abnormalities in protein structure, conformation, together with its impaired clearance, led to its aggregation and loss-of-function. Depending on the main protein altered, these diseases can be divided in amyloidophaties, tauopathies, α-synucleinopathies or (TAR)DNA-binding protein 43 (TDP-43), and despite presenting different neurophysiopathology, protein aggregation remains common between them.

Maintaining an intact proteome, namely cellular protein homeostasis, or proteostasis, is achieved by a precise control of protein synthesis, folding, conformational maintenance, and degradation. It requires a strict control of the initial production and folding of proteins, their conformational maintenance, quantity, and subcellular localization, and finally, a correct degradation when they are no longer functional. Thus, proteostasis turns indispensable in the nervous system for maintaining synaptic homeostasis and neuronal functionality. This process is primarily carried out by the UPS, but other systems as the autophagy and lysosomal pathways help to maintain protein turnover rates. In the UPS, proteins are tagged with ubiquitin, a signal that serves for its degradation through the proteasome.

Ub is a small (76 residues), highly compact globular protein codified by 4 different genes (*UBB*, *UBC*, *RPS27* and *UBA52* genes). It is ubiquitous and only found in eukaryotes. Ub can be covalently attached to target proteins as

a signal for their degradation by a multi-compartmentalized protease called the 26S proteasome. However, it also participates in other cell functions ensuring the functional diversity of the proteome. Then, ubiquitination of proteins has also been involved in DNA repair, trafficking, or immunity[209,210]. Now, we will review the principal considerations regarding ubiquitination with special focus on the functions related to this type of signalling and its contribution to proteinopathies.

2.1 Ubiquitination process and types of ubiquitination

The union of Ub to target proteins is sequential and requires the action of three proteins: a ubiquitin-activating enzyme called enzyme-1 (E1), a ubiquitin-conjugating enzyme (E2) and a ubiquitin-protein ligase (E3). First, Ub is activated in an ATP-dependent manner by the E1 and then transferred to an active cysteine residue of the E2. Finally, the E3 enzyme attaches the Ub to the target protein. Once attached, E2 and E3 enzymes can continue lengthening the ubiquitin chain. To date, two E1s, almost 30 E2s and more than 600 E3s have been identified in humans. Attachment of Ub to a target protein is made by isopeptide bonds between the ε-amino group of a lysine (Lys) residue in the target protein and the C-terminus of Ub. Based on this, different Ub modifications can occur. They constitute the ‘‘Ub code’’ and determine the functional significance of protein ubiquitination (**Figure 24**).

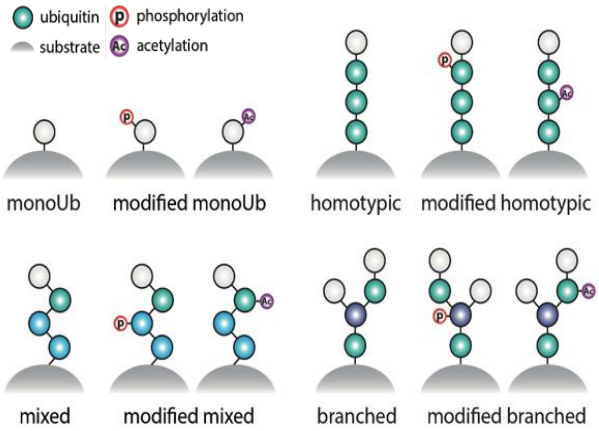

Figure 24. Schematic representation of the Ub code. Substrates can be mono-, multi- and poly- ubiquitinated. Also, branching of the chains and other PTMs can occur (*see legend*), amplifying the biological possibilities of Ub signaling. Ub, ubiquitin; PTMs, post-translational modifications. Adapted from (211).

Proteins can be mono- or multi-ubiquitinated, depending in the number of Ub molecules attached to different Lys residues of the target protein (one or several, respectively). Also, they can be poly-ubiquitinated by the addition of several Ubs to different Lys residues contained in Ub itself. Ub presents 8 amino groups where additional Ub monomers can be linked to. They are the N-terminal Met1 and 7 Lys residues (Lys6, Lys11, Lys27, Lys29, Lys33, Lys48, Lys63). When proteins are poly-ubiquitinated, several Ub monomers can be linked to one of the seven Lys residues or to Met1 residue and form Ub-chains. These chains present variable length, linkage type and configuration. Finally, the union to several amino groups in the same chain generates heterotypic or branched Ub chains.

2.2 Functions of covalently attached ubiquitin: more than protein degradation

The biological implications of Lys48- and Lys63-linked chains have been widely studied, while the function of others such as Lys6-, Lys11 or Lys-23 is still far away for being understood. As we have commented, one of the principal functions of ubiquitination is targeting proteins for proteasomal

degradation[212]. The successive conjugation of Ub to the Lys48 serves as a signal for recognition and degradation by the 26S proteasome (**Figure 25**).

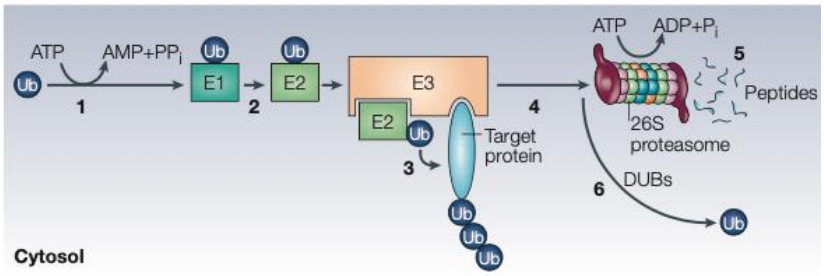

Figure 25. Ubiquitin conjugation for protein degradation in the proteasome. Sequential events (1-5) mediated by E1, E2 and E3 enzymes allow the attachment of a poly-Ub chain to the target protein and its degradation in the 26S proteasome. Finally, reusable ubiquitin is released by deubiquitylating enzymes (DUBs). Adapted from (212).

However, many other functions have been described, and most of them are linked to mono-ubiquitination or Lys63-linked poly-ubiquitination. They are resumed in the following paragraphs and synthetized in **Figure 26**.

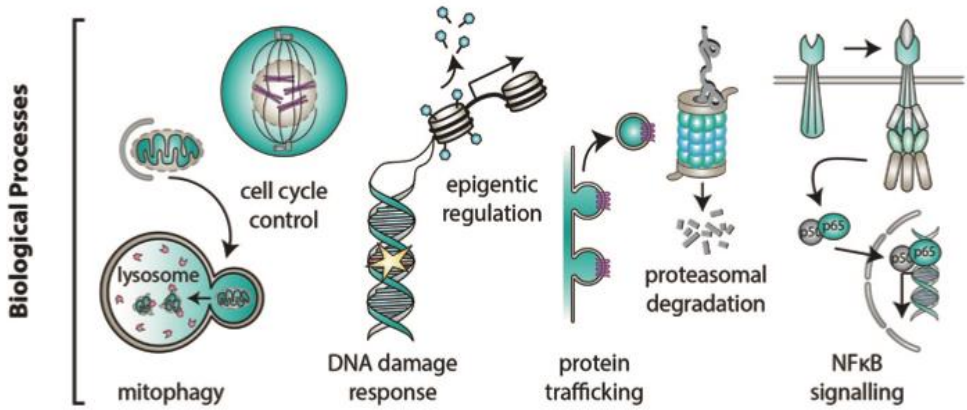

Figure 26. Biological processes regulated by ubiquitin. Differential linkage of ubiquitin allows regulating cellular processes such as mitophagy, intracellular signaling, protein traffiking or DNA damage. Adapted from (211).

2.2.1 DNA repair

Upon DNA damage, a family of proteins called RAD6 is required for activating the repair machinery[213]. This family of proteins includes E2 and E3 enzymes that mono-ubiquitinate or poly-ubiquitinate (Lys63-linked-chains) polymerases. After that, polymerases can interact with the DNA and the lesion is repaired.

2.2.2 Transcription

Histones can be modified by ubiquitin, generally being mono-ubiquitinated to enable the control of gene expression, DNA repair or replication. Transcription factors can be ubiquitinated as well, regulating its stability and activity[214].

2.2.3 Signal transduction

Signalling pathways can be regulated by ubiquitination. For example, the activation of the Nuclear Factor kappa-light-chain-enhancer of activated B cells (NF-κB) signalling pathway, under stimulus by tumor necrosis factor alpha (TNFα), requires the Lys63-linked polyubiquitination of the Receptor-Interacting Protein (RIP)[215]. This event allows a following Lys48-linked polyubiquitination, which permits the degradation of the inhibitor of NF-κB, IκB, and ensures NF-κB activation.

2.2.4 Endocytosis and sorting

Removal of growth factor receptors from the membrane and transportation to the endosomal compartment is controlled by K63-linked ubiquitination[216,217]. In addition, this type of poly-ubiquitination can regulate sorting and degradation of these receptors via the lysosomal pathway[218].

2.3 Functional relevance of other lys-linked chains

Met1-linked chains have been identified to regulate TNFα signalling through NF-κB activation[219,220]. *Lys6- and Lys33- linked chains* have been proposed as regulators of DNA damage[221]. In addition, Lys6-linked chains have been reported to play a role in mitochondrial homeostasis by regulating mitophagy[222]. *Lys11-linked chains* (especially those branched-conjugated) have been established as an additional proteasomal degradation signal in cell cycle regulation[223], and reported to be involved in NF-κB signalling regulation or during hypoxia[224,225]. Other chains such as *Lys27- or Lys29-* remain poorly understood. Recent studies regarding biological functions of Ub modification have been deeply reviewed by Swatek and colleagues[211].

2.4 Other proteins involved in the ubiquitination process

2.4.1 Deubiquitination proteins

Deubiquitinitating enzymes or deubiquitinases (DUBs) are specialized families of proteases that remove ubiquitin modifications. They are usually described in the context of proteasomal degradation, as they recuperate the Ub (**Figure 25**). However, they play an important role in orchestrating DNA damage response and DNA repair processes as well as in mediating signalling circuits such as the NF-κB pathway. Therefore, ubiquitinated RIP1 promotes cell survival while, by contrast, deubiquitination of RIP1 by A20, sifts this via to the induction of apoptosis[215]. Altered function of this DUB, among others, can aberrantly potentiate or reduce cell death, being related then, to cancer, neurodegenerative diseases or immune diseases[226].

2.4.2 Chaperones

Chaperones, also known as heat shock proteins (HSPs), constitute a family of proteins with the ability to bind and stabilize non-native conformation of proteins. They have been reported to directly cooperate with the UPS during protein quality control. For example, CHIP interacts with the Hsp70 and Hsp90 in order to ubiquitinate proteins such as tau. Also, they have been involved in regulating ATP binding and hydrolysis, an event required for Ub activation[227].

2.5 Ubiquitination in neurodegenerative diseases

Defects in Ub signalling have been linked to diseases such as cancer, diabetes, or muscle-wasting disorders[228], but they also have a special relevance in neurodegenerative diseases. As we have already mentioned, the basis of proteinopathies is the toxic accumulation of protein aggregates that perturb cellular homeostasis and neuronal function.

The protein aggregated, cells affected, and the localization of protein inclusions differ between diseases, but in each case, these aggregates are immunoreactive for Ub (**Box 2**). Furthermore, aberrations in Ub-dependent degradation systems (UPS or autophagy) have been linked to the aggregates formation and further neurodegeneration[229,230].

In Parkinson's disease (PD), the majority of α-synuclein present in Lewy bodies is mono- or di-ubiquitinated at several lysine residues. Also, mutations linked to familiar forms of PD include mutations in the Ub ligase Parkin (Park2)[231,232].

BOX 2

UB-POSITIVE AGGREGATES IN NEURODEGENERATIVE DISEASES

- **Parkison's disease**: Lewy Bodies (α-synuclein)
- **Alzheimer's disease**: Senile plaques (Aβ); NFTs (tau)
- **Huntington's disease**: mutant Htt aggregates (**Figure 27**)
- **Amyotrophic lateral sclerosis**: TDP43 aggregates

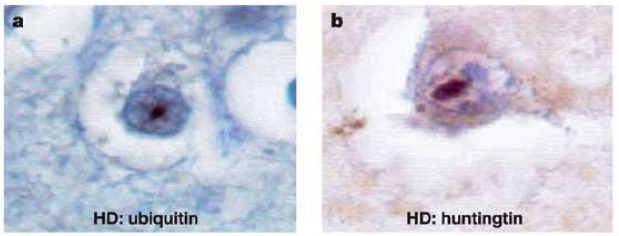

Figure 27. Htt aggregates present in HD. Htt aggregates are stained with both ubiquitin (a) and Htt (b) antibodies. Adapted from (393).

In Huntington's disease (HD), upregulation of TRAF6 enhances aggregate formation by mediating atypical ubiquitination of huntingtin (Htt) (*see Figure 27 in Box 2*)[233]. Accumulation of Lys48-, Lys63- and Lys11-linked chains has been also reported in HD.

In AD, the selective autophagy adaptor p62 acts as a scaffold protein for tau polyubiquitination by TRAF6. Its reduction has been found to promote tau pathology and NFTs formation[234]. In fact, as we have deeply reviewed in the previous *section 1.3.6.2*, tau is a highly post-translationally modified protein and its ubiquitination plays important roles in both physiological and pathological conditions.

3. MOLECULAR MECHANISMS OF CELL SURVIVAL AND TISSUE HOMEOSTASIS: MORE THAN PROGRAMMED CELL DEATH

Indisputably, the final event occurring in neurodegenerative diseases is the progressive loss of different populations of neurons. Along this text, we have summarized and explained the theory of the main pathological processes that underlie this massive cell death in tauopathies. Now, and for the rest of this section, we will review the basic concepts of the process leading to this aberrant neuronal death and also present the central protein of this Thesis: FAIM-L.

Programmed cell death (PCD) is an active and highly regulated process that ensures tissue homeostasis during development and in the adulthood. Current classification includes many types of PCD but places apoptosis, autophagy, and necrosis as the main ones[235]. Among them, apoptosis is especially relevant for the correct function of the nervous system during development, and it has been also considered the principal orchestrator of the neuronal loss underlying neurodegenerative diseases and its symptomatology [236–238]. However, cell death regulation is not the only function of this process, as we will see after mentioning the basic concepts involving this type of PCD.

3.1 Basic concepts of apoptosis

Apoptosis was firstly described by Kerr et al.,[239] in 1972. This type of PCD is based on a sequence of concrete biochemical and morphological changes which avoid the affection of neighbour cells and an inflammatory response.

These changes include rounding-up of the cell, chromatin condensation and nuclear fragmentation or the formation of apoptotic bodies (**Figure 28**)[239,240].

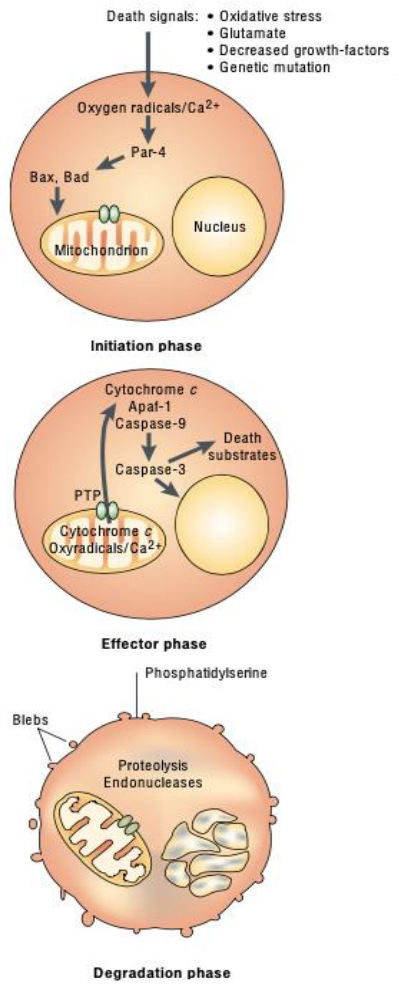

Figure 28. Morphological and biochemical features of the apoptotic process. Progressive activation of initiator and effector caspases during the 3 consecutive indicated phases leads to cell changes such as membrane blebbing, DNA condensation or exposition of phosphatidylserine in the membrane to promote phagocytosis of the dying cell. Adapted from (236).

Apoptosis is a multi-step process highly regulated by anti- and pro-apoptotic factors. Initially, an intra- or extracellular apoptotic stimulus triggers a cascade of events (grouped into the intrinsic or extrinsic pathways, respectively), which converges in the activation of a specific group of proteases known as caspases. This activation results in the cleavage of different cellular substrates that provokes those characteristic morphological changes that finally lead to cell death.

3.1.1 Caspases

Caspases constitute the main executors of the apoptotic process[235]. They are a group of highly specificity cysteine-aspartic proteases synthesized inactivated as zimogens (pro-caspases) that are progressively activated during the apoptotic process. Based on that, they can be grouped into initiator (caspase-2, -8, -9, -10) or effector (caspase-3, -6 and -7) caspases. The first ones are recruited differently through intrinsic or extrinsic pathway and are responsible

of activating of second ones. Effector caspases act on multiple and selective substrates ensuring the dismantling of the cell.

3.1.2 The intrinsic and extrinsic pathways

Effector caspases activation can be achieved, as mentioned above, through two pathways: the intrinsic and extrinsic pathways. The *intrinsic pathway* (**Figure 29,** *right*) is activated by intracellular stimulus such as hypoxia, DNA damage or reactive oxygen species (ROS)[241,242]. This stimulation leads to the permeabilization of the outer membrane of the mitochondria (MOMP) and the consecutive release of pro-apoptotic factors. Specifically, it courses with the release of cytochrome c from the mitochondria and the activation of caspase-9[243].

The *extrinsic pathway* (**Figure 29,** *left*) is activated by extracellular ligands that bind to cell surface transmembrane receptors (known as death receptors, DRs)[244,245]. In this case, ligand binding to DRs induces the recruitment of caspase-8[246]. Then, both activation of caspase-9 and -8 converge in the cleavage and further activation of the effector caspase-7 and -3 and the consequent cell death.

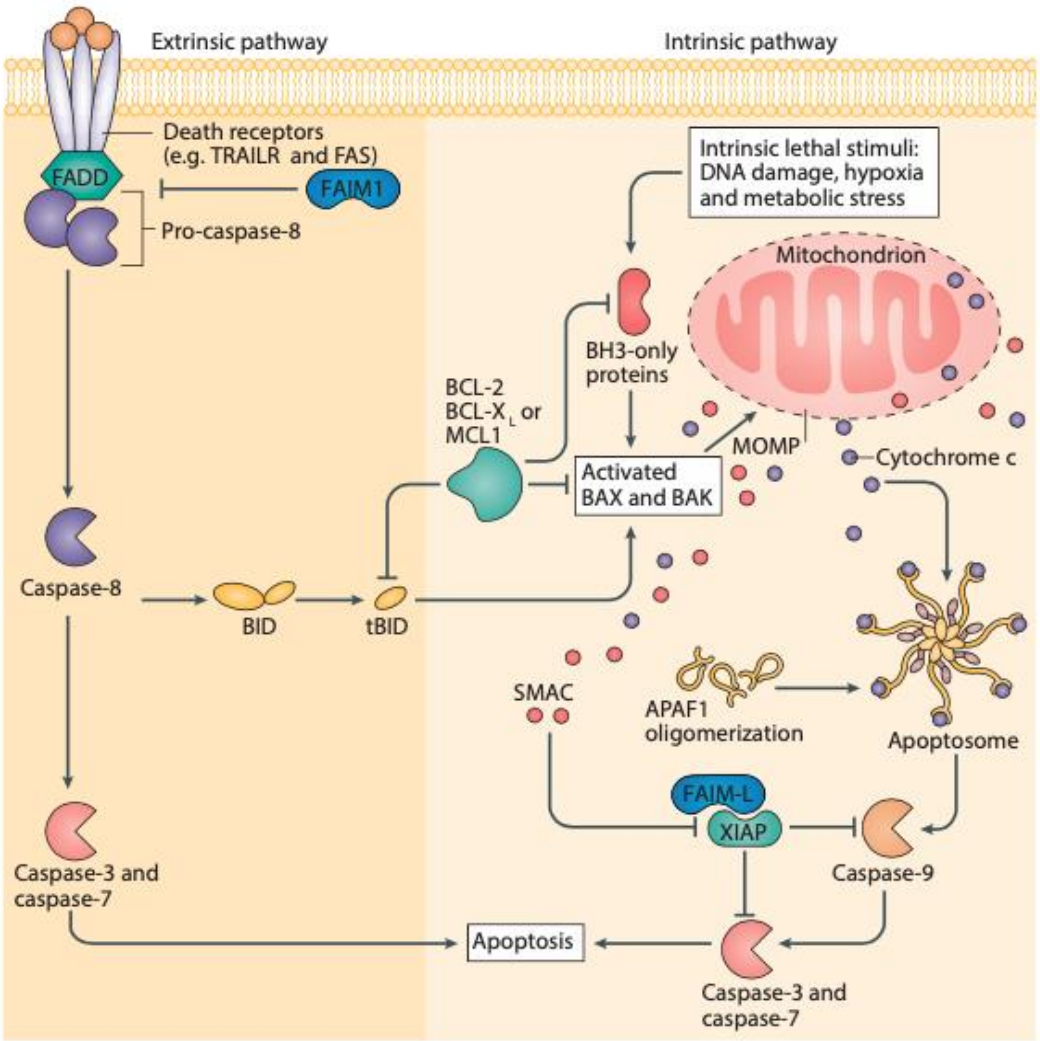

Figure 29: Extrinsic and intrinsic pathways of the apoptotic cascade. Ligand binding to death receptors (DRs) at the cell membrane or intracellular stimulus can activate the apoptotic process. Then, recruitment of caspase-8 and mitochondrial outer membrane permeabilization (MOMP) induce activation of caspase-3 and -7, which will mediate cell death. Importantly, mediators such as the BCL-2 protein family, SMAC, XIAP or FAIM1 (FAIM-S and FAIM-L) can regulate the process as indicated in the figure. Adapted from (247).

3.1.3 Pro- and anti-apoptotic regulators

During this cascade, the apoptotic process requires a fine control of all the steps. This is achieved by the participation of several pro- and anti-apoptotic molecules, which interfere at different levels in the chain and ensure its correct activation. In the following paragraphs, we will describe the IAPs and FAIM families, although this accurate regulation includes other mediators, in which we will not get focus, such as the Bcl-2 family, c-FLIP or the pro-apoptotic protein SIVA-1.

3.1.3.1 Inhibitors of apoptotic proteins: XIAP

Inhibitors of apoptotic proteins (IAPs) constitute a conserved family of proteins that carries its function by preventing caspases activation (Silke et al., 2014)[248]. To date, 8 human proteins have been identified to belong to the IAP family, being the X-linked Inhibitor of Apoptosis Protein (XIAP) the most relevant element. XIAP is a cytosolic protein that binds to caspase-3, -7 and -9 and potently blocks their activation. As other IAPs, XIAP presents a RING domain, which confers it a ubiquitin E3 ligase activity. Importantly, XIAP can use this E3 activity to ubiquitinate itself to provide an accurate regulation of its function and caspase inhibition.

3.1.3.2 Fas Apoptotic Inhibitory Molecules, FAIMs

Fas Apoptotic inhibitory molecules (FAIMs) are a family of proteins firstly reported to counteract apoptosis by inhibiting the activation of the family of DRs, Fas receptors. It is composed by FAIM1, FAIM2 and FAIM3, which inhibit Fas-induced cell death after the union of ligands such as TNFα, TRAIL or the Fas ligand, FasL. In this work, we are interested in FAIM1, which includes FAIM long (FAIM-L) and FAIM short (FAIM-S) isoforms, and which will be further explained in the following **section 3.2**.

Apart from those two families, other proteins regulate the apoptotic process, several of them indicated in **Figure 29**. They include the Bcl-2 family, which can either promote (BAK and BAX) or inhibit (BID and PUMA) mitochondrial permeabilization; c-FLIP, which can interfere in the binding of caspases to the DRs[249]; or SIVA-1, which can promote apoptosis by inducing the degradation of XIAP[250].

3.2 FAIM: more than an anti-apototic protein

The importance of apoptosis does not only rely in the regulation of cell death with a minimum environmental impact. Same machinery can also regulate other cellular processes without involving cell death. These events are mostly regulated by caspases but also include other apoptotic modulators that can participate in these non-cell-death-related processes (from now referred as non-apoptotic processes)[76,251]. They can mediate them either by regulating caspases or by presenting independent roles on their own. Among these mentioned regulators of apoptosis, FAIM develops an important role. FAIM has been object of study in our group for several years, and despite it was firstly defined as a DR-induced apoptosis inhibitor, it has become confirmed as an important regulator of a wide number of non-apoptotic functions. Here, we will review the basis of FAIM protein and its apoptotic and non-apoptotic functions.

3.2.1 FAIM1 gene

The human *FAIM1* gene is located in the long arm of the chromosome 3 (3q22.3) and contains six exons and three putative translational start sites. It is highly conserved between species and codifies for a group of proteins initially described as inhibitors of the DR Fas. Its expression is positively

regulated by the ERK pathway and negatively regulated by micro-RNAs such as miR-206, miR-1-3p and miR133b[252].

Alternative splicing of the exons 2a and 2b of FAIM1 gene results in 4 isoforms (**Figure 30**). FAIM-L and FAIM-S are the most commonly expressed isoforms and differ between them by the inclusion of the exon 2b. The incorporation of the exon 2a to these already mentioned isoforms was described in 2017 by our group[253] and generates the isoforms FAIM-L_2a and FAIM-S_2a.

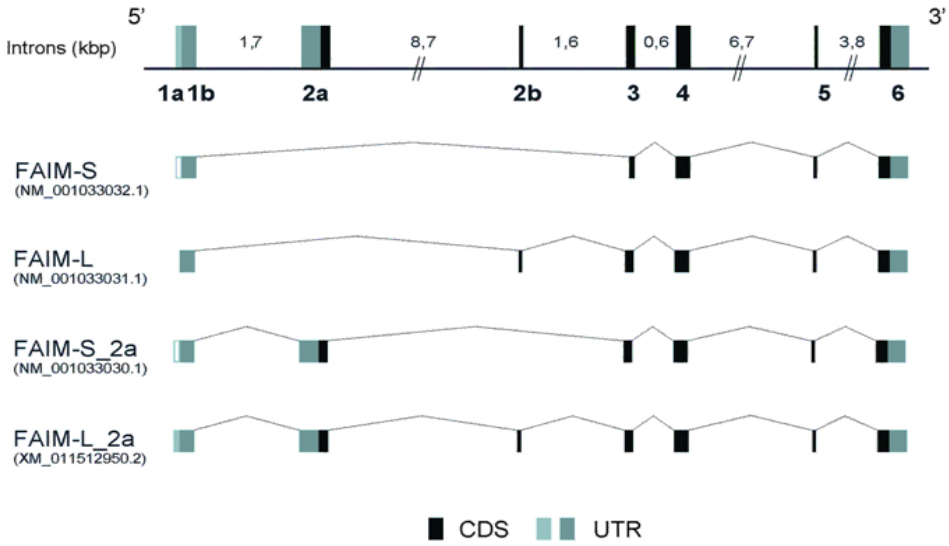

Figure 30. Schematic representation of FAIM isoforms. FAIM1 alternative splicing results in 4 isoforms, named following HUGO nomenclature Coding sequences (CDS, black boxes) and non-coding alternative exons (untranslated regions, UTR, light blue boxes) are indicted in both *FAIM1* gene and isoforms. Intron length (kbp) and GenBank accession number for all isoforms are also provided. Adapted from (253).

Focusing on FAIM-L and FAIM-S, the presence of exon 2b is translated to the incorporation of 22 additional amino acids to the N-terminal domain of the protein, which confers FAIM-L exclusive properties, as we will see next.

3.2.2 FAIM-S

FAIM-S is a 20 kDa soluble protein, highly evolutionary-conserved and ubiquitously expressed in cells. It was first identified by Schneider et al.,[254] in 1999. In this work, they isolated FAIM-S from B lymphocytes and described that it protected them against DR-induced (CD-40) cell death. Interestingly, FAIM-S does not exert death protection at DR level in neurons.

3.2.3 FAIM-L

FAIM-L is the obtained isoform after 2b exon inclusion, which as mentioned, results in the presence of 22 additional aminoacids at the N-terminal end as compared to FAIM-S. It was firstly described in 2001 by Zhong and colleagues[255]. FAIM-L is almost exclusively expressed in neuronal cells and becomes especially relevant during brain development. In fact, FAIM-L major levels of expression are reported in foetal and early post-natal stages, having established as an early and specific neuronal marker[256].

FAIM-L is able of inhibit apoptosis in neurons. This blockage of apoptosis can be produced at two levels. First, it can inhibit Fas DRs-induced cell death after FasL or TNFα stimulus by the prevention of caspase-8 activation (*see Figure 29*)[249]. Secondly, FAIM-L can exert its cellular protection by interacting with XIAP. XIAP presents E3 ligase activity, which can auto-ubiquitinate it. FAIM-L binds to XIAP and prevents its ubiquitination and subsequent proteasomal degradation[257]. This binding also avoids the interaction between XIAP and the pro-apoptotic protein SIVA-1, which by contrast is known to stimulate XIAP ubiquitination and degradation[250].

Through this mechanism, FAIM-L is able to, indirectly, regulate caspase-3 activation (**Figure 31**).

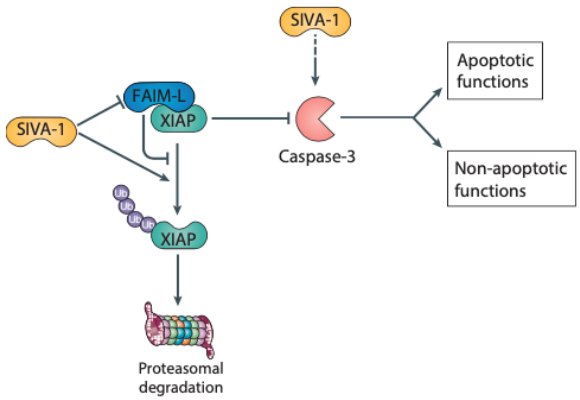

Figure 31. FAIM-L blocks caspase-3 activation through XIAP stabilization. Preventing from XIAP proteasomal degradation, and counteracting SIVA's function, FAIM-L regulates apoptotic and non-apoptotic functions of caspase-3. From Coccia, E. Thesis dissertation, 2020.

3.2.4 FAIM non-apoptotic functions

As we have mentioned at the beginning of this section, FAIM becomes an important regulator of several non-apoptotic processes, and it is able to perform them in different tissues. These functions become especially relevant in the nervous system, where FAIM helps to set the basis of neuronal differentiation and plasticity (**Box 3**). However, its wide participation is extended to peripheric tissues by the hand of FAIM-S. In order to better explore them, we have divided the functions in FAIM-S- and FAIM-L-specific and in those that are common for both isoforms.

BOX 3
SYNAPTIC PLASTICITY

Physical changes in the brain are the base of adaptation, learning and memory. While generation of new neurons mostly occurs under specific situations (e.g. brain recovery after a stroke), microscale modifications in the connections existing between neurons occur constantly. This concept is called **synaptic plasticity** and firstly emerged in 1894 when Santiago Ramon y Cajal proposed that memories were formed by strengthening of existing neuronal connections (Cajal, 1984)[192]. Nowadays several modifications are known to be responsible of this long-lasting synaptic plasticity (**Figure 32**):

- **LTP**: long-lasting increase in synapse strength after brief and repetitive periods of synaptic activity. Requires increases intracellular calcium and NMDA receptors activation.
- **LTD**: long-lasting reduction in synapse strength. Course with the dephosphorylation of the NMDA and AMPA receptors and its internalization from the cell membrane. Has been implicated in the removal of old memories and in executing motor memories.
- **Spine remodelling**: occurs with the induction of synaptic modifications (LTP or LTD). Spines constitute a platform for receptors, channels or scaffolding and signalling proteins which ensure synaptic transmission (193).
- **Pruning**: selective elimination of synapses in axons and dendrites. It is required for the establishment of functional neuronal connections. It is mainly mediated by growth factors and especially important during development.

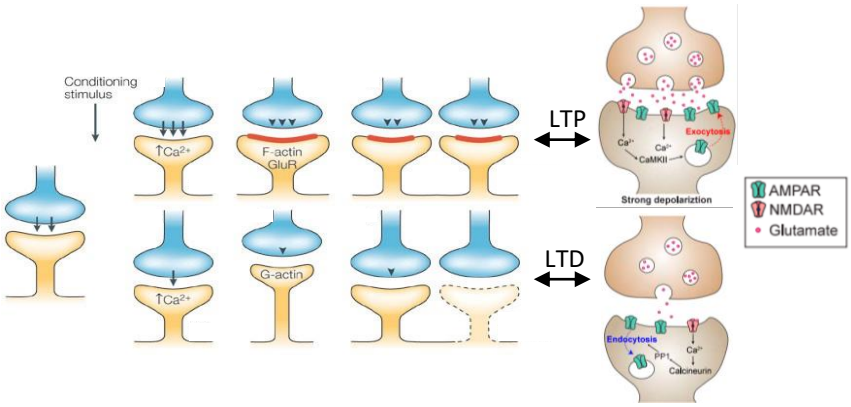

Figure 32. Long-lasting synaptic modifications are the basis of memory and learning. The ativity-dependent LTP and LTD processes and the generation of new spines or its pruning set up the basis of synaptic plasticity. Adapted from (394,395).

3.2.4.1 FAIM-S specific non-apoptotic functions

FAIM-S ubiquitous localization has involved it in insulin signalling regulation and energy homeostasis. In fact, the *FAIM1* KO mouse presents obesity, increased fatty acid synthesis and reduced insulin receptor β (ISRβ)[258,259]. In neurons, FAIM-S can regulate nerve growth factor (NGF)-dependent differentiation and branching in an ERK and NF-κB dependent manner[260].

3.2.4.2 FAIM-L specific non-apopotic functions

The neuronal specificity of FAIM-L, together with its ability to indirectly regulate non-apoptotic caspase-3 activation, places it as an important regulator of caspase-dependent plasticity processes in the brain (*Box 3)*.

Caspases has been reported to control dendrite spine density (caspase-2)[261], neurite outgrowth and arborization (caspase-9)[262], LTD and dendrite pruning. This las two processes, deeper explained just below, are controlled by caspase-3[76,263], and consequently, by FAIM-L (**Figure 33**).

3.2.4.2.1 Long-term depression, LTD

LTD involves a decrease in synaptic strength resulting from the internalization of the ionotropic glutamate receptors (AMPA and NMDA receptors) in the post-synaptic unit. Then, they can be recycled or eliminated in lysosomes[264]. Mattson and colleagues[79,265] first proposed that active caspase-3 could force LTD and this has been proved since then in several studies[76]. The mechanism is still unknown but seems to be controlled in an AKT- and GKS-3 dependent dependent way [73]. As we have already mentioned, FAIM-L inhibits caspase-3 activation, therefore, it is able to, through this mechanism, counteract caspase-3 activity and avoid LTD induction[266] (**Figure 33A**).

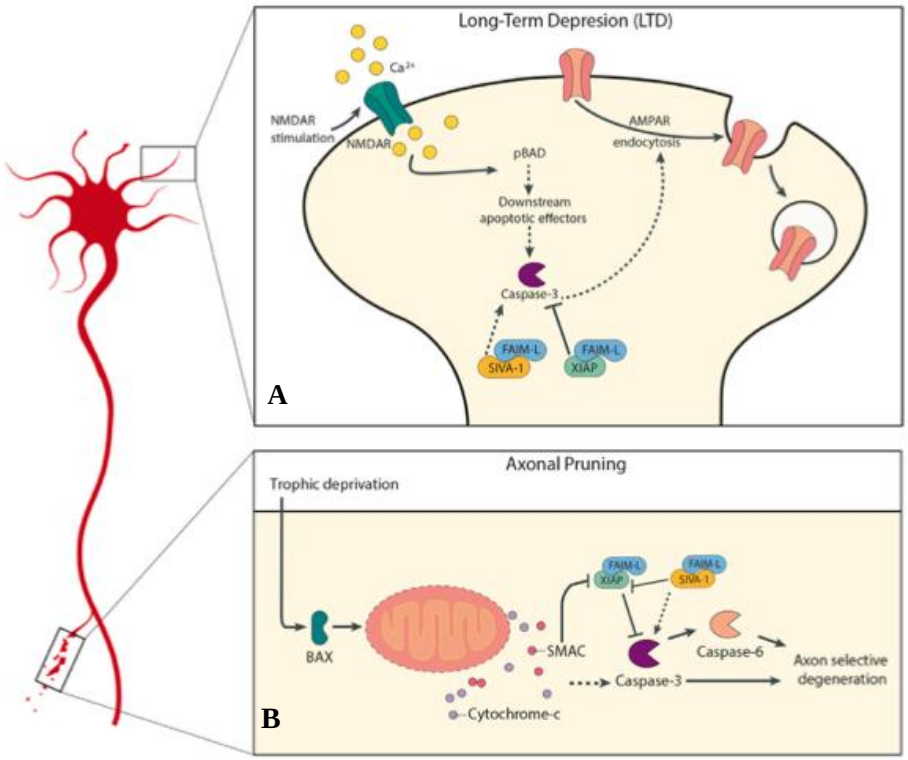

Figure 33. FAIM-L non-apoptotic functions. (A) During LTD, NMDA stimulation and calcium increase in the post-synaptic compartment activate the apoptotic machinery and caspase-3, resulting in AMPA receptor internalization. (B) Trophic deprivation results in the activation of caspase-3 through cytochrome c release, therefore inducing axonal degeneration. In both situations, the presence of FAIM-L stabilizes XIAP and indirectly blocks caspase-3 activation, avoiding both LTD and axonal pruning (250).

3.2.4.2.2 Dendritic pruning

Pruning and selective elimination of synapses in axon and dendrites are required for the establishment of functional neuronal connections. Pruning requires cytoskeletal destabilization and the degradation of axonal components. During development, NGF deprivation ensures axonal pruning and remodelling without causing neuronal death[267,268]. This mechanism converges in caspases-3 and -6 activation, together with cytoskeleton fragmentation and organelle degradation[269]. However, out of this context,

activation of axonal pruning can turn into axonal degeneration. Martínez-Mármol et al.,[266] described that FAIM-L was able to regulate this process, again through XIAP stabilization (**Figure 33B**).

3.2.4.3 Common non-apoptotic functions for FAIM

Apart from these relevant functions in the nervous system developed by both isoforms of FAIM, and the role of FAIM-S in lipid homeostasis, research performed by Dr. Rothstein's group in the past few years has proposed new and unique non-apoptotic functions for FAIM. By preventing ubiquitination and the consequent aggregation of proteins, it has been placed as a possible regulator of proteostasis under stress conditions. In that sense, they found that, under these mentioned stress conditions, whole FAIM-deficient (both isoforms) mice and cells lines presented accumulation of ubiquitinated proteins[270] while, by contrast, FAIM addition counteracted it. In fact, it was reported to reduce the intracellular accumulation of the protein responsible of the amyotrophic lateral sclerosis, the superoxide dismutase 1 (SOD1) [271] and, in collaboration with small HSPs, shifted to detergent-insoluble fractions and prevented the aggregation of Aβ[272]

3.2.5 FAIM-L and neurodegeneration

Properties and functions of FAIM, and specially FAIM-L, described during this section have placed it not only as an anti-apoptotic protein but also a regulator of proteostasis and synaptic plasticity. Importantly, these events are quite relevant in the pathology of neurodegenerative diseases. Then, in this last part of the section, we will comment several results obtained by our group that support the importance and contribution of this protein to neurodegeneration, specifically to retinopathies and AD.

3.2.5.1 FAIM and retinal degeneration

Recent studies from our group have also placed FAIM as potential regulator of retinal homeostasis and an early marker of retinal degeneration. Sirés et al,[273] demonstrated that absence of FAIM leads to a progressive photoreceptor death and a misfunction of ganglion cells in the retinas of FAIM KO mice. Also, these retinas present ubiquitin-positive aggregates and reactive gliosis (**Figure 34**). Recently, we have proved that these alterations are traduced to an impaired retinal functionality, with a malfunction of rod-driven pathways and a delayed dark adaptation (*article in review*).

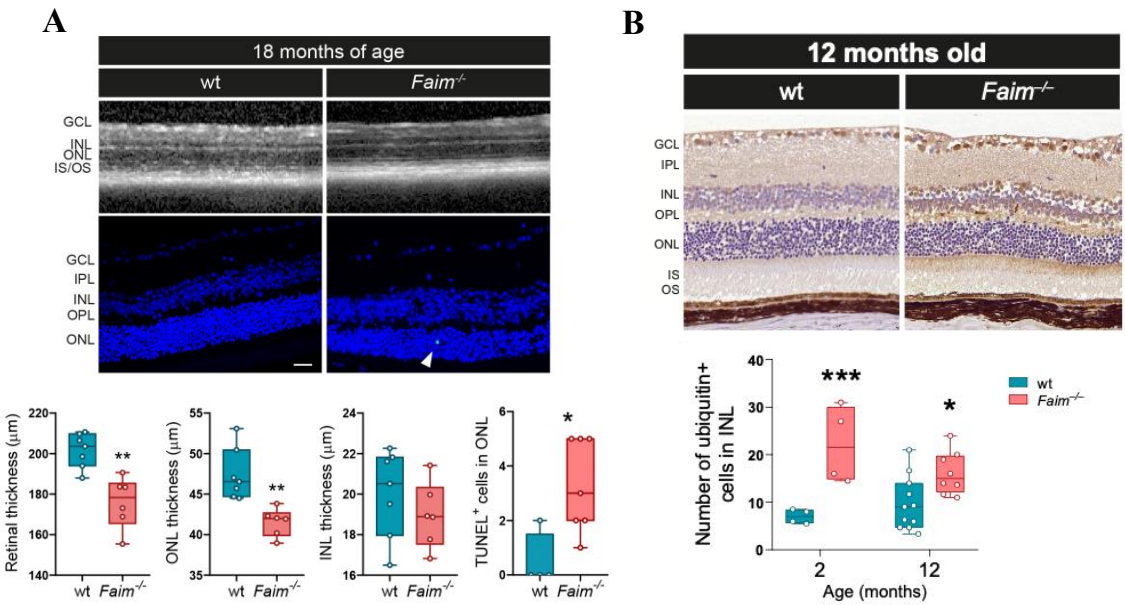

Figure 34. Photoreceptor degeneration and ubiquitin aggregates in FAIM1 KO mice (Faim−/−) retinas mice. (A) Retinas and retinal sections of wild-type (wt) and Faim−/− mice from 18-months-old mice visualized by the OCT technique (*upper panel*) and stained with TUNEL (green; *lower panel*). By this age, significant a reduction in the thickness of the ONL and a significative ($p < 0.05$) increase in the number of apoptotic nuclei of photoreceptors was observed in the 18-month-old Faim−/− mice. (B) Ubiquitin aggregation as increased in Faim−/− mice at 2 and 12 months-of-age, as shown by the quantification of the number of Ub positive cells. Representative images are shown for 12 months. GCL, ganglion cellular layer; IPL, inner plexiform layer; INL, inner nuclear layer; OPL, outer plexiform layer; ONL, outer nuclear layer; and IS/OS, inner/outer segment. Adapted from (273).

3.2.5.2 FAIM-L in Alzheimer's Disease

Importantly, first insights in this direction were made by our group, by establishing FAIM-L as a potential element in AD. Also, constitute the basis of the further analysis that has been made during this Thesis. Briefly, in 2015, Carriba et al.,[274] described that FAIM-L protein and mRNA levels were reduced at late stages in patients of AD and in the mouse model APPxPS1. Indeed, *in vitro* approximations allowed to demonstrate that FAIM-L was reduced in presence of Aβ-derived diffusible ligands (ADDLs) or cortical soluble fractions from the APPxPS1 mice. Finally, they also demonstrated that the protection afforded by TNFα against Aβ toxicity was only maintained in presence of FAIM-L, therefore, being deleterious upon FAIM-L reduction.

In summary, tauopathies are a group of neurodegenerative disease characterized by the progressive loss of protein and cellular homeostasis. Initially, alterations in the ubiquitination process led to the malfunction of the protein tau. Then, UPS dysfunction causes its aggregation into NFT, PiD or other fibrillar forms. Consequently, relevant cellular functions such as mitogenesis, DNA repair or synaptic functions become impaired. Neurons present a highly controlled machinery to maintain both cellular functionality survival. Caspase-3 and its indirect regulator FAIM-L can control from synaptic plasticity to apoptosis. Therefore, alteration in these proteins is related to neurodegeneration. In this Thesis, we have been centred in the role of FAIM-L in AD. Thus, along this work we will deeply analyse its contribution to the pathology of this disease.

HYPOTHESIS AND OBJECTIVES

V. HYPOTHESIS AND OBJECTIVES

In AD, neuronal dysfunction is highly dependent on the synaptic failure mostly caused by the synergy of both amyloid-β and tau pathology. Consequently, cellular homeostasis is lost, leading to progressive neuronal death and the subsequent cognitive decline characteristic of the disease. Caspases are important mediators of this scenario by being the principal executors of the apoptotic death process but also due to their participation in synaptic plasticity. In neurons, the antiapoptotic protein FAIM-L prevents XIAP ubiquitination and its further degradation. Through this mechanism, it can indirectly inhibit caspase-3 activation, therefore being able to protect from cell death but also to regulate caspase-dependent plasticity processes.

Based on the previous reports from our laboratory, which reported a reduction of FAIM-L levels in AD and given its capacities to regulate synaptic homeostasis and apoptosis, we postulate that FAIM-L reduction may be prompting AD progression. Therefore, we hypothesize that the exogenous recovery of FAIM-L levels at early stages of the disease may prevent synaptic and neuronal loss, and eventually, cognitive failure. Therefore, FAIM-L could be a potential therapeutic target for AD.

To prove this hypothesis, our main aim was to describe FAIM-L contribution to the progression of AD both by studying the cellular and molecular mechanisms in which it is involved and by determining the effect of its restoration mediated by adeno-associated viral expression using a mouse model of the disease. For that, we proposed the following specific objectives:

1. To perform a screening of FAIM-L levels among different AD mouse models and to select the most appropriate one for our main objective.

2. To relate the time-course of FAIM-L reduction with other pathological hallmarks in the selected model of AD.
3. To determine direct implications of FAIM-L loss-of-function in our mice by analyzing its capacity to regulate XIAP degradation and global ubiquitination.
4. To explore the cause of FAIM-L downregulation in AD and to determine possible functional associations between FAIM-L and AD pathological hallmarks based on its caspase-3 and ubiquitination regulatory capacities.
5. To explore the behavioral and biochemical implications of restoring FAIM-L expression *in vivo* to establish it as a possible therapeutic target for AD.

MATERIALS AND METHODS

IV. MATHERIALS AND METHODS

4. CELL LINES AND *IN VITRO* PROCEDURES

4.1 Cell lines

PC12 and HEK293T cells were used in this Thesis for different experimental purposes. They were commercially obtained from the American Type Culture Collection (ATCC, Manassas, VA, USA), amplified, and stored in liquid nitrogen.

4.1.1 HEK293T cell line

HEK293T cells are an epithelial-like variant of the Human Embryonic Kidney 293 (HEK293), an immortalized cell line derived from human embryonic kidney. HEK293T contain the SV40 Large T-antigen that enables them to produce recombinant proteins within plasmid vectors containing the SV40 promoter. For this reason, they are usually used for retroviral production[275,276]. HEK293T is an easily maintaining cell line, as well as highly resistant to stressful conditions, which ensures consistent results and high reproducibility. We used HEK293T cells for transient overexpression of proteins and for the study of molecular mechanisms that did not require a neuronal context (e.g. protein-protein interactions).

4.1.2 PC12 cell line

PC12 cell line is derived from a pheochromocytoma of rat adrenal medulla. Its neural crest embryonic origin confers it neuronal characteristics that can be enhanced under specific stimulus. The addition of NGF to cell media induces the acquisition of a dopaminergic neuronal phenotype in a reversible manner. Differentiated PC12 cells become able to synthetize and release dopamine and norepinephrine. They express neuronal markers such as NeuN and present

neurite outgrowth capacities[277]. Its unlimited proliferation capacity (compared to neuronal primary cultures), their homogeneity, their easy and efficient genetic manipulation, and its fast differentiation make this line a good *in vitro* model for studying neuronal events. For these reasons, in this Thesis we used PC12 cells for the understanding of Tau-related events under physiological and pathological conditions.

4.2 General cell culture maintenance and storage

For *general cells subculture*, ATCC recommendations were followed to preserve the characteristics of the original population and to avoid modifications of cellular genotype due to manipulation. Maximum passage numbers of cell lines and seeding densities for each cell type were determined according to this. For regular subculture (generally, once a week), cells were harvested, centrifuged for 3 min at 200 x g and seeded (generally a 1/5 dilution) in 100 mm Ø culture dishes with fresh media. Both cell types were maintained at 37ºC in 5% CO_2 atmosphere in a humidified incubator. Cell media components differ between both cell types:

- HEK293T cell media was composed by DMEM containing 10% heat-inactivated fetal bovine serum (iFBS) and Penicillin and Streptomocin (Pen/Strp) antibiotics (20U/ml; 20µg/ml)
- PC12 cells were maintained in DMEM supplemented with 6% iFBS, 6% heat-inactivated horse serum (iHS), 10mM HEPES and Pen/Strep (20U/ml; 20µg/ml).

For *cryopreservation of cell lines*, they were harvested and pelleted by centrifugation (3 min x 200 g). Then, cells were resuspended in iFBS containing 10% of dimethylsulfoxide (DMSO). DMSO is a cryoprotectant agent which prevents from damage and disruption of cell membranes. It helps

avoiding the formation of ice crystals during freezing procedure. Cells were aliquoted in 1 -ml cryovials and progressively cooled at -80ºC using a Mr. Frosty™ Freezing Container filled with 2-propanol, which ensures an optimal rate of cooling close to a -1ºC/min (Thermo-Fisher, Waltham, MA, USA). After 48h, cells were transferred to a liquid nitrogen tank for long-term storage.

For *thawing*, cells were withdrawn from liquid nitrogen and rapidly thawed in a water bath at 37ºC. To ensure the highest viability of cells and avoid DMSO-associated toxicity, cell suspension was diluted in the adequate cell culture media and centrifuged. Then, the supernatant was discarded, eliminating the residual DMSO, and cells were resuspended in fresh media and seeded into the most adequate culture dish depending on the quantity of cells.

The basic reagents used for cell maintenance and storage are resumed in the following **Table 5**.

Table 5: List of reagents used for cell culture general procedures

Reagent	Description	Supplier
Cell media		
DMEM	Dulbecco's Modified Eagle Medium	Thermo-Fisher
PBS	Phosphate saline solution buffer	Sigma-Aldrich
Cell media supplements		
iFBS	Heat-inactivated Fetal Bovine Serum	Thermo-Fisher
iHS	Heat-inactivated horse serum	Thermo-Fisher
HEPES	4-(2-hydeoxyethil)-1-Piperazineethanesulonic acid	Thermo-Fisher
Pen/Strep	Penicillin and Streptomicin antibiotics	Thermo-Fisher
DMSO	Dimethylsulfoxide	Thermo-Fisher

4.3 PC12 cell differentiation

For induction of neuronal phenotype in PC12 cells, they were seeded in pre-coated culture plates with Type I rat collagen (BD Biosciences; Franklin Lakes, NJ, USA) at a concentration of 10^5 cells/ml in maintenance media. In all conditions requiring coating, an adequate volume of collagen (1/50 dilution in sterile Milli-Q water) was added until complete coverage of the plate surface and allowed to polymerize for at least 20 min at 37ºC. Then, plates were washed twice with PBS 1X and cells were seeded. The next day, cells were deprived from serum (which was reduced up to 0,75% of both iFBS and iHS), and NGF (Sigma-Aldrich, St Louis, MO, USA) was added to a final concentration of 100 ng/ml **(Table 6).** Cells were considered as fully differentiated after 3 days of NGF addition, according to previous studies from the group[260]. In our experiments, this procedure was performed simultaneously with cell transfection as indicated in *section 1.4*.

Table 6: Comparison of the components of PC12 maintenance and differentiation cell media.

PC12 cell media components	
PC12 maintenance media	PC12 differentiation media
6% FBS	0.75% FBS
6% HS	0.75% HS
10mM HEPES	10mM HEPES
(+) Pen/Strep	(-) Pen/Strep
(-) NGF	(+) NGF
In DMEM	In DMEM

4.4 Cell transfection

HEK293T and PC12 cells were used to perform studies of protein-protein interactions, post-translational modifications of proteins and protein activity and as an approximation to study protein regulatory events. This was achieved by transient overexpression of the proteins of interest. Depending on the cell line, different protocols were used to efficiently deliver the corresponding plasmid DNA into the cell nucleus.

4.4.1 Cell transfection methods and cell culture specifications

4.4.1.1 Polyethylenimine

HEK293T cells were transfected using Polyethylenimine (PEI; Polysciences, Inc., Warrington, PA, USA). PEI-mediated transfection (**Figure 35**) involves the formation of nanoparticles called polyplexes, which include plasmid DNA.

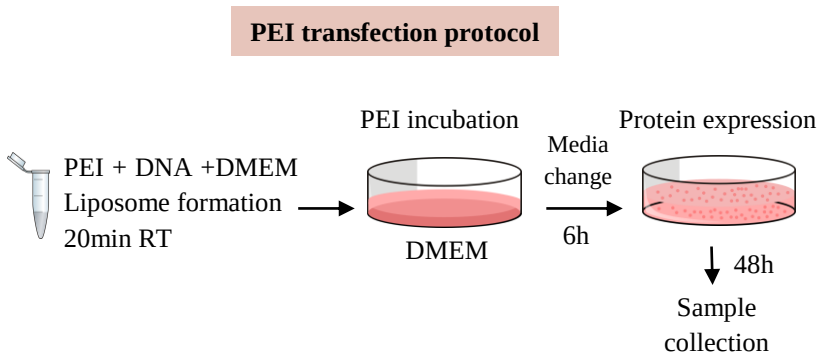

Figure 35. Graphical representation of PEI-mediated cell transfection. After *ex vivo* formation of polyplexes, they were added to cells and incubated for 6h. Then, media was changed, and cells were let overexpress proteins of interest for 48h.

For HEK293T cell transfection, cells were seeded in collagen pre-coated 100-mm Ø culture plates 24h before transfection. After this time and for each condition, a maximum of 15 µg of plasmid DNA and 75 µl PEI (final concentration of 133 µg/µl) were incubated in 3 ml of DMEM at RT.

Twenty min later, cell media was changed to DMEM (7 ml), and the mixture was added to the cell plate. After 6h, media was changed again, this time to new HEK293T full media without antibiotics. Cells were allowed to overexpress proteins of interest for 48h, then washed in ice-cold PBS 1X twice and processed as required for the corresponding subsequent experiment.

4.4.1.2 Lipofectamine2000

PC12 cells were transfected using Lipofectamine2000 (Lipo2000, Invitrogen, Carlsbad, CA, USA). Lipo2000 is a cationic liposome-based reagent. By forming these liposomes, it makes complexes with the nucleic acid molecules and overcomes the electrostatic repulsion of the cell membrane, ensuring its entrance to the cell. Lipo2000 technique (**Figure 36**) presents higher efficiency in neuronal-like cells and lower toxicity than other transfection methods.

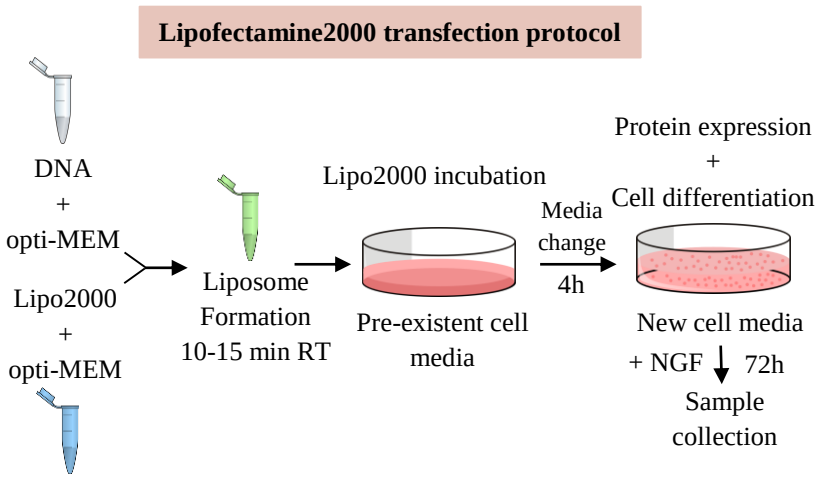

Figure 36. Graphical representation of Lipofectamine2000-mediated cell transfection. First, formation of liposomes was achieved by mixing Lipofectamine2000 reagent and de DNA plasmid for 10-15 min. Then, they were added to cells and incubated for 4h. Finally, media was substituted for PC12 deprivation media (+NGF), and cells were let overexpress proteins of interest and differentiate to neurons for 72h.

For this work, PC12 cells were seeded in collagen pre-coated 6-wells cell culture plates 24h before transfection. Then, for each condition, cells were transfected with a maximum of 5 µg of plasmid DNA and 12.5 µl of Lipo2000. Both reagents were diluted separately in 500 µl of Opti-MEM. Then mixed, incubated for 10 min at RT, and added to the cell plate. Transfection experiments in PC12 cells were performed simultaneously with cell differentiation. For that reason, 4h after transfection, the media was changed for new deprivation media (without antibiotics) and supplemented with NGF. Also, in these experiments, cells were let overexpress proteins for 72h, because is the time required for PC12 cells differentiation. Again, for collection, cells were washed in ice-cold PBS 1X twice and processed as required for the experiment.

Transfection procedures are synthesized in the following **Table 7**.

Table 7: Scheme of reagents and transfection protocols used for cell transient protein expression.

	PEI method (HEK293T cells)	Lipofectamine2000 method (PC12 cells)
Reagent preparation and liposome formation		
Reagent concentration	5 µl/µg of plasmid DNA	2.5 µl/µg of plasmid DNA
Plasmid DNA	15 µg	5 µg
Media	DMEM	Opti-MEM
Time of incubation	20 min	10 min
Reagent incubation in cells		
Time	6h	4h
Media	DMEM	Pre-existent media
Protein overexpression in cells		
Time	48h	72h
Media	HEK293T cell media (without antibiotics)	PC12 deprivation cell media (without antibiotics)

4.4.2 Plasmids

Plasmids used for this thesis are resumed in **Table 8.** Ubiquitin plasmid was kindly provided by Dr. Bohmann (University of Rochester Medical Center, New York, USA). Tau^{WT} plasmid was a kind gift from Dr. Ávila (Severo Ochoa Centre for Molecular Biology, Madrid, Spain). GSK3-β_HA (Ref# 14753) and Tau^{P301L} (Ref# 46908) plasmids were purchased at Addgene (Watertown, MA, USA). The rest of the constructs mentioned were previously generated in our laboratory.

Table 8: List of plasmids used in this Thesis. Backbone and tags of each plasmid are specified in the appropriate column.

Plasmid	Protein expressed	Backbone	Tag
FAIM-L_FLAG	FAIM-L	pcDNA3	3xFLAG
FAIM-S_FLAG	FAIM-S	pcDNA3	3xFLAG
XIAP	XIAP	pcDNA3	6xMyc
GSK3-β_HA	GSK3-β	pcDNA3	HA
Tau^{P301L}	EGPF-Tau^{P301L}	pRK5	EGFP
Tau^{WT}	Human Tau (1N2R)	pSGT42ATG	None
His-Ub	Human Ubiquitin	pCI	6xHis
FAIM-L_e2a_mCherry	FAIM-L	pcDNA	mCherry

Backbones of the plasmids mentioned were pCDNA3, pRK5, pSGT42ATG and pCI. The structure specifications of them are resumed in the following table (**Table 9**).

Table 9: Structure and specifications of the backbones used for the generation of the plasmids used in this thesis

Backbone	pcDNA3	pRK5	pSGT42ATG	pCI
Plasmid type	Mammalian expression	Mammalian expression	Unspecified	Mammalian expression
Promotor	CMV	CMV, SP6	SV40	CMV
Size	5446 bp	4754 bp	5449 bp	4006 bp
Bacterial resistance	Ampicilin	Ampicilin	Ampicilin	Ampicilin

For all the experiments involving transfections, control condition was added to the experimental design using a pcDNA3 backbone (empty vector).

4.4.3 Plasmid transformation and storage

DH5α competent cells (E. coli; Thermo-Fisher) were used for the generation of plasmid DNA libraries. Bacterial transformation was performed using manufacturer's instructions with some modifications. Briefly, 25 µl of competent cells were mixed with 5 µl of sample DNA and mixed gently. Cells were incubated on ice for 30 min. Then, cells were heat-shocked for 30 s using a 42ºC water bath and transferred to ice for 2 min. A volume of 250 µl of S.O.C medium (Thermo-Fisher) was added to the cells and shaken at 37ºC and 150 rpm in an incubator for 1 h. Two different volumes (20 and 200 µl) of cells from the transformation were plated in LB-agar plates (35g/L agar) and incubated inverted overnight at 37ºC. LB-agar plates were supplemented with ampicillin to ensure cell selection by antibiotic resistance (which depends on the backbone of the plasmid DNA; *see Table 9)***.** The next day, several colony-formation units (CFUs) were individually picked from LB-agar plates and independently suspended in 3 ml of LB broth medium (10g/L tryptone, 5g/L yeast extract, 5g/L NaCl) plus 1 µg/µl ampicillin (miniprep) and incubated in a shaker incubator at 150 rpm for 6-8h and at 37ºC. Fifty µl of each miniprep were mixed with 500 µl of a 50% glycerol solution (1:1 dilution in sterile Milli-Q water) and stored at -80ªC in cryovials to generate a glycerinate stock of each transformed competent cell.

4.4.4 Plasmid amplification

Plasmid amplification was achieved after bacteria growth (mini and maxipreps) followed by plasmid DNA extraction and purification. First, a small amount (1-2 µl) of the glycerinate stock was plated in an ampicillin LB-

agar plate and let grow over-night at 37ºC in the incubator. The next day, a miniprep was prepared by picking a single CFU and suspending it in 3 ml of LB broth medium plus ampicillin. Then, cells were incubated for 6-8h at 37ºC at 150 rpm. For extended amplifications, maxiprep was prepared by diluting 50 µl of the already grown miniprep in 250 µl of LB-broth plus antibiotic and incubated at 37ºC overnight in a shaker incubator at 150 rpm. Finally, for both mini and maxipreps, cells were pelleted by centrifugation for 30 min at 5.000 x g and plasmid DNA was extracted and purified using the commercial kit Qiaprep Spin Miniprep Kit (QUIAGEN, Hilden, Germany) or the Nucleobond Xtra Maxi kit (Macheley-Nage, Düren, Germany). Cells could also be stored as pellet at -20ºC for short-term periods before being processed.

5. ANIMALS AND *IN VIVO* PROCEDURES

5.1 PS19 mouse model and healthcare

The main animal model used in this Thesis was the Tau^{P301S} (line PS19) mouse model of tauopathy. Colony progenitors were kindly provided by Dr. Carles Saura (Neuroscience Institute, Department of Biochemistry and Molecular Biology, Unviersitat Autònoma de Barcelona (UAB), Barcelona, Spain) As explained in the introduction, this mouse was developed in 2007 by Virginia Lee and colleagues [92]. PS19 mouse expresses mutant human *Mapt* driven by the mouse Prnp promoter. The transgene encodes the 1N4R isoform of tau with the FTDP17-associated P301S mutation and results in a fivefold higher expression of mutant tau compared to the endogenous mouse protein. PS19 mouse was received and maintained in a C56BL/6J genetic background. Equal proportion of female and male mice were used in all the experiments, and their non-transgenic *wild-type* (WT) age-matched littermates served as controls.

All mice were bred and maintained in the Animal Core Facility of the Universitat Autònoma de Barcelona (UAB) and moved to the Animal Core Facility of the Universitat de Barcelona (UB), Mundet Campus for specific experimental procedures. Sex-matched mice were housed together in numerical birth order in groups of mixed genotypes (maximum five mice per cage), with access to food and water *ad libitum* in a colony room kept at 19-22ºC and 40-60% humidity, under a 12:12 h light/dark cycle.

All *in vivo* procedures were performed in compliance with the NIH Guide for the Care and Use of Laboratory Animals and approved by the local animal care committee of the Universitat Autònoma de Barcelona (3781-CEEA-UAB) following European (2010/63/EU) and Spanish (RD53/2013) regulations for the use and care of laboratory animals.

5.1.1 Genotyping

Mouse genotyping was performed by conventional PCR using primers to expand the exon 10 of mutant *Mapt* gene, only present in transgenic mice. First, DNA was extracted by digesting mouse tails in 300 µl of a lysis buffer containing 10 mM Tris-HCl pH 8, 100 mM NaCl, 10 mM EDTA, 0.5% SDS plus 3 µl of proteinase K (0.24 units/sample) (Sigma-Aldrich) and 50 µl of 3 M potassium acetate pH 5.5 (Invitrogen) for 90 min at 55ºC. DNA precipitation was achieved by adding the same amount of isopropanol (Sigma-Aldrich) to the supernatant and incubating the mixture overnight at 4ºC. The next day, samples were centrifuged at 1200 x g during 4 min and pellets were washed once in 300 µl of 70% Ethanol and let dry. Then, pellets were resuspended during 1h at 65ºC in 50 to 100 µl of TE buffer (10 mM Tris-HCl pH 8.0, 1 mM EDTA; Invitrogen). DNA was stored at -20ºC (or -80ºC for longer periods).

For conventional PCR, each condition was prepared by mixing 2 µl of DNA sample with 23 µl of Master Mix. An adequate volume of Master Mix (23 µl x Number of samples plus two additional conditions) was prepared as a stock and then distributed within the samples (**Table 10**). The primers used were purchased to Life Technologies (Carlsbad, CA, USA):

- P16134: 5´GGC ATC TCA GCA ATG TCT CC 3´
- P12473: 5´GGT ATT AGC CTA TGG GGG ACA C 3´
- OIMR8744: 5´CAA ATG TTG CTT GTC TGG TG 3´
- OIMR8745: 5´GTC AGT CGA GTG CAC AGT TT 3´

Table 10: Reagents used for the genotyping PCR reaction

PCR reaction reagents			
Stock Reagent [Concentration]		**Work Volume/sample [Concentration]**	**Supplier**
Master Mix	PCR buffer [10X]	2.5µl [1x]	Invitrogen
	dNTPs [10mM]	0.5µl [0.2mM]	Roche
	$MgCl_2$ [50mM]	1µl [2mM]	Invitrogen
	Primers [10µM]	1.25ul (each) [0.5µM]	Life Technologies
	Taq DNA polymerase [5U/µl]	0.25µl [0.05U/µl]	Invitrogen
	DNAse/RNAse free water	13.75 µl	Thermo-Fisher
DNA sample		2µl	-

PCR was performed using the 2790 Thermal cycler (Applied Biosystems, Walthman, MA, USA) and the following settings: 40 repeated cycles of 45 seconds at 94ºC, 45 seconds at 62ºC and 1 min at 72ºC. They corresponded to DNA denaturalization, primers annealing, and DNA elongation, respectively. Once finished, samples were incubated for 10 min at 72ºC **(Figure 37A).** Then, they were stored at 4ºC (or at -20ºC for longer periods) until being processed. Finally, 10X DNA gel loading dye buffer (Thermo-Fisher) was added to the PCR products (up to a 1X concentration) and ran in an agarose gel during at least 1h at 90 volts. Gel was prepared by dissolving agarose at 2.5% (NBS Biologicals, Huntingdon, Cambs, UK) in hot TAE 1X buffer (40 mM Tris-HCl, 2.5 mM EDTA, 1.14% acetic acid). Intercalant dye SYBER Safe (Invitrogen) was added to the mixture in a 1:1000 dilution and let it polymerize. Bands of the PCR product were visualized using U.V. light (GeneGenius Bio Imagen System, Syngene, Cambrigde, UK). Amplification of the exon 10 of Tau was evidenced by the presence of a 300bp band (**Figure 37B)**.

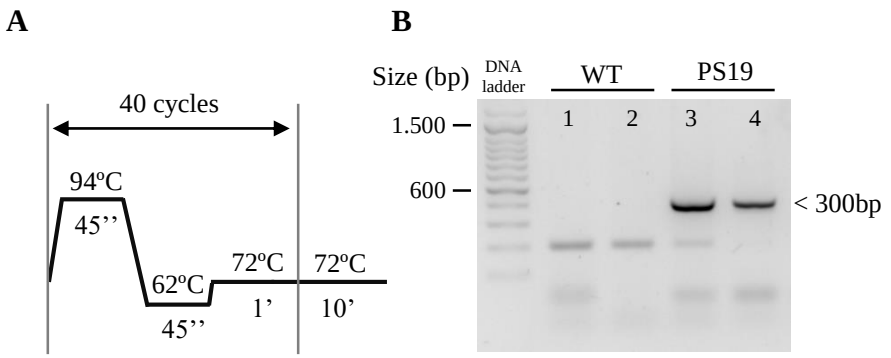

Figure 37. Mouse genotyping protocol. (A) Graphical scheme of PCR setting used for the amplification of exon 10 of *Mapt* gen. (B) PCR product visualization upon U.V. light in a 2,5% agarose gel. The 300bp band correspond to the presence of mutant Tau, therefore considering those animals as PS19 (lines 3 and 4), while the others were identified as WT (lines 1 and 2). 100 bp DNA ladder was used as weight marker (Invitrogen; 15628-019).

5.2 FAIM-L viral constructs design

For neuronal-specific overexpression of FAIM-L *in vivo*, FAIM-L sequence was cloned in adeno-associated viral vectors (AAVs) with the serotype 9 (AAV9). In this vector, FAIM-L sequence was linked to mCherry sequence by the self-cleaving peptide e2a (**Figure 38**). Once translated, several fragments can be obtained depending on the e2a cleavage ratio (FAIM-L_e2a_mCherry / FAIM-L_e2a / FAIM-L and mCherry).

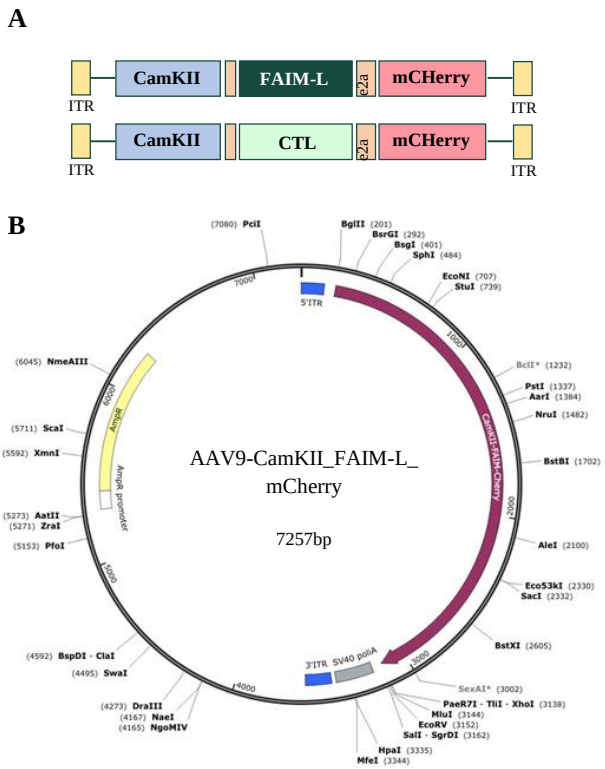

Figure 38. Structure of FAIM-L viral construct. (A) Graphical scheme of the construct incorporated to the AAV9 for overexpression of FAIM-L (dark green) or the control sequence (light green), in both cases under CamKII promotor control and linked to mCherry trough the e2a sequence (B) Map of the viral construct used for the incorporation of FAIM-L. Restriction sites, ampicillin resistance and mCherry location and length of the construct are indicated.

Expression of both proteins was under CamKII promoter regulation, ensuring only a neuronal expression pattern. As a control, an AAV9 construct substituting FAIM-L sequence for a non-coding control sequence was

generated. Both viral constructs were generated by the "Unitat de Producció de Vectors" from the Center of Animal Biotechnology and Gene Therapy at the UAB, Barcelona, Catalonia. Constructs were precipitated with polyethylene glycol (PEG) and purified by iodixanol gradient and stored al -80ºC in PBS-MK (PBS 0.1 M pH 7.4 plus 1 mM $MgCl_2$ and 2.5mM KCl) plus 40% of iodixanol. Viral constructs were aliquoted after the first thawing in order to avoid repeated cycles of freezing. Physical titers of AAV9-CamKII-CTL-E2A-mCherry (AAV:CTL) and AAV9-CamKII-FAIM-L-E2A-mCherry (AAV:FAIM-L) were 1.65E+13 genome copies (gc)/ml and 1,79E+13 gc/ml, respectively.

5.3 Intrahippocampal injection of adenoassociated viruses

Six-month-old WT and PS19 mice were weighted and deeply anesthetized with a mixture of oxygen and isofluorane (4-5% isofluorane for induction and 1-2% for maintenance; 21% oxygen; 1L/min flux) and placed in a stereotaxic apparatus for bilateral intrahippocampal injections of AAV9-expressing FAIM-L or CTL constructs. Injections were performed in the dentate gyrus (DG) and the CA1 region of the hippocampus (**Figure 39**). First, a small incision was performed in the head skin of the mice and once the cranium was accessible, two small cavities were made with a micro drill at the appropriate coordinates to facilitate the injection (**Figure 39B**). These coordinates were (relative to bregma): - 2 mm anteroposterior (AP); +/- 1.5 mm mediolateral (ML) and - 2.1 mm dorsoventral (DV) for DG injection; and -2 mm AP, +/- 1.5 mm ML and - 1.3 mm DV for hippocampal injection. DV coordinates were measured below dural surface with the incisor bar at 2,1 mm above the interaural line (**Figure 39A**).

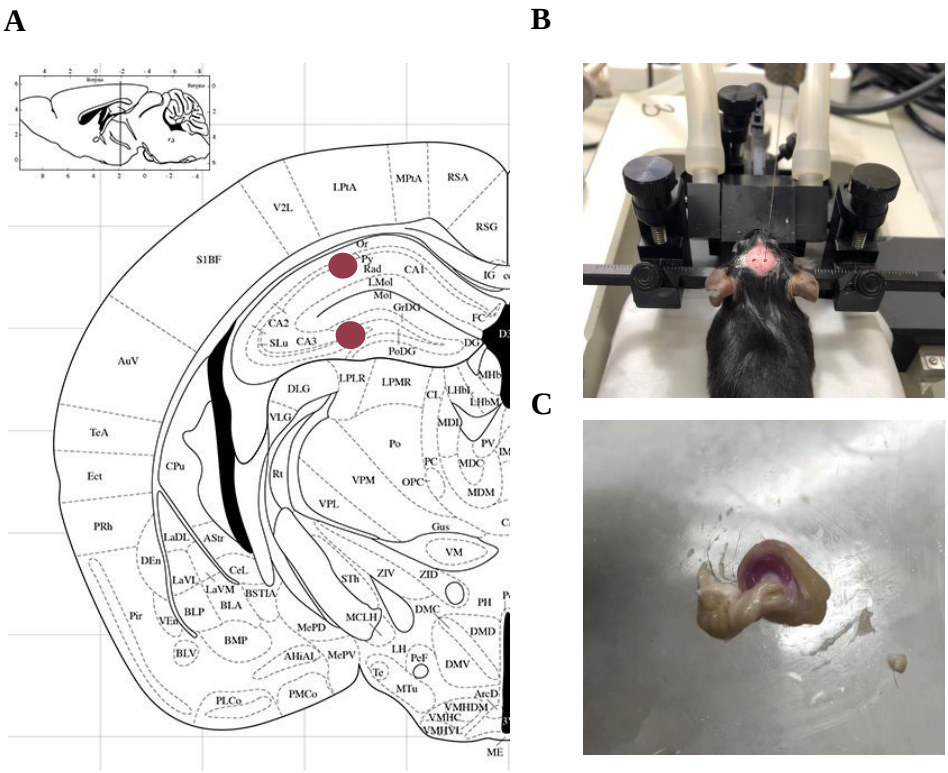

Figure 39: Representative images of intrahippocampal injection in mice. **(A)** Location of the coordinates selected for the injection in Mouse Brain Atlas (image adapted from (278). Coordinates (red dot) were determined using Mouse Brain Atlas tool designed by Matt Gaidica (http://labs.gaidi.ca). **(B)** Mice were fixed onto the stereotaxic apparatus provided with anesthetic and oxygen supply, as shown in the image. **(C)** Representative image of the area injected with the AAV, as shown by the red coloration of the hippocampus due to expression of mCherry.

The volume delivered in each location consisted in 1 µl (2 µl per injection and hemisphere) and was performed using a 10 µl-Hamilton microliter syringe at an infusion rate of 200 µl/min. The syringe was firstly placed in the deepest coordinate (DG injection; -2.1 mm DV). After the injection, it was left in the position for 2 min to ensure complete diffusion of the viruses and proceed to the next injection (hippocampal injection; -1.3 mm DV). Needle was slowly retracted each time, to the next position or from the brain to avoid liquid reflux. Both hemispheres were injected with the same AAV9 construct. Three

independent sets of animals with balanced sex, genotype and viral injection were used to cover all the experimental design.

5.4 Behavioral analysis

Three months after injections, a battery of cognitive tests was performed to evaluate hippocampal memory in injected mice. Until then, animal wellbeing was controlled monthly, registering body weight and spontaneous animal death.

5.4.1 Open Field test

To analyze spontaneous locomotion activity and anxiety, we used the Open Field (OF) test. OF consists of an open-top square arena measuring 40 X 40 X 40 cm in length, width, and height, respectively. Light intensity through the arena was maintained at 40 lux and the RT was kept at 19-22ºC and 40-60% humidity. For the test, animals were placed in the center of the arena and allowed to explore it freely for 30 min. Distal clues were positioned in one of the walls to guarantee accurate navigation of mice in their environment. Zones were divided into a central zone (3/4 of the arena) and a peripheral zone (1/4 of the arena) **(Figure 40).**

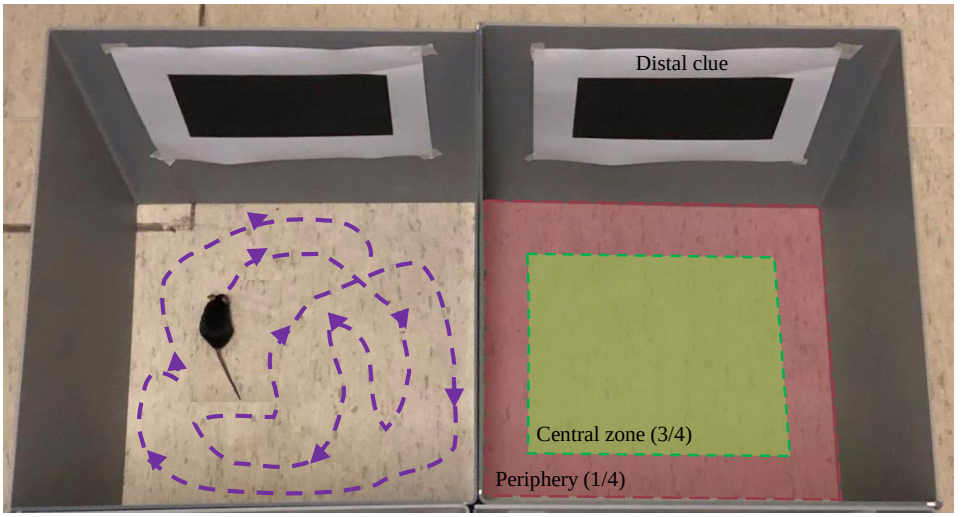

Figure 40. Open Field test set up. Animals were let to freely explore the arena and its activity (purple arrows) was recorded (left). The floor of the arena was divided into center (3/4) and periphery (1/4) (right). To provide spatial references to mice, a distal clue (black rectangle) was placed in one of the walls of the apparatus.

At the end of each trial, any defecation was removed, and the apparatus was cleaned with 30% ethanol for the next animal. Animals were tracked and recorded (in this and all the other tests) with SMART v3.0 junior software (Panlab, Barcelona, Spain). Distance travelled and the time expended in the different zones of the arena were recorded. Percentage (%) of time spent in the center [(Time in center of the arena / Total time) x 100], % of distance travelled in the center [Distance travelled in the center of the arena / Total distance) x 100], distance travelled each minute of the test, and the parallel index (measures the natural exploration capacity; 1.0 means walking straight) were measured.

5.4.2 NOL and NOR tests

To study hippocampal-dependent spatial and recognition memory, we used the Novel Object Location (NOLT) and Novel Object Recognition Tests (NORT). Both tests were performed in the same white arena and same

conditions of light and temperature abovementioned, with a first day of habituation, where mice were allowed to freely explore the arena for 30 min, and then, two days for the test (one day for the training and another one for the testing).

Spatial long-term memory was assessed using the NOLT. During the training session, animals were allowed to explore two identical objects placed in the far walls of the arena (4 cm distal to both walls) for 10 min (**Figure 41,** *left)*. One distal clue (**Figure 41;** *black box*) was placed in the same wall of the arena as the objects. Twenty-four hours later, one of the objects was moved to the opposite corner of the arena maintaining all the other conditions (**Figure 41,** *right*). Then, the same animals were let to explore the area for 6 min (testing). The new position was counterbalanced between mice. Preference for the new location was measured.

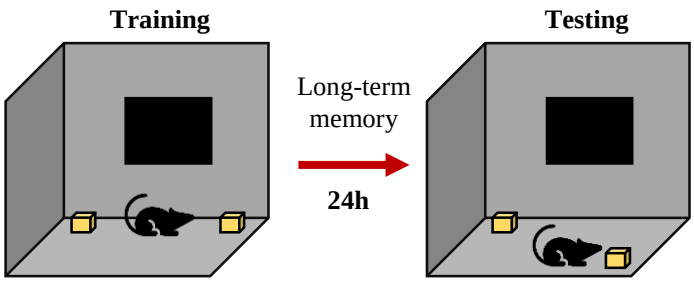

Figure 41: Novel object location test (NOLT). Representation of the squared arena with the distal cues and object location in each day of the test (training or test).

To study recognition memory, NORT was assessed. Same arena and conditions as before were settled, except for the distal clues. Two identical objects, different from those used in NOLT, were presented to each mouse during 10 min (training) (**Figure 42,** *left*). Again, twenty-four hours later, the same animals were tested for 6 min (test). In case of NORT, one of the objects was replaced for a new one (**Figure 42**, *right*). The new object was also

counterbalanced in order to exclude object preference due to non-controlled external stimuli (e.g. light, sounds…). Long-term memory was measured by analyzing the preference for the new object.

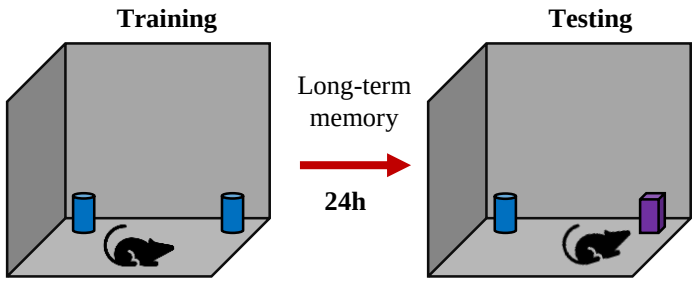

Figure 42: Novel Object Recognition Test (NORT). Representation of the squared arena with the distal cues and object location in each day of the test (training or test).

Preference for the new location or object were measured as the time exploring each object/time exploring both objects x 100.

5.4.3 T-MAZE test

Spatial long-term memory was also assessed using T-maze apparatus (**Figure 43**). T-maze consists in one vertical arm and two horizontal ones. Access to all arms is regulated by doors. The task was divided in two steps. For the training, mice were placed at the bottom of vertical arm of the T-maze. After 10 seconds, the guillotine door was opened and animals were let to explore freely during 10 min one horizontal arm of the maze, while the other remained closed. After training, animals were returned to their home cage.

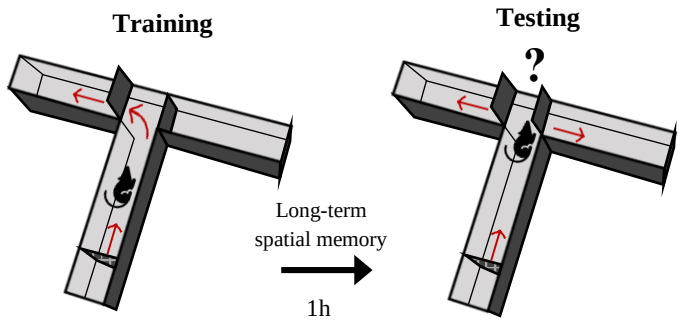

Figure 43: T-maze test (NORT). Representation of the T-maze apparatus and the door aperture sequence during training (left) and testing (right). Animals remained in the compartment of the vertical arm for 10s before the test started and then let explore freely.

The test was performed 1 hour after the training. Same procedure was executed but with the two horizontal arms opened this time. Mice were let to explore the full maze during 6 min. First arm choice, number of entries in each arm and distance and time exploring each arm were measured using SMART v3.0 junior software. The arm preference was measured as time exploring each arm/time exploring both arms x 100, and as distance in each arm/total distance x 100. First arm choice was also analyzed, considering as value of 1 the selection of the newly opened arm and value of 0 if animals firstly entered the already explored arm.

5.4.4 Y-MAZE test

To study working memory, spontaneous alternation performance was determined using the Y-maze test (**Figure 44**).

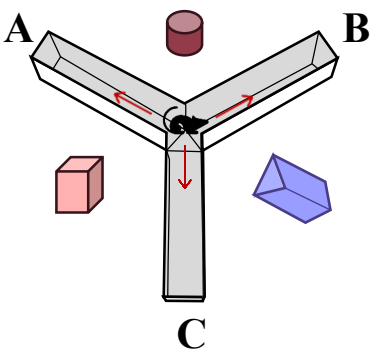

Figure 44: Y-maze Test. Graphical representation of the transparent Y-maze apparatus and distal clues location. Arms of the maze are named as A, B and C.

Each mouse was placed in the center of a symmetrical transparent Y-maze (three arms named as A, B and C of 35 cm length, 25 cm height and 15 cm width) and let explore freely through the maze during 10 min. Distal clues were placed between arms as indicated in Figure 44 to add a hippocampal memory component to the test. The sequence of entrances and total number of arms entered were recorded. We considered a complete arm entry when the hind paws of the mouse were completely placed in the arm. Percentage of spontaneous alternation was calculated as the number of triads containing entries into all three arms divided by the maximum possible alternations (the total number of arms entered – 2), as follows: (number of triads/total number of arms entered - 2) x 100. As the reentry into the same arm was off counted for analysis, the chance performance level in this task was 50% in the choice between the arm mice visited more recently (non-alternation) and the other arm visited less recently (alternation).

5.4.5 Passive Avoidance test

Associative memory was assessed using the passive avoidance test. This test is based in the passive avoidance paradigm, centered on the innate tendencies of mice for preference of dark areas and the avoidance of the bright ones. The paradigm was conducted using a 2-compartment box which allows light-dark conditions. One compartment was dimly lit (20 lux) and the other was brightly lit (200 lux). Both chambers were connected by a door (5 cm x 5 cm) **(Figure 45).**

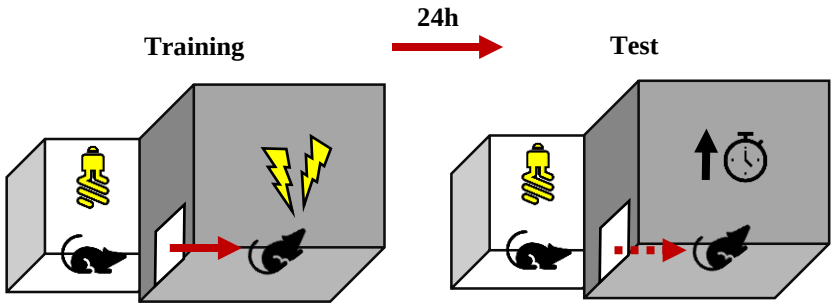

Figure 45. Passive Avoidance Test. Graphical representation of the 2-compatiment box used for analyzing associative memory in mice.

During training, mice were placed into the aversive brightly lit compartment. After 10 s, the door was opened, and animals were let to entry the preferred compartment (the darker one). Once the animal had all four paws inside the dark chamber, the door was closed, and mice were exposed to a mild foot shock (2 s, 1 mA intensity). To guarantee the association between the chamber and the footshock, animals remained twenty seconds in the dark compartment after the shock and returned to the home cage until test. The latency to enter the dimly lit compartment was recorded. Twenty-four hours after the training, animals were tested for retention, allowing us to analyze long-term memory and capacity of association. In the test, animals were returned to the brightly lit compartment and the latency to enter the shock-paired compartment was measured (retention or recall latency). Ten minutes were used as a time cutoff for the test. Animals that learned the task would avoid the location associated with the shock, even the light preferences, showing a greater recall latency. Time to enter was measured during training and testing, and recall latency was determined by comparing them and calculating the delay.

6. SAMPLE COLLECTION AND PROCESSING FOR PROTEIN EXTRACTION

6.1 Cell samples

Both PC12 and HEK293T cells were first washed with ice-cold PBS 1X to eliminate the residual cell media. Then, PBS was removed, and cells were immediately processed. A volume between 50-150 µl of SET lysis buffer (10 mM Tris-HCl pH 7.4, 150 mM NaCl, 1 mM EDTA and 1% SDS) was added to the cell culture plate. Using a cell scrapper, the cellular lysate was collected and sonicated for 15 s. The protein concentration was also determined using Dc protein assay kit and stored at −20°C until further processing.

6.2 Brain tissue samples from PS19 mouse model

Animals were deeply anesthetized with a mixture of isofluorane and oxygen (4-5% isofluorane; 1.8-2% oxygen) and transcardially perfused with ice-cold saline (0.9% NaCl solution). Brains were quickly removed and weighted after discarding the olfactory bulbs. The cortex, entorhinal cortex, hippocampus, striatum, and cerebellum were immediately dissected out and stored at -80ºC until being processed. For that, brain tissue was homogenized in ice-cold lysis buffer containing 1% Triton X-100, 50 mM Tris-HCl (pH 7.5), 10 mM EGTA, 150 mM NaCl and protease inhibitors (cOmplete, EDTA-free Protease Inhibitor Cocktail; 11873580001; Roche, Basilea, CH) and phosphatase inhibitors (Pierce Phosphatase inhibitor Mini Tablets; A32957; Thermo-Fisher). Samples were centrifuged at 16,000 x g for 30 min at 4ºC, the supernatants were collected, and the protein concentration was determined using the Dc Protein assay kit (Bio-Rad Laboratories, Hercules, CA, USA).

6.3 Samples from other Alzheimer's Disease mouse models

Brain tissue from mouse models different from our own colony of PS19 mice were provided from different researchers. Regarding *MAPT* mouse models, cortico-hippocampal samples from Tau^{VLW} mouse model were kindly provided by Dra. Marta Pascual and Dr. Eduardo Soriano (Department of Cell Biology, Physiology and Immunology, Universitat de Bacerlona (UB), Barcelona, Spain). Hippocampal samples from 3xTg mice were a kind gift from Dra. Sandra Villegas (Department of Biochemistry and Molecular Biology, UAB, Barcelona, Spain). PS19 hippocampal lysates (not originated from our colony) were a gift from Dr. Carles Saura. Hippocampal homogenates from *APP* mouse models were provided by Dra. Mar Hernández-Guillamon (Vall d'Hebron Research Institute (VHIR), UAB, Barcelona, Spain) in case of APP3 and 5xFAD, and by Dr. Javier Vitorica (Department of Biochemistry and Molecular Biology, UB, Seville, Spain) in case of APPsl samples and processed as indicated in *section 3.2*. The rest of samples were already lysed and re-quantified if required.

7. RNA ISOLATION AND QUANTIFICATION BY PCR ANALYSIS

7.1 RNA extraction

Total RNA from frozen hippocampus was isolated using RNAeasy kit (Qiagen) according to manufacturer's instructions. Briefly, tissue was homogenized under denaturing conditions and purified using spin columns by selective binding of the RNA to silica membranes. RNA was eluted using RNAse/DNAse-free double distilled water. Concentration and integrity of the RNA was determined using NanoDrop 2000 spectrophotometer (Thermo-Fisher). Purity of the RNA was determined by the 260/280 ratio (absorbance

at 260 and 280 nm). Only samples with a 260/280 ratio of 1.8-2.2 were included in the analysis.

7.2 Conversion of RNA to cDNA

At least 250 ng of RNA were reverse-transcribed using High cDNA Reverse Transcription kit (Thermo-Fisher; 4387406). Nine µl of each RNA sample was mixed with 11 µl of the RT Mix (previously prepared together as a stock for all the samples plus two additional samples by mixing 10 µl of the RT Buffer Mix plus 1 µl of the RT Enzyme Mix). Then, samples were subjected to reverse transcription, which was composed of two steps: 60 min at 37ºC and 5 min at 95ºC. Immediately after, samples were short-term stored at 4ºC or at -20ºC for longer periods.

7.3 Quantitative real time PCR (qRT-PCR)

qRT-PCR was performed in a 384 well-plate (BioRad, Hercules, CA, USA) by adding 4 µl of pre-diluted cDNA sample (at 1:5 ratio in RNAse/DNAse-free double distilled water) to the plate together with 6 µl of a mix containing 5 µl of iTaq Universal Syber Green Supermix (BioRad) and 0.25 µl of each appropriate primer (at 10 µM) in RNAse/DNAse-free double distilled water. The procedure was carried out using a CFX384 Touch Real-Time PCR System (BioRad) on standard conditions: 2 min at 50ºC, 10 min at 95ºC and 40 cycles of 15 seconds at 95ºC and 1 min at 60ºC, followed by 5 seconds at 95ºC, 5 seconds at 60ºC and 5 seconds at 95ºC. Each sample was measured in triplicate and mRNA expression was normalized against *Gapdh*. Primers used to perform RT-PCR are summarized in **Table 11**.

qRT-PCR data was analyzed using Bio-Rad CFX Maestro 2.2 Software (Bio-Rad, version 5.2.008.0222). Expression levels were expressed as mRNA relative units, corresponding to the relative fold-change in expression

determined by the comparative 2eΔΔCt method[279]. Ct corresponds to the cycle were the probe-induced fluorescent signal reaches a threshold value. ΔCt corresponds to the normalization of the Ct of the gene of interest to the housekeeping gene. ΔΔCt corresponds to the normalization of ΔCt to the control sample.

Table 11: List of primers used for qRT-PCR. Primers were designed using the NCBI primer designing tool Primer-BLAST, considering an optimal temperature of melting (Tm) of 60ºC and a product size between 80 and 150 nucleotides.

Gene	Primer sequence	
Faiml	Forward	5'-GCGCGGAGCAGACTGT-3'
	Reverse	5'-TCCAGGCTATAGAGAGGGCTT-3'
Mapt	Forward	5'-CCTGAGCAAAGTGACCTCCAAG -3'
	Reverse	5'- CAAGGAGCCAATCTTCGACTGG -3'
Gfap	Forward	5'-GGCGCTCAATGCTGGCTTCA-3'
	Reverse	5'- TCTGCCTCCAGCCTCAGGTT -3'
Gapdh	Forward	5'-TGTGAACGGATTTGGCCGTA -3'
	Reverse	5'- ACTGTGCCGTTGAATTTGCC -3'

8. WESTERN BLOTTING (WB)

Proteins were denatured using 4X SDS sample buffer (Tris-HCl pH 6.8, % Glycerol, 4,4% SDS, 10% β-mercaptoethanol, 0.1% bromophenol blue). For that, an appropriate volume of SDS sample buffer was added to the samples (*processed as indicated in 5.1*) up to 1X concentration and heated at 95ºC for 5 min. Unless otherwise indicated, 15 µg of protein per condition were resolved in denaturing polyacrylamide gels at constant voltage (90 volts for the first 10 min and 125 volts for at least 1h and 30 min). After the electrophoresis, proteins were transferred to nitrocellulose membranes (Hybond-C nitrocellulose membranes; GE Healthcare, Illinois, USA) at 100 volts during 1h and 30 min. After washing twice in PBS-buffered saline containing 0.1% Tween 20 (PBS-T) membranes were blocked during 1h at room temperature (RT) in a PBS-T solution containing 10% non-fat dry milk (PanReac). Then, membranes were blotted overnight at 4ºC with the primary antibodies detailed in **Table 12** in PBS-T plus 5% non-fat dry milk and 0.02% Sodium Azide. Primary antibodies used for detection of phosphorylations were diluted in PBS-T without containing non-fat dry milk.

Table 12: Primary antibodies used for Western Blot. A list is provided together with the expected molecular weight of the target protein, the dilution used, host species and the commercial identification. GAPDH was used as loading control. Regarding Tau antibodies, Tau5 recognizes total levels of tau independent of its phosphorylation status while AT8 antibody recognizes phosphorylated tau in Ser202 and Thr205. *MW*: molecular weight. *Abcam (Cambridge, UK); BD Bioscience (San Jose, CA, USA); Cell Signaling (Danvers, MA, USA); DAKO (Jena, DEU); Santa Cruz (Santa Cruz, CA, USA)

Antigen	MW (kDA)	Working dilution	Host	Source	Identifier
FAIM-L	23	1:1000	Rabbit	In House	Homemade
FLAG	10	1:10000	Mouse	Sigma-Aldrich	F3165
GAPDH	36	1:8000	Mouse	Enzo Life Sciences	ADI-CSA-335-E
GFAP	50	1:1000	Rabbit	Dako	Z033429.2
mGluR2	100	1:1000	Mouse	Merk Millipore	MAB397
HA	5	1:2000	Rat	Roche	1-867-423
mCherry	28	1:1000	Chicken	SICGEN	AB0081-200
Phospho-Tau (AT8)	49-75	1:250	Mouse	Thermo-fisher	MN1020
PSD95	95	1:1000	Mouse	Abcam	ab5417
Tau5	49-75	1:250-1:500	Mouse	Thermo-fisher	AHB0042
Ubiquitin	8.5	1:4000	Mouse	SantaCruz	sc-8017
XIAP	60	1:1000	Mouse	BD Bioscience	610762

After primary antibody incubation, the membranes were washed twice with PBS-T and incubated for 1h at RT with the appropriated horseradish peroxidase-conjugated secondary antibody diluted in 10% non-fat dry milk (**Table 13**).

Table 13: Secondary antibodies used for Western Blot. A list of the antibodies is provided, with the dilution used and the commercial identification. Anti-mouse IgG and Veriblot for IP detection reagents were used exclusively for IP assays (as they do not detect denaturalized IgG procedents from de IP assay).

Secondary antibody	Working dilution	Host	Source	Identifier
Anti-Chicken IgY-HRP	1:4000	Goat	Sigma-Aldrich	SAB3700226
Anti-Mouse IgG-HRP	1:4000	Goat	Sigma-Aldrich	A9044
Anti-Rabbit IgG-HRP	1:4000	Goat	Sigma-Aldrich	A0545
Anti-Rat IgG-HRP	1:4000	Goat	Sigma-Aldrich	A9037
Anti-mouse IgG for IP (HRP)	1:2000	Rat	Abcam	ab131368
VeriBlot for IP Detection Reagent (HRP)	1:200	-	Abcam	ab131366

After washing three times with PBS-T, the reaction was visualized with the Western Blotting Luminol Reagent (Santa Cruz Biotechnology; Santa Cruz, CA, USA). Chemiluminescence was captured using SuperRX Fuji Medical X-

RAY Films (Fujifilm Corporation, Minato, Tokyo, Japan). WB replicates were scanned and quantified using a computer-assisted densitometric analysis software (Fiji, Image-J, versionv1.53c, GNU General Public License).

9. SOLUBLE AND AGGREGATED FRACTIONS ISOLATION

Soluble Fractions from mouse hippocampus were obtained as previously described in ([280]) with several modifications. First, mouse tissue was processed and homogenized (in 100 µl per hippocampus) as mentioned just before. Then, supernatants (*S1 fraction*: combination of extracellular and cytosolic proteins and intracellular particulate proteins) were collected and pellets were re-extracted using buffered-SDS (2% SDS in 20 mM Tris–HCl, pH 7.4, 140 mM NaCl) and centrifuged at 4ºC for 1h at 100,000 x g. Finally, supernatants (*S2 fraction*: SDS releasable proteins) were also collected and resultant pellets (*P1 fraction*: highly aggregated proteins) were resuspended in a buffer containing 4% SDS plus 8M Urea and sonicated in short pulses for 15 s. All isolated fractions were immediately aliquoted and stored at −80°C until further processed by WB.

10. CO-IMMUNOPRECIPITATION ASSAY (co-IP) IN CELLS

10.1 Sample processing

After cell transfection with the appropriate plasmids, cells were collected in ice-cold PBS 1X and centrifuged for 5 min at 1,000 x g. Pellets were immediately lysed in immunoprecipitation (IP) buffer containing 150 mM NaCl, 20 mM HEPES, 5mM EDTA, 0.8% Igepal and 10% Glycerol pH 6.8 for 30 min in a rotary mixer at 4ºC. Lysates where then centrifuged, and supernatants were quantified. One mg of total protein was used for every condition in the IP assays, while 15 µg were processed as indicated for WB and used as a control of proper protein expression (inputs).

10.2 FLAG IPs

For FAIM co-IP assays, as FAIM-L and FAIM-S plasmids contain 3xFLAG tag, an IP of FLAG was performed. Briefly, lysates were incubated overnight at 4ºC in an orbital shaker with 40 µl of pre-diluted (1:1 ratio in IP buffer) FLAG M2 Affinity monoclonal agarose beads (Sigma-Aldrich; F2426). The next day, beads were pelleted by short centrifugations (1 min; 1,000 x g) and washed in 200 µl of IP buffer twice, afterwards in IP buffer/TBS (1X) in a 1:1 ratio twice, and finally in TBS 1X four times. Elution was performed by competition using 3xFLAG peptide (Sigma-Aldrich; F4799). For that, beads were resuspended in 37.5 µl of a mix of TBS 1X and 3xFLAG (to a final peptide concentration of 150µg/ml) and incubated on ice for 30 min. Supernatant was finally collected by short centrifugation (1 min; 1000 x g) and a volume of 12.5 µl of SDS sample buffer was added and boiled for 10 min.

10.3 Tau IPs

For tau co-IP assays, a pre-clearing step for avoiding unspecific unions was required before antibody incubation. Samples were incubated during 4h with mouse-IgG (0.5 µg/mg protein) and 20 µl of pre-diluted (1:1 ratio in IP buffer) Protein-G Sepharose FastFlow. Then, supernatants (diluted in 700 µlof IP buffer) were incubated overnight at 4ºC in a rotary mixer with anti-Tau5 antibody (1µg/mg protein) or mouse-IgG at the same concentration (Santa Cruz; sc-2025) as a negative control. The immune complexes were precipitated by the addition of 40 µl of diluted Protein-G Sepharose FastFlow (Sigma- Aldrich; GE17-0618-01) and its overnight incubation in an orbital shaker at 4ºC. Beads were collected by centrifugation (1 min; 1,000 x g) and washed in 200 µl IP buffer eight times. Beads were finally resuspended in 37.5

µl of IP buffer plus 12.5 µl of SDS buffer, boiled for 10 min at 95ºC and collected with an insulin syringe.

The total volume of the immunocomplexes and the inputs of both IP assays were resolved by SDS-PAGE in 12% acrylamide gels and analyzed by WB (*see section 10.3*).

11. PROTEIN UBIQUITINATION ANALYSIS IN CELLS

Ubiquitination status of Tau and XIAP proteins was assessed *in vitro* by immunoprecipitation of ubiquitinated proteins using the Ubiquitination Assay developed by Tansey Laboratory (Department of Cell and Developmental Biology, Vanderbilt University Medical Center, Nashville, TN, USA). For this assay, every condition was also transfected with the 6xHis-Ubiquitin plasmid. This way, once the plasmid is translated, 6xHis-Ubiquitin is covalently attached to ubiquitin-target proteins, allowing us to efficiently immunoprecipitate ubiquitinated proteins by specifically targeting the tag His instead the endogenous ubiquitin.

11.1 Sample processing

Briefly, HEK293T were transfected as described before with the appropriate plasmids (one 100 mm culture plate per condition). After 48h of transfection, cells were treated with 10 µM MG132 for 6h to inhibit the proteasome and avoid the degradation of ubiquitinated proteins. Then, cells were collected as usual. Pellet was resuspended again in 750 µl of ice-cold PBS 1X and 20 µl of the suspension was separated and processed as indicated for WB (input). Cells were centrifuged again and lysed in 750 µl of Buffer A (6 M Guanidine-HCl, 0.1 M NaH_2PO_4, 10 mM Imidazole; pH 8). Lysates were then sonicated in short pulses for a total of 15s.

11.2 Ubiquitin Assay

To purify ubiquitinated proteins, 50 µl of pre-diluted (1:1 ratio in buffer A) ProBondTM Ni-NTA agarose resin (Thermo-fisher Scientific; 46-0019) were added and let bind to 6xHis tag of the ubiquitin for 4h at RT in an orbital shaker. Later, resin was repeatedly precipitated (by centrifugations of 1min, 1,000 x g) and washed in the following order: twice in Buffer A, twice in Buffer A/T1 (1:3 ratio) and two more times in Buffer T1 (25 nM Tris-HCl, 20 mM Imidazole, pH=6,8). Finally, ubiquitinated proteins were eluted by adding 50 µl of a mix of 250mM Imidazole and SDS sample buffer and boiled for 10 min at 95ºC and then collected using an insulin syringe. Eluted proteins were considered as ubiquitin pull-down and the whole samples were ran in a WB all together with the inputs.

12. Mass Spectometry (MS) and protein identification

To identify potential partners of FAIM-L, we performed a proteome-wide analysis using co-immunoprecipitation coupled to mass spectrometry (IP-MS). Briefly, PC12 cells were transfected with FAIM-L_FLAG or pCDNA3 (as a negative control) and a FLAG IP was performed (*as described in section 6.2*). Then, samples were subjected to MS at the Proteomic Unit from the Centre for Genomic Regulation (CRG) at the Parc de Recerca Biomedica de Barcelona (PRBB), Barcelona Spain.

12.1 Bioinformatic analysis of MS

Members from the Proteomic Unit provided us a filtered and accurate list of the peptides (and the corresponding proteins) detected by the MS assay. Only those proteins detected in two independent samples of FLAG

immunoprecipitates but not in the negative control (pCDNA3 condition) were considered as potential partners for FAIM-L. A Gene Ontology (GO) analysis was performed with this data and the enriched pathways (KEGG and compartment categories; strength≤0.05) were determined. Considering this results more relevant proteins were summarized and information regarding to the percentage of protein covered and the peptide spectrum matches (PSMs) were provided.

13. GOLGI-COX STAINING AND ANALYSIS

Golgi-Cox staining allows the visualization neuronal morphology and dendritic spines by staining them with silver and mercury deposits through a mechanism still unknown[281,282].

13.1 Solutions preparation and storage

Golgi-Cox solution consists in a mixture of three reagents: (A) 1% potassium dichromate, (B) 1% mercury chloride and (C) 0.8% potassium chromate. All reagents were initially prepared in a 5% stock solution in distilled water and mixed properly up to the desired concentration. For 500 ml of Golgi-Cox solution, 80 ml of C were diluted in 220 ml of distilled water. Then, A and B were mixed in a 1:1 ratio (100ml for each reagent) and poured into C dilution under continuous stirring. Solution was stored in darkness and at RT at least five days to allow precipitate formation, and then transferred to another bottle avoiding the precipitate and stored in the same conditions up to 1 month.

13.2 Brain tissue staining

For staining, one hemisphere per animal was transferred immediately after euthanasia, into a urine pot and incubated in 10ml of Golgi-Cox-Solution in the dark and RT for 15-20 days. After incubation, brains were transferred to a

cell dish plate washed in continuous agitation; first, in distilled water three times for 2 min each and, second, 30 min in 90% ethanol to eliminate the excess of solution and to avoid needle-like precipitates. Then, brains were transferred to 70% ethanol and cut using a vibratome in 200 μm slices. Vibratome chamber was filled with 70% ethanol solution. Slices were collected in culture plates also filled with 70% ethanol and immediately processed. Slices were incubated in fresh 16% ammonia solution for 60 min. Then, samples were washed once for 2 min in distilled water and fixed with 1% sodium thiosulfate ($Na_2S_2O_3$) solution for 7 min. After a final wash of 2 min in distilled water, slices were mounted in super-frost Leica Bond coverslips (Leica, Wetzlar, Germany; S21.2113.A) and let dry. Dehydration of samples was performed using a battery of 3 min incubations in different percentage of ethanol solutions (50%, 70%, 80%, and 100% ethanol), two incubations of 5 min in a 2:1 Isopropanol:100% ethanol, once in 100% isopropanol and twice in 100% xylol. Finally, slides were mounted in DPX.

Stratum radiatum dendrites from hippocampal CA1 pyramidal neurons were analyzed using x 100 oil objective of Nikon Eclipse E600 light microscope. Bright-field images were captured with a Nikon DXM 1200F digital camera attached to the microscope. Only fully impregnated pyramidal neurons with their soma entirely within the thickness of the section were used. Z-stacks of each dendrite were taken every 0.2 μm, at 1024 × 1024 pixel resolution, yielding an image with pixel dimensions of 49.25 × 49.25 μm. Z-stacks were deconvolved using the Huygens software (Scientific volume imaging, Hilversum, Netherlands) to improve voxel resolution and to reduce optical aberration along the Z axis. Only fully visible segments of proximal apical dendrites were selected for the analysis of spine density. For that, segments overlapping with other branches were avoided in order not to obscure visualization of spines. Segments either ‘parallel’ to or ‘at acute angles’

relative to the coronal surface of the section were also discarded to avoid ambiguous identification of spines. Given that spine density increases as a function of the distance from the soma, reaching a plateau of 45 μm away from the soma, only dendritic segments of basal dendrites 45 μm away from the cell body were analyzed. Also, the first 10 μm of the dendrite were discarded and only spines arising from the lateral surfaces of the dendrites were included in the study. The total number of spines and the longitude of the dendrite analyzed were obtained using the cell counter tool in the ImageJ software. At least 60 dendrites per group from at least three mice per genotype were counted and expressed as a ratio of number of dendrites/μm of dendrite.

14. STATISTICAL ANALYSIS

Data was analyzed using GraphPad Prism v9 (GraphPad software, La Jolla, CA, USA). All the results are expressed as mean ± SEM. Statistical tests were performed using: Student's t test (for comparing one variable between two groups), one-way ANOVA (for one variable between more than two groups) and two- or three-way ANOVA for multi-component variables between more than two groups. ANOVA tests were followed by Bonferroni's post hoc test. For XY statistical analyses, simpler lineal regression was performed. Outlier values were excluded from the analysis according to the ROUT test (Q=1%). For *in vitro* experiments, unless otherwise stated, at least three independent replications of the same experiment were performed to confirm the results. A 95 % confidence interval was used and values with a $p < 0.05$ were considered as statistically significant.

RESULTS

V. RESULTS

15. FAIM-L reduction is linked to the presence of tau pathology in ad mouse models.

As previously mentioned, the first linkage of FAIM-L to neurodegenerative diseases was assessed by our group. We described the downregulation of FAIM-L levels in AD patients and in the AD mouse model APPxPS1[274]. Thus, we wanted to further analyse the consequences of its reduction in the progression of AD. To achieve this, we decided to search for any involvement of FAIM-L loss-of-function in the pathological events of AD by using mouse models as the main tool.

In their work, Carriba et al, reported FAIM-L reduction in the APPxPS1 mouse model. However, these mice do not report neuronal loss and its maintenance is high time- and cost-consuming. To accurately find the most appropriate model for our study, we performed a two-criteria selection based on the early manifestation of synaptic and cognitive deficits and the presence of neuronal loss. Additionally, we wanted to address both hallmarks of AD by including mouse models with Aβ and tau pathology or the combination of both. Finally, as diverse mutations have different impact depending on the level where pathways are altered (e.g. increasing total production of Aβ vs. directly modifying Aβ cleavage, or affecting differentially to tau isoforms), we also considered the nature of the mutations present. Then, we performed a first screening using samples from the 5xFAD, APP23, APPsl, PS19, Tau^{VLW} and 3xTg mouse models. We determined FAIM-L protein levels in cortico-hippocampal or hippocampal lysates from these mice at ages where the pathology was already present.

WB analysis revealed that only those mice showing tau pathology presented a decrease in FAIM-L levels comparing to its WT littermates. We observed a decrease of FAIM-L levels in PS19 by 2 months of age, in Tau^{VLW} at 8 months old, and in 22-month-old 3xTg mice (**Figure 46A**).

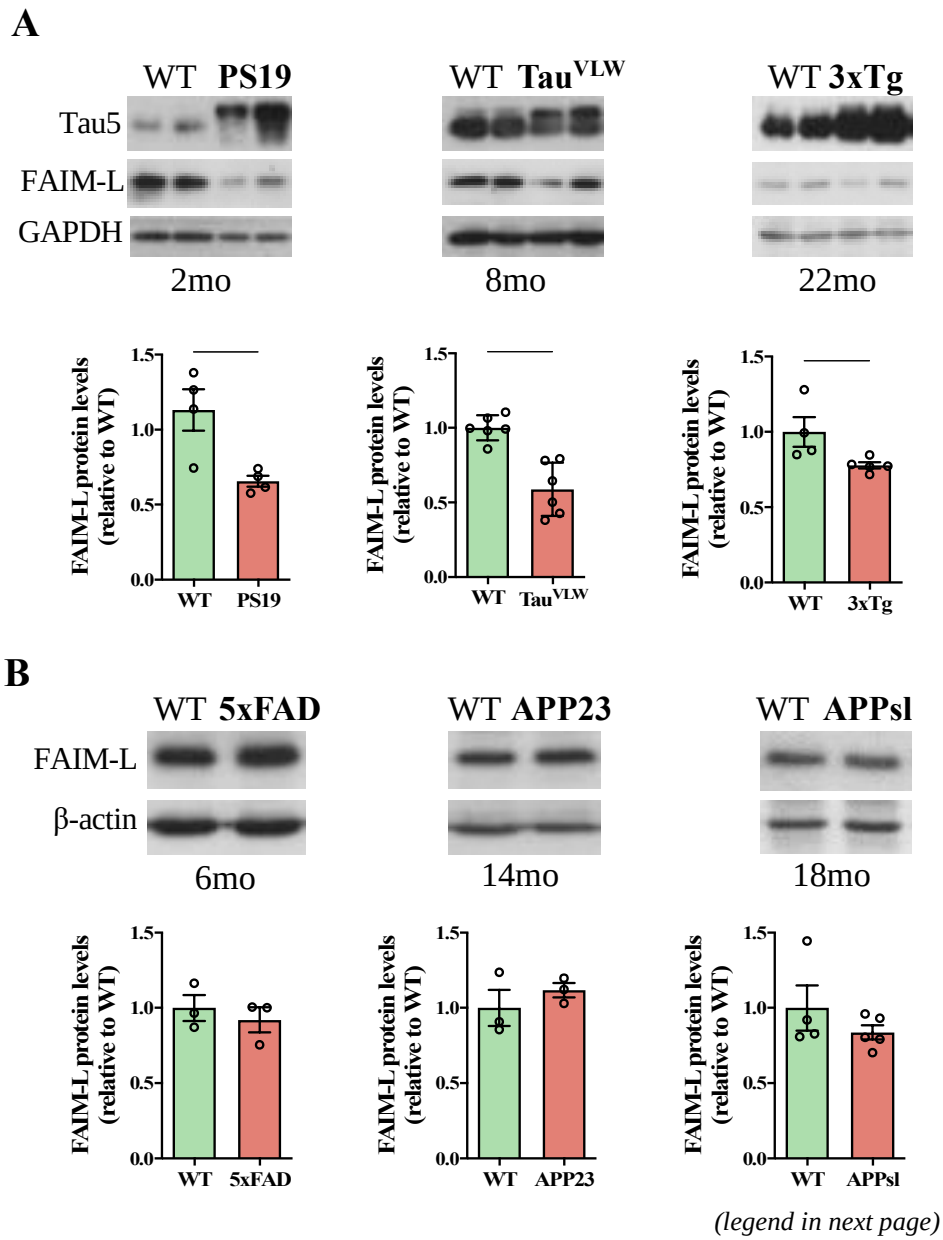

(legend in next page)

Figure 46. FAIM-L is reduced only in AD mouse models that present tau pathology. FAIM-L and total tau protein levels were analyzed by WB in protein extracts obtained from hippocampus of WT and AD mouse models at ages where the pathological alterations have been reported (mo, months): (A) PS19 (2mo), VLW (cortico-hippocampal samples; 8mo) or 3xTg (22mo), and (B) 5xFAD (12mo), APP23 (14mo) or APPsl (18mo) mice. Graphs represent arbitrary units (obtained by densitometric analysis of immunoblot images; (A) FAIM-L/GAPDH and (B) FAIM-L/β-actin ratio) and are compared to their WT littermates. Data is shown as mean ± SD (n=3-6). Representative immunoblots are shown. *$P < 0.05$; *** $P < 0.001$ (Student's t test). Each point corresponds to the value from an individual mouse.

In contrast, results showed that FAIM-L levels remained unchanged in the *APP* mouse models analysed. Neither the exhibition of a highly aggressive Aβ pathology (as happens in the 5xFAD model), nor the presence of the same *APP* mutation present in the APPxPS1 mice (as happens in the APPsl model) were able to induce a reduction of FAIM-L levels in these models. Twelve-month-old 5xFAD mice, 14-month-old APP23 mice and 18-month-old APPsl mouse models presented equivalent levels of FAIM-L to their WT littermates (**Figure 46B**).

16. FAIM-L reduction occurs simultaneously with an abnormal increase in tau phosphorylation

This screening reported an exclusive reduction of FAIM-L in *MAPT* mouse models. Considering that our proposal was based on an early dysregulation of FAIM-L in the progression of AD, we hypothesized that its decrease might be linked to one of the initial PTM that trigger tau toxicity and aggregation, its hyperphosphorylation. Then, to deeper analyse the effects of FAIM-L loss in the progression of the disease, we first decided to establish a colony of the PS19 mouse model in our laboratory. Although P301S is strictly a FTDP-17 mutation and *MAPT* mutations have not been described in familiar AD, tau mouse models are considered an effective tool for the study tau-mediated alterations in this pathology. We selected this mouse model because of the early reduction of FAIM-L reported in the hippocampal samples we had

analysed (**Figure 46A**) and due to the severity of tau pathology and the associated alterations (synaptic failure or cognitive deficits) reported in these mice[92]. Also, as FAIM-L loss was observed at ages were NFTs are still not formed (6-months-old)[92], it correlated with our idea of being dependent on the early aberrant modifications of tau. Then, we proceeded to temporally characterize the decrease of FAIM-L in the most affected area of the brain in this model: the hippocampus[92]. Also, we chronologically related it with the increase in pTau. To do so, we selected three time points corresponding to the presence of low, mild, and severe pathology, according to the bibliography[92]: 3, 6 and 9 months-of age. When levels of FAIM-L were analysed by WB at the selected ages, results revealed a significative decrease in FAIM-L levels by 6 months-of-age (**Figure 47A**; *second panel*). This reduction was observed together with an increase in pTau levels (**Figure 47B**; *second panel*). According to this, FAIM-L levels remained unchanged in 3-month-old mice (**Figure 47A**; *first panel*), when we did not detect an increase in pTau levels (**Figure 47B**; *first panel*). Finally, FAIM-L downregulation and pTau increase were maintained by 9 months-of age (**Figure 47A,B**; *third panel*).

Figure 47. Hippocampus of PS19 mice show a decrease in FAIM-L protein levels by 6 months of age, concurrently with an increase in pTau levels. FAIM-L, total tau (Tau5) and pTau (AT8) protein levels were analyzed by WB in protein extracts obtained from the hippocampus of WT and PS19 mice at 3, 6, and 9 months-of-age (mo), in the newly established colony. (A) A decrease in FAIM-L levels and (B) an increase in pTau protein levels were firstly detected at 6 mo and maintained at 9 mo. Graphs represent arbitrary units (obtained by densitometric analysis of immunoblot images; (A) FAIM-L/GAPDH and (B) pTau/Tau ratios) and are compared to their WT littermates. Data is shown as mean ± SEM (n=6-15). Representative immunoblots are shown. ***P < 0.01;* *** *P < 0.001* (Student's t test). Each point corresponds to the value from an individual mouse.

(figure in nex page)

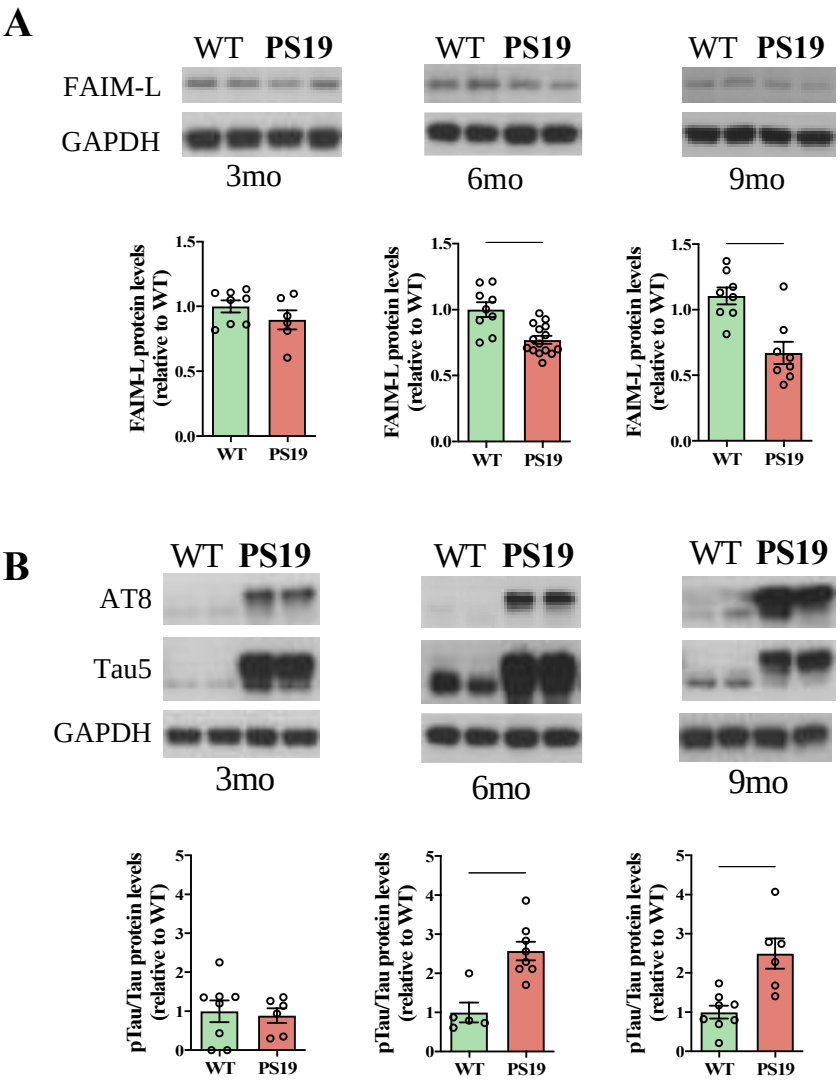

This temporal coincidence suggested us that FAIM-L reduction might be specifically dependent on the hyperphosphorylation of tau. To determine that, we increased phosphorylation levels of tau (pTau) in differentiated PC12. Recent studies have shown that 4R tau isoforms are more prone to phosphorylation[283], so the first strategy followed was to overexpress the 1N4R tau isoform (Tau^{WT}) in our cells. P301L mutation makes tau more prone to phosphorylation and aggregation. Then, the second one was to overexpress a

mutated form of tau (Tau^{P301L}). Finally, we decided to transfect cells with the GSK-3β, known to be the main kinase phosphorylating tau[284]. Then, we overexpress with Tau^{WT}, Tau^{P301L} and GSK-3β in our cells. We to transfected GSK-3β alone to increase the phosphorylation of endogenous tau, and together with Tau^{WT} and Tau^{P301L} to potentiate the phosphorylation of the overexpressed forms. Then, we analysed FAIM-L endogenous levels by WB. Results revealed that co-transfection of either Tau^{WT} or Tau^{P301L} with GSK-3β plasmid resulted in a significant reduction of FAIM-L protein levels (**Figure 48**) in cells.

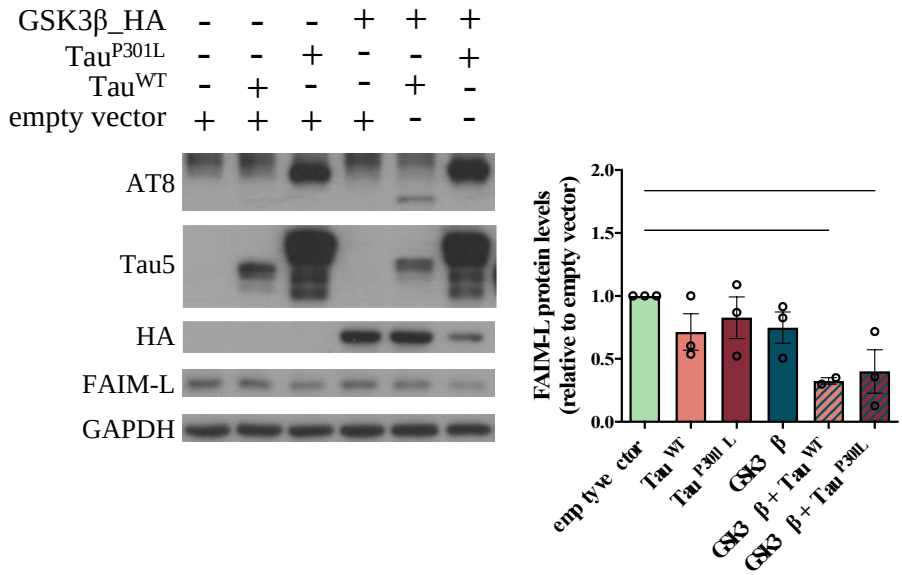

Figure 48: Aberrant increase in phosphorylation levels of Tau results in a reduction of FAIM-L protein levels *in vitro*. FAIM-L, total tau (Tau5) and pTau (AT8) protein levels were analyzed by WB in protein extracts obtained from transfected and differentiated PC12 cells. PC12 cells were transfected with Tau^{WT}, Tau^{P301L}, GSK3β_HA or empty vector. The presence or absence of each plasmid is indicated with a (+) or a (-), respectively. Reduction in FAIM-L levels was observed exclusively after co-transfection of GSK-3β with one of Tau plasmids, where increased pTau levels (AT8) was also detected. Membranes were immunoblotted against Tau5 and HA as a control of successful transfection of Tau^{WT}, Tau^{P301L} and GSK-3β, respectively. Values represent arbitrary units (obtained by densitometric analysis of immunoblot images; FAIML/GAPDH ratio) and compared to the empty vector condition (considered as one for each independent replicate). Data is shown as mean ± SEM (n=2-3). Representative immunoblots are shown. *$P < 0.05$ compared to empty vector (one-way ANOVA followed by Bonferroni's post hoc test).

The sole overexpression of GSK-3β, Tau^{WT} or Tau^{P301L} barely permitted pTau detection in the WB. Conversely, when tau and GSK-3β were coexpressed we were able to observe an increase in pTau (reflected by the immunodetection of pTau in the WB). Therefore, this result indicated that FAIM-L decrease was dependent on an increase in pTau, induced in this system by the co-expression of GSK-3β.

17. FAIM-L is reduced in the hippocampus of PS19 mice before the onset of other pathological hallmarks

This last result strongly supports the association between tau hyperphosphorylation and FAIM-L decrease, and places it as an early modification in the course of the pathology. However, it counteracts the temporal characterizacion reported for this model. On one side, Yoshiyama et al[92], reported an increase in pTau in 3 months-old animals. BY contrast, despite we were detected an increase in both mRNA (**Figure 49**) and protein levels of tau by this age, we were not able to detect an increase in pTau levels until 6 months (**Figure 47**).

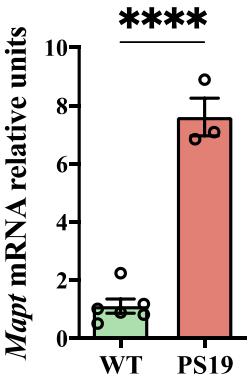

Figure 49. Hippocampus of PS19 mice show an increase in *Mapt* mRNA levels by 3 months of age. *Mapt* mRNA levels were analyzed by qRT-PCR in the hippocampus of 3 months-old (mo) WT and PS19. mRNA expression levels were normalized to *Gapdh* and plotted relative to values from the corresponding age-matched WT mice. Values are expressed as fold change compared to WT and shown as mean ± SEM (n=4-6). ****$P < 0.0001$ compared to respective WT mice (Student's t test). Each point corresponds to the value from an individual mouse.

On the other side, we found a delay in FAIM-L decrease when compared to the results obtained from Dr. Saura's laboratory samples. Several groups have

proposed a retardation in the onset of the pathology in their home-breed PS19 colonies[95,285,286]. To confirm this possibility and to determine the sequence of events in our mice, we decided to situate other pahological markers in the time-couse of the disease. Both synaptic failure and neuroinflammation were reported to be early alterated in the PS19 model by their developers (3 and 6 months, respectively). Therefore, we analysed levels of synaptic markers and the gliotic protein GFAP at these two ages and later, at 9 months-of-age. We found that neither PSD95 (**Figure 50A**) nor mGlurR2 (**Figure 50B**) levels were decreased in 3- or 6-months-old mice. A similar temporal delay was observed for GFAP (**Figure 50C**). By contrast, we found an impairment in synaptic post-synaptic integrity and astrogliosis at the elder age (9 months), where both synaptic markers were significantly decreased (**Figure 50A,B**; *third panel*) and GFAP increased (**Figure 50C**; *third panel*).

Figure 50: Synaptic alterations and astrogliosis are only detected in the hippocampus of PS19 at elder ages, and after FAIM-L decrease. PSD95 (A), mGluR2 (B) and GFAP (C) protein levels were analyzed by WB in protein extracts obtained from the hippocampus of WT and PS19 mice at 3, 6 and 9 months-of-age (mo). (A, B) A significant decrease in the synaptic markers PSD95 and mGluR2 levels was firstly detected at 9 mo. (C) A significant increase in GFAP protein levels was detected by 9mo. Graphs represent arbitrary units (obtained by densitometric analysis of immunoblot images; GAPDH ratio) and are compared to their WT littermates. Data is shown as mean ± SEM (n=6-15). Representative immunoblots are shown. *$P < 0.05$; ** $P < 0.01$ compared to respective WT mice (Student's test test). Each point corresponds to the value from an individual mouse.

(figure in next page)

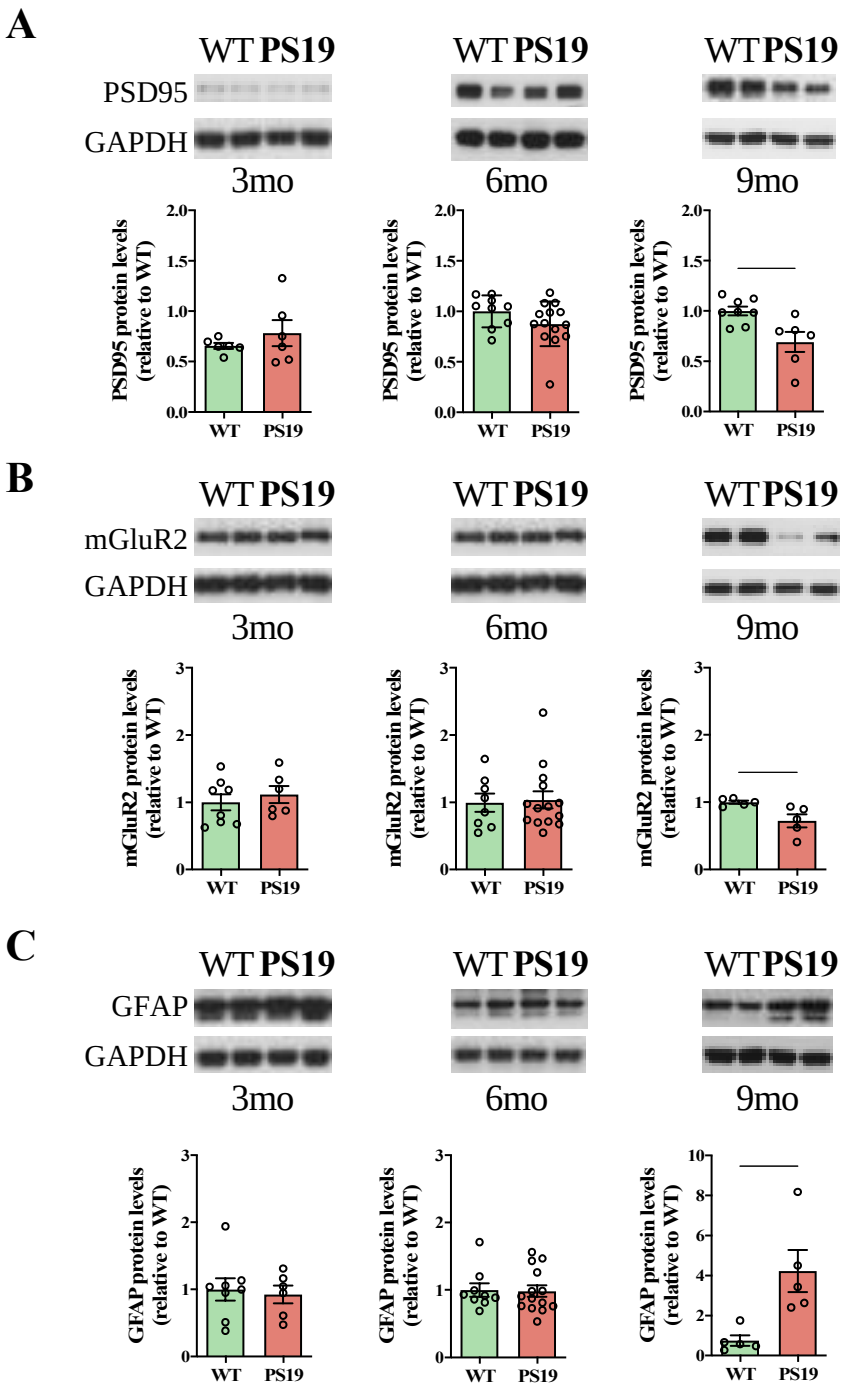

With this delay in the emergence of synaptic alterations and gliosis, (compared to that one reported in Yoshiyama et al[92]) we can conclude that our model

develops tau-related pathology later in time. Indeed, and more importantly, we definitely can place FAIM-L decrease as an early event in the progression of the pathology. So far, FAIM-L reduction is not only linked to one of the first alterations in tau pathology, the phosphorylation of tau, but also precedes the rest of pathological hallmarks.

18. *Faim-l* transcription is not altered in PS19 mice

After the newly discovered relatiopship between FAIM-L reduction and pTau increase, we next wanted to determine if FAIM-L reduction could be caused by a decrease in its transcription rates. Then, we performed a RT-qPCR in hippocampal samples of 3 and 6 months-of-age PS19 mice. Results revealed that there was no reduction in *Faim-l* mRNA levels at either of the ages analysed (**Figure 51**). As FAIM-L protein levels are already reduced by 6 months, we can conclude that FAIM-L reduction is not caused by an aberrant reduction in its transcription.

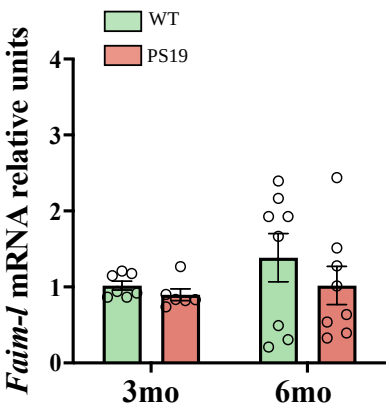

Figure 51. FAIM-L reduction in the hippocampus of PS19 mouse is not caused by a reduction in its transcription. *Faim-l* mRNA levels were analyzed by qRT-PCR in the hippocampus of 3 and 6 months-old (mo) WT and PS19 mice. No differences were observed in *Faim-l* mRNA either between genotypes, or with age. mRNA expression levels were normalized to *Gapdh* and plotted relative to values from the corresponding age-matched WT mice. Values are expressed as fold change compared to WT and shown as mean ± SEM (n=6-8) (Student's test test). Each point corresponds to the value from an individual mouse.

19. FAIM-L loss results in a reduction in xiap levels and an increase in global protein ubiquitination

Once explored FAIM-L reduction in the course of the disease and placed it as an early event in the progression of the pathology, we proceeded to explore functional implications of FAIM-L downregulation in the hippocampus of the PS19. For that, we focused on the principal molecular process in which FAIM-L has been involved so far: ubiquitination.

FAIM-L is able to regulate both apoptotic and non-apoptotic caspase-3 processes by the stabilization of XIAP and the prevention of its ubiquitination and degradation[266]. Thus, we first hypothesized that FAIM-L loss would supose a reduction in XIAP protein levels in our *in vivo* model. To explore this possibility, we determined by WB XIAP hippocampus of the PS19 mice before and once FAIM-L levels had been decreased. WB analysis revealed a slight but significant decrease in XIAP levels by 9 month-of-age, consistent with a settled reduction of FAIM-L levels from 6 months of age (**Figure 52A**; *third panel*). No differences in XIAP were observed at earlier stages of the disease (3 and 6 months, **Figure 52A**; *first and second panel*).

The role of FAIM-L in ubiquitination is not only limitted to the avoidance of XIAP's ubiquitination. Our group has reported that FAIM KO retinas accumulate Ub-immunopositive protein aggregates[273]. Similar results have been obtained by Kaku and colleges, which have proposed FAIM as a proteostasis regulator. FAIM was reported to avoid the accumulation of aggregated proteins under cellular stress[270]. Thus, we decided to also check for global ubiquitination status in the hippocampus of PS19 mice at the ages selected. As for XIAP, we demonstrated an increase in global protein ubiquitination in 9-months-old hippocampus (**Figure 52B**; *third panel*). Again, we did not observe changes in total ubiquitination by 3 months-of-age

(**Figure 52B**; *first panel*). Interstingly, at 6 months, we observed a slight increase in total ubiquitination even it was statically non-significant (p-value=0.077) (**Figure 52B**; *second panel*).

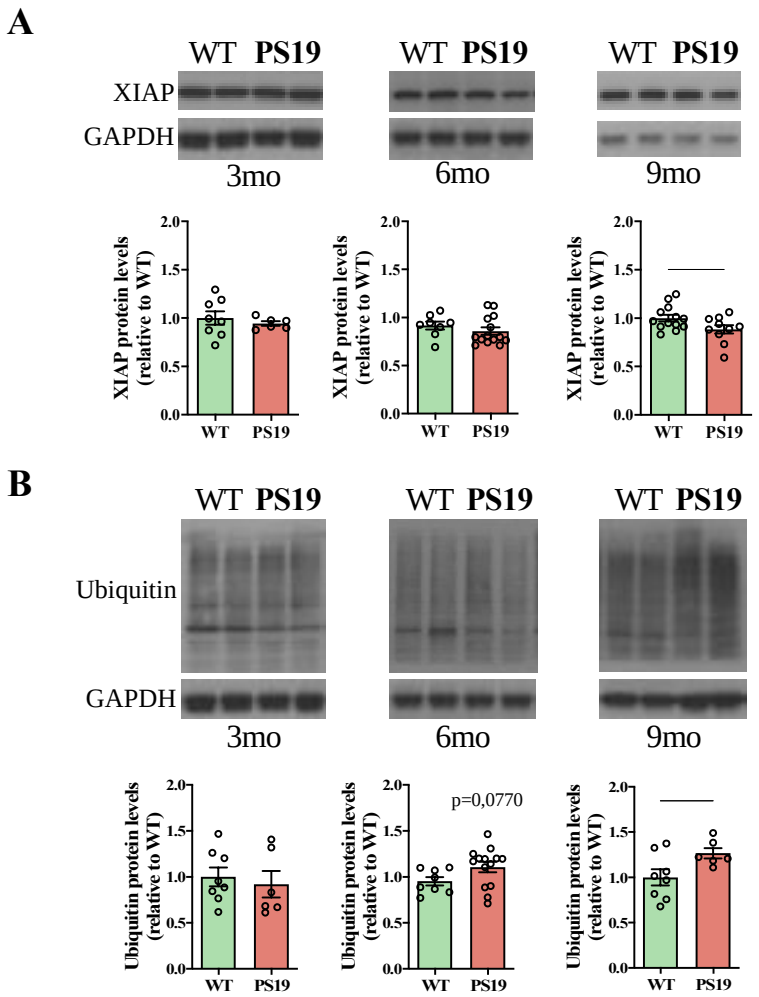

Figure 52: FAIM-L-dependent processes are altered by 9 months-of age in the hippocampus of PS19 mice. XIAP protein levels (A) and global ubiquitination levels (B) were analyzed by WB in protein extracts obtained from the hippocampus of WT and PS19 at 3, 6 and 9 months-of-age (mo). (A) A significant decrease in the anti-apoptotic protein XIAP was detected at 9mo. (B) Ubiquitination levels presented a tendency to increase by 6mo (p-value= 0.077) and it was significantly increased by 9mo. Graphs represent arbitrary units (obtained by densitometric analysis of immunoblot images; GAPDH ratio) and are compared to their WT littermates. Data is shown as mean ± SEM (n=6-15). Representative immunoblots are shown. *$P < 0.05$ (Student's test test). Each point corresponds to the value from an individual mouse.

20. Both FAIM-L and FAIM-S interact with tau but only FAIM-L prevents its ubiquitination

Ubiquitination is an important process for proteostasis, early impaired in AD[229,230]. Thus, NFTs and other tau aggregates are highly ubiquitinated[287]. Abnormal ubiquitination of tau leads to its caspase-3-mediated cleavage and to the formation of Tau-C3, a highly toxic and pro-aggregant fragment of the protein[288,289]. Our results suggested a potential role of FAIM-L in the regulation of ubiquititination processes in the PS19 mice, so we wondered whether FAIM-L could be able to directly prevent tau ubiquitination by interacting with it in a similar manner as it does with XIAP[250,266]. Then, its absence could be promoting the aberrant Ub incorporations in tau, leading to derived alterations such as its further cleavage, loss-of-function and tau-associated toxicity. Finally, FAIM-L could be mediating its consecutive aggregation.

To address this hypothesis, we first determined FAIM-L ability to interact with tau. As an initial approximation, we performed an immunoprecipitation followed by mass spectrometry (IP-MS) assay. With this strategy we massively identified possible partners of FAIM-L. We performed a FLAG co-IP from differentiated PC12 cells transfected with FAIM-L_FLAG plasmid. Then, the immunoprecipitates (which would include those proteins interacting with FAIM-L) were analysed by MS at the Proteomic Unit of the CRG (see *matherials and methods section X* for details). From the provided data, we performed a GO analysis and determined the enriched KEGG pathways (**Figure 53B**) and comparments (**Figure 53B**). Interestingly, this bioinformatic analysis revealed an enrichment in proteins related to the proteasome system and to AD. Also, FAIM-L most relevant partners were

implicated in the calpain complex, endoplasmic reticulum (ER) and the PSD complex.

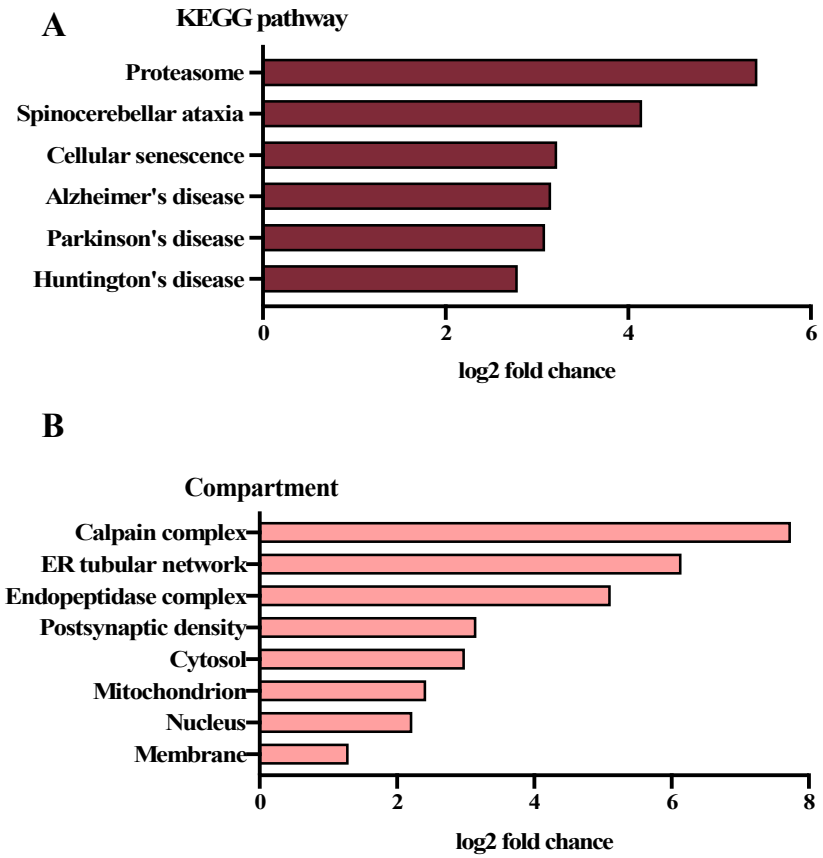

Figure 53. The gene ontology annotation and pathway enrichment analysis of all the FAIM-L interacting proteins obtained by MS. Representation of the top (A) 6 GO KEGG pathway and (B) 8 GO cellular components. *KEGG, Kyoto Encyclopedia of Genes and Genomes.*

Then, we performed a selection of several potential partners according to this information and based on the realiability of detection (**Table 14)**.

Table 14. Selection of proteins reported to interact with the FAIM-L in the IP-MS. Two pools of PC12 cells overexpressing FAIM-L were used to isolate and identify possible partners of FAIM-L. Predicted FAIM-L-interacting proteins were identified by MS and reported to interact with the common domain of the protein. A list of potential partners detected are grouped in the table according to GO enriched pathways. Peptide spectrum matches (PSMs) and percentage of coverage for each protein detected are also provided.

Gene	Protein	Σ#PSMs	ΣCoverage	GO
Mapt	Microtubule-associated protein tau	10	9,57	**Alzheimer's disease**
Ube2v1	Ubiquitin-conjugating enzyme E2 variant 1	5	36,05	**Proteasome**
Psme1	Proteasome Activator Subunit 1	5	6,43	**Proteasome**
Capn2	Calpain 2 catalytic subunit	3	5,57	**Alzheimer's disease**
Capn1	Calpain-1 catalytic subunit	2	2,95	**Alzheimer's disease**
Psma4	Proteasome subunit alpha	2	6,51	**Alzheimer's disease Proteasome**
Rtn4	Reticulon-4	2	3,78	**Alzheimer's disease**

Of note, all the proteins detected in the assay were predicted to interact with FAIM-L by the common domain of the protein, therefore, not excluding a possible interaction also with FAIM-S. Interestingly, among the protein identified, we detected tau protein. It was one of the more accurately detected proteins. Ten PSMs of tau were detected in the MS analysis. Also, a 9,52% of the protein was covered by these identified peptide sequences.

To validate the predicted partnership and further characterize this interaction, we transfected HEK293T cells with FAIM-L_FLAG, FAIM-S_FLAG and Tau^{WT}, and performed a co-IP of Tau^{WT}. WB analysis of the proteins

immunoprecipitated in the assay revealed an interaction between Tau^{WT} and both isoforms of FAIM. For quantificate this interaction, we normalize the signal detected in the WB for FAIM-L and FAIM-S, with the corresponding amount of tau immunoprecipitated. Then, using a FAIM/Tau ratio we could compare the amount of FAIM-L or FAIM-S immunoprecipitated with tau. Here, we observed that, for an equal quantity of tau, FAIM-L interacts with it over 5 times more than FAIM-S (**Figure 54**). This result confirmed MS results and setted the basis for the study of FAIM-L regulation of tau ubiquitination.

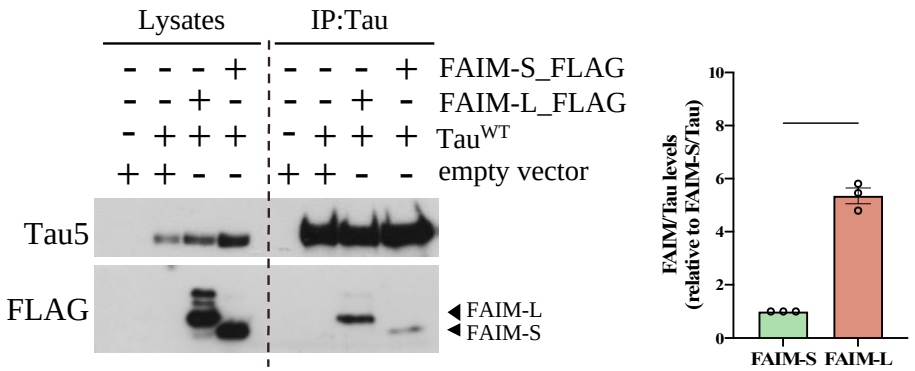

Figure 54. Tau interacts with both FAIM isoforms under physiological conditions but presents higher affinity for FAIM-L. Interaction between FAIM and Tau was analyzed by co-immunoprecipitation in protein extracts obtained from transfected HEK293T cells. HEK293T cells were transfected with FAIM-L_FLAG, FAIM-S_FLAG, Tau^{WT} or an empty vector. The presence or absence of each plasmid is indicated with a (+) or a (-), respectively. Tau was immunoprecipitated (IP) and processed by WB with the total lysates from the original sample (lysates). The membranes were immunoblotted with Tau5 and FLAG antibodies, as indicated in the representative immunoblot. Graphs represent arbitrary units (obtained by densitometric analysis of immunoblot images; FAIML/Tau^{WT} ratio) and are compared to FAIM-S/Tau^{WT} ratio (considered as one for each independent replicate). Data is shown as mean ± SEM (n=3). *** $P < 0.001$ (Student's test test). Each point corresponds to the value from an individual experiment.

To assess this end, we performed a Ub Assay by transfecting HEK293T cells with Tau^{WT}, FAIM-L, FAIM-S and His-Ub plasmids. Then, we carried out an IP for the His tag of the Ub and specifically analyzed by WB the ubiquitination levels of tau in the ubiquitin-pull down. Results confirmed that tau became ubiquitinated in a cell aproximation assay (**Figure 55,** *lines 3 and 7*) and, as

we expected, FAIM-L prevented this ubiquitination (**Figure 55,** *lines 4 and 8*). Interestingly, FAIM-S was not able to reduce Tau^{WT} ubiquitination, indicating that, although both isoforms were able to interact with tau, only FAIM-L exerted a modulatory function over its ubiquitination.

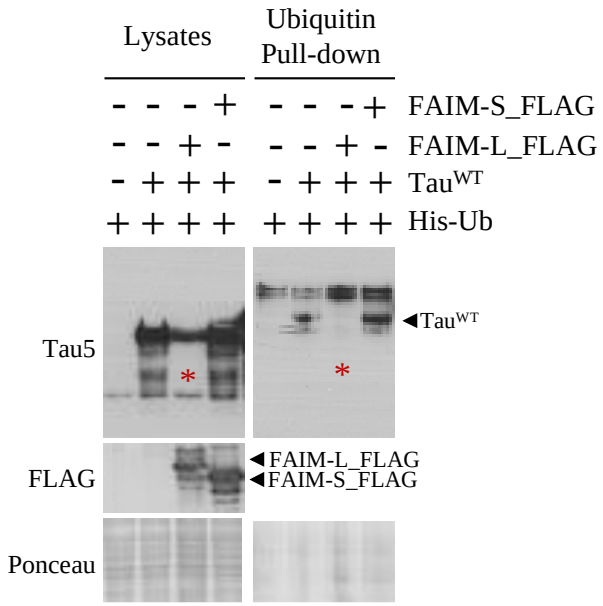

Figure 55: Only FAIM-L, but not FAIM-S, is able to reduce ubiquitination levels of Tau^{WT}. Ubiquitination levels of Tau^{WT} were analyzed in protein extracts obtained from transfected HEK293T cells after a Ubiquitination Assay. HEK293T cells were transfected with 6xHis-Ubiquitin (Ub), FAIM-L_FLAG, FAIM-S_FLAG, Tau^{WT} or empty vector. The presence or absence of each plasmid is indicated with a (+) or a (-), respectively. Ubiquitin pull-down was performed and analyzed by WB. Membranes from the ubiquitin pull-down were immunoblotted against Tau5 to detect levels of ubiquitinated tau. Membranes from total lysates (lysates) were blotted against Tau5 and FLAG and used as a control of succesful transfection. Reduction in Tau^{WT} ubiquitination was detected in presence of FAIM-L (red asterisk) but not in presence of FAIM-S. Ponceau staining is used as a loading control.

Different types of ub chains can be attached to a protein. When poly-Ub chains are linked to it, several high molecular bands can be detected in the ubiquitin pull-down. In our Ub pull-down, we only detected one tau ubiquitinated band at the same molecular weight of tau. This pattern suggested that tau was being mono or di-ubiquitinated. Additionally, when we analysed the input, we

observed that tau ubiquitination leads to its cleavage and the emergence of non-ubiquitinated fragments of lower molecular weight. As mono-ubiquitination usually serves as a signal for protein[290], this observation further supporting our idea. Again, this cleavage is reduced in presence of FAIM-L.

Lys48-linked Ub chains can bind to proteins and target them to degradation. Usually, this abovementioned multi-band pattern in the WB reflects this type of ubiquitation. To definitely confirm that, treatments with MG132, wich inhibit the proteasome and avoid protein degradation, can be used. If a protein is ubiquitinated and degraded, the inhibition of the proteasome leads to its accumulation in the cytosol. Then, one observes a higher amount of protein when the proteasome is inhibited as compared when it is not. Our results suggested that tau is presenting other type of ubiquitination. Nevertheless, we proceeded to inhibit the proteasome to further confirm our proposal. We then repeated this experiment and overexpressed HEK293T cells with FAIM-L and Tau^{WT}. Then, we treated, or not, the cells with MG132 (**Figure 56**).

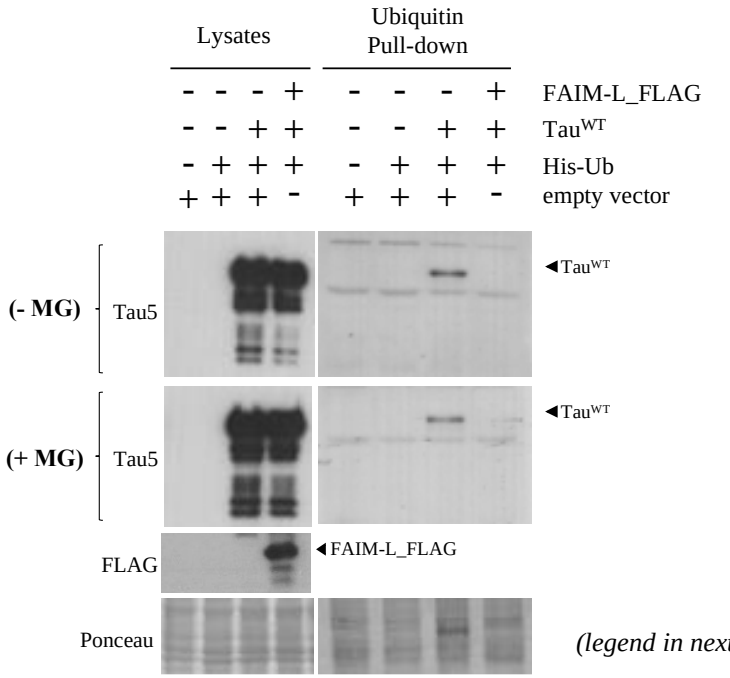

(legend in next page)

Figure 56: ubiquitination levels of Tau^{WT}. Ubiquitination levels of Tau^{WT} were analyzed in protein extracts obtained from transfected HEK293T cells after a Ubiquitination Assay. HEK293T cells were transfected with 6xHis-Ubiquitin (Ub), FAIM-L_FLAG, Tau^{WT} or empty vector and treated *(lower panel*) or not (*upper panel*) for 6h with MG132 (MG). The presence or absence of each plasmid is indicated with a (+) or a (-), respectively. Ubiquitin pull-down was performed and analyzed by WB. All the samples (-MG and +MG) from the Ubiquitin pull-down and those from the input were anlaysed in the same membrane but showed separated to facilitate visualization. Membranes from the ubiquitin pull-down were immunoblotted against Tau5 to detect levels of ubiquitinated Tau, and membranes from total lysates (lysates) were blotted against Tau5 and FLAG, and used as a control of successful transfection. Ponceau staining is used as a loading control.

When we analysed the Ubiquitin pull-down, we observed that the type of ubiquitination that FAIM-L was preventing did not change. Thus, we can confirm that FAIM-L is preventing a non-degradative ubiquitination of tau, which indeed is probably mono-ubiquitinated.

21. FAIM-L interaction with mutant tau did not result in a blocking its ubiquitination

Mutations in tau such as the P301S (present in our mouse model) or the P301L (one of the most common mutations in FTDP-17[291] present high rates of self-assembly[143]. P301L, for example, estimulates the adquisition of transient conformations which expose the PHF6 and PHF6* motifs of tau and promote its aggregation[143,208]. Indeed, *MAPT* mutations are reported to reduce tau capacity to bind to MTs[291]. Importantly, both the loss of affinity or conformational changes can affect the interaction with other proteins. For this reason, we wanted to determine any possible modifications in the interaction between FAIM-L and tau interaction under these pathological conditions. Then, we wanted to define if it also modified the capacity of FAIM-L to avoid the ubiquitination of mutant tau. For that, we repeated the same experimental design used above but including the transfection of a plasmid for a mutant form of tau (Tau^{P301L}).

First, we determined the interaction between FAIM and Tau^{P301L} by immunoprecipitating FAIM's tag FLAG. Results obtained from WB, showed that both FAIM-L and FAIM-S were also capable of interacting with Tau^{P301L} (**Figure 57**), as previously showed with Tau^{WT}.

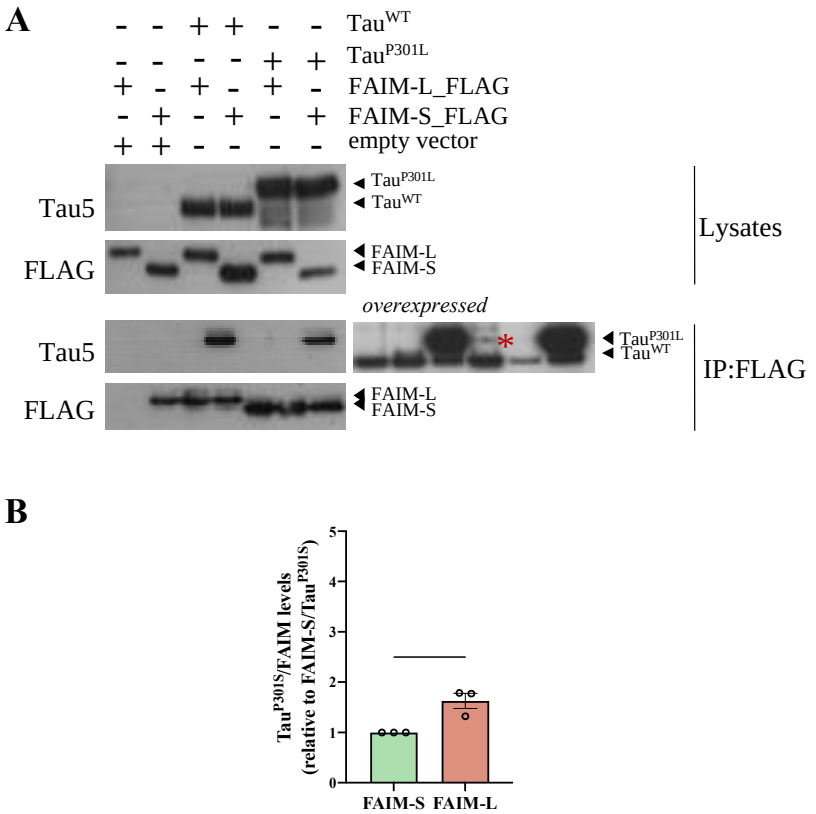

Figure 57. Mutant tau also interacts with FAIM, with higher affinity for the longer isoform FAIM-L. Interaction between FAIM and tau was analyzed by co-immunoprecipitation in protein extracts obtained from transfected HEK293T cells. HEK293T cells were transfected with FAIM-L_FLAG, FAIM-S_FLAG, Tau^{WT}, Tau^{P301L} or an empty vector. The presence or absence of each plasmid is indicated with a (+) or a (-), respectively. FLAG was immunoprecipitated (IP) and processed by WB with the total lysates from the original sample (lysates). The membranes were immunoblotted with Tau5 and FLAG antibodies, as indicated in the representative immunoblot (A). FAIM interaction with Tau^{WT} was hardly detected after immunoprecipitation of FLAG (*overexpressed* blot in A, right, and indicated with a red asterisk). (B) Graphs obtained from WB quantifications represent arbitrary units (obtained by densitometric analysis of immunoblot images; FAIML/Tau^{P301L} ratio) and are compared to FAIM-S/Tau^{P301L} ratio (considered as one for each independent replicate). Data is shown as mean ± SEM (n=3). *$P < 0.05$ (Student's t test). Each point corresponds to the value from an individual experiment.

As we did before, we calculated the appropriate ratio of immunoprecipitation (this time Tau / FAIM ratio). Co-IP quantification indicated that the affinity between FAIM-L and Tau^{P301L} was higher compared to FAIM-S (**Figure 57B**). However, in this assay we were not able to detect the presence of Tau^{WT} in the immunoprecipitate at first moment. As we already have confirmed the interaction between FAIM and the native form of tau, we first overexposed the WB. After that, we were able to detect a faint band corresponding to the Tau^{WT} form (**Figure 57,** *red asterisk*), confirming the interaction with both isoforms. Since we have made previous comparisons by immunoprecipitating tau, we repeated the analysis by immunoprecipitating tau instead of FLAG. Also, as the high expression and immunoprecipitation of Tau^{P301L} (*see lysates and IP:FLAG in* **Figure 57**) had interfered the detection of Tau^{WT} in the FLAG IP, we included a condition with half quantity of DNA of the Tau^{P301L} plasmid. Once again, our results confirmed the interaction between both tau proteins and both FAIM isoforms (**Figure 58**).

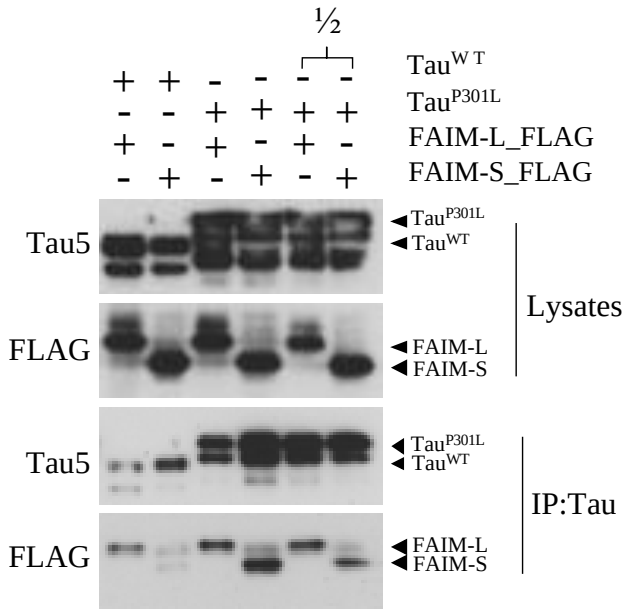

(legend in next page)

Figure 58. Immunoprecipitation of tau also shows FAIM interaction with both Tau^{WT} and Tau^{P301L}, but with higher affinity for the WT form. Interaction between FAIM and tau was analyzed by co-immunoprecipitation in protein extracts obtained from transfected HEK293T cells. HEK293T cells were transfected with FAIM-L_FLAG, FAIM-S_FLAG, Tau^{WT}, Tau^{P301L} or an empty vector. The presence or absence of each plasmid is indicated with a (+) or a (-), respectively. Tau was immunoprecipitated (IP) and processed by WB with the total lysates from the original sample (lysates). The membranes were immunoblotted with Tau5 and FLAG antibodies, as indicated in the representative immunoblot. Only one replicate was used for this experiment. ½, half quantity of DNA for Tau^{P301L} plasmid transfected.

Then, we proceeded to quantify FAIM-L and Tau^{P301L} interaction and to compare it to the interaction with the WT form. On one side, the limited detection of Tau^{WT} in the FLAG co-IP suggested that that FAIM affinity for Tau^{P301L} was higher compared to Tau^{WT}. However, when we performed the Tau co-IP we reported opposite results. This time, we observed that more quantity of FAIM-L was immunoprecipitating with Tau^{WT} compared to Tau^{P301L}. It is worthy mentioned that detection of protein–protein interactions by co-IP is highly dependent on the procedure. Specifically, it can vary depending on the capacity to maintain stable physiological interactions during the process, the effectivity of the antibodies used, or the conformational state of the proteins analyzed. For this reason, the quantification of a specific interaction could lead to discrepancies depending on the antibody used. Then, after our results we can confirm that both FAIM-L and FAIM-S interact with Tau^{P301L}, but we cannot precisely define wether this interaction is increased or decreased compared to Tau^{WT}, requiring further analysis using other techniques.

So far, we were unable to determine if FAIM-L and Tau^{P301L} interaction was impaired *in vitro*. Still, we proceded to determine if, under these conditions, FAIM-L function was impaired. We then determined its capacity to prevent Tau^{P301L} ubiquitination. Again, we transfected HEK293T cells with both FAIM isoforms and both tau proteins and performed a Ubiquitin Assay. In this

assay, Ubiquitin pull-down WB results revealed that, while FAIM-L (and not FAIM-S) was able to reduce Tau^{WT} ubiquitination (**Figure 59**, *red asterisk*), neither of the isoforms were able to reduce Tau^{P301L} ubiquitination levels (**Figure 59,** *black asterisk*).

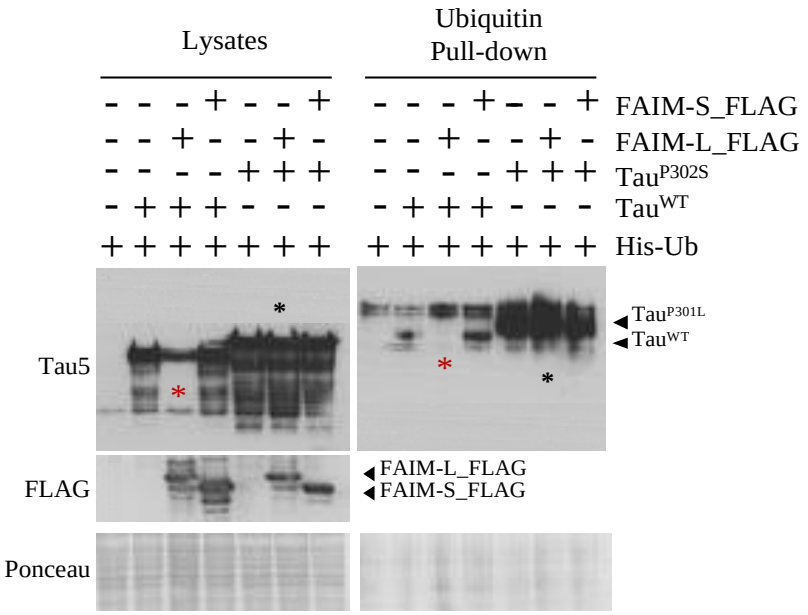

Figure 59: FAIM-L is not able to avoid ubiquitination of Tau^{P301L}. Ubiquitination levels of Tau^{WT} and Tau^{P301L} were analyzed in protein extracts obtained from transfected HEK293T cells after a Ubiquitination Assay. HEK293T cells were transfected with 6xHis-Ubiquitin (Ub), FAIM-L_FLAG, FAIM-S_FLAG, Tau^{WT}, Tau^{P301L} or empty vector. The presence or absence of each plasmid is indicated with a (+) or a (-), respectively. Ubiquitin pull-down was performed and analyzed by WB. Membranes from the ubiquitin pull-down were immunoblotted against Tau5 to detect levels of ubiquitinated Tau and membranes from total lysates (lysates) were blotted against Tau5 and FLAG, and used as a control of successful transfection. Reduction in Tau^{WT} ubiquitination was detected in presence of FAIM-L (and not in presence of FAIM-S), as described before (*red asterisk*). By contrast, FAIM-L was not able to reduce Tau^{P301L} ubiquitination (*black asterisk*). Ponceau staining is used as a loading control.

22. FAIM-L is not sequestered in PS19 aggregates

This last result confirmed us the inability of FAIM-L to regulate Tau^{P301L}, at least in the conditions we used. Unfortunately, we were not able to determine if the amount or strength of interaction between FAIM-L and Tau^{P301L} was affected due to the mutation. Misfolded proteins habitually sequester their cellular partners into the inclusions, interfering with their funcionality[292]. Tau has been described to sequester elements of the ribosome into its aggregates, therefore causing ribosomal loss of integrity and dysfunction[293]. We hypothesized that FAIM-L could be sequestered by tau aggregates and, as a consequence, it would be losing its functionality. This fact would explain FAIM-L inability to reduce tau ubiquitination during pathology and help us to infers if their interaction is increased or decreased.

To further analyse whether FAIM-L could be sequestered in tau aggregates, we decided to analyse it in hippocampal samples of the PS19 mice. Then, we processed hippocampus of 9-months-old PS19 mice, once tau pathology has been settled and stable aggregates have been defined[92]. Then, we determined the presence of FAIM-L in the different fractions obtained by using a sequential lysis protocol. This protocol allowed us to separate both soluble and cytosolic fractions (S1) from encapsulated (SDS-soluble, S2) and highly aggregated (SDS-insoluble, P1) proteins. Results obtained by WB showed that by 9 months-of age, tau was slightly aggregated in the hippocampus of PS19 mice, but those aggregates did not include FAIM-L (as shown by its non-detection in the P1 fractions). By contrast, it remained in the cytoplasmic fraction (**Figure 60**).

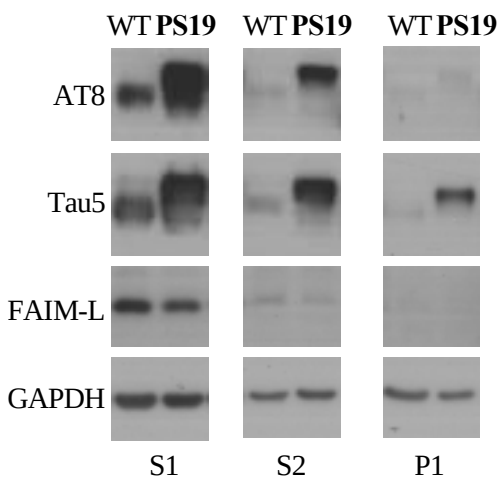

Figure 60: FAIM-L is not sequestered in tau aggregates. FAIM-L and Tau levels were analyzed by WB in sub-fractionated protein extracts from in hippocampus of 9 months-old WT and PS19 mice. Protein extracts were separated depending on protein solubility in: soluble and cytoplasmic proteins (S1), encapsulated and SDS-soluble proteins (S2) and highly aggregated and SDS-Urea soluble proteins (P1). FAIM was only detected in S1 and S2 fractions in both PS19 mice and WT littermates. Tau protein was detected in S1 and S2 in both genotypes, but almost exclusively in the P1 fraction when the PS19 mice was analysed.

23. Intrahippocampal injection of neuronal-specific AAVs allow us to overexpress FAIM-L in the hippocampus of PS19 mice

So far, we had identified FAIM-L as an early downregulated protein in the progression of tau pathology present in AD. We had observed a decrease of its protein levels in the hippocampus of our 6-months-old PS19 mouse model. Also, we observed that this reduction coincided with one of the first aberrant modifications in tau protein, its hyperphosphorylation. Indeed, this decrease occurred before the onset of other pathological hallmarks. Consequently, FAIM-L function became impaired leading to a decrease of XIAP protein and an increase in global protein ubiquitination. We had also demonstrated that FAIM-L is able to reduce tau ubiquitination, by interacting with it. Based on our results, and on its anti-apoptotic known action, we propose that FAIM-L loss could be promoting AD progression. Therefore, we suggest that the restoration of its levels could play a neuroprotective role *in vivo* by regulating these processes.

To address this hypothesis, we decided to overexpress FAIM-L protein levels specifically in the neurons of the hippocampus of the PS19 mice. Then, we

proceeded to analyse any functional repercussions of this exogenous restoration of FAIM-L. For that, we intrahippocampally injected PS19 and WT mice with AAV9s, which overexpress FAIM-L, or with a non-coding CTL sequence (see *matherials and methods, section 2.3*). Then we determined behavioural capacities, synaptic functionality, ubiquitination processes, tau and XIAP stability and neuroinflammation in these treated mice after three months of FAIM-L overexpression. Surgery and behavioural analysis were performed in collaboration with Dr. Albert Giralt (Department of Biomedicine, UB, Barcelona, Spain).

Before performing the experiment, we determined the effectiveness of the infection of the AAVs after 3 months, its pattern of expression, and the functionality of the constructs. First of all, we injected WT animals with AAV:FAIM-L and AAV:CTL and euthanized them 3 months after the injection. In these animals, we then performed an immunostaining of mCherry (as FAIM-L viral construct incorporates the mCherry tag; see *matherials and methods, section 2.2*). Results obtained confirmed us the expression of the viral constructs in the hippocampus of the WT mice (**Figure 61A)**. We could corroborate the maintenance of FAIM-L expression until the final time point of the procedure, 3 months. Indeed, we could observe that mCherry expression was majorly concentrated in CA3 and DG, with practically no expression detected in the CA2 region. Finally, we performed a WB of different brain regions of these injected animals. With this assay, we could confirm a main expression of FAIM-L in the hippocampus and a low diffusion to adjacent areas (**Figure 61B**).

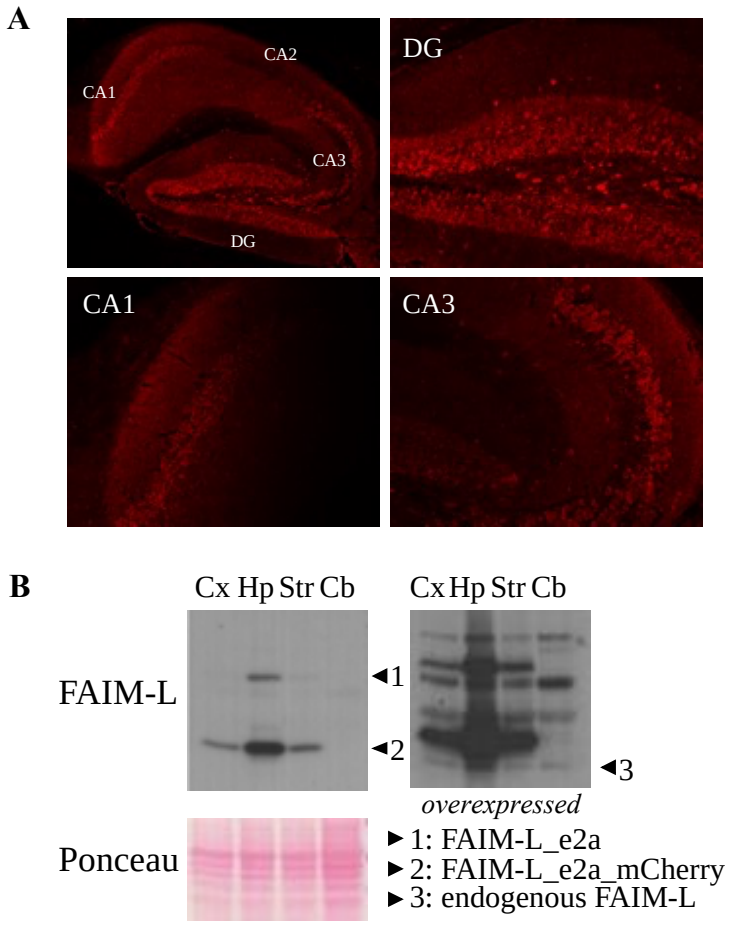

Figure 61: Designed AAVs effectively infect the hippocampus of WT mice for 3 months and show low diffusion to adjacent brain areas. WT animals were bilaterally and intrahippocampally injected with AAVs overexpressing FAIM-L (AAV:FAIM-L) or a control sequence (AAV:CTL) for 3 months according to the coordinates established. (A) mCherry immunostaining was analyzed in hippocampal sections from paraffin-embedded brains. Immunolabeling showed specific expression of mCherry in dentate gyrus (DG), and CA3 and CA1 regions of the hippocampus. Each region is indicated in the corresponding magnified image. Representative images are shown. (B) Overexpression of FAIM-L in the hippocampus of injected mice was analyzed by WB. FAIM-L was mostly detected in the hippocampus (Hp) while low or none FAIM-L overexpression was detected in the cortex (Cx), striatum (Str) and cerebellum (Cb). 1 and 2 refers to entire and cleaved constructs of viral FAIM-L, respectively; 3 corresponds to the endogenous FAIM-L (only observed in the overexposed immunoblot). Scale bar: 50 µm and 100 µm for the amplified images.

Only a slight signal was detected in the adjacent brain areas to the point of injection (cortex and striatum) while no overexpression was detected in distant

regions (cerebellum). Indeed, it permitted us to detect all the constructs derived from FAIM-L sequence processing. FAIM-L is attached to the mCherry tag by the e2a peptide. After translation, the e2a peptide is proteolytically cleaved, liberating mCherry and FAIM-L. In the WB we could detect that the e2a linker remained predominantly attached to FAIM-L. FAIM-L pattern showed an initial translate (1), the FAIM-L_e2a composite (2) and FAIM-L protein (3), being FAIM-L_e2a the most expressed construct.

After this result, we decided to determine the functionality of this construct. To this end, we performed a Ubiquitin Assay and analysed the capacity of the viral construct of FAIM-L_e2a to inhibit XIAP ubiquitination. We tranfected HEK293T cells with XIAP and the FAIM-L_e2a plasmid (containing the exact same sequence present in the virus construct) and determined the ubiquitination status of XIAP. WB results showed that that FAIM-L_e2a was capable of reducing XIAP ubiquitination in the same manner as FAIM-L itself (**Figure 62)**. It confirms, therefore, that this FAIM-L_e2a structure is functional and thus we can study the effect of FAIM-L independently of the ratio of cleavage from the e2a linker.

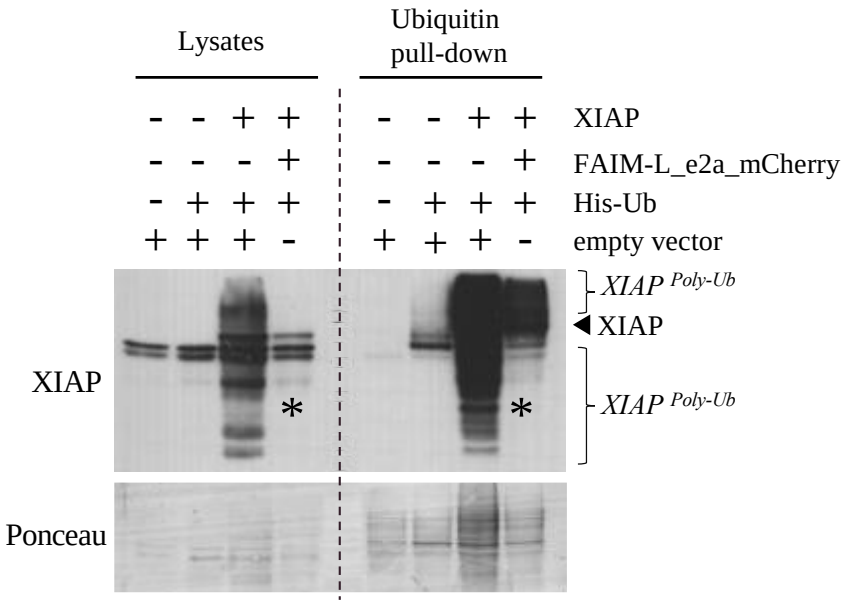

Figure 62: FAIM-L viral construct is functional, showing ability to reduce XIAP's ubiquitination *in vitro*. Ubiquitination levels of XIAP were analyzed in protein extracts obtained from transfected HEK293T cells after a Ubiquitination Assay. HEK293T cells were transfected with 6xHis-Ubiquitin (Ub), XIAP, FAIM-L_e2a_mCherry or or an empty vector. The presence or absence of each plasmid is indicated with a (+) or a (-), respectively. Ubiquitin pull-down was performed and analyzed by WB. Total lysates (lysates) were used as a control of successful transfection. Membranes were immunoblotted against XIAP to detect levels of ubiquitinated XIAP. Reduction in XIAP ubiquitination (referred as $XIAP^{Poly\text{-}Ub}$) was detected in presence of FAIM-L_e2a_mcherry in both lysates and ubiquitin pull-down and indicated with a red asterisk (*). Ponceau staining is used as a loading control.

Once we proved that we were able to overexpress functional FAIM-L in the hippocampus of WT mice with at least 3 months of durability, we proceeded with our experimental design (**Figure 63)**.

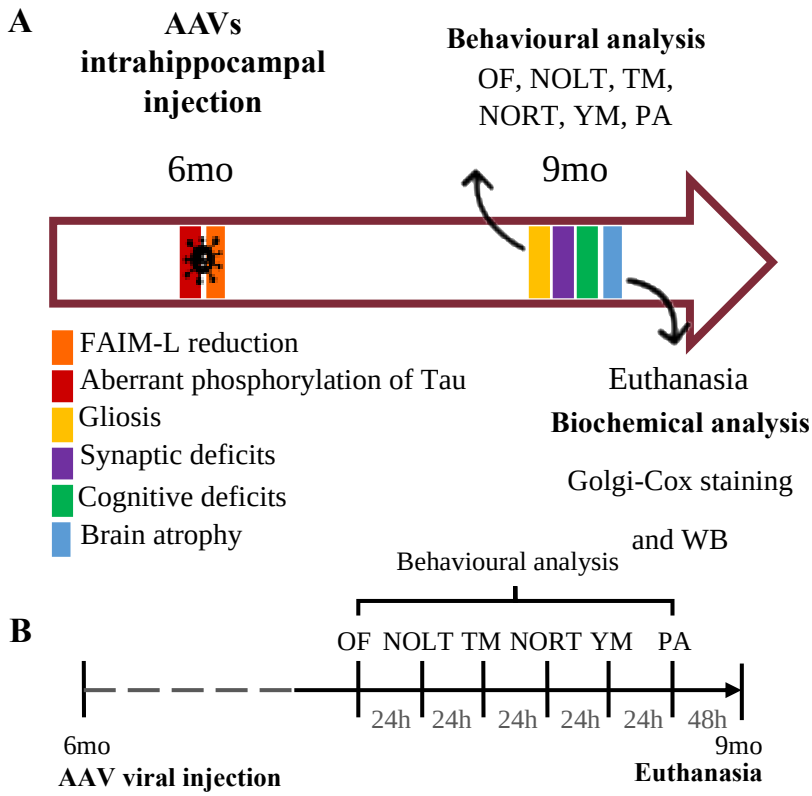

Figure 63: Experimental design used for *in vivo* analysis of FAIM-L overexpression effects in the progression of tau pathology in PS19 mice. (A) Scheme of all procedures performed in injected animals. 6 months-old (mo) WT and PS19 mice were bilaterally and intrahippocampally injected and maintained for 3 months. After this time, animals were subjected to a battery of cognitive tests to determine alterations in hippocampal-dependent memories. Then, animals were euthanized, and brains were processed for biochemical analysis. Sequence of pathological events reported for PS19 mouse model in this work are also provided, according to the legend. (B) Scheme of cognitive tests performed in injected animals. Animals were let resting for 24h between one test and the next one. A total of 3 independent sets of animals (with balanced genotypes and injection conditions) were injected to cover all the analyses. Two sets of animals were used for behavioral analyses and Golgi-Cox staining and another set weas destinated exclusively to WB analysis. OF, Open Field; NOLT, Novel Object Location Test; TM, T-Maze Test; NORT, Novel Object Recognition Test; YM, Y-Maze Test; PA, Passive Avoidance Test.

Briefly, we injected our animals when FAIM-L is already decreased but the rest of biochemical and cognitive alterations are still not developed (6 months-of-age). Then, we analysed them at 9 months-of-age, coinciding with the

emergence of synaptic deficits, neuroinflammation and alterations in proteostasis. Our design included four experimental groups: WT and PS19 mice both injected with AAVs containing CTL (AAV:CTL) or FAIM-L (AAV:FAIM-L) sequence. These groups presented balanced females and males individuals and are named as WT:CTL (n=17), PS19:CTL (n=8), WT:FAIM-L (n=7) and PS19:FAIM-L (n=10), respectively.

24. Intrahippocampal injection of FAIM-L AAVs ameliorates body weight loss in PS19 mice and avoids brain atrophy

General health conditions of PS19 mice decrease progressively after 8 months of age according to bibliography[92]. For this reason, during the 3 months period after injection we determined the wellbeing of our animals by determining the body weight every month. This evaluation showed that, while there were no differences in body weigh between genotypes at the moment of injection (6 months; **Figure 64A,**), In particular, whiel WT groups increased their weigh during the 3 months, PS19 mice progressively lost weight. Thus, significant differences were reported by 9 months of age (**Figure 64B**). Interestingly, viral injection of FAIM-L partially reduces weight loss in PS19 mice (**Figure 64A**), as shown by the significant reduction in weight differences between PS19:FAIM-L and WT animals ($p < 0.05$) compared to PS19:CTL ($p < 0.001$). (**Figure 64B**), indicating a improvement in general wellbeing in these animals.

Then, as PS19 mice show neuronal loss at later stages of the disease[92], and hippocampal atrophy has been detected in these mice by 12 months[96], we explored if FAIM-L overexpression was able to reduce brain atrophy in our mice. For that, we measured total brain weight in the moment of euthanasia. Results confirmed that, while PS19:CTL showed a reduced brain weight

compared to WT animals, FAIM-L injection completely avoided brain atrophy (**Figure 64C**).

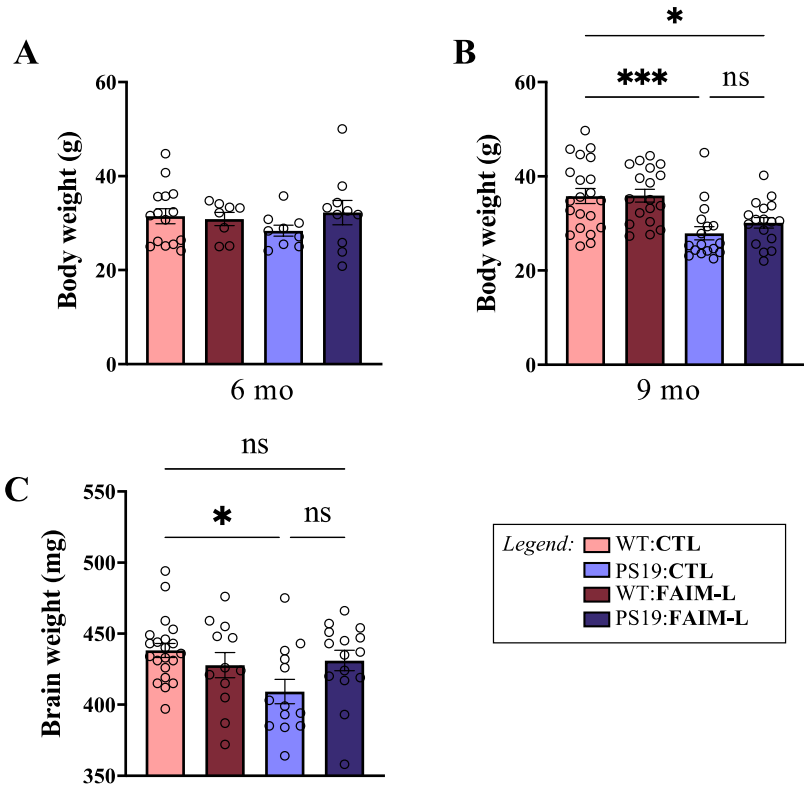

Figure 64: FAIM-L restoration in the hippocampus of PS19 mice prevents from body weight loss and brain atrophy. Body (A, B) and brain weight (C) were measured in 9 months-old WT and PS19 mice injected with AAV:CTL or AAV:FAIM-L. In (A) progressive loss of body weight was registered by measuring body weight monthly. Graphs are represented by the mean ± SEM (n = 17-21 per group). *$P < 0.05$; ***$P < 0.001$ when comparing to WT:CTL mice in (A,B and C). Genotype effect ($F_{(1, 69)} = 22.85$: $P < 0.0001$) in (A); Interaction [genotype x treatment] effect ($F_{(1, 57)} = 4.986$: $P = 0.0295$) in (B) (two-way ANOVA followed by Bonferroni's post hoc test. g, grams; mg, milligrams; ns, non-significant. Each point corresponds to the value from an individual mouse.

Alltogether, the improved health conditions and the absence of brain atrophy in PS19:FAIM-L mice, reinforced our hypothesis of FAIM-L preventing tau-associated pathology.

25. Viral overexpression of FAIM-L partially prevents cognitive deficits in PS19 mice

Importantly, all the molecular and cellular alterations that occur in patients of neurodegenerative diseases converge in a general health decline and an accurate representation of different clinical symptoms. Among them, cognitive alterations and loss of memory are classically observed in frontotemporal dementias. For this reason, and before analyzing other biochemical parameters, we studied hippocampal-dependent learning and memory in our animals. With a battery of behavioural tests (**Figure 63B**), we wanted to explore the functional implications of FAIM-L in the progression of these diseases.

25.1 Lack of habituation is partially prevented after FAIM-L normalization in 9-months-old PS19 mice

Initially, animals were tested in the OF test to exclude any motor deficit and anxious/hyperactive behaviours. In this test, the arena is divided in central and peripheric areas. The measurement of the time spent in each area allows to determine if the animal presents anxiety or hyperactive behaviours. Calmed animals tend to spend more time in the centre while anxious animals preferentially go to the periphery, close to the walls. This type of behaviour is called thigmotaxis, and despite being normal at the beginning of the text, its maintenance along time is a clear sign of anxiety[294]. Results showed that there were no differences in the time spent in the centre of the arena between genotypes (**Figure 65A**). To corroborate it, we also determined the parallel index. This parameter is based on spatial navigation strategy in mice and delimit mice tendency to walk straight (when the value is 1.0). Then, straights movements are usually associated with thigmotaxis and a major localization

of the animals close to the walls. Again, no differences were observed between groups (**Figure 65B**), helping us to discard anxiety in our mice.

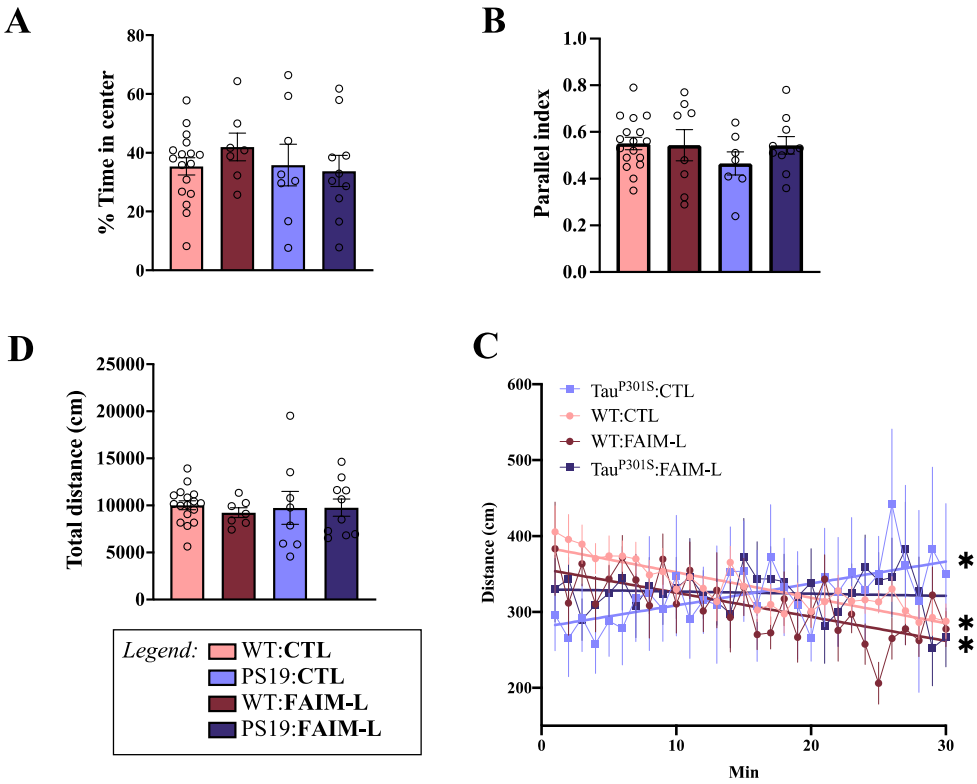

Figure 65: 9-months-old PS19 lack of habituation is amoliorated by the overexpression of FAIM-L. Locomotor activity and anxiety in the OF test were assessed for 30 min in 9 months-old WT and PS19 mice injected with AAV:CTL and AAV:FAIM-L. (A) Percentage of time spent in the center of the arena. (B) Parallel index was used to determine spatial navigation strategy in mice (1.0 means walking straight. (C) Total distance travelled in the arena during the test. (D) Distance travelled in the whole arena per minute. Graphs represent mean ± SEM (n = 7-17 per group). In (D) WT:CTL *(R^2 = 0.7728; $F_{(1,28)}$ = 95.23; *P < 0.0001)*; WT:FAIM-L *(R^2 = 0.4663; $F_{(1,28)}$ = 24.46; *P < 0.0001)*; PS19:CTL *(R^2 = 0.4169; $F_{(1,28)}$ = 20.02; *P = 0.0001)* and PS19:FAIM-L (R^2 = 0.007973; $F_{(1,28)}$ = 0.2250; P = 0.6389); *P < 0.001* when slopes from PS19:CTL and PS19:FAIM-L are compared. Two-way ANOVA followed by Bonferroni's post hoc test in (A, B, C) and linear simple regression in (D). Each point corresponds to the value from an individual mouse in (A, B, C).

Distance travelled in the arena is usually used to determine the presence of motor impairment when decreased, or hyperactive behaviour when it is increased. Also, by measuring the distance travelled per minute of the test, we

can determine deficits in habituation[295]. No differences were observed regarding total distance (**Figure 65C**), further discarding hyperactivity in PS19 mice. However, a differential pattern of activity was observed when distance travelled every minute was checked (**Figure 65D**). Both WT:CTL and WT:FAIM-L showed an progressive habituation to the environment as shown by a reduced exploration within time (and measured by a significant negative correlation between distance and time in both treated WT groups) **(Figure 65D,** *light and maroon lines*, respectively) Conversely, PS19:CTL mice showed an increase in distance travelled among time, as shown, in this case, by a significant positive correlation (**Figure 65D**, *light purple line*). Interestingly, this behaviour was slightly reduced in PS19:FAIM-L mice. (**Figure 65D,** *dark purple line*).

In summary, by 9 months-of-age, PS19 mice did not show motor impairment, anxiety, or hyperactivity. However, they were unable to progressively familiarizate to the arena of the OF. FAIM-L restoration partially prevented this lack of habituation.

25.2 Long-term spatial and recognition memory are not affected in 9-months-old PS19 mice

Impaired locomotion, anxiety or hyperactivity may interfer with the results in other behavioural tests. As we did not report any of them, we were able to correctly analyse the other tests planned. Long-term spatial and recognition memory are two types of non-associative memories based on a feeling of familiarity. They have been widely considered dependent on the hippocampus integrity[296,297]. In animals, we can evaluate the status of these long-term memories through the NOL and NOR tests. This is achieved by calculating the preference for a newly located object (NOLT) and a new object (NORT),

compared to a familiar one. This preference is calculated by measuring the percentage of time (% time, s) that the animal explores each object during a testing session and comparing them (old location or old object compared to the new one).

Results showed that, in the NOLT, PS19 mice had preference for the new located object (**Figure 66A**). Surprisingly, WT mice did not show a significant higher exploration of the object in the new location comparing to the non-moved ones. Instead, both PS19:CTL and PS19:FAIM-L mice presented higher preference for the object in the new location when tested (**Figure 66A**), showing intact spatial memory. To further explore this phenomenon, we analysed animal performance separating them by sex. When only males were considered for the analysis, all genotypes correctly discriminated the new location (**Figure 66B**).

Figure 66: PS19 mice present intact long-term spatial and recognition memories. NOLT (A,B) and NORT (C) were performed in 9 months-old WT and PS19 mice injected with AAV:CTL or AAV:FAIM-L. In (B) only males were considered in the analysis of the NOLT. Graphs show the percentage of time exploring old (O) and new (N) location (L) or object with respect to the total exploration time in the testing session of each test. Graphs represent mean ± SEM (n = 7-17 per group). ** $P < 0.01$; *** $P < 0.001$ compared to the old location in each group; location effect ($F_{(1, 76)} = 31.05$; $P < 0.0001$) in (A). * $P < 0.01$; ** $P < 0.001$; *** $P < 0.0001$ when compared with the old object of each group; object effect ($F_{(1, 76)} = 98.17$: $P < 0.0001$) in (B) (three-way ANOVA followed by Bonferroni's post hoc test). Each point corresponds to the value from an individual mouse.

(figure in next page)

A

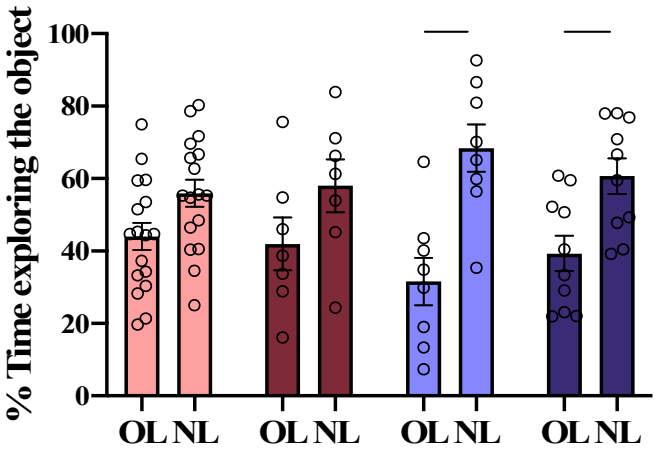
% Time exploring the object
100
80
60
40
20
0
OL NL
OL NL
OL NL
OL NL

B

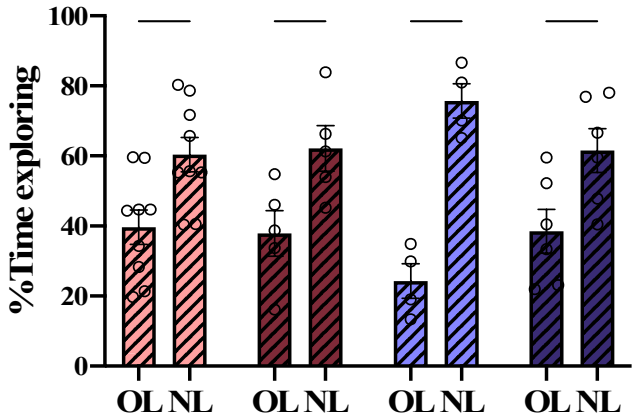
%Time exploring
100
80
60
40
20
0
OL NL
OL NL
OL NL
OL NL

C

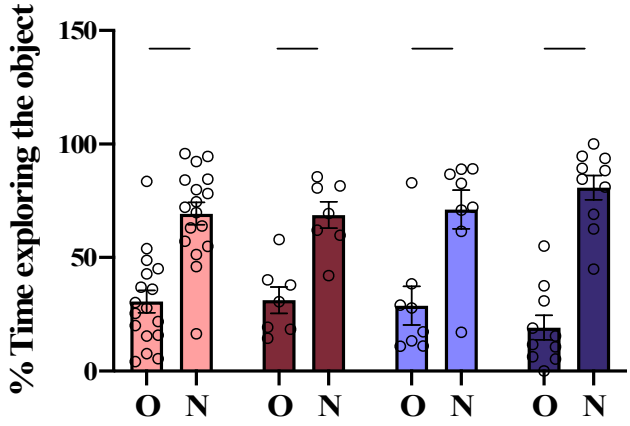
% Time exploring the object
150
100
50
0
O N
O N
O N
O N


Legend:
WT:CTL
PS19:CTL
WT:FAIM-L
PS19:FAIM-L
Male
All animals

Regarding NORT, all animals significantly spent more the time exploring the new object compared to the old ones (**Figure 66C**). Then, we confirmed discriminatory capacity and intact hippocampal recognition memory in PS19 mice but also in WT animals. This result suggested some environmental interference in the NOLT and helped us to dismiss any severe memory alterations in WT animals. Unfortunately, the absence of impairment in long-term spatial and recognition memories by 9 months in the control PS19 impeded us to determine the effect of FAIM-L regarding to these cognitive capacities.

25.3 FAIM-L injection enhances discriminatory capacities in PS19 mice

Another classical test for measuring spatial memory is the T-maze. As for the other tests, it is based on the discrimination by familiarity. This time, the preference for a novel arm (closed in the training) versus the familiar (opened in the training) during a testing session (**Figure 67**).

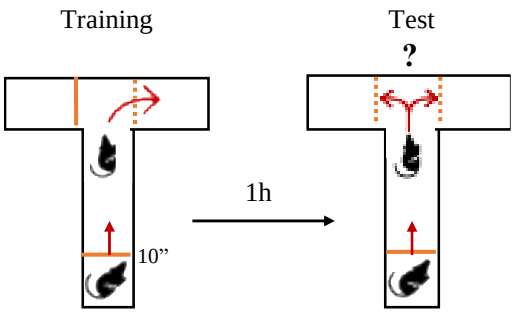

Figure 67. Graphical diagram of the T-Maze apparatus. Diagrams of the training (left) and testing (right) sessions of the T-maze test. Lines represent closed arms and dotted lines represent accessible arms. Animals were placed for 10 s in the vertical arm before starting the test. During the test, their preference for the new open arm was tested.

We measured the percentage of time exploring both arms and the distance travelled in each arm, and the number of entries in the new and the familiar arms. When we analyzed the percentage of time exploring each arm, we observed an improvement in the performance in those animals injected with FAIM-L (**Figure 68A**). In this regard, PS19:FAIM-L mice showed a

significantly higher preference for the new arm and WT:FAIM-L animals presented the same tendency (non-significant; *p = 0.082*). By contrast, both WT and PS19 mice injected with CTL AAV did not show significant discrimination between arms. This increased preference was also observed in the PS19:FAIM-L when distance travelled was measured (**Figure 68B**), but not observed when number of entries to the new arm were calculated (**Figure 68C**).

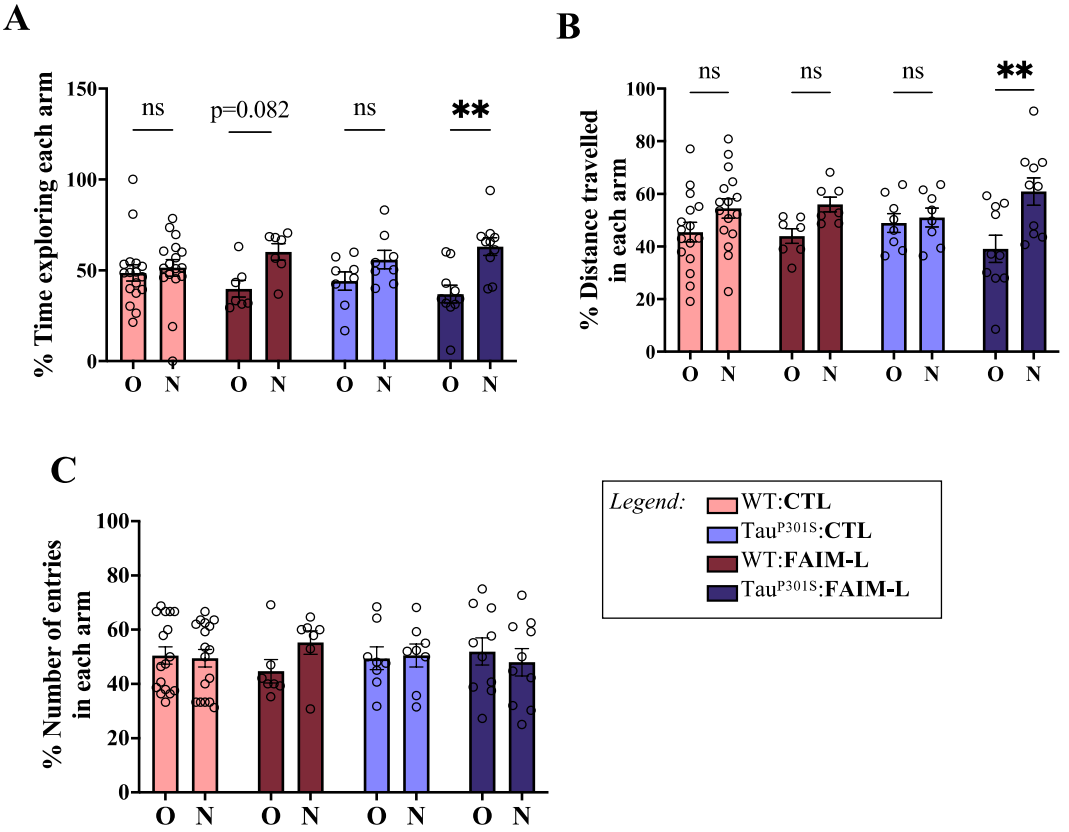

Figure 68: FAIM-L overexpression enhances spatial discrimination in 9 months-old mice. Spatial memory was tested in 9 months-old WT and PS19 mice injected with AAV:CTL or AAV:FAIM-L using the T-maze test. Preference for the newly opened arm (N) compared to the arm opened during training (O) was measured in the testing session by analyzing the time exploring (A), the distance travelled (B) and the number of entries (C) to each arm and expressed as percentage of the total time, distance or number of entries, respectively. Graphs represent mean ± SEM (n = 7-17 per group). In (A) * $P < 0.05$ when comparing the new the old arm in each group; arm effect ($F_{(1, 76)} = 16.40$: $P = 0.0001$); Interaction [arm x treatment] effect ($F_{(1, 76)} = 4.522$: $P = 0.0367$). In (B) ** $P <$

0.01 when comparing the new with the old arm in each group; arm effect ($F_{(1, 74)} = 12.85$: $P = 0.0006$); Three-way ANOVA followed by Bonferroni's post hoc test. Each point corresponds to the value from an individual mouse. ns, non-significant.

Altogether, these results showed that FAIM-L overexpression enhanced discriminatory capacity of mice, which even not entering more times to the new arm, spent more time exploring it. Finally, as we had observed an anomalous behaviour in WT mice, we decided to determine locomotion activity and exploration in our mice. Then, we measured the total number of entries (**Figure 69A**) and the total distance travelled (**Figure 69B**) in each group. We did not observe differences in either of them. Thus, we could not justify unexpected WT performance in the T-maze by the presence of any pattern of anxiety, hyperactivity or altered motility.

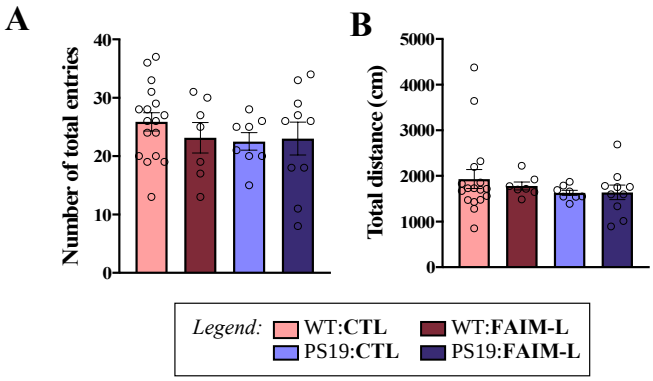

Figure 69: 9-months-old animals did not show locomotor impairment or hyperactivity during the T-maze test. (A) Total number of entries in the testing session (B) Total distance travelled during the test (three-way ANOVA followed by Bonferroni's post hoc test).

25.4 FAIM-L overexpression does not recover the impaired working memory present in PS19 mice

The hippocampus has been also found to get recruited during working memory[298]. In order to determine any possible effect of FAIM-L restoration in working memory, we performed the Y-maze test. This test is based on innate curiosity of rodents to explore previously unvisited areas. Then, working memory was analysed by calculating the spontaneous alternation performance. As healthy mice show less tendency to enter to most recently visited areas, the arm entrance record is mostly altern (**Figure 70A**; *correct vs. incorrect*) and superior to the spontaneous alternance (by chance = 50%). Results showed that only WT:CTL and WT:FAIM-L were significantly above the chance (**Figure 70B**). Number of total entries was also registered in order to analyse animals' exploratory capacity and locomotion. We observed that PS19:CTL mice showed significant less arm entrances compared to WT animals, and that FAIM-L injection reduced this difference respect WT animals ($p < 0.05$) when compared to PS19:CTL mice ($p < 0.01$) (**Figure 70C**). The absence of any major locomotor impairment suggested us that this reduced distance travelled could be caused by a lesser exploration. However, we could not completely exclude it here since we did not dispose of information regarding to total distance travelled by each group or the time spent in each arm. In any case, we observed how FAIM-L injection slightly improved mice predisposition to explore the maze. However, it was unable to restore working memory in PS19 mice.

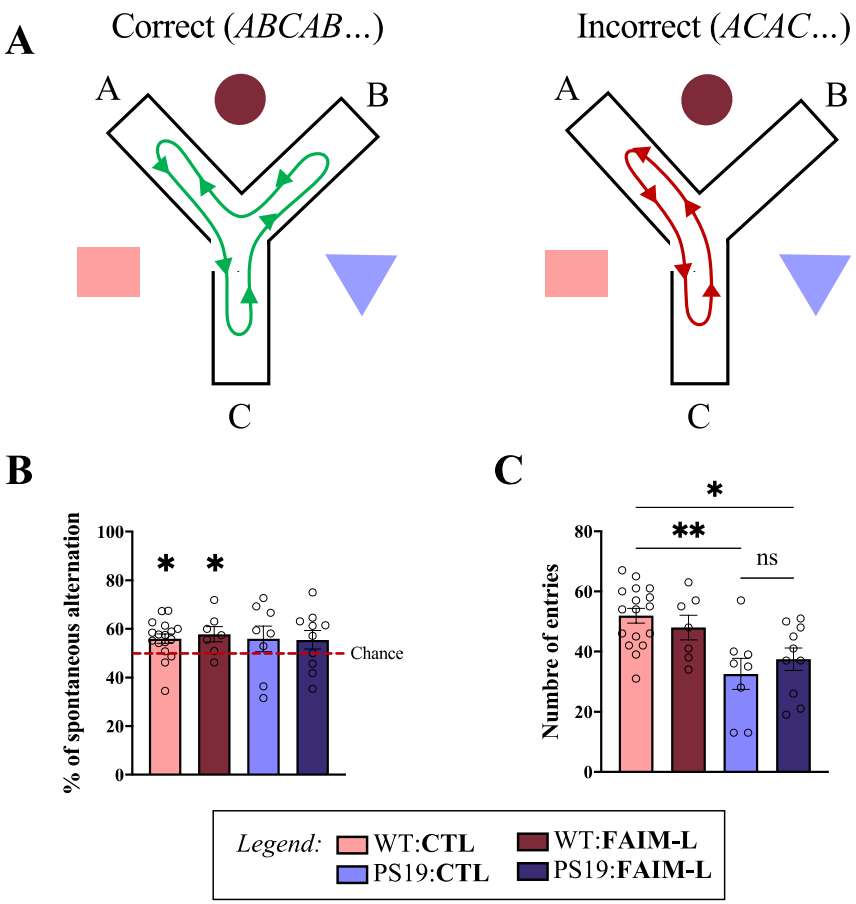

Figure 70: FAIM-L levels restoration does not rescue spatial working memory in PS19 mice. Y-Maze test was performed in 9 months-old WT and PS19 mice injected with AAV:CTL or AAV:FAIM-L, and the sequence of entries was registered during 10 min. (A) Diagrams of the correct (left; entry in a non-visited arm) and incorrect (right; entry in a recently visited arm) alternations in the Y-maze. Distal clues (represented as geometric figures) were located next to each arm of the maze. (B) Percentage of spontaneous alternance measured as triades. 50% of alternation is considered as chance. (C) Total number of entries in all arms during the test. Graphs represent mean ± SEM (n = 7-17 per group). * $P < 0.05$ when compared to Chance (Student's t-test for each group) in (B). * $P < 0.05$; ** $P < 0.01$ when compared with WT:CTL mice (Two-way ANOVA followed by Bonferroni's post hoc test) in (C). Each point corresponds to the value from an individual mouse. ns, non-significative.

25.5 FAIM-L restoration in the hippocampus of PS19 mice is able to prevent associative memory deficits

Associative memory is defined as the ability to learn and remember the relationship between unrelated items in one scenario. The hippocampus has been considered to play a critical role in binding together all those different attributes of the episode (Borders et al., 2017)[299]. To analyse this type of memory in our animals, we performed the Passive Avoidance Test and measured the latency to cross from the bright compartment to the darker one.

We measured this time to step-through at the training and testing phases and compared them (recall latency) (**Figure 71**). First, results showed that there were no differences in the time to step-through during the training session between the four groups. Only in the PS19:CTL group, one animal presented an increased latency to cross. This type of behaviour can be considered a signal of neophobia. Howewer, no reports of this kind of behaviour have been described for this mouse model. When we recorded the time to step-trough in the testing session, we observed an increased recall latency for both WT:CTL and WT:FAIM-L. Interestingly, a similar delay was observed in the PS19:FAIM-L group, being statistically indistinguishable from WT mice. By contrast, PS19:CTL did not required more time to step-through the chambers during the test, showing deficient associative memory.

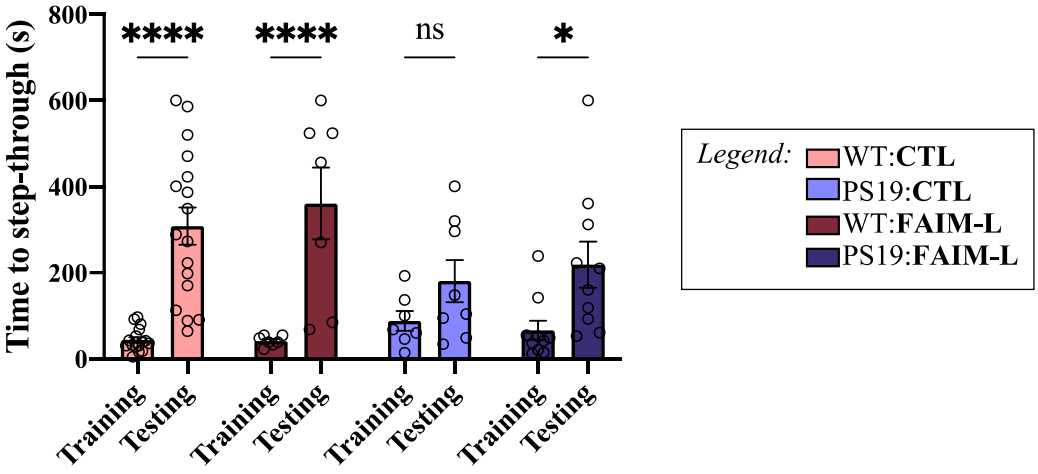

Figure 71: Restoration of FAIM-L levels completely avoids associative memory loss in 9-months-old PS19 mice. Capacity of association was analyzed in 9 months-old WT and PS19 mice injected with AAV:FAIM-L and AAV:CTL using the Passive Avoidance paradigm. Recall latency was measured during the training and the testing sessions. Graphs represent mean ± SEM (n = 7-17 per group). * *P < 0.05;* **** *P < 0.0001* when comparing to time to step-through in the training vs the testing session. Testing/training effect ($F_{(1, 76)}$ = 44.15*: P < 0.0001*); Interaction [Training/Testing x Genotype] effect ($F_{(1, 76)}$ = 9.179*: P = 0.0033*); (three-way ANOVA followed by Bonferroni's post hoc test). Each point corresponds to the value from an individual mouse. s, seconds; ns, non-significant.

Altogether, the data we have presented so far demonstrate that, even PS19 mice still do not present prominent cognitive deficits by 9 months-of-age, the restoration of FAIM-L levels in the hippocampus of these mice enhanced discrimination capacities and spatial learning and, more importantly, rescued associative memory deficits already observed in PS19 mice by this age.

26. FAIM-L rescues synaptic loss in the hippocampus of PS19 mouse model

Synaptic plasticity is a prime process underlying learning and memory formation. Abnormalities involving dendritic spines, postsynaptic density, or LTP/LTD-like plasticity are usually impaired in neurodegenerative diseases and lead to cognitive dysfunction[68,69]. Here, we have demonstrated the ability of FAIM-L to enhance spatial memory and discrimination and the rescue of

associative memory in affected mice after its overexpression in the hippocampus. Interestingly, this improvement in memory functionality agrees with the known participation of FAIM-L in plasticity processes through indirect caspase-3 regulation (LTD or axonal pruning). For this reason, we next wanted to determine the status of synaptic plasticity after the viral injection of FAIM-L in the hippocampus of PS19 mice. One of the most direct consequences of these impaired activity-dependent adaptations is the pruning of dendritic spines[300]. Under abnormal LTP/LTD processes, maturation and maintenance of these synaptic platforms are altered.

CA3 connection to the CA1 is essential for LTP and correct hippocampal memory function[301–303]. By analysing these neurons, we can determine the integrity of the post-synaptic compartment and then infers the functional status of these connections. Thus, we analysed spine density in post-synaptic CA1 pyramidal neurons. Golgi-Cox staining is a useful method for study neuronal morphology and visualization of dendritic spines[282]. For that, we counted spine boutons in the apical dendrites of these neurons (**Figure 72A,B;** *red box*). Spines density impairment was clearly visualized by comparing PS19:CTL mice with the other three groups (**Figure 72B**). Then, quantification of the number of spines (per μm of dendrite) confirmed this spine density reduction in PS19 mice (**Figure 72C**). More interestingly, it revealed that this reduction was prevented in PS19:FAIM-L, reaching equivalent values to the WT, and significantly different compared to the PS19:CTL group. Then, Golgi-Cox results confirmed that the restoration of FAIM-L levels in the hippocampus of PS19 totally prevented spine loss.

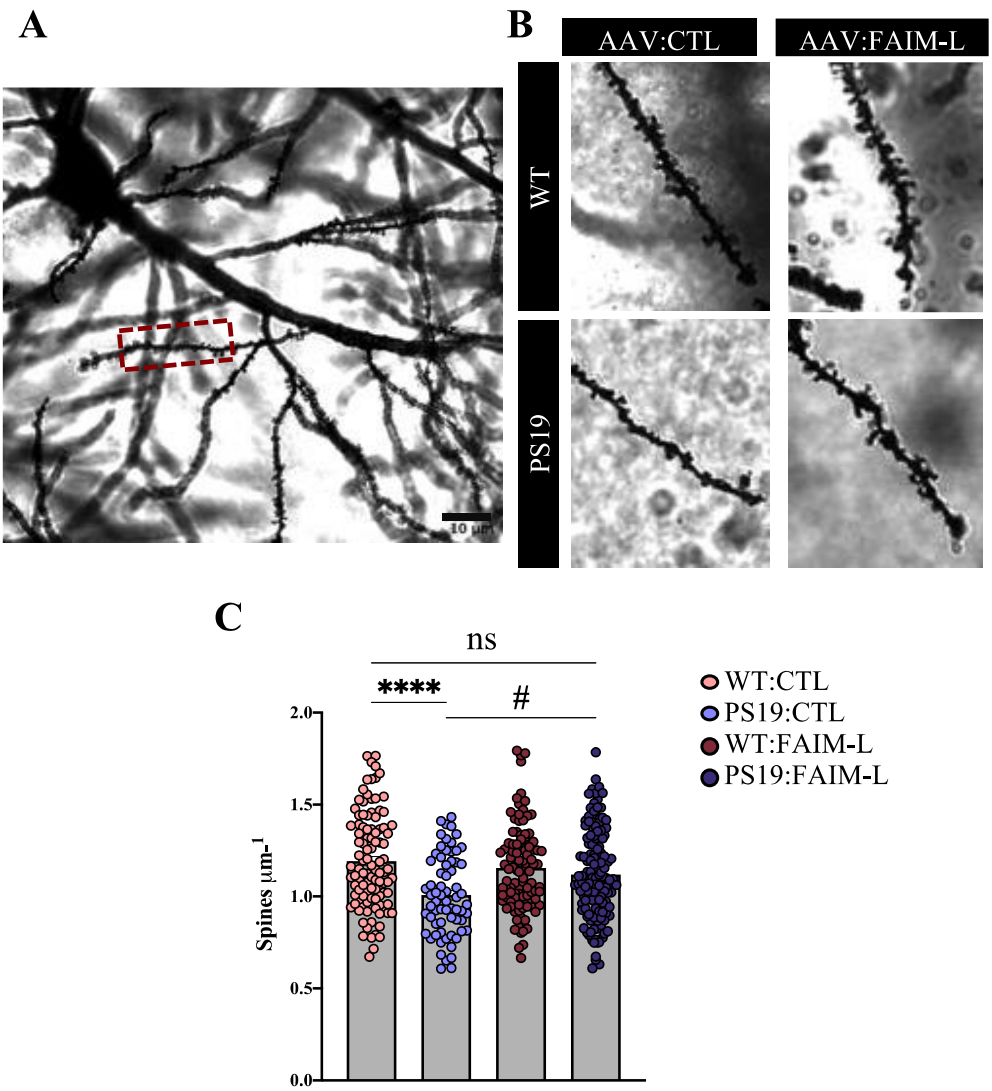

Figure 72: Overexpression of FAIM-L mice prevents synaptic loss in the CA1 region of the hippocampus in 9 month-old PS19 mice. Golgi-Cox staining was performed in hippocampal slices from 9 months-old WT and PS19 mice injected with AAV:CTL or AAV:FAIM-L. (A) Representative image of a Golgi-Cox stained CA1 pyramidal neuron at stratum radiatum area. (B) Representative images of Golgi-Cox stained apical dendrites from CA1 pyramidal neurons in WT and PS19 mice injected with AAV:CTL and AAV:FAIM-L. (C) Quantification of spine density in dendrites as in (B), represented as number of spines x μm^{-1}. Graphs represent mean ± SEM (n = 67-135 spines per group). # $P < 0.05$ when comparing with PS19:CTL; **** $P < 0.0001$ when comparing with WT:CTL. Interaction [Genotype x Treatment] effect ($F_{(1, 409)} = 9.270$; $P = 0.0025$); (two-way ANOVA followed by Bonferroni's post hoc test). Each point corresponds to the value from an individual dendrite. ns, non-significant.

27. FAIM-L overexpression helps preventing the loss of post-synaptic components observed in the hippocampus of PS19 mice

Post-synaptic density (PSD) maintenance and dynamism, and NMDA receptors trafficking in glutamatergic synapses are essential for the preservation of spines[304]. Consequently, mislocalization of PSD elements or internalization of glutamate receptors and their degradation leads to impaired LTP and enhanced LTD and to spine degeneration[70,305]. Here, we had confirmed a spine loss in PS19 mice and a total avoidance of this degeneration through FAIM-L overexpression. For that, we hypothesized that FAIM-L could also be preventing alterations in the post-synaptic unit components.

When we characterized the time-course of the disease in our model, we reported PSD95 and mGluR2 downregulation in the hippocampus by 9-months-old. Thus, we decided to determine the levels of these proteins after the hippocampal injection. We first determined the integrity of PSD compartment by checking PSD95 levels. WB results showed that FAIM-L was able to prevent the reduction of PSD95 obseved in PS19:CTL when compared to both WT groups (**Figure 73A**). Then, we analysed mGluR2 levels. Our laboratory had previously reported the role of FAIM-L in avoiding the internalization of the mGluR2 receptor[250]. Now, our results revealed that FAIM-L restoration partially prevented mGluR2 loss also in our mice, although the effect remained statistically non-significant (**Figure 73B**).

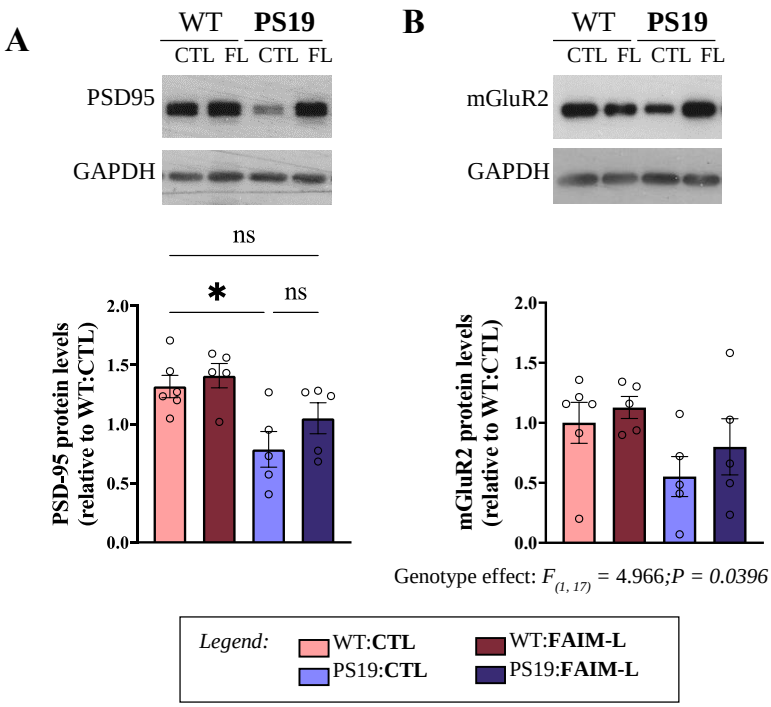

Figure 73: FAIM-L partially prevents post-synaptic protein loss in 9 months-old PS19 mice. PSD95 (A) and mGluR2 (B) protein levels were analyzed by WB in protein extracts obtained from the hippocampus of 9 months-of-age WT and PS19 mice injected with AAV:CTL or AAV:FAIM-L. Graphs represent arbitrary units (obtained by densitometric analysis of immunoblot images; GAPDH ratio) and are compared to AAV:CTL. Data is shown as mean ± SEM (n=5-6). Representative immunoblots are shown. *$P < 0.05$ when comparing as indicated; Genotype effect ($F_{(1, 17)}$ = 13.85*: P = 0.0017*) in (A); Genotype effect ($F_{(1, 17)}$ = 4.966*: P = 0.0396*) (two-way ANOVA followed by Bonferroni's post hoc test). Each point corresponds to the value from an individual mouse. ns; non-significant.

With these results, we concluded that FAIM-L also contributed to the restoration of synaptic plasticity in the hippocampus PS19 mice by partially preventing classical post-synaptic proteins loss, and especially by maintaining PSD integrity.

28. Restoration of FAIM-L levels in hippocampal neurons is not sufficient to prevent XIAP degradation neither the increased ubiquitination pattern present in PS19 mice

This protection of synaptic integrity could be explained by FAIM-L capacity to regulate non-apoptotic caspase-3 functions through the stabilization of XIAP protein and the prevention of its ubiquitination. We had observed a reduction in XIAP protein levels and an increase in global protein ubiquitination by 9 months of age. Thus, we proceded to determine the effect of FAIM-L restoration regarding these two parameters. WB results revealed that XIAP was decreased in PS19 hippocampus, but the recovery of FAIM-L levels was not able to prevent this XIAP loss (**Figure 74A**). Similar results were obtained when ubiquitination was analyzed. It was significantly increased in transgenic mice, but not normalized after the overexpression of FAIM-L (**Figure 74B**). Therefore, we can conclude that FAIM-L restoration in neurons was not sufficient to observe a prevention in XIAP levels reduction or to normalize ubiquitination rates in the hippocampus of our mice.

Figure 74: FAIM-L overexpression in the hippocampus of 9 months-old PS19 mice is not able to normalize XIAP and ubiquitin levels. XIAP (A) and global protein ubiquitination (B) levels were analyzed by WB in protein extracts obtained from the hippocampus of 9 months-of-age WT and PS19 mice injected with AAV:CTL or AAV:FAIM-L. Graphs represent arbitrary units (obtained by densitometric analysis of immunoblot images; XIAP/GAPDH ratio or Ubiquitin/Ponceau ratio) and are compared to WT:CTL. Data is shown as mean ± SEM (n=5-6). Representative immunoblots are shown. Genotype effect ($F_{(1, 17)}$ = 4.467*: P = 0.0497*) in (A); Genotype effect ($F_{(1, 16)}$ = 5.546*: P = 0.0316*) in (B); (two-way ANOVA followed by Bonferroni's post hoc test). Each point corresponds to the value from an individual mouse.

(figure in next page)

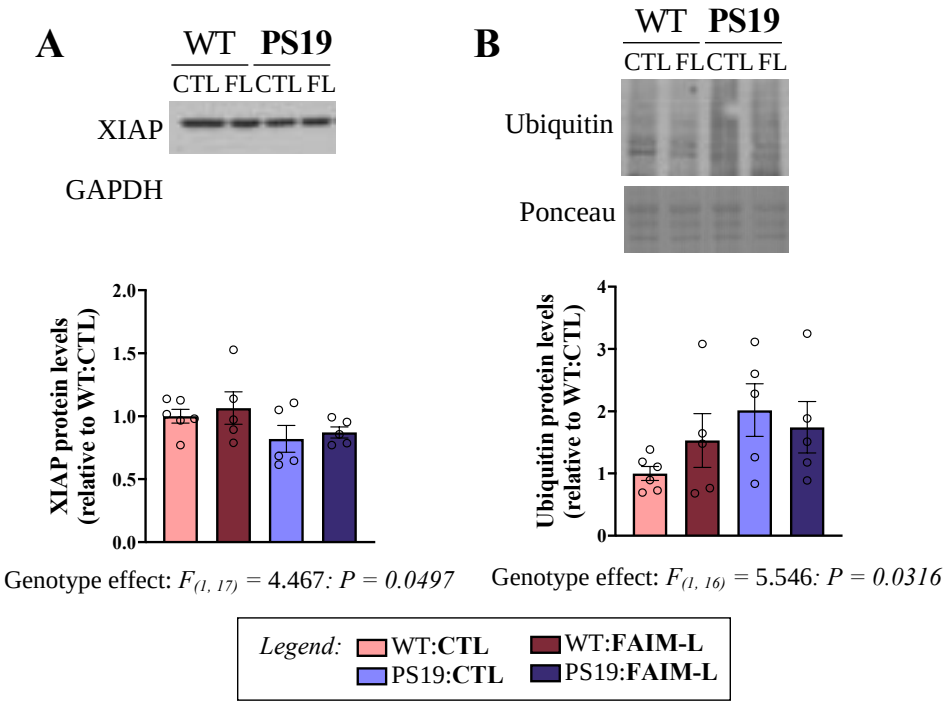

29. Restoration of FAIM-L levels does not affect phosphorylation status of tau

We were unable to detect effects in global ubiquitination after FAIM-L overexpression. However, in this work we have proved that FAIM-L is capable of directly prevent tau ubiquitination, which has been related to tau aggregation[288,289]. Interestingly, a positive loop between these two PTMs has been established. Both ubiquitination and phosphorylation can enhance the aberrant accumulation of the other PTM, facilitating tau aggregation[306,307]. Unfortunately, as we disposed of a limited amount of sample of injected animals, we could not specifically check for tau ubiquitination and its further aggregation in these conditions. For that and based on this mentioned relationship between ubiquitination and phosphorylation, we decided to analyse pTau levels in injected mice as a distant approximation. However, WB

analysis did not reveal major changes in pTau / Tau ratio after FAIM-L overexpression (**Figure 75**).

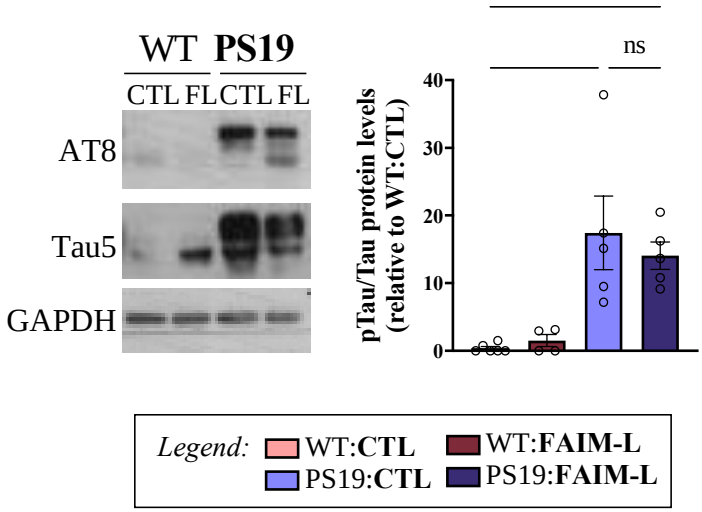

Figure 75: Phosphorylated Tau was not reduced after FAIM-L overexpression in the hippocampus of PS19 mice. Phosphorylated Tau (AT8) and total Tau levels were analyzed by WB in protein extracts obtained from the hippocampus of 9 months-of-age WT and PS19 injected with AAV:CTL and AAV:FAIM-L. Graphs represent arbitrary units (obtained by densitometric analysis of immunoblot images; pTau/Tau Ratio or Tau5/GAPDH ratio) and are compared WT:CTL. Data is shown as mean ± SEM (n=5-6). Representative immunoblots are shown. * *P < 0.05;* ** *P < 0.01*; Genotype effect ($F_{(1, 16)}$ = 25.16*: P = 0.0001*); (two-way ANOVA followed by Bonferroni's post hoc test). Each point corresponds to the value from an individual mouse.

30. FAIM-L overexpression does not reduce inflammation in the hippocampus of PS19 mice

Astroglia and microglia play an important role in neurodegenerative diseases. In AD, aberrant activation of glial cells is also reported increased in response to the toxicity derived from tau hyperphosphorylation and its pathological processing as well as after synaptic failure[81,308,309]. Based on that, we finally determined the levels of GFAP in the hippocampus of our injected mice at 9 months-of-age. However, we did not see any effect of FAIM-L restoration in

the reduction of reactive astrogliosis associated to the pathology in the PS19:FAIM-L mice (**Figure 76**). This result suggested that despite FAIM-L restoration protected from synaptic failure and ameliorated the progression of the disease, it was not able to reduce the neuroinflammation associated to the pathology.

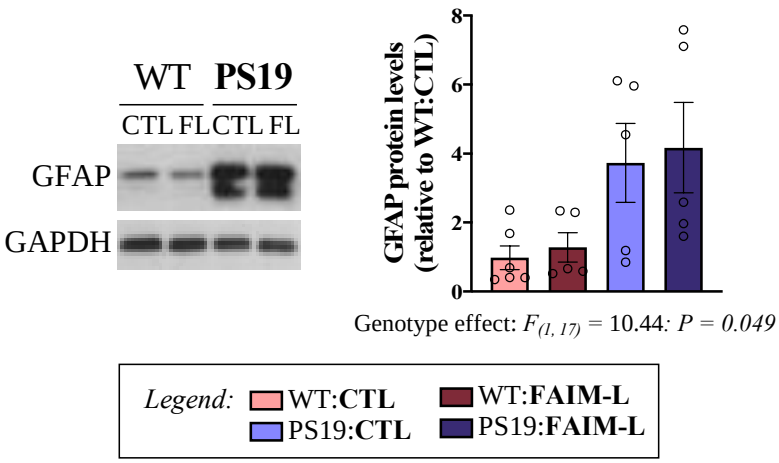

Figure 76: FAIM-L restoration is not able to reduce astrogliosis in PS19 mice. GFAP protein levels were analyzed by WB in protein extracts obtained from the hippocampus of 9 months-of-age WT and PS19 injected with AAV:CTL or AAV:FAIM-L. Graphs represent arbitrary units (obtained by densitometric analysis of immunoblot images; GAPDH ratio) and are compared to WT:CTL and shown as mean ± SEM (n=5-6). Representative immunoblots are shown. Genotype effect ($F_{(1, 17)} = 10.44$*: P = 0.049*); (two-way ANOVA followed by Bonferroni's post hoc test). Each point corresponds to the value from an individual mouse.

In summary, along this work, we have been able to establish FAIM-L contribution to AD by directly relating it to tau pathology. Using mouse models of the disease, we have proved that this protein is downregulated only in mouse models coursing with severe tau alterations. This reduction is dependent on one of the prime aberrant modifications of tau, its phosphorylation. Indeed, as FAIM-L reduction occurs before the onset of the other pathological hallmarks, its exogenous overexpression in the hippocampus of the PS19 mouse model, protects from the progressive

neurodegeneration. Importantly, FAIM-L expression recovery maintains post-synaptic and dendritic spine integrity that finally leads to the prevention of the brain atrophy and memory loss observed in this mouse. Interestingly, its protective effect may be achieved by an additional function of FAIM-L that we have discovered here: its ability to prevent a non-degradative form of tau ubiquitination.

DISCUSSION

VI. DISCUSSION

AD is the most prevalent neurodegenerative disease nowadays. It affects more than 40 million people affected worldwide. Its exponential increase and the high socio-economic impact associated have made crucial to find a successful treatment. However, the complexity, heterogeneity, and its late onset, make the discovery of potential treatable targets especially challenging. Therefore, it is essential to dismantle the early and direct pathological mechanisms that underly AD. By studying them, we will be closer to prevent neurodegeneration.

Synaptic impairment, mitochondrial malfunction and alterations in proteostasis are directly related to the progressive neuronal dysfunction and loss[310,311]. Thus, in order to avoid aberrant cell death, neurons dispose of an accurate machinery to regulate these processes. Usually, this control is orchestrated by the same elements that mediate cell death. Caspases are the executors of apoptosis but also maintain cell homeostasis. The effector caspase-3, for example, is involved in mitochondrial biogenesis[312], autophagy [313], and, more importantly, in synaptic plasticity[314,315]. Increased caspase-3 activity leads to axonal selective degeneration and pruning[315], spine loss [316] and enhanced LTD due to an excessive AMPA internalization at the post-synaptic membrane[317]. Then, aberrant caspase-3 activity becomes highly related to neurodegeneration[192]. Importantly, several modulators control the correct function and activation of caspases. In case of caspase-3, its activity is inhibited by XIAP. Additionally, XIAP function is controlled by FAIM-L. FAIM-L avoids XIAP ubiquitination and degradation[266], and thus, indirectly regulates caspase-3 activation. Therefore, FAIM-L, XIAP and caspase-3 participates in a complex and multi-step mechanism that maintains synaptic function and cell homeostasis[250,266].

During the past years, our group has stablished the role of FAIM-L in the central nervous system (CNS). We have described the aforementioned capacity to prevent XIAP ubiquitination and degradation[266]. In addition, we have associated FAIM-L to neurodegeneration. First, Carriba et al.,[274] reported a loss of FAIM-L in the hippocampus of AD patients and in the mouse model APPxPS1 before the onset of the pathology. More recently, Sirés et al., [273] have demonstrated that the FAIM KO mouse develops retinal degeneration. In this mouse, FAIM absence is associated to an impaired proteostasis and an accumulation of ubiquitin aggregates. FAIM was already described to regulate ubiquitination and protein aggregation *in vivo* and *in vitro* by Kaku and colleagues[270–272]. Then, our group have firstly linked this capacity to the progressively loss of function and aberrant death of photoreceptors.

Based on this evidence, we suggested that an early loss of FAIM-L in AD might have an impact in neuronal degeneration and in the progression of the disease. Therefore, we proposed this protein as a compelling candidate for the treatment of AD. In the present Theis, we further explored this hypothesis by characterizing FAIM-L decrease, determining the consequences of its downregulation in the course of AD pathology, and studying the effect of its restoration in a mouse model of the disease. The present results demonstrate that FAIM-L loss is directly related to tau pathology. Indeed, they show that FAIM-L reduction precedes the rest of tau-derived alterations. Finally, they prove that FAIM-L restoration counteracts degenerative and functional alterations reported in the PS19 mice. We have demonstrated that, when we overexpressed FAIM-L in the hippocampus of the PS19 mice, we prevented synaptic impairment and avoided brain atrophy and cognitive deficits.

One of our central objectives consisted in counteracting FAIM-L decrease *in vivo*. Thus, we first performed a screening of FAIM-L loss in different mouse

models of AD. Conventionally, *APP* mouse models pathology coursed without tau alterations. However, recent studies have shown some insights of tau pathology in these animals. Females from the 5xFAD mouse model present tau-positive Aβ aggregates by 7 months-of-age[318]. Nevertheless, these animals already present synaptic impairment, cognitive deficits, and neuronal loss by this age[319]. Indeed, they require the exogenous injection of pathological tau for the induction of tangle formation and the acceleration of disease progression[320]. Likewise, the APP23 mouse model shows an increase in pTau levels once the disease has already been settled [321,322,323]. Also, it requires to be crossed with the JNPL3 model to develop a more aggressive and tau-related pathology[324]. In definitive, *APP* mice can develop slight tau pathology, but it usually appears after the manifestation of the rest of pathological alterations. Thus, it suggests a low participation of tau in the course of the pathology in these mice.

We analysed FAIM-L status when Aβ and tau pathology are present both separately and combined. Thus, we included *APP* mouse models, *MAPT* models and a double-transgenic mouse model (3xTg). Our analyses revealed that only *MAPT* mice and double-transgenic mice showed a decrease in FAIM-L protein levels. Thus, we reported for the first time, that FAIM-L decrease is directly related to tau and not to Aβ pathology. Carriba's findings[274] reported a decrease of FAIM-L levels in the entorhinal cortex of APPxPS1 mice by 6 months. Interestingly, these mice presented an early appearance of tau alterations (2 months), before the onset of other hallmarks of the disease[325]. Loss of PSEN function has reported to enhance tau phosphorylation and pathology[326], explaining the early increase in pTau in this model. Indeed, it correlates with the reported decrease in FAIM-L.

Altogether, we suggest that tau alterations must be severe enough to induce a decrease in FAIM-L levels *in vivo*. Then, the tau pathology that develops most of the *APP* mouse models may be insufficient to cause tau-derived alterations and consequently, FAIM-L decrease.

For a better understanding of the causes leading to FAIM-L reduction, we considered essential to perform our research using a *MAPT* mouse model. We selected the PS19 mouse model. This mouse presents one of the most aggressive tau mutations, the P301S. Also, it presents a fast and severe tau pathology progression[92]. Finally, it has been widely used for AD research[93,327–330].

Using this model, we first observed a temporal coincidence between the decrease in FAIM-L levels and the increase in pTau. Then, we confirmed that FAIM-L reduction was specifically dependent on the phosphorylation status of tau. Finally, we have observed that the reduction of FAIM-L was not caused by an alteration in transcription of FAIM-L. Tau is widely known to regulate the transcription of certain genes[149,161,162]. However, whether aberrantly phosphorylated tau is able to regulate proteins degradation remains to be studied. Yin et al.,[331] reported that overexpression and hyperphosphorylation of tau *in vivo* and *in vitro* resulted in a reduction of nicotinic acetylcholine receptor (nAChR) α4. They observed that tau activated calpain-2. Then, calpain-2 cleaved and degraded the α4 nAChR.

So far, little is known about FAIM-L degradation mechanisms, but a calpain-mediated cleavage may be plausible. Our laboratory has recently discovered that FAIM-L present PEST-like motifs in its sequence (*non-published data*). Therefore, FAIM-L could be degraded after protease-mediated cleavage. Second, we have identified calpain-1 and -2 as potential partners of FAIM-L in our MS analysis. Thus, it is reasonable to think that increased pTau could

activate calpains, which in turn, could cleave and degrade FAIM-L. Interestingly, calpain system is altered in other neurodegenerative diseases, such as spinal muscular atrophy (SMA)[332], where protein levels of FAIM-L are also reduced[333].

As mentioned, we observed that FAIM-L loss was dependent on the phosphorylation status of tau. In this work, we modulated pTau levels in PC12 cells and determined FAIM-L protein levels. By doing this, we observed that, when pTau was increased after GSK-3β overexpression, FAIM-L was significantly decreased. This result suggests that FAIM-L loss may depend on an increase in pTau, possibly mediated by GSK-3β. Aβ activates GSK-3β by interfering with the insulin and the canonical wnt signalling pathway[334–336] and by binding to the α2A adrenergic receptor[337]. As a result, active GSK-3β promotes tau phosphorylation and calpain-1 activation[338]. When Carriba and colleagues[274] linked FAIM-L downregulation to AD, they observed that FAIM-L was reduced in neuronal cultures after amyloid treatments. In this regard, these results would be apparently contradictory. However, we think that they represented upstream events that lead to FAIM-L decrease. They found a reduction in FAIM-L levels after Aβ treatments *in vitro*. Now, we hypothesize that Aβ may be causing an aberrant GSK-3β-mediated phosphorylation of tau. This, at last instance, would reduce FAIM-L in a calpain-mediated way.

Neither GSK-3β nor calpain levels have been determined in our mice. However, their inhibition has been proved to prevent synaptic failure, cognitive deficits and neuronal loss in the PS19 and the APPxPS1mice[339,340341,342]. Thus, we propose that this same mechanism may be also occurring *in vivo*. Altogether, this hypothesis would support our results

and explain FAIM-L decrease in a tau-dependent manner, but also observed it in the context of Aβ.

Our preliminary data reported altered pTau and FAIM-L levels in hippocampal samples of the PS19 mice by 2 months-of-age. However, in our colony, we detected a delayed manifestation of these two pathological hallmarks. Many factors can influence the phenotype manifestation in genetically modified animals. Changes in husbandry or environmental conditions may explain delayed phenotypes[343]. However, mouse background is one of the most important modificatory elements. While backcrossing ensures colony stability and prevents genetic drift accumulation, progressive modifications in background strain may have an impact on mice development. PS19 model was generated using B6C3F1/J genetic background. Our animals have been maintained in C57/BL6 background. Thus, these changes may have impacted progression of tau pathology in our mice.

We have selected this model because FAIM-L decrease was reported before the onset of the rest of tau-derived alterations[92]. Thus, we needed to re-position these alterations in the course of our mice pathology. The first characterization of PS19 disease showed an early increment in tau phosphorylation. It was reported by 3 months-of-age, concomitant with reactive gliosis and synaptic impairment[92]. By contrast, recent findings from other authors have not observed these alterations until 6 or 9 months-of-age[285,344]. Similarly, hippocampal spine loss, reduction in synaptic density and reactive gliosis are not observed until 9 months [95,285]. We also reported an increased reactive gliosis and synaptic impairment from 9 months-of-age. Consequently, we found a delayed appearance of cognitive deficits. By 9 months-of-age we were only able to detect an impairment in the associative memory, suggesting that the other alterations such as motor deficits may appear at later ages. In

definitive, our PS19 mice showed a delayed course of the pathology but still, FAIM-L reduction was previous to the other alterations. Thus, FAIM-L could be a relevant contributor to AD progression.

To address that, we injected FAIM-L or CTL AAVs in 6 months-old PS19 and WT mice. Then, we determined the effect of its restoration in the progression of the pathology by 9 months. After our analysis, we report for the first time that the sole FAIM-L overexpression in the hippocampus of PS19 mice changes the progression of tau-linked pathology. FAIM-L normalization protects from synaptic impairment, brain atrophy and memory loss in AD.

Caspase3-related apoptotic and non-apoptotic functions of FAIM-L can explain by themselves the effects observed in synaptic homeostasis and cell survival. Additionally, FAIM can regulate it by controlling protein ubiquitination and proteostasis. Our group firstly established that FAIM-L was capable of preventing XIAP ubiquitination[266]. Later, we reported that its absence courses with the global accumulation of ubiquitin aggregates in the retina of the FAIM KO mouse[273]. Similarly, Kaku et al., observed that FAIM absence increased global protein ubiquitination under stress conditions[270–272]. In this work we have proved that FAIM-L can directly avoid tau ubiquitination. Thus, we provide a new promising capacity of FAIM-L that may contribute to proteostasis and cellular protection in AD.

Under physiological conditions, tau is ubiquitinated and targeted for degradation. Then, when proteostasis is impaired, ubiquitin accumulation induces tau aggregation[179,180]. While adequate Lys63-linked poly-Ub of tau mediates its autophagy and degradation, aberrant CHIP and TRAF6-mediated Lys63-linked poly-Ub enhances its aggregation[345,346]. However, the beneficious or detrimental effect of ubiquitination during tau pathology is

controversial. On one hand, soluble and highly phosphorylated forms of tau are especially toxic for neurons. Counteracting the action of E3 ligases such as CHIP or TRAF6 reduces tau aggregation but results in the accumulation of non-aggregated, Ub-negative, and hyperphosphorylated tau in the cytoplasm[345,347]. Thus, some studies have proposed that ubiquitination may be beneficial for the cell[157,191,192,348]. On the other hand, pre-tangled forms are also highly neurotoxic. Ubiquitination enhances tau oligomerization, and these intermediate Ub-positive oligomers, impair proteasome activity[349,350], promote seeding and propagation of tau, and activate apoptosis through the NFκ-B pathway[351]. Then, intermediate aggregates could be promoted by ubiquitination and be detrimental as well.

Importantly, some studies have observed that PHFs are mostly mono-ubiquitinated and Lys6-, Lys11-, and Met1-linked poly-ubiquitinated. These type of Ub codes are used as a signal to control protein function and not for its proteasomal or lysosomal degradation[179,183,184]. Then, they are more responsible for tau loss of function and cellular altered functionality than for protein aggregation[352,353]. Therefore, we suggest that the effect of ubiquitination in the progression of tau pathology is dependent on the type of ubiquitination and the signalling derived from it.

When we analysed tau ubiquitination, we measured tau global ubiquitination (by determining the incorporation of His-Ub). However, WB pattern can usually give some insights on the type of ubiquitination attached to the protein. XIAP is Lys48-linked poly-ubiquitinated[354]. Thus, when we analyse its ubiquitination by WB, we observe the accumulation of various bands with higher molecular weights. These bands correspond to the protein of interest attached to Ub chains of different lengths. Also, when cells are treated with the proteasome inhibitor MG132, we can detect an accumulation of

ubiquitinated XIAP. Conversely, mono-ubiquitinated proteins incorporates a unique Ub molecule and are not targeted for degradation[211]. Thus, we only observe a band in the WB that correspond to the protein of interest attached to one Ub that do not change after MG132 treatments. Ub molecule weight is ~ 8.5 kDa. Then, the band is approximately of the same molecular weight as the protein being ubiquitinated[355]. Our Ub-pull down showed that FAIM-L was inhibiting a non-degradative ubiquitination of tau. Additionally, we only observed a unique band for tau, suggesting that FAIM-L is indeed preventing tau mono-ubiquitination.

Functional implications of tau mono-ubiquitination have not been identified yet. So far, Axotrophin/MARCH7 E3 Ub ligase has been reported to mono-ubiquitinate tau protein, and to impair its binding to microtubules[185]. Thus, at first place, this ubiquitination would be interfering with tau function in the same manner as phosphorylation does. The rest of plausible implications must be extrapolated from general physiological functions of this type of ubiquitination and the effect in other neuronal proteins. We propose that mono-ubiquitination of tau might have an impact in its nuclear functions, its mislocalization and its truncation. Classically, mono-ubiquitination was related to transcriptional regulation and DNA repair though histone activity modulation[213,214]. Tau is especially relevant in the nucleus and mediates these two processes[149,161]. Then, an aberrant mono-ubiquitination of tau could be impairing some of its nuclear functions. Additionally, mono-ubiquitylation can serve as a signal for protein translocation. Mono-ubiquitination of the proteins p53 and NEMO triggers its export from the nucleus[356,357]. Similarly, mono-ubiquitination of DLG3, induces its transference to the plasma membrane[358]. Aberrant hyperphosphorylation of tau results in its mislocalization and loss-of-function[178]. Thus, we suggest that mono-ubiquitination may have a similar effect.

Finally, mono-ubiquitination of the PP2A protein promotes its calpain-mediated cleavage[290]. Also, ubiquitin has been associated with the early caspase-3 mediated and the formation of the tau-C3 component[289]. Thus, we propose that this type of ubiquitination might stimulate tau truncation. In this work, we have observed that tau ubiquitination results in the accumulation of tau fragments. Further analysis will be required to determine if these fragments are in fact tau-C3. However, we suggest that cleavage might be consequence of tau mono-ubiquitination, and then, FAIM-L will be also protecting from the formation of these highly toxic truncated-forms of tau[288].

In summary, we have reported that FAIM-L is preventing non-degradative tau ubiquitination. This fact, and the observation of a unique band in the WB, suggests that tau is being mono-ubiquitinated. This type of ubiquitination regulates protein activity and translocation. Thus, FAIM-L could be safeguarding tau correct function and location within the cell.

We also characterized FAIM-L capacity to block tau ubiquitination under pathological conditions. We analysed the effect of FAIM-L in the ubiquitination of a mutant form of tau. However, we did not observe any effect of FAIM-L preventing Tau^{P301L} ubiquitination. Usually, tau can trap other proteins into its aggregates. Therefore, these sequestered proteins are unable to perform their function. The RNA binding proteins (RBPs) Musashi1 and Musashi2 co-aggregate with tau both *in vitro* and in the Tau^{P301L} mouse model. Then, their function is impaired, provoking Lamin alterations[359,360]. Similarly, tau can also interact and sequester nRNA ribosomal proteins, impairing ribosome physical integrity and functionality[293]. Based on this, we proposed that FAIM-L could be sequestered into tau aggregates, losing its function. To assess this possibility, we determined the co-aggregation of FAIM-L with tau

in vivo. We analysed tau insoluble aggregates in our PS19 mice, but we did not detect the presence of FAIM-L.

Importantly, conformational changes of tau may differ *in vivo* and *in vitro*. WT tau rapidly aggregates spontaneously *in vitro*[361]. Also, the addition of mutations such as the P301L, can promote a faster aggregation of tau in this system[2,116]. Thus, we propose that, *in vitro*, tau abnormal aggregation could still trap FAIM-L justifying its loss-of-function. Musashi co-aggregation with tau resulted from an increased interaction between both proteins [359,360]. However, when we analysed Tau^{P301L} and FAIM-L interaction we were unable determine if it was increased. While tau co-IP indicated a decreased interaction between Tau^{WT} and FAIM-L, FAIM-L co-IP showed it increased. Therefore, further analysis should be required to decipher if FAIM-L is co-aggregating with Tau^{P301L} *in vitro*. First, we should analyse if Tau^{P301L} is aggregated in our cell system. Then, we should determine if FAIM-L is present in those aggregation. Finally, we should define the status of FAIM-L and Tau^{P301L} interaction *in vitro* using other approximation (e.g. Proximity Ligation Assay).

So far, we have reported new findings that relate FAIM-L to AD. We have found it due to the presence of tau pathology and we have defined its capacity to inhibit tau ubiquitination. However, the most relevant finding of our work is to demonstrate that FAIM-L present a protective role of FAIM-L in the progression of this disease.

We have demonstrated that FAIM-L restoration in a PS19 mouse model prevents brain atrophy. Tau aberrant malfunction and aggregation has been related to the activation of regulated to pyroptosis[362], parthanatos[363] and ferroptosis[364]. Also, it has been directly involved in necroptosis[365,366]. Here, we have proved that FAIM-L avoids tau ubiquitination and to protect from its

toxicity. Then, we hypothesize that, through this regulation, FAIM-L could have an impact in the promotion of these types of PCD and, thus, protecting from brain atrophy. Additionally, FAIM-L anti-apoptotic function could explain this increased neuronal survival. Thus, further investigation would allow us to also determine if FAIM-L restoration is also protecting against apoptosis in AD.

FAIM-L restoration in PS19 mice also ensured synaptic integrity. Again, FAIM-L action over tau ubiquitination[367]. Spine alterations have been observed in the CA3 region of the hippocampus in patients of AD[368] and mouse models[176,369] after hyperphosphorylated and pre-tangled tau. Also, aberrant tau impairs spine remodelling[75,155], NMDA receptor recruitment[157] and induces PSD95 detachment[157–159]. Similarly, FAIM-L control of non-apoptotic caspase-3 functions could explain its effect on synaptic function. Caspase-3 provokes mGluR2 internalization[250], impairs LTD[79,265], and promotes axonal pruning[76,263,266]. Indeed, it also promotes tau pathology by cleaving tau and forming the tau-C3 fragment[191].

Importantly, FAIM-L regulation of caspase-3 non-apoptotic functions are mediated by XIAP stabilization. However, we analysed XIAP levels in hippocampal lysates after FAIM-L overexpression and we did not to detect a restoration of XIAP levels in our animals. FAIM-L overexpression in the hippocampus of our mice avoided spine loss and maintained post-synaptic integrity. Both processes are highly dependent on caspase-3. Thus, we suggest the possibility of an under-detected restoration of XIAP. We propose that XIAP restoration could be occurring only in certain populations of neurons and/or exclusively in the synaptic compartment. First, FAIM-L expression is controlled by CaMKII promoter, which ensured FAIM-L neuronal specificity. Also, it resulted in a differential FAIM-L distribution among the hippocampus.

CaMKII expression depends on the phenotypic and functional characteristics of neurons. Thus, both CaMKII and FAIM-L are barely expressed in CA2 neurons[370,371]. By contrast, XIAP is ubiquitously expressed in the brain. Then, if FAIM-L overexpression is limited to certain populations of hippocampal neurons, the normalization of XIAP levels should be hindered when analysed in whole hippocampal lysates. Second, the apoptotic machinery activates local and transiently in the synaptic compartment to exert its non-apoptotic functions[372,373]. Then, XIAP restoration in synapsis would be undetectable in total lysates. At this point, we consider essential to study FAIM-L participation in XIAP maintenance by accurately delimiting the area of study (e.g. by immunofluorescence analysis). Also, we propose to specifically evaluate the status of this protein and other mediators precisely in subcellular fractions. In definitive, we considered that FAIM-L relevant role in synaptic maintenance results from the combination of its non-apoptotic functions and the regulation of tau aberrant modifications.

Neuronal dysfunction and cognitive impairment are strongly related to the progressive neuronal loss happening in AD[374]. However, it is especially related to synaptic dysfunction[68,69,375]. Here, we have demonstrated that FAIM-L prevents from both neuronal loss and synaptic impairment in the hippocampus of our mice. Therefore, its restoration resulted also, in the prevention of memory impairment.

Importantly, only slight cognitive deficits were observed in our mice. First, we could discard neophobic behaviour in our mice. Habitually, mice performance in the Passive Avoidance test reflects neophobic behaviours[376]. In our transgenic mice, we observed a slight increase in the time to step-trough during the training session. However, it was non-significant and consistent with the absence of reports about neophobia in this model. Second, we did not

find motor deficits, anxiety or hyperactivity in our mice when tested in the OF. Several groups have reported hyperactive behaviour in PS19 mice using this test[96,97]. They have reported an increased total distance travelled in the OF. However, we only observed an increased exploration within time. Thus, we propose that our mice present limited capacity of adaptation to the environment. In fact, we think that this probably might evolve to hyperactive behaviour at later stages. Importantly, when FAIM-L was overexpressed, we observed that this lack of adaptation was partially reverted. By extrapolation, we propose that FAIM-L may be delaying the start of this aforementioned behaviour. Finally, they did not present hippocampal spatial and recognition memory deficits. While some authors have reported impaired recognition memory in this model by 6 months-of-age[377], others have not reproduced this phenotype until 10 months-of-age[378]. Indeed, to observe an earlier recognition memory impairment, they needed to cross PS19 mice with an *APP* mouse[379].

Accordingly, our NOLT and T-maze results showed intact spatial and recognition memory by 9 months-of-age. However, they revealed some disparities regarding animal performance. First, we observed an absence of discrimination between objects during the training during the NOLT in WT mice. Then, we observed that only PS19 mice injected with FAIM-L recognized the newly opened arm in the T-maze. By contrast WT and PS19:CTL animals did not showed increased time, distance or number of entries to the new arm in this test.

Behavioural analyses are exposed to numerous influences that can interfere with the results, hindering their interpretation. Some of them can be attributed to sex. Only sexual differences in PS19 mice have been reported by other authors in the Morris Water Maze task [329,380]. However, after this result, we decided to study animal performance by analysing both sexes independently.

When only males were considered in the NOLT, all groups were able to discriminate the newly located object. Positively, we did not find differences in the other tests, including T-maze. In our experimental design, we divided animals in two independent batches. Then, to further analyse this situation, we also analysed both sets of animals separately. Interestingly, only WT animals for the first set of animals aberrantly performed NOLT test. Again, no differences were observed in the T-maze. Thus, we suggest that deficits in habituation of WT mice might have occurred in first set of animals during the training session of the NOLT. As a result, it would have hindered some animals to discriminate during this test, justifying our results. Unfortunately, technical difficulties impeded us to re-analyse training archives in order to further explore this possibility.

As mentioned, no differences between sexes or animals' sets were reported for the T-maze test. However, we only overserved that only those animals injected with FAIM-L correctly discriminated the new arm. This effect was significant for the PS19:FAIM-L mice, while WT:FAIM-L mice showed a tendency to improve its performance. Habedank and colleagues[381] reported that C57BL/6 mice did not always show preference or learning behaviour in the T-maze. Thus, we suggest that the background of our mice might explain mice aberrant performance in the T-maze test. Additionally, FAIM-L would be counteracting the effect of mice strain, preventing spatial memory deficits associated to C57/BL6 mice.

Our PS19 mice showed impaired working memory and associative memory, consistent with other authors reports. They have described working memory deficits in PS19 mice from 10 months-of-age[378] and altered associative memory from 8-month[382]. Importantly, after FAIM-L overexpression, we were able to prevent associative memory defects, but we could not recover

working memory. Working memory present a hippocampal component. However, it is mainly controlled by the prefrontal cortex (PFC)[383,384]. Specifically, it seems to highly depend on the correct function of NMDA receptors in the pyramidal neurons of the PFC[385]. Therefore, elements such as the transcription factor TFEB, had to be specifically overexpressed in this region to exert its protective role and preserve working memory in the PS19 mice[386,298]. Importantly, tau pathology and a spine density impairment are already present in the PFC by 9 months-of-age in PS19 mice[344]. For this reason, we suggest that the exclusive overexpression of FAIM-L in the hippocampus is not sufficient to prevent the loss of this type of memory in our mice. According to this idea, FAIM-L hippocampal overexpression would be able to preserve those memory functions mostly controlled by this area. Successfully, after performing the Passive Avoidance test, we were able to confirm it. With this test, we found that the impaired associative memory observed in the PS19 mice was completely prevented by FAIM-L overexpression. Therefore, we can conclude that FAIM-L protection at molecular and cellular levels, prevents, at last instance, memory loss.

Our data points FAIM-L as a highly potential therapeutical target for AD and opens new windows for its treatment. Despite the contribution of both Aβ and tau pathology to AD have been deeply explored during the past few years, the translation of this research into therapeutic strategies has recurrently failed. Aβ offers an early prevention of the disease and has been considered as a causal and central event of the disease. However, the development of therapies against Aβ have not provided successful results in the clinical trials performed so far. Thus, recent research has proposed that Aβ accumulation may not directly cause neurodegeneration[54,387]. After that, efforts were progressively placed into tau. Its pathology strongly correlates with dementia severity and cognitive deficits[56,57]. Also, its pathology has been strongly related to neuronal

degeneration[367,374,388]. Finally, tau does not require additional alterations for being responsible of primary tauopathies. Thus, the suppression or deletion of tau has had a profound protective effect against brain damage and neurological deficits[389,390]. Unfortunately, the extreme complexity of these pathologies has difficulted the direct targeting of this protein. Neither GSK-3β inhibitors (e.g. Tideglusib)[391], nor direct inhibitors of tau aggregation (Trx0014 and LMTM9[392], have shown significant clinical benefits. Based on that, we consider that trying to modulate downstream elements that control those neurotoxic effects of tau may have a greater therapeutical impact.

Here, we have discovered that FAIM-L is bounded to tau pathology and that its sole overexpression of inverts the progression of the disease in the PS19 mice. In addition, we have proposed FAIM-L as a multifunctional that regulates caspase-3 non-apoptotic functions and avoids tau aberrant ubiquitination. Thus, FAIM-L prevents synaptic impairment, cell death and memory loss. Finally, we present FAIM-L as common element in both Aβ and tau pathologies. Carriba's findings[274], showed FAIM-L reduced after Aβ. Now, have directly relate it to tau pathology. Altogether, FAIM-L relevance in AD is highly increased.

In summary, we have provided new relevant information regarding to the mechanisms underlying tau pathology. More importantly, we have pointed to useful strategies for its prevention. We have confirmed the protective role of FAIM-L in synaptic function, proteostasis and cell survival. Therefore, FAIM-L arises as a therapeutical target for AD, the rest of tauopathies and, hopefully, other neurodegenerative diseases.

CONCLUSIONS

VII. CONCLUSIONS

1. FAIM-L levels are exclusively reduced in mouse models coursing with severe tau pathology.
2. In the FTDP-17 mouse model PS19, FAIM-L decrease occurs together with an aberrant increase in phosphorylated tau and before synaptic impairment and astrogliosis.
3. FAIM-L protein decrease in PS19 mice is not caused by a reduction in its mRNA levels.
4. FAIM-L reduction is dependent on an increase in phosphorylation of tau *in vitro*.
5. FAIM-L loss-of-function results in an increased global protein ubiquitination and a reduction of XIAP levels.
6. Tau^{WT} and Tau^{P301L} are able to interact with the two isoforms of FAIM, showing in both cases, more affinity for the longer isoform, FAIM-L.
7. FAIM-L, but not FAIM-S, is able control tau post-translational modifications of Tau^{WT} protein preventing its non-degradative ubiquitination.
8. Restoration of FAIM-L in the hippocampus of the PS19 mice allows expressing functional FAIM-L for at least 3 months without notable diffusion to other brain regions such as the cortex, the striatum or the cerebellum.
9. The simple restoration of FAIM-L in the hippocampus of 6-months-old PS19 mice improves general wellbeing in the transgenic mice, as shown by a delayed body weight loss, and completely prevents brain atrophy by 9 months of age.
10. FAIM-L normalization in the hippocampus of PS19 mice prevents spine loss and partially avoids the instability of the post-synaptic density compartment.

11. FAIM-L restoration in specific hippocampal neurons of PS19 mice does not avoid neuroinflammation neither normalizes global protein ubiquitination and XIAP protein levels.
12. PS19 mice did not show altered spatial and reference memory by 9 months-of-age. Still, the overexpression of FAIM-L in the hippocampus of PS19 mice results in an improved spatial reference memory when tested in the T-maze.
13. Overexpression of FAIM-L in the hippocampus is not sufficient to prevent working memory deficits, that are mainly controlled by the prefrontal cortex.
14. FAIM-L restoration in the hippocampus of PS19 mice prevents associative memory impairment and partially reduces the absence of habituation observed in 9-months-old transgenic mice.

Final conclusion. FAIM-L arises as a major player in amyloid-β and tau pathology, which is capable of modifying its progression by protecting neurons from tau toxicity. Therefore, although these results deserve further analysis, FAIM-L emerges as a potential therapeutic target for AD and other tauopathies in very early stages of the disease.

REFERENCES

VIII. REFERENCES

1. Lee, V. M. Y., Goedert, M., & Trojanowski, J. Q. Neurodegenerative tauopathies. *Annual Review of Neuroscience* ***24***, 1121–1159 (2001).
2. Dickson, D. W., Kouri, N., Murray, M. E. & Josephs, K. A. Neuropathology of frontotemporal lobar degeneration-Tau (FTLD-Tau). *Journal of Molecular Neuroscience* **45**, 384–389 (2011).
3. Spillantini, M. G. & Goedert, M. Tau pathology and neurodegeneration. *The Lancet Neurology* **12**, 609–622 (2013).
4. Kovacs, G. G. Invited review: Neuropathology of tauopathies: Principles and practice. *Neuropathology and Applied Neurobiology* **41**, 3–23 (2015).
5. 2022 Alzheimer's disease facts and figures. *Alzheimers Dement* **18**, 700–789 (2022).
6. Lalli, M. A. *et al.* Origin of the PSEN1 E280A mutation causing early-onset Alzheimer's disease. *Alzheimers Dement* **10**, S277-S283.e10 (2014).
7. Husna Ibrahim, N. *et al.* Pharmacotherapy of Alzheimer's Disease: Seeking Clarity in a Time of Uncertainty. *Front Pharmacol* **11**, (2020).
8. Alzheimer, A. Über eigenartige Krankheitsfälle des späteren Alters: (On certain peculiar diseases of old age. *Hist Psychiatry* **2**, 74–101 (1991).
9. Tanzi, R. E. The Genetics of Alzheimer Disease. *Cold Spring Harb Perspect Med* **2**, (2012).
10. Strittmatter, W. J. *et al.* Apolipoprotein E: high-avidity binding to beta-amyloid and increased frequency of type 4 allele in late-onset familial Alzheimer disease. *Proc Natl Acad Sci U S A* **90**, 1977–1981 (1993).
11. Liu, C. C., Kanekiyo, T., Xu, H. & Bu, G. Apolipoprotein E and Alzheimer disease: risk, mechanisms, and therapy. *Nat Rev Neurol* **9**, 106 (2013).
12. Cheng, G. W. Y. *et al.* Apolipoprotein E ε4 Mediates Myelin Breakdown by Targeting Oligodendrocytes in Sporadic Alzheimer Disease. *J Neuropathol Exp Neurol* **81**, 717–730 (2022).
13. Corder, E. H. *et al.* Gene dose of apolipoprotein E type 4 allele and the risk of Alzheimer's disease in late onset families. *Science* **261**, 921–923 (1993).
14. Haass, C., Kaether, C., Thinakaran, G. & Sisodia, S. Trafficking and proteolytic processing of APP. *Cold Spring Harb Perspect Med* **2**, (2012).
15. D'Onofrio, G. *et al.* Neuropsychiatric symptoms and functional status in Alzheimer's disease and vascular dementia patients. *Curr Alzheimer Res* **9**, 759–771 (2012).
16. Schott, J. M. *et al.* Consensus classification of posterior cortical atrophy. *Alzheimers Dement* **13**, 870–884 (2017).
17. Graff-Radford, J. *et al.* New insights into atypical Alzheimer's disease in the era of biomarkers. *Lancet Neurol* **20**, 222–234 (2021).
18. Haass, C. & Selkoe, D. J. Soluble protein oligomers in neurodegeneration: lessons from the Alzheimer's amyloid beta-peptide. *Nat Rev Mol Cell Biol* **8**, 101–112 (2007).

19. Serrano-Pozo, A., Frosch, M. P., Masliah, E. & Hyman, B. T. Neuropathological alterations in Alzheimer disease. *Cold Spring Harb Perspect Med* **1**, (2011).
20. Spires-Jones, T. L. & Hyman, B. T. The intersection of amyloid beta and tau at synapses in Alzheimer's disease. *Neuron* **82**, 756–771 (2014).
21. de Loof, A. & Schoofs, L. Alzheimer's Disease: Is a Dysfunctional Mevalonate Biosynthetic Pathway the Master-Inducer of Deleterious Changes in Cell Physiology? *OBM Neurobiol* **3**, (2019).
22. Jarero-Basulto, J. J. *et al.* Current Evidence on the Protective Effects of Recombinant Human Erythropoietin and Its Molecular Variants against Pathological Hallmarks of Alzheimer's Disease. *Pharmaceuticals 2020* **13**, 424 (2020).
23. Cras, P. *et al.* Senile plaque neurites in Alzheimer disease accumulate amyloid precursor protein. *Proc Natl Acad Sci U S A* **88**, 7552 (1991).
24. Taylor, C. J. *et al.* Endogenous secreted amyloid precursor protein-alpha regulates hippocampal NMDA receptor function, long-term potentiation and spatial memory. *Neurobiol Dis* **31**, 250–260 (2008).
25. Habib, A., Sawmiller, D. & Tan, J. Restoring Soluble Amyloid Precursor Protein α Functions as a Potential Treatment for Alzheimer's Disease. *J Neurosci Res* **95**, 973–991 (2017).
26. Hampel, H. *et al.* The Amyloid-β Pathway in Alzheimer's Disease. *Molecular Psychiatry* **26**, 5481–5503 (2021).
27. Boespflug, E. L. & Iliff, J. J. The Emerging Relationship Between Interstitial Fluid-Cerebrospinal Fluid Exchange, Amyloid-β, and Sleep. *Biol Psychiatry* **83**, 328–336 (2018).
28. Benarroch, E. E. Glutamatergic synaptic plasticity and dysfunction in Alzheimer disease: Emerging mechanisms. *Neurology* **91**, 125–132 (2018).
29. Tabaton, M. & Piccini, A. Role of water-soluble amyloid-beta in the pathogenesis of Alzheimer's disease. *Int J Exp Pathol* **86**, 139–145 (2005).
30. Chen, G. F. *et al.* Amyloid beta: structure, biology and structure-based therapeutic development. *Acta Pharmacol Sin* **38**, 1205–1235 (2017).
31. Moloney, C. M., Lowe, V. J. & Murray, M. E. Visualization of neurofibrillary tangle maturity in Alzheimer's disease: A clinicopathologic perspective for biomarker research. *Alzheimers Dement* **17**, 1554–1574 (2021).
32. Brion, J. P. Neurofibrillary tangles and Alzheimer's disease. *Eur Neurol* **40**, 130–140 (1998).
33. Metaxas, A. & Kempf, S. J. Neurofibrillary tangles in Alzheimer's disease: elucidation of the molecular mechanism by immunohistochemistry and tau protein phospho-proteomics. *Neural Regen Res* **11**, 1579–1581 (2016).
34. Yamada, K. *et al.* Neuronal activity regulates extracellular tau in vivo. *J Exp Med* **211**, 387–393 (2014).
35. de Calignon, A. *et al.* Propagation of tau pathology in a model of early Alzheimer's disease. *Neuron* **73**, 685–697 (2012).

36. d'Errico, P. & Meyer-Luehmann, M. Mechanisms of Pathogenic Tau and Aβ Protein Spreading in Alzheimer's Disease. *Front Aging Neurosci* **12**, (2020).
37. Masters, C. L. *et al.* Amyloid plaque core protein in Alzheimer disease and Down syndrome. *Proc Natl Acad Sci U S A* **82**, 4245–4249 (1985).
38. Kamenetz, F. *et al.* APP Processing and Synaptic Function. *Neuron* **37**, 925–937 (2003).
39. Shankar, G. M. *et al.* Natural oligomers of the Alzheimer amyloid-beta protein induce reversible synapse loss by modulating an NMDA-type glutamate receptor-dependent signaling pathway. *J Neurosci* **27**, 2866–2875 (2007).
40. Li, S. *et al.* Soluble Aβ oligomers inhibit long-term potentiation through a mechanism involving excessive activation of extrasynaptic NR2B-containing NMDA receptors. *J Neurosci* **31**, 6627–6638 (2011).
41. Snyder, E. M. *et al.* Regulation of NMDA receptor trafficking by amyloid-beta. *Nat Neurosci* **8**, 1051–1058 (2005).
42. Busche, M. A. *et al.* Clusters of hyperactive neurons near amyloid plaques in a mouse model of Alzheimer's disease. *Science* **321**, 1686–1689 (2008).
43. Latif-Hernandez, A. *et al.* The two faces of synaptic failure in App NL-G-Fknock-in mice. *Alzheimers Res Ther* **12**, 1–15 (2020).
44. Mucke, L. & Selkoe, D. J. Neurotoxicity of amyloid β-protein: synaptic and network dysfunction. *Cold Spring Harb Perspect Med* **2**, (2012).
45. Lalli, M. A. *et al.* Origin of the PSEN1 E280A mutation causing early-onset Alzheimer's disease. *Alzheimers Dement* **10, Suppl 5**, S277-S283.e10 (2014)
46. Schindler, S. E. *et al.* High-precision plasma β-amyloid 42/40 predicts current and future brain amyloidosis. *Neurology* **93**, e1647–e1659 (2019).
47. Khan, A., Corbett, A. & Ballard, C. Emerging amyloid and tau targeting treatments for Alzheimer's disease. *Expert Rev Neurother* **17**, 697–711 (2017).
48. Zhao, J., Liu, X., Xia, W., Zhang, Y. & Wang, C. Targeting Amyloidogenic Processing of APP in Alzheimer's Disease. *Front Mol Neurosci* **13**, 137 (2020).
49. Cummings, J. L. *et al.* ABBY: A phase 2 randomized trial of crenezumab in mild to moderate Alzheimer disease. *Neurology* **90**, e1889–e1897 (2018).
50. Honig, L. S. *et al.* Trial of Solanezumab for Mild Dementia Due to Alzheimer's Disease. *N Engl J Med* **378**, 321–330 (2018).
51. Salloway, S. *et al.* Two Phase 3 Trials of Bapineuzumab in Mild-to-Moderate Alzheimer's Disease. *New England Journal of Medicine* **370**, 322–333 (2014).
52. Rygiel, K. Novel strategies for Alzheimer's disease treatment: An overview of anti-amyloid beta monoclonal antibodies. *Indian J Pharmacol* **48**, 629–636 (2016).
53. Budd Haeberlein, S. *et al.* Two Randomized Phase 3 Studies of Aducanumab in Early Alzheimer's Disease. *J Prev Alzheimers Dis* **9**, 197–210 (2022).

54. Morris, G. P., Clark, I. A. & Vissel, B. Inconsistencies and controversies surrounding the amyloid hypothesis of Alzheimer's disease. *Acta Neuropathol Commun* **2**, (2014).
55. Sasaguri, H. *et al.* APP mouse models for Alzheimer's disease preclinical studies . *EMBO J* **36**, 2473–2487 (2017).
56. Bejanin, A. *et al.* Tau pathology and neurodegeneration contribute to cognitive impairment in Alzheimer's disease. *Brain* **140**, 3286–3300 (2017).
57. Muralidar, S., Ambi, S. V., Sekaran, S., Thirumalai, D. & Palaniappan, B. Role of tau protein in Alzheimer's disease: The prime pathological player. *Int J Biol Macromol* **163**, 1599–1617 (2020).
58. DuBoff, B., Götz, J. & Feany, M. B. Tau promotes neurodegeneration via DRP1 mislocalization in vivo. *Neuron* **75**, 618–632 (2012).
59. Busche, M. A. & Hyman, B. T. Synergy between amyloid-β and tau in Alzheimer's disease. *Nat Neurosci* **23**, 1183–1193 (2020).
60. Weickenmeier, J., Jucker, M., Goriely, A. & Kuhl, E. A physics-based model explains the prion-like features of neurodegeneration in Alzheimer's disease, Parkinson's disease, and amyotrophic lateral sclerosis. *J Mech Phys Solids* **124**, 264–281 (2019).
61. Fornari, S., Schäfer, A., Jucker, M., Goriely, A. & Kuhl, E. Prion-like spreading of Alzheimer's disease within the brain's connectome. *J R Soc Interface* **16**, (2019).
62. Kametani, F. & Hasegawa, M. Reconsideration of amyloid hypothesis and tau hypothesis in Alzheimer's disease. *Frontiers in Neuroscience* **12**, (2018).
63. Chabrier, M. A., Cheng, D., Castello, N. A., Green, K. N. & LaFerla, F. M. Synergistic effects of amyloid-beta and wild-type human tau on dendritic spine loss in a floxed double transgenic model of Alzheimer's disease. *Neurobiol Dis* **64**, 107–117 (2014).
64. Mori, H., Kondo, J. & Ihara, Y. Ubiquitin is a component of paired helical filaments in Alzheimer's disease. *Science* **235**, 1641–1644 (1987).
65. Perry, G., Friedman, R., Shaw, G. & Chau, V. Ubiquitin is detected in neurofibrillary tangles and senile plaque neurites of Alzheimer disease brains. *Proc Natl Acad Sci U S A* **84**, 3033–3036 (1987).
66. Myeku, N. *et al.* Tau-driven 26S proteasome impairment and cognitive dysfunction can be prevented early in disease by activating cAMP-PKA signaling. *Nature Medicine* **22**, 46–53 (2015).
67. Tai, H. C. *et al.* The Synaptic Accumulation of Hyperphosphorylated Tau Oligomers in Alzheimer Disease Is Associated With Dysfunction of the Ubiquitin-Proteasome System. *Am J Pathol* **181**, 1426–1435 (2012).
68. Zhou, L. *et al.* Tau association with synaptic vesicles causes presynaptic dysfunction. *Nature Communications* **8**, 1–13 (2017).
69. Lleó, A. *et al.* Changes in Synaptic Proteins Precede Neurodegeneration Markers in Preclinical Alzheimer's Disease Cerebrospinal Fluid. *Mol Cell Proteomics* **18**, 546–560 (2019).
70. Chen, Y., Fu, A. K. Y. & Ip, N. Y. Synaptic dysfunction in Alzheimer's disease: Mechanisms and therapeutic strategies. *Pharmacol Ther* **195**, 186–198 (2019).

71. Maor-Nof, M. *et al.* Axonal Pruning Is Actively Regulated by the Microtubule-Destabilizing Protein Kinesin Superfamily Protein 2A. *Cell Rep* **3**, 971–977 (2013).
72. Horowitz, P. M. *et al.* Early N-terminal changes and caspase-6 cleavage of tau in Alzheimer's disease. *Journal of Neuroscience* **24**, 7895–7902 (2004).
73. Hernández, F., Gómez de Barreda, E., Fuster-Matanzo, A., Lucas, J. J. & Avila, J. GSK3: A possible link between beta amyloid peptide and tau protein. *Exp Neurol* **223**, 322–325 (2010).
74. Kimura, T. *et al.* Microtubule-associated protein tau is essential for long-term depression in the hippocampus. *Philosophical Transactions of the Royal Society B: Biological Sciences* **369**, (2014).
75. Regan, P. *et al.* Tau Phosphorylation at Serine 396 Residue Is Required for Hippocampal LTD. *Journal of Neuroscience* **35**, 4804–4812 (2015).
76. Mukherjee, A. & Williams, D. W. More alive than dead: non-apoptotic roles for caspases in neuronal development, plasticity and disease. *Cell Death Differ* **24**, 1411–1421 (2017).
77. Barth, N. D., Marwick, J. A., Vendrell, M., Rossi, A. G. & Dransfield, I. The 'Phagocytic synapse' and clearance of apoptotic cells. *Front Immunol* **8**, 1708 (2017).
78. Nonaka, S. & Nakanishi, H. Microglial clearance of focal apoptotic synapses. *Neurosci Lett* **707**, (2019).
79. M P Mattson & W Duan. 'Apoptotic' biochemical cascades in synaptic compartments: roles in adaptive plasticity and neurodegenerative disorders - PubMed. *J Neurosci Res* **58**, 152–166 (1999).
80. Wang, J. *et al.* UBE3A-mediated PTPA ubiquitination and degradation regulate PP2A activity and dendritic spine morphology. *Proc Natl Acad Sci U S A* **116**, 12500–12505 (2019).
81. Heneka, M. T. *et al.* Neuroinflammation in Alzheimer's disease. *The Lancet Neurology* **14**, 388–405 (2015).
82. Nimmerjahn, A., Kirchhoff, F. & Helmchen, F. Neuroscience: Resting microglial cells are highly dynamic surveillants of brain parenchyma in vivo. *Science (1979)* **308**, 1314–1318 (2005).
83. Rodríguez-Arellano, J. J., Parpura, V., Zorec, R. & Verkhratsky, A. Astrocytes in physiological aging and Alzheimer's disease. *Neuroscience* **323**, 170–182 (2016).
84. Schofield, E., Kersaitis, C., Shepherd, C. E., Kril, J. J. & Halliday, G. M. Severity of gliosis in Pick's disease and frontotemporal lobar degeneration: tau-positive glia differentiate these disorders. *Brain* **126**, 827–840 (2003).
85. Bellucci, A., Bugiani, O., Ghetti, B. & Spillantini, M. G. Presence of Reactive Microglia and Neuroinflammatory Mediators in a Case of Frontotemporal Dementia with P301S Mutation. *Neurodegener Dis* **8**, 221 (2011).
86. Laurent, C. *et al.* Hippocampal T cell infiltration promotes neuroinflammation and cognitive decline in a mouse model of tauopathy. *Brain* **140**, 184–200 (2017).
87. Josephs, K. A. Rest in peace FTDP-17. *Brain* **141**, 324–331 (2018).

88. Knouff, C. *et al.* Apo E structure determines VLDL clearance and atherosclerosis risk in mice. *J Clin Invest* **103**, 1579–1586 (1999).
89. Youmans, K. L. *et al.* APOE4-specific changes in Aβ accumulation in a new transgenic mouse model of Alzheimer disease. *J Biol Chem* **287**, 41774–41786 (2012).
90. Hall, A. M. & Roberson, E. D. Mouse models of Alzheimer's disease. *Brain Research Bulletin* **88**, 3–12 (2012).
91. Lewis, J. *et al.* Neurofibrillary tangles, amyotrophy and progressive motor disturbance in mice expressing mutant (P301L) tau protein. *Nature Genetics* **25**, 402–405 (2000).
92. Yoshiyama, Y. *et al.* Synapse loss and microglial activation precede tangles in a P301S tauopathy mouse model. *Neuron* **53**, 337–351 (2007).
93. Takeuchi, H. *et al.* P301S Mutant Human Tau Transgenic Mice Manifest Early Symptoms of Human Tauopathies with Dementia and Altered Sensorimotor Gating. *PLoS One* **6**, (2011).
94. Lasagna-Reeves, C. A. *et al.* Tau oligomers impair memory and induce synaptic and mitochondrial dysfunction in wild-type mice. *Mol Neurodegener* **6**, (2011).
95. Romero-Molina, C. *et al.* Distinct Microglial Responses in Two Transgenic Murine Models of TAU Pathology. *Front Cell Neurosci* **12**, (2018).
96. Ahmad, F., Mein, H., Jing, Y., Zhang, H. & Liu, P. Behavioural Functions and Cerebral Blood Flow in a P301S Tauopathy Mouse Model: A Time-Course Study. *Int J Mol Sci* **22**, (2021).
97. Patel, H. *et al.* Pathological tau and reactive astrogliosis are associated with distinct functional deficits in a mouse model of tauopathy. *Neurobiol Aging* **109**, 52–63 (2022).
98. DeVos, S. L. *et al.* Tau Reduction Prevents Neuronal Loss and Reverses Pathological Tau Deposition and Seeding in Mice with Tauopathy. *Sci Transl Med* **9**, (2017).
99. Vieira, R. T. *et al.* Epidemiology of early-onset dementia: a review of the literature. *Clinical Practice and Epidemiology in Mental Health* **9**, 88–95 (2013).
100. Forrest, S. L. *et al.* Retiring the term FTDP-17 as MAPT mutations are genetic forms of sporadic frontotemporal tauopathies. *Brain* **141**, 521–534 (2018).
101. Armstrong, R., Cairns, N. & Lantos, P. The spatial patterns of Pick bodies, Pick cells and Alzheimer's disease pathology in Pick's disease. *Neuropathology* **19**, 64–70 (1999).
102. Buée, L., Bussière, T., Buée-Scherrer, V., Delacourte, A. & Hof, P. R. Tau protein isoforms, phosphorylation and role in neurodegenerative disorders. *Brain Res Rev* **33**, 95–130 (2000).
103. Arima, K. Ultrastructural characteristics of tau filaments in tauopathies: immuno-electron microscopic demonstration of tau filaments in tauopathies. *Neuropathology* **26**, 475–483 (2006).
104. Williams, D. R. *et al.* Pathological tau burden and distribution distinguishes progressive supranuclear palsy-parkinsonism from Richardson's syndrome. *Brain* **130**, 1566–1576 (2007).

105. Togo, T., Cookson, N. & Dickson, D. W. Argyrophilic grain disease: neuropathology, frequency in a dementia brain bank and lack of relationship with apolipoprotein E. *Brain Pathol* **12**, 45–52 (2002).
106. Petersen, R. C. *et al.* Neuropathologic features of amnestic mild cognitive impairment. *Arch Neurol* **63**, 665–672 (2006).
107. Dickson, D. W. The pathogenesis of senile plaques. *J Neuropathol Exp Neurol* **56**, 321–339 (1997).
108. Ahmed, Z. *et al.* Globular glial tauopathies (GGT): consensus recommendations. *Acta Neuropathol* **126**, 537–544 (2013).
109. Roberts, G. W. Immunocytochemistry of neurofibrillary tangles in dementia pugilistica and Alzheimer's disease: evidence for common genesis. *Lancet* **2**, 1456–1458 (1988).
110. Alonso, A. D. *et al.* Hyperphosphorylation of Tau Associates with changes in its function beyond microtubule stability. *Frontiers in Cellular Neuroscience* **12**, (2018).
111. Cherry, J. D. *et al.* Tau isoforms are differentially expressed across the hippocampus in chronic traumatic encephalopathy and Alzheimer's disease. *Acta Neuropathol Commun* **9**, 1–17 (2021).
112. Dugger, B. N. & Dickson, D. W. Pathology of neurodegenerative diseases. *Cold Spring Harbor Perspectives in Biology* **9**, (2017).
113. Caroppo, P., Prioni, S., Maderna, E., Grisoli, M. & Rossi, G. New MAPT variant in a FTD patient with Alzheimer's disease phenotype at onset. *Neurol Sci* **42**, 2111–2114 (2021).
114. Wszolek, Z. K. *et al.* Frontotemporal dementia and parkinsonism linked to chromosome 17 (FTDP-17). *Orphanet Journal of Rare Diseases* **1**, (2006).
115. Lossos, A. *et al.* Frontotemporal dementia and parkinsonism with the P301S tau gene mutation in a Jewish family. *Journal of Neurology* **250**, 733–740 (2003).
116. Goedert, M. & Spillantini, M. G. Tau mutations in frontotemporal dementia FTDP-17 and their relevance for Alzheimer's disease. *Biochim Biophys Acta Mol Basis Dis* **1502**, 110–121 (2000).
117. Schellenberg, G. D. & Montine, T. J. The genetics and neuropathology of Alzheimer's disease. *Acta Neuropathol* **124**, 305–323 (2012).
118. Höglinger, G. U., Respondek, G. & Kovacs, G. G. New classification of tauopathies. *Rev Neurol (Paris)* **174**, 664–668 (2018).
119. Irwin, D. J. Tauopathies as clinicopathological entities. *Parkinsonism Relat Disord* **22 Suppl 1**, S29–S33 (2016).
120. Zhang, Y., Wu, K. M., Yang, L., Dong, Q. & Yu, J. T. Tauopathies: new perspectives and challenges. *Molecular Neurodegeneration* **17**, (2022).
121. Tsuchiya, K. *et al.* Argyrophilic grain disease mimicking temporal Pick's disease: a clinical, radiological, and pathological study of an autopsy case with a clinical course of 15 years. *Acta Neuropathol* **102**, 195–199 (2001).
122. Ishihara, K. *et al.* Argyrophilic grain disease presenting with frontotemporal dementia: a neuropsychological and pathological study of an autopsied case with presenile onset. *Neuropathology* **25**, 165–170 (2005).
123. van Swieten, J. C. *et al.* The DeltaK280 mutation in MAP tau favors exon 10 skipping in vivo. *J Neuropathol Exp Neurol* **66**, 17–25 (2007).

124. Josephs, K. A. *et al.* Voxel-based morphometry patterns of atrophy in FTLD with mutations in MAPT or PGRN. *Neurology* **72**, 813–820 (2009).
125. Buchman, A. S. & Bennett, D. A. Loss of motor function in preclinical Alzheimer's disease. *Expert Rev Neurother* **11**, 665–676 (2011).
126. Gültekin, M. Phenotypic Variants of Patients with Progressive Supranuclear Palsy. *Archives of Neuropsychiatry* **57**, 61 (2020).
127. Spillantini, M. G. *et al.* Mutation in the tau gene in familial multiple system tauopathy with presenile dementia. *Proc Natl Acad Sci U S A* **95**, 7737–7741 (1998).
128. Spillantini, M. G., Crowther, R. A. & Goedert, M. Comparison of the neurofibrillary pathology in Alzheimer's disease and familial presenile dementia with tangles. *Acta Neuropathol* **92**, 42–48 (1996).
129. Venkatramani, A. & Panda, D. Regulation of neuronal microtubule dynamics by tau: Implications for tauopathies. *Int J Biol Macromol* **133**, 473–483 (2019).
130. Weingarten, M. D., Lockwood, A. H., Hwo, S. Y. & Kirschner, M. W. A protein factor essential for microtubule assembly. *Proc Natl Acad Sci U S A* **72**, 1858–1862 (1975).
131. Cleveland, D. W., Hwo, S. Y. & Kirschner, M. W. Physical and chemical properties of purified tau factor and the role of tau in microtubule assembly. *J Mol Biol* **116**, 227–247 (1977).
132. Fellous, A., Francon, J., Lennon, A. M & Nunez, J. Microtubule assembly in vitro. Purification of assembly-promoting factors. *Eur J Biochem* **78**, 167–174 (1977).
133. Andreadis, A., Brown, W. M. & Kosik, K. S. Structure and novel exons of the human tau gene. *Biochemistry* **31**, 10626–10633 (1992).
134. Neve, R. L., Harris, P., Kosik, K. S., Kurnit, D. M. & Donlon, T. A. Identification of cDNA clones for the human microtubule-associated protein tau and chromosomal localization of the genes for tau and microtubule-associated protein 2. *Brain Res* **387**, 271–280 (1986).
135. Schweers, O., Mandelkow, E. M., Biernat, J. & Mandelkow, E. Oxidation of cysteine-322 in the repeat domain of microtubule-associated protein tau controls the in vitro assembly of paired helical filaments. *Proc Natl Acad Sci U S A* **92**, 8463 (1995).
136. Trabzuni, D. *et al.* MAPT expression and splicing is differentially regulated by brain region: relation to genotype and implication for tauopathies. *Hum Mol Genet* **21**, 4094–4103 (2012).
137. Sadot, E., Heicklen-Klein, A., Barg, J., Lazarovici, P. & Ginzburg, I. Identification of a tau promoter region mediating tissue-specific-regulated expression in PC12 cells. *J Mol Biol* **256**, 805–812 (1996).
138. Caillet-Boudin, M. L., Buée, L., Sergeant, N. & Lefebvre, B. Regulation of human MAPT gene expression. *Mol Neurodegener* **10**, 1–14 (2015).
139. Pîrşcoveanu, D.F.V. *et al*. Tau protein in neurodegenerative diseases - a review. *Rom J Morphol Embryol* **58**, 1141-1150 (2017).
140. Goedert, M., Spillantini, M. G., Jakes, R., Rutherford, D. & Crowther, R. A. Multiple isoforms of human microtubule-associated protein tau: sequences and localization in neurofibrillary tangles of Alzheimer's disease. *Neuron* **3**, 519–526 (1989).

141. Holper, S., Watson, R. & Yassi, N. Tau as a Biomarker of Neurodegeneration. *International Journal of Molecular Sciences* **23**, (2022).
142. Bachmann, S., Bell, M., Klimek, J. & Zempel, H. Differential Effects of the Six Human TAU Isoforms: Somatic Retention of 2N-TAU and Increased Microtubule Number Induced by 4R-TAU. *Front Neurosci* **15**, 547 (2021).
143. von Bergen, M. *et al.* Mutations of Tau Protein in Frontotemporal Dementia Promote Aggregation of Paired Helical Filaments by Enhancing Local β-Structure. *Journal of Biological Chemistry* **276**, 48165–48174 (2001).
144. Luo, Y., Ma, B., Nussinov, R. & Wei, G. Structural Insight into Tau Protein's Paradox of Intrinsically Disordered Behavior, Self-Acetylation Activity, and Aggregation. *J Phys Chem Lett* **5**, 3026–3031 (2014).
145. Zeng, Y. *et al.* The structure and phase of tau: from monomer to amyloid filament. *Cellular and Molecular Life Sciences* **78**, 1873–1886 (2020).
146. McKenzie-Nickson, S. *et al.* Modulating Protein Phosphatase 2A Rescues Disease Phenotype in Neurodegenerative Tauopathies. *ACS Chem Neurosci* **9**, 2731–2740 (2018).
147. Brandt, R., Léger, J. & Lee, G. Interaction of tau with the neural plasma membrane mediated by tau's amino-terminal projection domain. *J Cell Biol* **131**, 1327–1340 (1995).
148. Farah, C. A. *et al.* Tau interacts with Golgi membranes and mediates their association with microtubules. *Cell Motil Cytoskeleton* **63**, 710–724 (2006).
149. Sotiropoulos, I. *et al.* Atypical, non-standard functions of the microtubule associated Tau protein. *Acta Neuropathologica Communications* **5**, 1–11 (2017).
150. Kanaan, N. M. *et al.* Pathogenic Forms of Tau Inhibit Kinesin-Dependent Axonal Transport through a Mechanism Involving Activation of Axonal Phosphotransferases. *Journal of Neuroscience* **31**, 9858–9868 (2011).
151. Magnani, E. *et al.* Interaction of tau protein with the dynactin complex. *EMBO J* **26**, 4546–4554 (2007).
152. He, H. J. *et al.* The proline-rich domain of tau plays a role in interactions with actin. *BMC Cell Biol* **10**, 1–12 (2009).
153. Yu, W. *et al.* The Microtubule-severing Proteins Spastin and Katanin Participate Differently in the Formation of Axonal Branches. *Mol Biol Cell* **19**, 1485 (2008).
154. Shahani, N. & Brandt, R. Functions and malfunctions of the tau proteins. *Cell Mol Life Sci* **59**, 1668–1680 (2002).
155. Frandemiche, M. L. *et al.* Activity-Dependent Tau Protein Translocation to Excitatory Synapse Is Disrupted by Exposure to Amyloid-Beta Oligomers. *Journal of Neuroscience* **34**, 6084–6097 (2014).
156. Mondragón-Rodríguez, S. *et al.* Interaction of endogenous tau protein with synaptic proteins is regulated by N-methyl-D-aspartate receptor-dependent tau phosphorylation. *J Biol Chem* **287**, 32040–32053 (2012).
157. Ittner, L. M. *et al.* Dendritic function of tau mediates amyloid-beta toxicity in Alzheimer's disease mouse models. *Cell* **142**, 387–397 (2010).

158. Kornau, H. C., Schenker, L. T., Kennedy, M. B. & Seeburg, P. H. Domain interaction between NMDA receptor subunits and the postsynaptic density protein PSD-95. *Science* **269**, 1737–1740 (1995).
159. Robbins, M., Clayton, E. & Kaminski Schierle, G. S. Synaptic tau: A pathological or physiological phenomenon? *Acta Neuropathologica Communications* **9**, 1–30 (2021).
160. Pooler, A. M., Noble, W. & Hanger, D. P. A role for tau at the synapse in Alzheimer's disease pathogenesis. *Neuropharmacology* **76 Pt A**, 1–8 (2014).
161. Frost, B., Hemberg, M., Lewis, J. & Feany, M. B. Tau promotes neurodegeneration through global chromatin relaxation. *Nature Neuroscience* **17**, 357–366 (2014).
162. Loomis, P. A., Howard, T. H., Castleberry, R. P. & Binder, L. I. Identification of nuclear tau isoforms in human neuroblastoma cells. *Proceedings of the National Academy of Sciences* **87**, 8422–8426 (1990).
163. Talbot, K. *et al.* Demonstrated brain insulin resistance in Alzheimer's disease patients is associated with IGF-1 resistance, IRS-1 dysregulation, and cognitive decline. *J Clin Invest* **122**, 1316–1338 (2012).
164. Marciniak, E. *et al.* Tau deletion promotes brain insulin resistance. *J Exp Med* **214**, 2257–2269 (2017).
165. Seiberlich, V. *et al.* Downregulation of the microtubule associated protein Tau impairs process outgrowth and myelin basic protein mRNA transport in oligodendrocytes. *Glia* **63**, 1621–1635 (2015).
166. Limorenko, G. & Lashuel, H. A. Revisiting the grammar of Tau aggregation and pathology formation: how new insights from brain pathology are shaping how we study and target Tauopathies. *Chem Soc Rev* **51**, 513–565 (2022).
167. Wesseling, H., Mair, W., Hyman, B. T., Steen, H. & Steen Correspondence, J. A. Tau PTM Profiles Identify Patient Heterogeneity and Stages of Alzheimer's Disease. *Cell* **183**, 1699-1713 (2020).
168. Wegmann, S., Biernat, J. & Mandelkow, E. A current view on Tau protein phosphorylation in Alzheimer's disease. *Curr Opin Neurobiol* **69**, 131–138 (2021).
169. Johnson, G. V. W. & Stoothoff, W. H. Tau phosphorylation in neuronal cell function and dysfunction. *Journal of Cell Science* **117**, 5721–5729 (2004).
170. Maas, T., Eidenmüller, J. & Brandt, R. Interaction of tau with the neural membrane cortex is regulated by phosphorylation at sites that are modified in paired helical filaments. *J Biol Chem* **275**, 15733–15740 (2000).
171. Pooler, A. M. *et al.* Dynamic association of tau with neuronal membranes is regulated by phosphorylation. *Neurobiol Aging* **33**, 431.e27-431.e38 (2012).
172. Pooler, A. M. & Hanger, D. P. Functional implications of the association of tau with the plasma membrane. *Biochem Soc Trans* **38**, 1012–1015 (2010).
173. Aoki, K., Yoshida, K., Aoki, K. & Yoshida, K. Biological Consequences of Priming Phosphorylation in Cancer Development. *Protein Phosphorylation* (2017)

174. Butler, V. J. *et al.* Tau/MAPT disease-associated variant A152T alters tau function and toxicity via impaired retrograde axonal transport. *Hum Mol Genet* **28**, 1498–1514 (2019).
175. Grundke-Iqbal, I. *et al.* Abnormal phosphorylation of the microtubule-associated protein tau (tau) in Alzheimer cytoskeletal pathology. *Proc Natl Acad Sci U S A* **83**, 4913–4917 (1986).
176. Hoover, B. R. *et al.* Tau Mislocalization to Dendritic Spines Mediates Synaptic Dysfunction Independently of Neurodegeneration. *Neuron* **68**, 1067–1081 (2010).
177. Crimins, J. L., Pooler, A., Polydoro, M., Luebke, J. I. & Spires-Jones, T. L. The intersection of amyloid β and tau in glutamatergic synaptic dysfunction and collapse in Alzheimer's disease. *Ageing Res Rev* **12**, 757–763 (2013).
178. Polanco, J. C. *et al.* Amyloid-β and tau complexity - Towards improved biomarkers and targeted therapies. *Nature Reviews Neurology* **14**, 22–40 (2018).
179. Morishima-Kawashima, M. *et al.* Ubiquitin is conjugated with amino-terminally processed tau in paired helical filaments. *Neuron* **10**, 1151–1160 (1993).
180. Tan, J. M. M. *et al.* Lysine 63-linked ubiquitination promotes the formation and autophagic clearance of protein inclusions associated with neurodegenerative diseases. *Hum Mol Genet* **17**, 431–439 (2008).
181. Li, L., Jiang, Y., Wang, J. Z., Liu, R. & Wang, X. Tau Ubiquitination in Alzheimer's Disease. *Frontiers in Neurology* **12**, (2022).
182. Brickner, J. R. *et al.* A ubiquitin-dependent signalling axis specific for ALKBH-mediated DNA dealkylation repair. *Nature* **551**, 389–393 (2017).
183. Cripps, D. *et al.* Alzheimer disease-specific conformation of hyperphosphorylated paired helical filament-Tau is polyubiquitinated through Lys-48, Lys-11, and Lys-6 ubiquitin conjugation. *Journal of Biological Chemistry* **281**, 10825–10838 (2006).
184. Nakayama, Y. *et al.* Identification of linear polyubiquitin chain immunoreactivity in tau pathology of Alzheimer's disease. *Neurosci Lett* **703**, 53–57 (2019).
185. Flach, K. *et al.* Axotrophin/MARCH7 acts as an E3 ubiquitin ligase and ubiquitinates tau protein in vitro impairing microtubule binding. *Biochimica et Biophysica Acta (BBA) - Molecular Basis of Disease* **1842**, 1527–1538 (2014).
186. Seibenhener, M. L. *et al.* Sequestosome 1/p62 Is a Polyubiquitin Chain Binding Protein Involved in Ubiquitin Proteasome Degradation. *Mol Cell Biol* **24**, 8055–8068 (2004).
187. Puangmalai, N. *et al.* Lysine 63-linked ubiquitination of tau oligomers contributes to the pathogenesis of Alzheimer's disease. *Journal of Biological Chemistry* **298**, 101766 (2022).
188. Drubin, D. G. & Kirschner, M. W. Tau protein function in living cells. *J Cell Biol* **103**, 2739–2746 (1986).
189. D'Souza, I. & Schellenberg, G. D. Determinants of 4-repeat tau expression. Coordination between enhancing and inhibitory splicing sequences for exon 10 inclusion. *J Biol Chem* **275**, 17700–17709 (2000).

190. Crowther, R. A., Olesen, O. F., Jakes, R. & Goedert, M. The microtubule binding repeats of tau protein assemble into filaments like those found in Alzheimer's disease. *FEBS Lett* **309**, 199–202 (1992).
191. de Calignon, A., Spires-Jones, T. L., Pitstick, R., Carlson, G. A. & Hyman, B. T. Tangle-Bearing Neurons Survive Despite Disruption of Membrane Integrity in a Mouse Model of Tauopathy. *J Neuropathol Exp Neurol* **68**, 757–761 (2009).
192. Avila, J. Alzheimer disease: Caspases first. *Nature Reviews Neurology* **6**, 587–588 (2010).
193. Kovacech, B. & Novak, M. Tau truncation is a productive posttranslational modification of neurofibrillary degeneration in Alzheimer's disease. *Curr Alzheimer Res* **7**, 708–716 (2010).
194. Rissman, R. A. *et al.* Caspase-cleavage of tau is an early event in Alzheimer disease tangle pathology. *Journal of Clinical Investigation* **114**, 121–130 (2004).
195. Rohn, T. T., Rissman, R. A., Head, E. & Cotman, C. W. Caspase Activation in the Alzheimer's Disease Brain: Tortuous and Torturous. *Drug News Perspect* **15**, 549–557 (2002).
196. Lefebvre, T. *et al.* Evidence of a balance between phosphorylation and O-GlcNAc glycosylation of Tau proteins - A role in nuclear localization. *Biochim Biophys Acta Gen Subj* **1619**, 167–176 (2003).
197. Minoura, K. *et al.* Amphipathic helical behavior of the third repeat fragment in the tau microtubule-binding domain, studied by (1)H NMR spectroscopy. *Biochem Biophys Res Commun* **294**, 210–214 (2002).
198. Ledesma, M. D., Bonay, P., Colaço, C. & Avila, J. Analysis of Microtubule-associated Protein Tau Glycation in Paired Helical Filaments. *Journal of Biological Chemistry* **269**, 21614–21619 (1994).
199. Avila, J., Lucas, J. J., Pérez, M. & Hernández, F. Role of tau protein in both physiological and pathological conditions. *Physiol Rev* **84**, 361–384 (2004).
200. Jeganathan, S., von Bergen, M., Brutlach, H., Steinhoff, H. J. & Mandelkow, E. Global hairpin folding of tau in solution. *Biochemistry* **45**, 2283–2293 (2006).
201. Barré, P. & Eliezer, D. Folding of the Repeat Domain of Tau Upon Binding to Lipid Surfaces. *J Mol Biol* **362**, 312–326 (2006).
202. Niewiadomska, G., Niewiadomski, W., Steczkowska, M. & Gasiorowska, A. Tau Oligomers Neurotoxicity. *Life (Basel)* **11**, 1–28 (2021).
203. Goedert, M., Yamaguchi, Y., Mishra, S. K., Higuchi, M. & Sahara, N. Tau filaments and the development of positron emission tomography tracers. *Front Neurol* **9**, 70 (2018).
204. Hasegawa, M., Smith, M. J. & Goedert, M. Tau proteins with FTDP-17 mutations have a reduced ability to promote microtubule assembly. *FEBS Lett* **437**, 207–210 (1998).
205. Alonso, A. D. C., Mederlyova, A., Novak, M., Grundke-Iqbal, I. & Iqbal, K. Promotion of hyperphosphorylation by frontotemporal dementia tau mutations. *J Biol Chem* **279**, 34873–34881 (2004).
206. Khandelwal, P. J., Dumanis, S. B., Herman, A. M., Rebeck, G. W. & Moussa, C. E. H. Wild type and P301L mutant Tau promote neuro-

inflammation and α-Synuclein accumulation in lentiviral gene delivery models. *Mol Cell Neurosci* **49**, 44 (2012).
207. Nacharaju, P. *et al.* Accelerated filament formation from tau protein with specific FTDP-17 missense mutations. *FEBS Lett* **447**, 195–199 (1999).
208. Kawasaki, R. & Tate, S. I. Impact of the Hereditary P301L Mutation on the Correlated Conformational Dynamics of Human Tau Protein Revealed by the Paramagnetic Relaxation Enhancement NMR Experiments. *Int J Mol Sci* **21**, (2020).
209. Varshavsky, A. The early history of the ubiquitin field. *Protein Sci* **15**, 647 (2006).
210. Kulathu, Y. & Komander, D. Atypical ubiquitylation — the unexplored world of polyubiquitin beyond Lys48 and Lys63 linkages. *Nature Reviews Molecular Cell Biology* **13**, 508–523 (2012).
211. Swatek, K. N. & Komander, D. Ubiquitin modifications. *Cell Research* **26**, 399–422 (2016).
212. Welchman, R. L., Gordon, C. & Mayer, R. J. Ubiquitin and ubiquitin-like proteins as multifunctional signals. *Nature Reviews Molecular Cell Biology* **6**, 599–609 (2005).
213. Prakash, S., Sung, P. & Prakash, L. DNA repair genes and proteins of Saccharomyces cerevisiae. *Annu Rev Genet* **27**, 33–70 (1993).
214. Muratani, M., Kung, C., Shokat, K. M. & Tansey, W. P. The F box protein Dsg1/Mdm30 is a transcriptional coactivator that stimulates Gal4 turnover and cotranscriptional mRNA processing. *Cell* **120**, 887–899 (2005).
215. O'Donnell, M. A., Legarda-Addison, D., Skountzos, P., Yeh, W. C. & Ting, A. T. Ubiquitination of RIP1 regulates an NF-κB-independent cell death switch in TNF signaling. *Curr Biol* **17**, 418 (2007).
216. Hicke, L., Schubert, H. L. & Hill, C. P. Ubiquitin-binding domains. *Nat Rev Mol Cell Biol* **6**, 610–621 (2005).
217. Katzmann, D. J., Odorizzi, G. & Emr, S. D. Receptor downregulation and multivesicular-body sorting. *Nat Rev Mol Cell Biol* **3**, 893–905 (2002).
218. Boname, J. M. *et al.* Efficient internalization of MHC I requires lysine-11 and lysine-63 mixed linkage polyubiquitin chains. *Traffic* **11**, 210–220 (2010).
219. Komander, D. *et al.* Molecular discrimination of structurally equivalent Lys 63-linked and linear polyubiquitin chains. *EMBO Rep* **10**, 466 (2009).
220. Rahighi, S. *et al.* Specific recognition of linear ubiquitin chains by NEMO is important for NF-kappaB activation. *Cell* **136**, 1098–1109 (2009).
221. Elia, A. E. H. *et al.* Quantitative Proteomic Atlas of Ubiquitination and Acetylation in the DNA Damage Response. *Mol Cell* **59**, 867–881 (2015).
222. Cunningham, C. N. *et al.* USP30 and parkin homeostatically regulate atypical ubiquitin chains on mitochondria. *Nat Cell Biol* **17**, 160–169 (2015).
223. Bremm, A. & Komander, D. Emerging roles for Lys11-linked polyubiquitin in cellular regulation. *Trends Biochem Sci* **36**, (2011).
224. Mevissen, T. E. T. *et al.* OTU Deubiquitinases Reveal Mechanisms of Linkage Specificity and Enable Ubiquitin Chain Restriction Analysis. *Cell* **154**, 169 (2013).

225. Bremm, A., Moniz, S., Mader, J., Rocha, S. & Komander, D. Cezanne (OTUD7B) regulates HIF-1α homeostasis in a proteasome-independent manner. *EMBO Rep* **15**, 1268–1277 (2014).
226. He, M. *et al.* The emerging role of deubiquitinating enzymes in genomic integrity, diseases, and therapeutics. *Cell & Bioscience* **6**, 1–15 (2016).
227. Esser, C., Alberti, S. & Höhfeld, J. Cooperation of molecular chaperones with the ubiquitin/proteasome system. *Biochim Biophys Acta* **1695**, 171–188 (2004).
228. Popovic, D., Vucic, D. & Dikic, I. Ubiquitination in disease pathogenesis and treatment. *Nature Medicine* **20**, 1242–1253 (2014).
229. Lam, Y. A. *et al.* Inhibition of the ubiquitin-proteasome system in Alzheimer's disease. *Proc Natl Acad Sci U S A* **97**, 9902–9906 (2000).
230. Bennett, E. J., Bence, N. F., Jayakumar, R. & Kopito, R. R. Global impairment of the ubiquitin-proteasome system by nuclear or cytoplasmic protein aggregates precedes inclusion body formation. *Mol Cell* **17**, 351–365 (2005).
231. Tofaris, G. K., Razzaq, A., Ghetti, B., Lilley, K. S. & Spillantini, M. G. Ubiquitination of alpha-synuclein in Lewy bodies is a pathological event not associated with impairment of proteasome function. *J Biol Chem* **278**, 44405–44411 (2003).
232. Spratt, D. E. *et al.* A molecular explanation for the recessive nature of parkin-linked Parkinson's disease. *Nature Communications* **4**, 1–12 (2013).
233. Zucchelli, S. *et al.* Tumor Necrosis Factor Receptor-associated Factor 6 (TRAF6) Associates with Huntingtin Protein and Promotes Its Atypical Ubiquitination to Enhance Aggregate Formation. *J Biol Chem* **286**, 25108 (2011).
234. Babu, J. R., Geetha, T. & Wooten, M. W. Sequestosome 1/p62 shuttles polyubiquitinated tau for proteasomal degradation. *J Neurochem* **94**, 192–203 (2005).
235. Green, D. R. & Llambi, F. Cell death signaling. *Cold Spring Harb Perspect Biol* **7**, (2015).
236. Mattson, M. P. Apoptosis in neurodegenerative disorders. *Nat Rev Mol Cell Biol* **1**, 120–129 (2000).
237. Kermer, P., Liman, J., Weishaupt, J. H. & Bähr, M. Neuronal Apoptosis in Neurodegenerative Diseases: From Basic Research to Clinical Application. *Review Neurodegenerative Dis* **1**, 9–19 (2004).
238. Erekat, N. S. Apoptosis and its therapeutic implications in neurodegenerative diseases. *Clinical Anatomy* **35**, 65–78 (2022).
239. Kerr, J. F. R., Wyllie, A. H. & Currie, A. R. Apoptosis: a basic biological phenomenon with wide-ranging implications in tissue kinetics. *Br J Cancer* **26**, 239–257 (1972).
240. Galluzzi, L. *et al.* Molecular mechanisms of cell death: Recommendations of the Nomenclature Committee on Cell Death 2018. *Cell Death and Differentiation* **25**, 486–541 (2018).
241. Tait, S. W. G. & Green, D. R. Mitochondria and cell death: outer membrane permeabilization and beyond. *Nature Reviews Molecular Cell Biology* **11**, 621–632 (2010).

242. Wu, C. C. & Bratton, S. B. Regulation of the intrinsic apoptosis pathway by reactive oxygen species. *Antioxid Redox Signal* **19**, 546–558 (2013).
243. Cai, J., Yang, J. & Jones, D. P. Mitochondrial control of apoptosis: the role of cytochrome c. *Biochim Biophys Acta* **1366**, 139–149 (1998).
244. Kumar, R., Herbert, P. E. & Warrens, A. N. An introduction to death receptors in apoptosis. *Int J Surg* **3**, 268–277 (2005).
245. Guicciardi, M. E. & Gores, G. J. Life and death by death receptors. *FASEB J* **23**, 1625–1637 (2009).
246. Kischkel, F. C. *et al.* Cytotoxicity-dependent APO-1 (Fas/CD95)-associated proteins form a death-inducing signaling complex (DISC) with the receptor. *EMBO J* **14**, 5579–5588 (1995).
247. Ichim, G. & Tait, S. W. G. A fate worse than death: apoptosis as an oncogenic process. *Nat Rev Cancer* **16**, 539–548 (2016).
248. Silke, J. & Vucic, D. IAP family of cell death and signaling regulators. *Methods Enzymol* **545**, 35–65 (2014).
249. Yu, J. W. & Shi, Y. FLIP and the death effector domain family. *Oncogene* **27**, 6216–6227 (2008).
250. Coccia, E. *et al.* SIVA-1 regulates apoptosis and synaptic function by modulating XIAP interaction with the death receptor antagonist FAIM-L. *Cell Death Dis* **11**, (2020).
251. Espinosa-Oliva, A. M., García-Revilla, J., Alonso-Bellido, I. M. & Burguillos, M. A. Brainiac Caspases: Beyond the Wall of Apoptosis. *Front Cell Neurosci* **13**, 500 (2019).
252. Coccia, E. *et al.* FAIM Is Regulated by MiR-206, MiR-1-3p and MiR-133b. *Front Cell Dev Biol* **8**, (2020).
253. Coccia, E. *et al.* Identification and characterization of new isoforms of human fas apoptotic inhibitory molecule (FAIM). *PLoS One* **12**, (2017).
254. Schneider, T. J., Fischer, G. M., Donohoe, T. J., Colarusso, T. P. & Rothstein, T. L. A novel gene coding for a Fas apoptosis inhibitory molecule (FAIM) isolated from inducibly Fas-resistant B lymphocytes. *Journal of Experimental Medicine* **189**, 949–955 (1999).
255. Zhong, X., Schneider, T. J., Cabral, D. S., Donohoe, T. J. & Rothstein, T. L. An alternatively spliced long form of Fas apoptosis inhibitory molecule (FAIM) with tissue-specific expression in the brain. *Mol Immunol* **38**, 65–72 (2001).
256. Segura, M. F. *et al.* The Long Form of Fas Apoptotic Inhibitory Molecule Is Expressed Specifically in Neurons and Protects Them against Death Receptor-Triggered Apoptosis. *The Journal of Neuroscience* **27**, 11228-12241 (2007).
257. Moubarak, R. S. *et al.* FAIM-L is an IAP-binding protein that inhibits XIAP ubiquitinylation and protects from fas-induced apoptosis. *Journal of Neuroscience* **33**, 19262–19275 (2013).
258. Huo, J., Xu, S., Guo, K., Zeng, Q. & Lam, K. P. Genetic deletion of faim reveals its role in modulating c-FLIP expression during CD95-mediated apoptosis of lymphocytes and hepatocytes. *Cell Death Differ* **16**, 1062–1070 (2009).
259. Huo, J. *et al.* Loss of Fas apoptosis inhibitory molecule leads to spontaneous obesity and hepatosteatosis. *Cell Death & Disease* **7**, e2091–e2091 (2016).

260. Sole, C. *et al.* The death receptor antagonist FAIM promotes neurite outgrowth by a mechanism that depends on ERK and NF-κB signaling. *Journal of Cell Biology* **167**, 479–492 (2004).
261. Pozueta, J. *et al.* Caspase-2 is required for dendritic spine and behavioural alterations in J20 APP transgenic mice. *Nat Commun* **4**, (2013).
262. Ohsawa, S. *et al.* Maturation of the olfactory sensory neurons by Apaf-1/caspase-9-mediated caspase activity. *Proc Natl Acad Sci U S A* **107**, 13366–13371 (2010).
263. Unsain, N., Higgins, J. M., Parker, K. N., Johnstone, A. D. & Barker, P. A. XIAP regulates caspase activity in degenerating axons. *Cell Rep* **4**, 751–763 (2013).
264. Lee, S. H., Simonetta, A. & Sheng, M. Subunit rules governing the sorting of internalized AMPA receptors in hippocampal neurons. *Neuron* **43**, 221–236 (2004).
265. Mattson, M. P., Keller, J. N. & Begley, J. G. Evidence for synaptic apoptosis. *Exp Neurol* **153**, 35–48 (1998).
266. Martínez-Mármol, R. *et al.* FAIM-L regulation of XIAP degradation modulates Synaptic Long-Term Depression and Axon Degeneration. *Sci Rep* **6**, (2016).
267. Cusack, C. L., Swahari, V., Hampton Henley, W., Michael Ramsey, J. & Deshmukh, M. Distinct pathways mediate axon degeneration during apoptosis and axon-specific pruning. *Nat Commun* **4**, (2013).
268. Nikolaev, A., McLaughlin, T., O'Leary, D. D. M. & Tessier-Lavigne, M. APP binds DR6 to trigger axon pruning and neuron death via distinct caspases. *Nature* **457**, 981–989 (2009).
269. Simon, D. J. *et al.* A Caspase Cascade Regulating Developmental Axon Degeneration. *Journal of Neuroscience* **32**, 17540–17553 (2012).
270. Kaku, H. & Rothstein, T. L. FAIM Is a Non-redundant Defender of Cellular Viability in the Face of Heat and Oxidative Stress and Interferes With Accumulation of Stress-Induced Protein Aggregates. *Front Mol Biosci* **7**, (2020).
271. Kaku, H., Ludlow, A. v., Gutknecht, M. F. & Rothstein, T. L. FAIM Opposes Aggregation of Mutant SOD1 That Typifies Some Forms of Familial Amyotrophic Lateral Sclerosis. *Front Neurosci* **14**, (2020).
272. Kaku, H., Balaj, A. R. & Rothstein, T. L. Small Heat Shock Proteins Collaborate with FAIM to Prevent Accumulation of Misfolded Protein Aggregates. *Int J Mol Sci* **23**, (2022).
273. Sirés, A. *et al.* Faim knockout leads to gliosis and late-onset neurodegeneration of photoreceptors in the mouse retina. *J Neurosci Res* **99**, 3103–3120 (2021).
274. Carriba, P. *et al.* Amyloid-β reduces the expression of neuronal FAIM-L, thereby shifting the inflammatory response mediated by TNFα from neuronal protection to death. *Cell Death Dis* **6**, (2015).
275. Campenot, R. B. Local control of neurite development by nerve growth factor. *Proc Natl Acad Sci U S A* **74**, 4516–4519 (1977).
276. DuBridge, R. B. *et al.* Analysis of mutation in human cells by using an Epstein-Barr virus shuttle system. *Mol Cell Biol* **7**, 379–387 (1987).

277. Greene, L. A. & Tischler, A. S. Establishment of a noradrenergic clonal line of rat adrenal pheochromocytoma cells which respond to nerve growth factor. *Proc Natl Acad Sci U S A* **73**, 2424–2428 (1976).
278. Paxinos, G. & Franklin, K. B. J. Paxinos and Franklin's the Mouse Brain in Stereotaxic Coordinates. *Academic Press* **2nd Edition**, (2001).
279. Livak, K. J. & Schmittgen, T. D. Analysis of relative gene expression data using real-time quantitative PCR and the 2(-Delta Delta C(T)) Method. *Methods* **25**, 402–408 (2001).
280. Jimenez, S. *et al.* Disruption of Amyloid Plaques Integrity Affects the Soluble Oligomers Content from Alzheimer Disease Brains. *PLoS One* **9**, (2014).
281. Bayram-Weston, Z., Olsen, E., Harrison, D. J., Dunnett, S. B. & Brooks, S. P. Optimising Golgi-Cox staining for use with perfusion-fixed brain tissue validated in the zQ175 mouse model of Huntington's disease. *J Neurosci Methods* **265**, 81–88 (2016).
282. Zaqout, S. & Kaindl, A. M. Golgi-cox staining step by step. *Front Neuroanat* **10**, 38 (2016).
283. Barron, M. R., Gartlon, J., Dawson, L. A., Atkinson, P. J. & Pardon, M. C. Increasing Tau 4R Tau Levels Exacerbates Hippocampal Tau Hyperphosphorylation in the hTau Model of Tauopathy but Also Tau Dephosphorylation Following Acute Systemic Inflammation. *Front Immunol* **11**, 293 (2020).
284. Hernández, F., Gómez de Barreda, E., Fuster-Matanzo, A., Lucas, J. J. & Avila, J. GSK3: a possible link between beta amyloid peptide and tau protein. *Exp Neurol* **223**, 322–325 (2010).
285. Dejanovic, B. *et al.* Changes in the Synaptic Proteome in Tauopathy and Rescue of Tau-Induced Synapse Loss by C1q Antibodies. *Neuron* **100**, 1322-1336.e7 (2018).
286. Neddens, J. *et al.* Correlation of pyroglutamate amyloid β and ptau Ser202/Thr205 levels in Alzheimer's disease and related murine models. *PLoS One* **15**, (2020).
287. Popovic, D., Vucic, D. & Dikic, I. Ubiquitination in disease pathogenesis and treatment. *Nature Medicine* **20**, 1242–1253 (2014).
288. Rohn, T. T. Caspase Cleaved Tau in Alzheimer's Disease: A Therapeutic Target Realized. *Int J Neurol Neurother* **2**, 014 (2015).
289. García-Sierra, F. *et al.* Ubiquitin is Associated with Early Truncation of Tau Protein at Aspartic Acid 421 during the Maturation of Neurofibrillary Tangles in Alzheimer's Disease. *Brain Pathol* **22**, 240-250 (2011).
290. Watkins, G. R. *et al.* Monoubiquitination Promotes Calpain Cleavage of the Protein Phosphatase 2A (PP2A) Regulatory Subunit 4, Altering PP2A Stability and Microtubule-associated Protein Phosphorylation. *J Biol Chem* **287**, 24207–24215 (2012).
291. Goedert, M. & Jakes, R. Mutations causing neurodegenerative tauopathies. *Biochimica et Biophysica Acta - Molecular Basis of Disease* **1739**, 240–250 (2005).
292. Yang, H. & Hu, H. Y. Sequestration of cellular interacting partners by protein aggregates: implication in a loss-of-function pathology. *FEBS Journal* **283**, 3705–3717 (2016).

293. Banerjee, S., Ferdosh, S., Ghosh, A. N. & Barat, C. Tau protein- induced sequestration of the eukaryotic ribosome: Implications in neurodegenerative disease. *Sci Rep* **10**, (2020).
294. Simon, P., Dupuis, R. & Costentin, J. Thigmotaxis as an index of anxiety in mice. Influence of dopaminergic transmissions. *Behavioural brain research* **61**, 59–64 (1994).
295. Kraeuter, A. K., Guest, P. C. & Sarnyai, Z. The Open Field Test for Measuring Locomotor Activity and Anxiety-Like Behavior. *Methods Mol Biol* **1916**, 99–103 (2019).
296. Broadbent, N. J., Squire, L. R. & Clark, R. E. Spatial memory, recognition memory, and the hippocampus. *Proc Natl Acad Sci U S A* **101**, 14515–14520 (2004).
297. Bird, C. M. & Burgess, N. The hippocampus and memory: insights from spatial processing. *Nature Reviews Neuroscience* **9**, 182–194 (2008).
298. Leszczynski, M. How does hippocampus contribute to working memory processing? *J Neurosci* **31**, 9032-9042 (2011).
299. Borders, A. A., Aly, M., Parks, C. M. & Yonelinas, A. P. The Hippocampus is Particularly Important for Building Associations Across Stimulus Domains. *Neuropsychologia* **99**, 335 (2017).
300. Wang, X. bin & Zhou, Q. Spine Remodeling and Synaptic Modification. *Molecular Neurobiology* **41**, 29–41 (2010).
301. Debanne, D., Gähwiler, B. H. & Thompson, S. M. Heterogeneity of Synaptic Plasticity at Unitary CA3–CA1 and CA3–CA3 Connections in Rat Hippocampal Slice Cultures. *The Journal of Neuroscience* **19**, 10671 (1999).
302. Dimsdale-Zucker, H. R., Ritchey, M., Ekstrom, A. D., Yonelinas, A. P. & Ranganath, C. CA1 and CA3 differentially support spontaneous retrieval of episodic contexts within human hippocampal subfields. *Nature Communications* **9**, 1–8 (2018).
303. Espadas, I. *et al.* Dopamine D2R is Required for Hippocampal-dependent Memory and Plasticity at the CA3-CA1 Synapse. *Cereb Cortex* **31**, 2187–2204 (2021).
304. Borczyk, M., Śliwińska, M. A., Caly, A., Bernas, T. & Radwanska, K. Neuronal plasticity affects correlation between the size of dendritic spine and its postsynaptic density. *Scientific Reports* **9**, 1–12 (2019).
305. Tsien, J. Z., Huerta, P. T. & Tonegawa, S. The essential role of hippocampal CA1 NMDA receptor-dependent synaptic plasticity in spatial memory. *Cell* **87**, 1327–1338 (1996).
306. Hunter, T. The Age of Crosstalk: Phosphorylation, Ubiquitination, and Beyond. *Mol Cell* **28**, 730–738 (2007).
307. Kim, J. H. *et al.* CHIP-mediated hyperubiquitylation of tau promotes its self-assembly into the insoluble tau filaments. *Chem Sci* **12**, 5599–5610 (2021).
308. Rao, J. S., Kellom, M., Kim, H. W., Rapoport, S. I. & Reese, E. A. Neuroinflammation and synaptic loss. *Neurochem Res* **37**, 903–910 (2012).
309. Cook, C. *et al.* Tau deposition drives neuropathological, inflammatory and behavioral abnormalities independently of neuronal loss in a novel mouse model. *Hum Mol Genet* **24**, 6198–6212 (2015).

310. Nakamura, T., Cho, D.-H. & Lipton, S. A. Redox regulation of protein misfolding, mitochondrial dysfunction, synaptic damage, and cell death in neurodegenerative diseases. *Exp Neurol* **238**, 10–21 (2012).
311. Taoufik, E., Kouroupi, G., Zygogianni, O. & Matsas, R. Synaptic dysfunction in neurodegenerative and neurodevelopmental diseases: an overview of induced pluripotent stem-cell-based disease models. *Open Biol* **8**, (2018).
312. Kim, J. S., Ha, J. Y., Yang, S. J. & Son, J. H. A Novel Non-Apoptotic Role of Procaspase-3 in the Regulation of Mitochondrial Biogenesis Activators. *J Cell Biochem* **119**, 347–357 (2018).
313. Wang, L. *et al.* The cytoplasmic nuclear shuttling of Beclin 1 in neurons with Alzheimer's disease-like injury. *Neurosci Lett* **661**, 63–70 (2017).
314. Li, Z. *et al.* Caspase-3 activation via mitochondria is required for long-term depression and AMPA receptor internalization. *Cell* **141**, 859–871 (2010).
315. Simon, D. J. *et al.* A caspase cascade regulating developmental axon degeneration. *J Neurosci* **32**, 17540–17553 (2012).
316. Ertürk, A., Wang, Y. & Sheng, M. Local pruning of dendrites and spines by caspase-3-dependent and proteasome-limited mechanisms. *J Neurosci* **34**, 1672–1688 (2014).
317. Gipson, C. D. & Olive, M. F. Structural and functional plasticity of dendritic spines – root or result of behavior? *Genes Brain Behav* **16**, 101–117 (2017).
318. Shin, J., Park, S., Lee, H. Y. & Kim, Y. S. Thioflavin-positive tau aggregates complicating quantification of amyloid plaques in the brain of 5XFAD transgenic mouse model. *Scientific Reports* **11**, 1–9 (2021).
319. Oakley, H. *et al.* Intraneuronal beta-amyloid aggregates, neurodegeneration, and neuron loss in transgenic mice with five familial Alzheimer's disease mutations: potential factors in amyloid plaque formation. *J Neurosci* **26**, 10129–10140 (2006).
320. He, Z. *et al.* Amyloid-β plaques enhance Alzheimer's brain tau-seeded pathologies by facilitating neuritic plaque tau aggregation. *Nature* **24**, 29–38 (2017).
321. Fang, Y. *et al.* The blockage of the Nogo/NgR signal pathway in microglia alleviates the formation of Aβ plaques and tau phosphorylation in APP/PS1 transgenic mice. *J Neuroinflammation* **13**, 1–17 (2016).
322. Feng, T. *et al.* Chronic cerebral hypoperfusion accelerates Alzheimer's disease pathology with the change of mitochondrial fission and fusion proteins expression in a novel mouse model. *Brain Res* **1696**, 63–70 (2018).
323. Sturchler-Pierrat, C. *et al.* Two amyloid precursor protein transgenic mouse models with Alzheimer disease-like pathology. *Proc Natl Acad Sci U S A* **94**, 13287–13292 (1997).
324. Bolmont, T. *et al.* Induction of tau pathology by intracerebral infusion of amyloid-beta -containing brain extract and by amyloid-beta deposition in APP x Tau transgenic mice. *Am J Pathol* **171**, 2012–2020 (2007).
325. Blanchard, V. *et al.* Time sequence of maturation of dystrophic neurites associated with Aβ deposits in APP/PS1 transgenic mice. *Exp Neurol* **184**, 247–263 (2003).

326. Soto-Faguás, C. M., Sanchez-Molina, P. & Saura, C. A. Loss of presenilin function enhances tau phosphorylation and aggregation in mice. *Acta Neuropathol Commun* **9**, (2021).
327. Zhang, Z. *et al.* Cleavage of tau by asparagine endopeptidase mediates the neurofibrillary pathology in Alzheimer's disease. *Nat Med* **20**, 1254–1262 (2014).
328. García-Arriaza, J. *et al.* Tauopathy Analysis in P301S Mouse Model of Alzheimer Disease Immunized With DNA and MVA Poxvirus-Based Vaccines Expressing Human Full-Length 4R2N or 3RC Tau Proteins. *Vaccines (Basel)* **8**, (2020).
329. Sun, Y. *et al.* The behavioural and neuropathologic sexual dimorphism and absence of MIP-3α in tau P301S mouse model of Alzheimer's disease. *J Neuroinflammation* **17**, 1–18 (2020).
330. Larson, T. *et al.* Mice expressing P301S mutant human tau have deficits in interval timing. *Behavioural Brain Research* **432**, (2022).
331. Yin, Y. *et al.* Accumulation of human full-length tau induces degradation of nicotinic acetylcholine receptor α4 via activating calpain-2. *Sci Rep* **6**, (2016).
332. de La Fuente, S. *et al.* Cell Death & Disease Calpain system is altered in survival motor neuron-reduced cells from in vitro and in vivo spinal muscular atrophy models. *Cell Death Dis* **11**, 487 (2020).
333. Sansa, A., de la Fuente, S., Comella, J. X., Garcera, A. & Soler, R. M. Intracellular pathways involved in cell survival are deregulated in mouse and human spinal muscular atrophy motoneurons. *Neurobiol Dis* **155**, 105366 (2021).
334. Townsend, M., Mehta, T. & Selkoe, D. J. Soluble Abeta inhibits specific signal transduction cascades common to the insulin receptor pathway. *J Biol Chem* **282**, 33305–33312 (2007).
335. Magdesian, M. H. *et al.* Amyloid-beta binds to the extracellular cysteine-rich domain of Frizzled and inhibits Wnt/beta-catenin signaling. *J Biol Chem* **283**, 9359–9368 (2008).
336. Lee, H. K., Kumar, P., Fu, Q., Rosen, K. M. & Querfurth, H. W. The insulin/Akt signaling pathway is targeted by intracellular beta-amyloid. *Mol Biol Cell* **20**, 1533–1544 (2009).
337. Zhang, F. *et al.* β-amyloid redirects norepinephrine signaling to activate the pathogenic GSK3β/tau cascade. *Sci Transl Med* **12**, (2020).
338. Aweida, D., Rudesky, I., Volodin, A., Shimko, E. & Cohen, S. GSK3-β promotes calpain-1-mediated desmin filament depolymerization and myofibril loss in atrophy. *J Cell Biol* **217**, 3698–3714 (2018).
339. Hurtado, D. E. *et al.* Selectively silencing GSK-3 isoforms reduces plaques and tangles in mouse models of Alzheimer's disease. *J Neurosci* **32**, 7392–7402 (2012).
340. Tan, X. *et al.* Isoorientin, a GSK-3β inhibitor, rescues synaptic dysfunction, spatial memory deficits and attenuates pathological progression in APP/PS1 model mice. *Behavioural brain research* **398**, (2021).
341. Liu, X. *et al.* Ubiquitin Specific Protease 13 Regulates Tau Accumulation and Clearance in Models of Alzheimer's Disease. *J Alzheimers Dis* **72**, 425–441 (2019).

342. Fan, Y. G. *et al.* Paricalcitol accelerates BACE1 lysosomal degradation and inhibits calpain-1 dependent neuronal loss in APP/PS1 transgenic mice. *EBioMedicine* **45**, 393–407 (2019).
343. Knoblaugh, S. E., Hohl, T. M. & Perle, K. M. D. la. Pathology Principles and Practices for Analysis of Animal Models. *ILAR J* **59**, 40–50 (2019).
344. Walker, C. K. *et al.* Dendritic Spine Remodeling and Synaptic Tau Levels in PS19 Tauopathy Mice. *Neuroscience* **455**, 195–211 (2021).
345. Petrucelli, L. *et al.* CHIP and Hsp70 regulate tau ubiquitination, degradation and aggregation. *Hum Mol Genet* **13**, 703–714 (2004).
346. Seibenhener, M. L. *et al.* Sequestosome 1/p62 Is a Polyubiquitin Chain Binding Protein Involved in Ubiquitin Proteasome Degradation. *Mol Cell Biol* **24**, 8055–8068 (2004).
347. Dickey, C. A. *et al.* Deletion of the Ubiquitin Ligase CHIP Leads to the Accumulation, But Not the Aggregation, of Both Endogenous Phospho- and Caspase-3-Cleaved Tau Species. *Journal of Neuroscience* **26**, 6985–6996 (2006).
348. Santacruz, K. *et al.* Medicine: Tau suppression in a neurodegenerative mouse model improves memory function. *Science (1979)* **309**, 476–481 (2005).
349. Keck, S., Nitsch, R., Grune, T. & Ullrich, O. Proteasome inhibition by paired helical filament-tau in brains of patients with Alzheimer's disease. *J Neurochem* **85**, 115–122 (2003).
350. Shin, S. K. *et al.* Docosahexaenoic acid-mediated protein aggregates may reduce proteasome activity and delay myotube degradation during muscle atrophy in vitro. *Exp Mol Med* **49**, (2017).
351. Puangmalai, N. *et al.* Lysine 63-linked ubiquitination of tau oligomers contributes to the pathogenesis of Alzheimer's disease. *Journal of Biological Chemistry* **298**, (2022).
352. Dittmar, G. & Selbach, M. Deciphering the Ubiquitin Code. *Mol Cell* **65**, 779–780 (2017).
353. Galves, M., Rathi, R., Prag, G. & Ashkenazi, A. Ubiquitin Signaling and Degradation of Aggregate-Prone Proteins. *Trends Biochem Sci* **44**, 872–884 (2019).
354. Yang, Y., Fang, S., Jensen, J. P., Weissman, A. M. & Ashwell, J. D. Ubiquitin protein ligase activity of IAPs and their degradation in proteasomes in response to apoptotic stimuli. *Science* **288**, 874–877 (2000).
355. Sugiyama, T., Li, S., Kato, M., Ikeuchi, K. & Ichimura, A. Sequential Ubiquitination of Ribosomal Protein uS3 Triggers the Degradation of Non-functional 18S rRNA. *CellReports* **26**, 3400-3415.e7 (2019).
356. Jin, H. S. *et al.* cIAP1, cIAP2, and XIAP act cooperatively via nonredundant pathways to regulate genotoxic stress-induced nuclear factor-kappaB activation. *Cancer Res* **69**, 1782–1791 (2009).
357. Kruse, J. P. & Gu, W. MSL2 Promotes Mdm2-independent Cytoplasmic Localization of p53. *J Biol Chem* **284**, 3250 (2009).
358. van Campenhout, C. A. *et al.* Dlg3 Trafficking and Apical Tight Junction Formation Is Regulated by Nedd4 and Nedd4-2 E3 Ubiquitin Ligases. *Dev Cell* **21**, 491 (2011).

359. Montalbano, M. *et al.* Tau oligomers mediate aggregation of RNA-binding proteins Musashi1 and Musashi2 inducing Lamin alteration. *Aging Cell* **18**, (2019).
360. Montalbano, M. *et al.* Tau Modulates mRNA Transcription, Alternative Polyadenylation Profiles of hnRNPs, Chromatin Remodeling and Spliceosome Complexes. *Front Mol Neurosci* **14**, 302 (2021).
361. García-Escudero, V. *et al.* A new non-aggregative splicing isoform of human Tau is decreased in Alzheimer's disease. *Acta Neuropathol* **142**, 159 (2021).
362. Shen, H. *et al.* Pyroptosis executive protein GSDMD as a biomarker for diagnosis and identification of Alzheimer's disease. *Brain Behav* **11**, (2021).
363. Salech, F., Ponce, D. P., Paula-Lima, A. C., SanMartin, C. D. & Behrens, M. I. Nicotinamide, a Poly [ADP-Ribose] Polymerase 1 (PARP-1) Inhibitor, as an Adjunctive Therapy for the Treatment of Alzheimer's Disease. *Front Aging Neurosci* **12**, (2020).
364. Esteras, N. *et al.* Insoluble tau aggregates induce neuronal death through modification of membrane ion conductance, activation of voltage-gated calcium channels and NADPH oxidase. *FEBS J* **288**, 127–141 (2021).
365. Caccamo, A. *et al.* Necroptosis activation in Alzheimer's disease. *Nature Neuroscience 2017 20:9* **20**, 1236–1246 (2017).
366. Moujalled, D., Strasser, A. & Liddell, J. R. Molecular mechanisms of cell death in neurological diseases. *Cell Death Differ* **28**, 2029–2044 (2021).
367. Avila, J. *et al.* Cognitive Decline in Neuronal Aging and Alzheimer's Disease: Role of NMDA Receptors and Associated Proteins. *Front Neurosci* **11**, (2017).
368. Blazquez-Llorca, L., Garcia-Marin, V., Merino-Serrais, P., Ávila, J. & DeFelipe, J. Abnormal Tau Phosphorylation in the Thorny Excrescences of CA3 Hippocampal Neurons in Patients with Alzheimer's Disease. *Journal of Alzheimer's Disease* **26**, 683–698 (2011).
369. Rodríguez-Urgellés, E. *et al.* Meridianins Rescue Cognitive Deficits, Spine Density and Neuroinflammation in the 5xFAD Model of Alzheimer's Disease. *Front Pharmacol* **13**, (2022).
370. Coultrap, S. J. *et al.* Autonomous CaMKII Mediates Both LTP and LTD Using a Mechanism for Differential Substrate Site Selection. *Cell Rep* **6**, 431–437 (2014).
371. Chang, J. Y. *et al.* CaMKII Autophosphorylation Is Necessary for Optimal Integration of Ca2+ Signals during LTP Induction, but Not Maintenance. *Neuron* **94**, 800-808.e4 (2017).
372. Unsain, N., Higgins, J. M., Parker, K. N., Johnstone, A. D. & Barker, P. A. XIAP Regulates Caspase Activity in Degenerating Axons. *Cell Rep* **4**, 751–763 (2013).
373. Jiao, S. & Li, Z. Non-apoptotic function of BAD and BAX in long-term depression of synaptic transmission. *Neuron* **70**, 758 (2011).
374. Di, J. *et al.* Abnormal tau induces cognitive impairment through two different mechanisms: synaptic dysfunction and neuronal loss. *Sci Rep* **6**, (2016).

375. Forner, S., Baglietto-Vargas, D., Martini, A. C., Trujillo-Estrada, L. & LaFerla, F. M. Synaptic Impairment in Alzheimer's Disease: A Dysregulated Symphony. *Trends Neurosci* **40**, 347–357 (2017).
376. Ögren, S. O. & Stiedl, O. Passive Avoidance. *Encyclopedia of Psychopharmacology* 1–10 (2013).
377. Apicco, D. J. *et al.* Reducing the RNA binding protein TIA1 protects against tau-mediated neurodegeneration in vivo. *Nature Neuroscience* **21**, 72–80 (2017).
378. Vagnozzi, A. N., Giannopoulos, P. F. & Praticò, D. The direct role of 5-lipoxygenase on tau pathology, synaptic integrity and cognition in a mouse model of tauopathy. *Psychiatry* **7**, (2017).
379. Zampar, S. & Wirths, O. Characterization of a mouse model of alzheimer's disease expressing aβ4-42 and human mutant tau. *Int J Mol Sci* **22**, 5191 (2021).
380. Berger-Sweeney, J., Arnold, A., Gabeau, D. & Mills, J. Sex differences in learning and memory in mice: effects of sequence of testing and cholinergic blockade. *Behavioral neuroscience* **109**, 859–873 (1995).
381. Habedank, A., Kahnau, P. & Lewejohann, L. Alternate without alternative: Neither preference nor simple learning behaviour shown by C57BL/6J mice in the T-maze. *bioRxiv*, (2020).
382. Tang, S. J. *et al.* Fyn kinase inhibition reduces protein aggregation, increases synapse density and improves memory in transgenic and traumatic Tauopathy. *Acta Neuropathol Commun* **8**, 1–21 (2020).
383. Kubota, K. & Niki, H. Prefrontal cortical unit activity and delayed alternation performance in monkeys. *J Neurophysiol* **34**, 337–347 (1971).
384. Fuster, J. M. Unit activity in prefrontal cortex during delayed-response performance: neuronal correlates of transient memory. *J Neurophysiol* **36**, 61–78 (1973).
385. Kilonzo, K. *et al.* Delayed-matching-to-position working memory in mice relies on NMDA-receptors in prefrontal pyramidal cells. *Scientific Reports* **11**, 8788 (2021).
386. Wang, H., Wang, R., Carrera, I., Xu, S. & Lakshmana, M. K. TFEB Overexpression in the P301S Model of Tauopathy Mitigates Increased PHF1 Levels and Lipofuscin Puncta and Rescues Memory Deficits. *eNeuro* **3**, 9340–9351 (2016).
387. Zigman, W. B. *et al.* Alzheimer's Disease in Adults with Down Syndrome. *Int Rev Res Ment Retard* **36**, 103 (2008).
388. Chen, X. *et al.* Synapse impairment associated with enhanced apoptosis in post-traumatic stress disorder. *Synapse* **74**, (2020).
389. Shipton, O. A. *et al.* Tau protein is required for amyloid {beta}-induced impairment of hippocampal long-term potentiation. *J Neurosci* **31**, 1688–1692 (2011).
390. Bi, M. *et al.* Tau exacerbates excitotoxic brain damage in an animal model of stroke. *Nature Communications* **8**, 1–15 (2017).
391. Lovestone, S. *et al.* A phase II trial of tideglusib in Alzheimer's disease. *J Alzheimers Dis* **45**, 75–88 (2015).
392. Medina, M. An Overview on the Clinical Development of Tau-Based Therapeutics. *Int J Mol Sci* **19**, (2018).

393. Ross, C. A. & Poirier, M. A. Protein aggregation and neurodegenerative disease. *Nat Med* **10**, (2004).
394. Gipson, C. D. & Olive, M. F. Structural and functional plasticity of dendritic spines – root or result of behavior? *Genes Brain Behav* **16**, 101–117 (2017).
395. Hyun, J. S., Inoue, T. & Hayashi-Takagi, A. Multi-Scale Understanding of NMDA Receptor Function in Schizophrenia. *Biomolecules* **10**, (2020).